Université catholique de Louvain

Faculté de Médecine

Unité de Néphrologie

Chloride Transporters and Vacuolar H^+-ATPase in Nephrogenesis and Congenital Tubulopathies

François JOURET

Docteur en Médecine

Promoteur : Prof. Olivier DEVUYST

Thèse présentée en vue de l'obtention du grade de

Docteur en Sciences Biomédicales

Orientation : Physiopathologie, Biologie Moléculaire

2006

Université catholique de Louvain

Faculté de Médecine

Unité de Néphrologie

Chloride Transporters and Vacuolar H^+-ATPase in Nephrogenesis and Congenital Tubulopathies

François JOURET

Docteur en Médecine

Promoteur : Prof. Olivier DEVUYST

Thèse présentée en vue de l'obtention du grade de

Docteur en Sciences Biomédicales

Orientation : Physiopathologie, Biologie Moléculaire

2006

à Céline,

à Chloé et Baptiste,

à mes parents,

Recognizing that we have the kind of blood we have
because we have the kind of kidneys we have,
we must acknowledge that our kidneys constitute
the major foundation of our philosophical freedom.

Only because they work the way they do
has it become possible for us to have bones, muscles, glands and brains.
Superficially, it might be said that the function of the kidney is to make urine;
but in a more considered view one can say that
the kidneys make the stuff of philosophy itself.

Homer W. Smith
Boston, 1953

AVANT-PROPOS

Au Professeur B. Coulie, Recteur, à son prédécesseur, le Professeur M. Crochet, au Professeur J-F. Denef, Prorecteur aux Affaires Médicales, aux Professeurs J-J. Rombouts et D. Moulin, respectivement actuel et ancien Doyens de la Faculté de Médecine, ainsi qu'au Professeur J. Melin, Coordonnateur Général des Cliniques Universitaires St-Luc, j'adresse toute ma reconnaissance pour la formation médicale et scientifique que j'ai reçue au sein de l'Université catholique de Louvain.

Dès ma deuxième candidature en Médecine (1996), le Professeur J-F. Denef m'accueille au sein du laboratoire d'Histologie, et m'initie à la démarche expérimentale avec beaucoup de disponibilité et de rigueur. Je tiens à lui exprimer ici ma profonde gratitude d'avoir suscité en moi l'attrait pour la recherche fondamentale.

Par la qualité de son enseignement et son enthousiasme scientifique, le Professeur O. Devuyst me convainc rapidement de la richesse clinique et fondamentale de la Néphrologie, et m'ouvre les portes de son laboratoire en 1999. Promoteur de cette thèse, puisse-t-il recevoir ici l'expression de mes sincères remerciements pour la qualité de son encadrement, son esprit d'analyse et sa motivation à toute épreuve. Merci d'avoir alimenté jour après jour ma curiosité scientifique, et d'avoir permis tant de collaborations nationales et internationales !

Qu'il me soit permis de remercier ici les Professeurs R. Beauwens (Université Libre de Bruxelles), E.I. Christensen (University of Aarhus, Aarhus, Denmark), J-P. Cosyns, P.J. Courtoy, Ph. Gailly, A. Goffinet et J-N. Octave, Président du Jury, d'avoir accepté de faire partie du jury de cette thèse. Leur « passion intellectuelle » ouverte à l'interprétation originale des données primaires et inscrite dans une approche critique et intégrative de la physiologie humaine a développé mon esprit de questionnement et d'investigation (*inquiry*, lat. *quaere verum*, chercher le vrai) tout au long de ce doctorat. Leurs conseils judicieux et commentaires constructifs lors de la rédaction m'ont en outre permis d'améliorer tant le fond que la forme de cette thèse.

Ce travail n'aurait pas été possible sans l'aide bienveillante et la qualité technique de V. Beaujean, Y. Cnops, H. Debaix, S. Druart et N. Van Oost au sein du laboratoire de Néphrologie. Je tiens à les remercier vivement pour leur temps consacré à mon apprentissage scientifique, leur engouement et leur complicité durant mon séjour au laboratoire. Merci à S. Ruttens, Ph. Camby et L. Wenderickx du laboratoire

d’Anatomo-Pathologie, à C. Auzanneau, G. Dom, T. Lac, M. Leruth, E. Marbaix, B. Marien, M-F. van den Hove et P. Van Der Smissen de l’unité CELL, à A. Bernard, C. Hermans, T. Leal et P. Lebecque des Cliniques Universitaires St-Luc, ainsi qu’à F. Jamar, S. Pauwels, et S. Walrand du laboratoire d’Imagerie Moléculaire et de Radiothérapie Expérimentale pour leur précieuse aide logistique, leur efficacité, et leurs conseils avisés lors de nos collaborations passés, présentes,… et, j’espère, à venir !

Nos travaux de recherche ont en outre bénéficié des échanges fructueux avec les équipes scientifiques de J-J. Cassiman (Katholieke Universiteit Leuven, Leuven), H.R. De Jonge (Erasmus Universiteit, Rotterdam), W.B. Guggino (Johns Hopkins University, Baltimore), F.E. Karet (University of Cambridge, Cambridge), S.J. Scheinman (State University of New-York, Syracuse), P. Steels (Universiteit Hasselt, Diepenbeek), R.V. Thakker (University of Oxford, Oxford), T. Willnow (Max Delbrück Center, Berlin).

During my stay in the lab, I got the unique opportunity to meet and work every day with people from (almost) all around the World. Cultural and scientific exchanges, as well as the daily practice of English, allowed me (… us) to learn more about our various traditions and lifestyle, thereby improving our own personality. Again, my thanks to you all, A. Ahrabi, H. Belge, P. Nguyen, J. Ni, T. Nishino, K. Parreira, E. Riveira-Munoz, A. Sacré, F. Turan, and J. Zhang, for being who you are. Merci également à tout le staff clinique du service de Néphrologie pour leur intérêt porté à nos travaux et leurs encouragements durant toute la durée de ce doctorat.

In fine, mes remerciements vont à mon épouse et mes enfants pour leur soutien et patience, ainsi qu’à mes parents, frère et sœur, pour l’exemple de vie qu’ils me donnent chaque jour et la confiance qu’ils m’ont toujours accordée. Qu’ils trouvent ici l’expression de toute mon affection.

Ces travaux ont bénéficié du soutien du Fonds National de la Recherche Scientifique au travers d’un mandat d’Aspirant, et se sont déroulés au sein de l’école doctorale de Physiologie, Pharmacologie et Morphologie Cellulaires de la Faculté de Médecine de l’Université catholique de Louvain.

TABLE OF CONTENTS

LIST OF ABBREVIATIONS

ABC	ATP-binding cassette
AE1/SLC4A1	Type I anion exchanger
AF	amniotic fluid
AFLP	amplified fragment length polymorphism
AMN	amnionless
AQP	aquaporin
ARF	ADP-ribosylation factor
CA	carbonic anhydrase
CaCC	Ca^{++}-activated Cl^- channel
CBAVD	congenital bilateral absence of the vas deferens
CC16	Clara cell protein 16kD
CD	collecting duct
CF	cystic fibrosis
CFTR	cystic fibrosis transmembrane conductance regulator
COP	coat protein
ΔF508	deletion of phenylalanine at position 508
E11	embryonic day 11
EBCR	epithelial basolateral Cl^- conductance regulator
EGF	epidermal growth factor
EM	electron microscopy
ENaC	epithelium Na^+ channel
ER	endoplasmic reticulum
GAPDH	glyceraldehyde 3-phosphate dehydrogenase
GFR	glomerular filtration rate
GW	gestational week
HE	hydroethidine
HK-2	human kidney (2) cells
HPRT	hypoxanthine guanine phosphoribosyltransferase
HRP	horseradish peroxidase
IC	intercalated cell
IF	intrinsic factor
KO	knock-out
LDL	low-density lipoprotein
LMW	low-molecular-weight
MDR	multidrug resistance
MRP	multidrug resistance protein
MM	metanephric mesenchyme
NaC	Na^+-dependent dicarboxylate transporter
NBC	$Na^+/HCO3^-$ co-transporter
NBD	nucleotide-binding domain
NHERF	Na^+/H^+ exchange regulator factor

NPD	nasal potential difference
NPT	Na^+-dependent phosphate transporter
OAT	organic anion transporter
OCRL	oculo-cerebro-renal syndrome of Lowe
OK	opossum kidney
OMIM	Online Mendelian Inheritance in Man^{TM}
ORCC	outwardly rectifying chloride channel
PCNA	proliferative cell nuclear antigen
PCT	proximal convoluted tubule
PET	positron emission tomography
PST	proximal straight tubule
PIP_2	phosphoinositide (4,5) bisphosphate
PKA	protein kinase A
PT	proximal tubule
PTH	parathyroid hormone
RAP	receptor-associated protein
ROS	reactive oxygen species
RTA	renal tubular acidosis
RT-PCR	reverse-transcription polymerase chain reaction
SOD	superoxide dismutase
SPECT	single-photon emission computed tomography
TAL	thick ascending limb
^{99m}Tc-DMSA	^{99m}Technetium dimercaptosuccinic acid
^{99m}Tc-MAG3	^{99m}Technetium mercaptoacetyltriglycine
TGN	*trans*-Golgi network
tnAP	tissue-nonspecific alkaline phosphatase
TMD	transmembrane domain
UB	ureteric bud
V-ATPase	vacuolar H^+-ATPase

Websites

http://mordor.cgb.ki.se/cgi-bin/CONSITE/consite
http://organogenesis.ucsd.edu/
http://us.expasy.org/
http://www.genet.sickkids.on.ca/cftr/
http://www.gene.ucl.ac.uk/nomenclature/
http://www.hgmd.cf.ac.uk/hgmd0.html
http://www.ncbi.nlm.nih.gov/BLAST/
http://www.ncbi.nlm.nih.gov/entrez/query.fcgi?db=OMIM

CHAPTER I. INTRODUCTION

The kidney serves essential functions in water, electrolyte, acid-base, and organic solute homeostasis by ultrafiltrating blood and producing urine. Likewise, the kidney removes metabolic products and exogenous toxins from the body, and excretes them into the urine. In addition, specialized renal cells are involved in hormone production, thereby participating in calcium metabolism, erythrogenesis, and blood pressure regulation. The functional unit of the kidney is the nephron consisting of a glomerulus responsible for blood ultrafiltration, and a tubule organized into structurally and functionally distinct epithelial segments. In this thesis, we address the role of chloride transporters and vacuolar proton-ATPase (V-ATPase) in the developing and mature tubule, and more specifically in the proximal tubule (PT) cells and the intercalated cells (IC) of the collecting duct (CD).

The general structure and main functions of the PT are summarized in **Section 1**, with a particular emphasis on the reabsorption of filtered low-molecular-weight (LMW) proteins. This function is ensured by the receptor-mediated endocytic pathway and plays a central role in hormone and vitamin homeostasis, as well as in the salvage of amino acids. The **Section 2** outlines the distribution and functional properties of the IC, as well as their crucial role in acid-base homeostasis.

The importance of Cl^- and H^+ transporters in the physiology of both PT cells and IC is highlighted by the severe phenotype observed in inherited and acquired human diseases affecting these proteins. The **Section 3** details the pathophysiology of two

"chloride channelopathies" further investigated in this project, i.e. Dent's disease (defect of the Cl^- transporter ClC-5) and cystic fibrosis (defect of the Cl^- channel CFTR). The attention is especially drawn on the mouse models available to further investigate these disorders.

The last part of the introduction addresses the embryonic development of the kidney. Consistent observations of early PT dysfunction and acid-base disorders in infants with mutations of genes encoding Cl^- and H^+ transporters support that the tubular maturation is essentially achieved around birth and during early infancy. Additional clinical and experimental evidences for such functional differentiation of kidney tubules during organogenesis are presented and discussed in **Section 4**.

The co-distribution of Cl^- and H^+ transporters in specialized cells along the nephron supports mutual interactions between these proteins, as well as their implication in various physiological processes disrupted in human diseases and animal models.

1. The proximal tubule

1.1. Anatomy and ultrastructure

Each kidney consists of 700,000 to 1,200,000 nephrons in man, and about 10,000 to 20,000 nephrons in mouse. Nephrons in the mammalian kidney can be classified according to the position of their glomerulus in the cortex (superficial, midcortical, or juxta-medullary) or according to the length (short or long) of their loop of Henle. The loop of Henle consists of the straight part of the PT, the descending thin limb, the ascending and thick ascending limb (Figure 1.1). Most superficial nephrons have short loops that bend within the outer medulla, whereas the loops of juxta-medullary nephrons extend to the inner medulla. However, all three types of glomeruli may be associated with short as well as long loops. The ratio of short to long loops is about 85:15 in man, 82:18 in mouse, 70:30 in rat, and 34:66 in rabbit, which reflects species differences in urine-concentrating mechanisms (Zhai, 2006). Such structural organization of the distinct segments of the nephron in the cortex and the medulla has important implications in understanding the mechanisms of renal function. Two architectural zones can particularly be distinguished in the mammalian cortex: the cortical labyrinth and the medullary rays (Figure 1.1). The medullary rays extend from

the outer stripe of the outer medulla and are regularly located between the larger tracts of the cortical labyrinth. The glomeruli, proximal and distal convoluted tubules, connecting tubules, initial CD, and most of the vascular network, are located within the cortical labyrinth, whereas the medullary rays carry the straight segments of proximal and distal tubules, the cortical CD, and associated capillaries. Within medullary rays, the straight tubules from the most superficial nephrons are arranged as central bundles which are surrounded by tubules originating in the deeper cortex. This illustrates the morphologic and likely also functional heterogeneity of the different zones of the renal cortex.

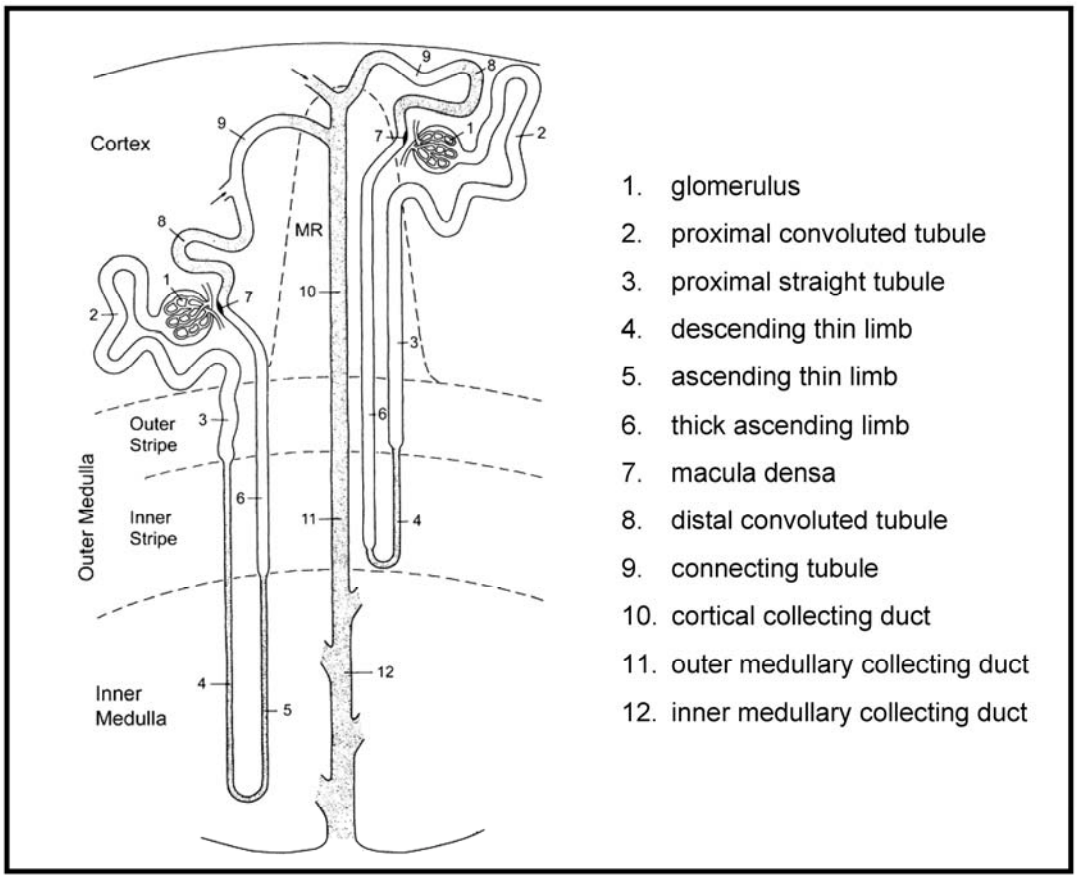

Figure 1.1. Anatomy of the nephron

The nephron represents the structural and functional unit of the kidney, and consists of a glomerulus and a tubule organized into distinct segments. The first segments of the tubule are the proximal convoluted tubule, further subdivided into S1 and S2, and the proximal straight tubule, S3. The loop of Henle includes the descending thin limb, the ascending thin limb, and the thick ascending limb (alias the distal straight tubule). The distal convoluted tubule continues into the connecting tubule (CNT). The CNT leads further into the cortical, outer medullary, and inner medullary collecting duct that joins the duct of Bellini.

Adapted from Kriz, 1988

The PT begins at the urinary pole of the glomerulus as a continuation of the parietal epithelium of the Bowman space (Figure 1.1). The PT is approximately 14 mm long in man, and between 8 to 10 mm in rodents. At low magnification, the PT can be divided into a convoluted part (proximal convoluted tubule, PCT) and a straight part (proximal straight part, PST). Furthermore, ultrastructural examinations distinguish three morphologically distinct consecutive segments: S1, S2, and S3. The S1 and S2 segments cover respectively the first and the second portions of the PCT located in the cortical labyrinth, whereas the S3 segment corresponds to the PST and runs in the medullary rays and the outer stripe of the outer medulla. At the junction of the outer and inner stripes of the outer medulla, the straight segments of PT end abruptly, and give rise to the descending thin limbs of the loops of Henle. Note that this segmental variation in the ultrastructure of the PT is not as clear in mouse as in rat and human kidney (Zhai, 2003).

The epithelial cells lining the PT are characterized by highly specialized apical and basolateral membrane domains (Figure 1.2). The luminal membrane shows a typical sensory primary cilium and long densely packed microvilli forming a “brush border” system. This enlargement of the apical surface area correlates with the main role of the PT, i.e. the reabsorption of the bulk of the ultrafiltrate. On the other side, the basolateral membrane shows numerous invaginations and interdigitations between adjacent cells. This rearrangement generates an extensive intercellular space that is separated from the tubular lumen by the tight junctions or *zonula occludens* and delimited from the interstitium by the basement membrane. In strong contrast with those found in the distal nephron, the structure of PT tight junctions is typical of “leaky epithelia”, which favours a number of paracellular transport mechanisms. In addition, PT cells are characterized by numerous mitochondria, a well-developed endocytic/lysosomal system, as well as a prominent Golgi apparatus responsible for protein synthesis, sorting and targeting. Cell complexity progressively declines from S1 to S3 segments, correlating with a gradual decrease of reabsorptive rates along the PT. Of note, differences in the volume density of lysosomes and large endosomes have been reported between man, rabbit, rat, and mouse, and may be related to species-

dependent variations in the glomerular filtration of macromolecules and the reabsorptive and degradative capacity of the endocytic apparatus in the PT (Zhai, 2003).

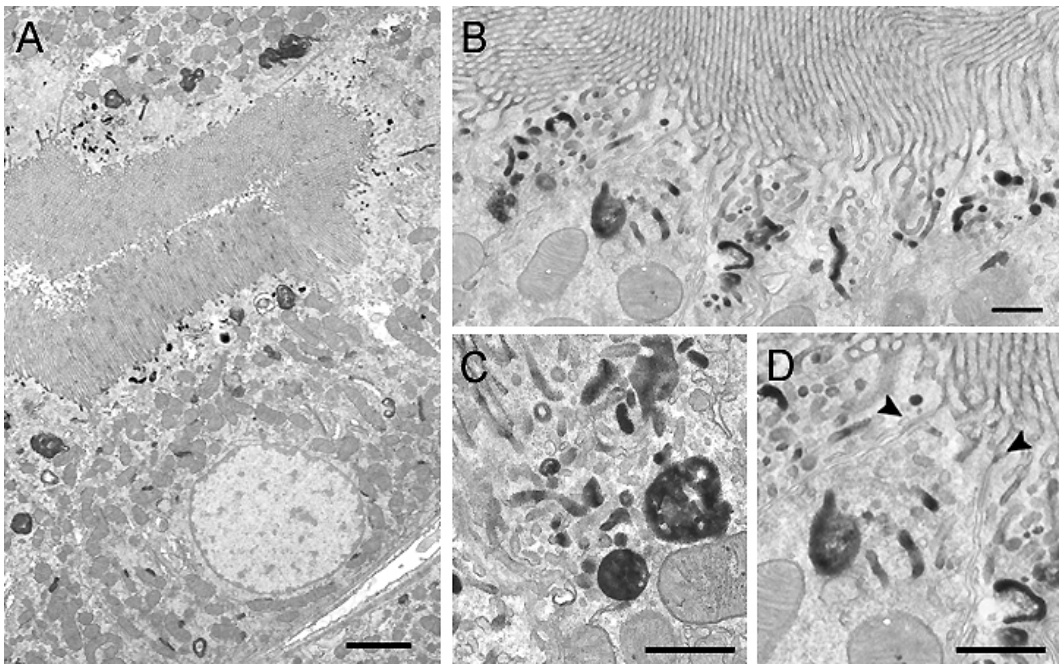

Figure 1.2. Electron microscopy of mouse PT cell

The ultrastructural morphology of PT epithelial cells includes a well-developed brush border and endosomal apparatus, numerous mitochondria, and a thin basement membrane (A). Higher magnification illustrates a tall and well-differentiated brush border (B), and numerous apical endosomes demonstrated here by peroxidase cytochemistry upon injection of horseradish peroxidase (C). PT cells are connected to each other by apical intercellular junctions (D, arrowheads).
Bars in (A), 5 μm; (B), 1 μm; (C), 0.5 μm; (D), 0.8 μm.

Courtesy of P.J. Courtoy and P. Van der Smissen

1.2. Main functions

The epithelial cells lining the PT are highly specialized to reabsorb the ultrafiltrate, including approximately two-thirds of the filtered salt and water and all filtered organic solutes (primarily glucose and amino acids). The solutes are absorbed isotonically, in that the osmotic potential of the fluid leaving the proximal tubule is the same as that of the initial glomerular filtrate. This is mainly ensured by the transport of Na^+ from the lumen into the blood driven by the Na^+/K^+-ATPase located at the basolateral side of PT cells, which in turn allows the reabsorption of glucose, amino acids, and inorganic phosphate via secondary active transport through apical

Na^+/solute co-transporters (Féraille, 2001). The uptake of albumin and LMW proteins is achieved by receptor-mediated endocytosis in the first PT segments (Birn, 2006). Such PT endocytic activity also prevents the urinary loss of essential hormones and vitamins like parathyroid hormone (PTH), vitamin D, retinol, vitamin B12, and folates, and participates in their processing, i.e. degradation, storage or activation and release into the bloodstream. In addition, PT cells are involved in the regulation of acid-base balance by reabsorbing the bulk of filtered HCO_3^- and secreting NH_4^+. This nephron segment also reabsorbs divalent ions, such as Ca^{2+}, HPO_4^{2-}, and SO_4^{2-}. Finally, several organic anion and cation transporters, mostly distributed along the S3 PT, actively secrete a variety of substances, including drugs and metabolites, from the blood into the urine (Wright, 2004).

1.3. Receptor-mediated endocytosis

A significant amount of albumin and plasma LMW proteins are filtered daily through the glomerulus and avidly reabsorbed in S1 and S2 segments of the PCT, as well as in the straight part S3 (Birn, 2006). As an example, albumin concentration in the renal ultrafiltrate has been estimated in the range of 22-32 mg/liter, which corresponds to a daily filtered load of albumin of 3300-5760 mg, but less than 1% of filtered albumin is excreted in the final urine (Gekle, 2005). By definition, LMW proteins are characterized by a molecular weight below that of albumin (~69kDa). They include hormones (PTH, insulin, growth hormone), carrier or storage proteins (retinol-, vitamin D- and folate-binding proteins), enzymes (cytochrome C, lysozyme), cell surface antigen components (β_2-microglobulin), immunoglobulin light chains, and other proteins (cystatin C, Clara cell CC16 protein, and α_1-microglobulin). Most of their filtered load is reabsorbed and catabolized by PT cells, and the human urine is virtually devoid of plasma proteins under physiological conditions. Such massive uptake of proteins accounts for as much as 80% of the total metabolic clearance of small proteins and peptides, and plays a key role in hormone and vitamin homeostasis. Of note, the fraction of reabsorbed albumin compared to the filtered load is smaller in rodents with relatively short PT than in larger species with longer PT.

This protein uptake mainly involves receptor-mediated (or adsorptive) endocytosis, while fluid-phase capture can be regarded as quantitatively negligible in

the PT. During receptor-mediated endocytosis, substances are concentrated at the cell membrane, and the concentration in the endocytic invagination exceeds the concentration in the extracellular space several fold. The mechanisms underlying receptor-mediated endocytosis can be roughly subdivided into three types with respect to vesicle formation: (i) endocytosis via clathrin-coated pits; (ii) caveolae-mediated endocytosis; and (iii) clathrin- and caveolae-independent endocytosis (for a detailed review, see Conner, 2003). Clathrin-mediated endocytosis represents the predominant pathway for protein uptake across the apical membrane of PT cells. The apical endocytic pathway of PT cells consists of five main interrelated compartments: (i) microvilli and clathrin-coated pits, (ii) early endosomes, (iii) dense apical tubules responsible for apical recycling, (iv) late endosomes, and (v) lysosomes (Figure 1.3).

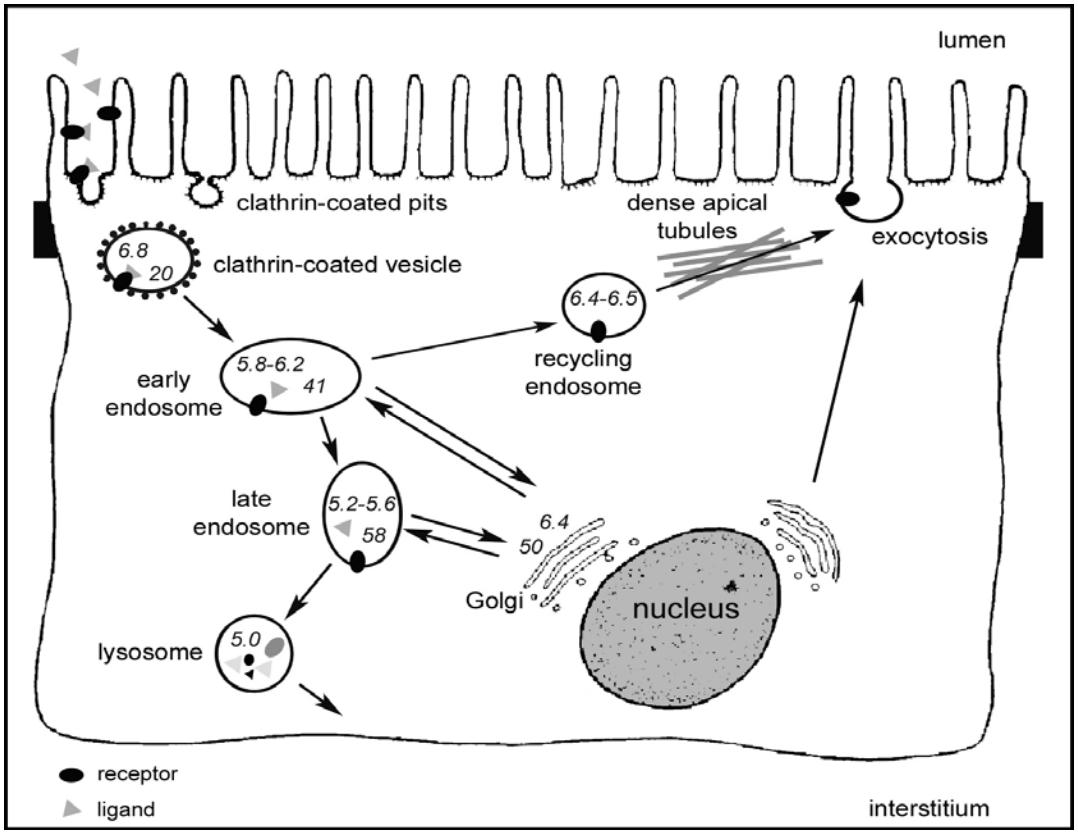

Figure 1.3. Organization of the endocytic apparatus in PT cell

The complex ligand-receptor forms at the apical brush border of PT cells, is internalized into coated vesicle, and transferred to the endosomal network. Progression along the endocytic pathway depends on the acidification of the intravesicular lumen, as well as on the actin cytoskeleton and the microtubules. Ligand-receptor complexes dissociate in early endosomes, with further recycling of the receptor through the DAT network and transfer of the ligand to lysosomes for degradation or storage. In each organelle lumen, the upper and lower figures represent pH and [Cl^-] concentration (mM) values, respectively.
Modified from Faundez, 2004.

Two multiligand receptors, megalin and cubilin, are abundantly expressed at the brush border of PT cells (Christensen, 2002a). Ligand binding and interactions between both receptors induce their internalization into coated vesicles and their subsequent delivery to endosomes and lysosomes for ligand processing and receptor degradation or recycling. Pharmacological studies have shown that receptor-mediated endocytosis of albumin depends on the integrity of the actin cytoskeleton (stabilization of the microvilli), as well as on the microtubules (acceleration of vesicle movement from the plasma membrane to the endocytic network) (Gekle, 1997). In addition, the endocytic process is dependent on a progressive acidification from early to late endosomes and finally to lysosomes (Shi, 1991; Faundez, 2004). Indeed, the drop in pH in the successive endocytic compartments triggers receptor-ligand dissociation and modulates vesicle trafficking, endosomal fusion events, and coat formation. In PT cells, the endosomal acidification is driven by the electrogenic V-ATPase (Figure 1.4), whose inhibition by pharmacological agents like bafilomycin A-1 or toxic agents like the heavy metal cadmium, has been demonstrated to severely impair the uptake of albumin and LMW proteins *in vitro* and *in vivo* (Wang, 2005; Herak-Kramberger, 1998). The translocation of H^+ from the cytoplasm into the endosomes generates a transmembrane electrical potential ($\Delta\Psi$), resulting in a rapid inhibition of V-ATPase activity. Thus, in order to limit the formation of an endosomal-positive membrane potential, either negative charge carriers have to concurrently enter vesicles or positive charge carriers have to leave. In most cases, the acidification of intracellular vesicles is dependent on a parallel Cl^- conductance that provides the electrical shunt necessary to neutralize the H^+ electrical gradient (Jentsch, 2002). Furthermore, the intravesicular Cl^- concentration itself could directly affect the activity of the V-ATPase (Moriyama, 1987), as well as the vesicle recycling, independently of its effect on pH (Faundez, 2004). Of note, the involvement of Na^+/H^+-exchanger isoform 3 (NHE-3) in endosomal acidification has been recently demonstrated in PT cells (Wang, 2005). Most likely, NHE-3 participates in the acidification of early endosomes, in which there is a sufficient Na^+ outward gradient (vesicle-to-cytosol) to drive NHE-3 in the appropriate direction. Indeed, pharmacological inhibition of NHE-3 *in vitro* disturbs the early vesicular acidification and retards albumin endocytosis. Moreover, genetic inactivation of NHE-3 in mice leads to significant tubular proteinuria (Gekle, 2005).

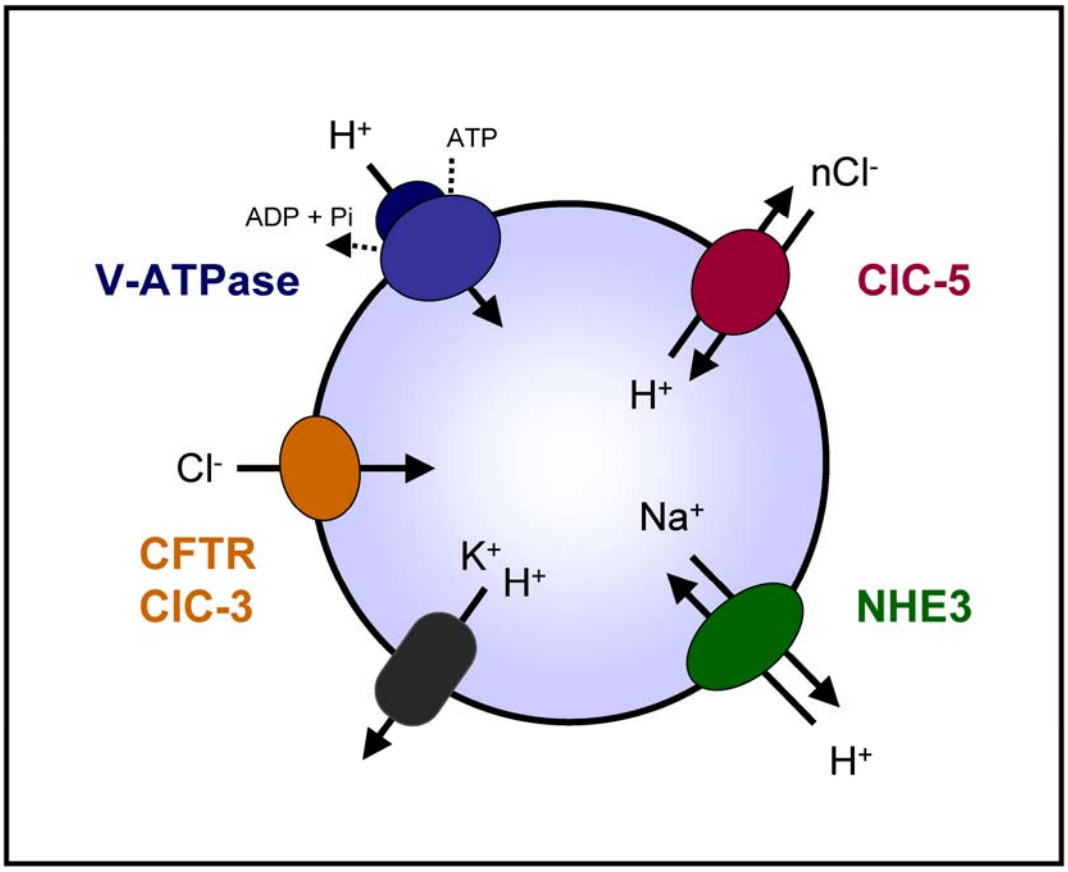

Figure 1.4. Partners of the endosomal acidification

The endosomal acidification is achieved by ATP-driven transport of cytosolic H^+ through the V-ATPase. The positive electrical gradient ($\Delta\Psi$) is dissipated by cation (H^+, K^+) leakage, as well as by parallel Cl^- permeability through ClC-5 and most likely other anion transporters. Two recent studies have demonstrated that ClC-5 acts as voltage-dependent Cl^-/H^+ exchanger (Picollo, 2005; Scheel, 2005). The electro-neutral Na^+/H^+ exchanger NHE3 also participates in endosomal pH regulation (Wang, 2005).

1.3.1. Megalin

Megalin is a multiligand endocytic receptor belonging to the low-density lipoprotein (LDL) receptor family, which was originally identified in rat glomerular podocytes as the antigen in Heymann membranous glomerulonephritis (Kerjaschki, 1982-83).

Megalin co-distributes with cubilin in many absorptive epithelia, like the small intestine, the renal PT, the visceral yolk sac and the placenta (Christensen, 2002a). In addition, megalin has been identified in the choroid plexus, endometrium, epididymis, lung, inner ear, parathyroid and thyroid glands. The subcellular distribution of megalin

in rodent and human kidney includes the brush border and the apical endocytic apparatus, as well as lysosomal structures, of PT cells (Chatelet, 1986; Christensen, 1995). Megalin has been shown to rapidly recycle between apical clathrin-coated pits and early and late endosomes, with delivery of luminal ligands to lysosomes for hormone and vitamin homeostasis and amino acid recovery (Christensen, 1998; Nagai, 2003). The normal expression of megalin is finely regulated by its interaction with the chaperone RAP (receptor-associated protein, 45 kDa) in the endoplasmic reticulum (ER), which protects freshly synthesized megalin from the premature binding of ligands and its subsequent degradation (Birn, 2000). In addition, RAP may be involved in the correct folding of megalin (Bu, 1996).

The structure of megalin is characterized by a large extracellular domain, a single transmembrane domain, and a short cytoplasmic tail harbouring two NPxY motifs necessary for the clustering into clathrin-coated pits (Takeda, 2003) (Figure 1.5). In addition to NPxY motifs, the C-terminal tail of megalin contains distinct targeting sequences, such as a related VENQNY motif involved in apical sorting and several Src homology 3 and 2 recognition sites likely implicated in signal transduction (Hjalm, 1996). The extracellular domain is made of four clusters of cysteine-rich complement-type/LDL-receptor type A repeats forming the ligand binding regions. These domains are separated by a total of 17 epidermal growth factor (EGF)-type repeats and eight spacer regions containing YWTD sequences. Ligand binding to megalin is considered as Ca^{++}-dependent and favored by cationic sites on the ligands (Christensen, 1992; Moestrup, 1995).

The role of megalin in kidney PT cells has been suggested by the investigations of megalin-deficient mouse models (Willnow, 1996; Leheste, 2003). The absence of megalin does not affect the overall architecture of the epithelial PT cells and no changes in glucose, electrolyte and amino acid transports have been reported in *megalin* knockout (KO) mice. In strong contrast, the loss of megalin causes a significant reduction in the number of coated pits, endosomes, and lysosomes in PT

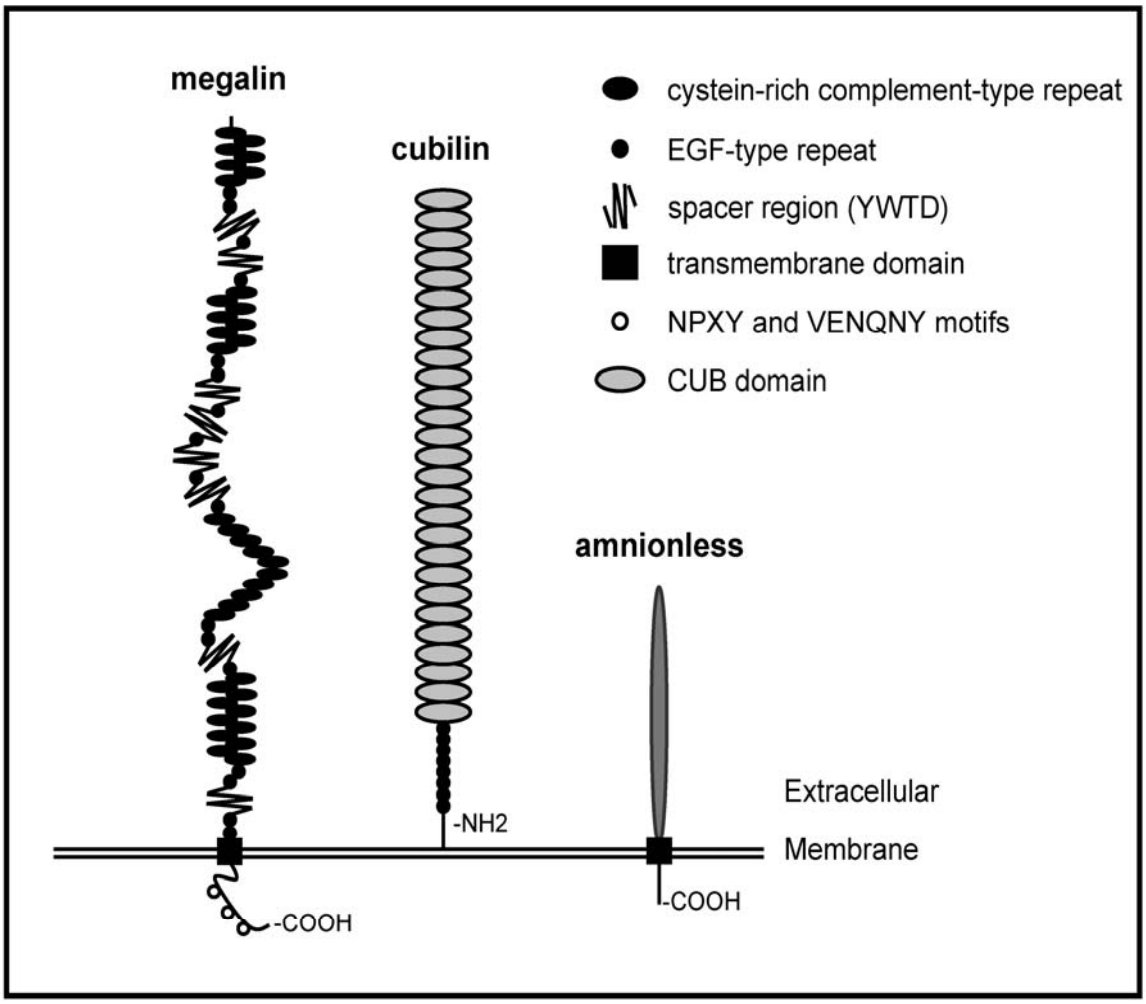

Figure 1.5. Structure of megalin, cubilin and amnionless

Megalin is a 4600-amino-acid transmembrane protein. The extracellular domain contains four cysteine-rich clusters of LDL receptor-type A repeats constituting the ligand binding regions separated and followed by a total of 17 EGF-type repeats and eight spacer regions containing YWTD repeats. The cytoplasmic C-terminal tail contains two NPXY sequences and one VENQNY sequence responsible for apical sorting.

Cubilin is a 3600-amino-acid protein with no transmembrane domain. The extracellular domain contains 27 CUB domains where interactions with multiple ligands take place. The CUB domains are preceded by a stretch of 106 amino acids followed by eight EGF-type repeats. The amino-terminal region contains a potential palmitoylation site and an amphipathic helix structure with some similarity to the lipid binding regions of apolipoproteins.

Amnionless (AMN) is a 434-amino-acid single-transmembrane protein, with no known, closely related proteins. The extracellular domain includes a cysteine-rich stretch of 70 amino acids that shares similarities with modules present in bone morphogenic protein (BMP) inhibitors. The cytoplasmic domain exhibits 2 highly conserved FXNPXF sequences implicated in ligand-independent internalization via clathrin-coated pits.

Redrawn from Birn, 2006

Table 1.1. Ligands for megalin and cubilin

Megalin	Cubilin
Vitamin carrier proteins	
transcobalamin II-vitamin B12 vitamin D-binding protein, vitamin D retinol-binding protein folate-binding protein sex hormones-binding globulin	intrinsic factor-vitamin B12 vitamin D-binding protein, vitamin D
Other carrier proteins	
albumin hemoglobin, myoglobin lactoferrin odorant-binding protein transthyretin	albumin hemoglobin, myoglobin transferrin
Lipid binding proteins	
apolipoproteins B, E, J, H, M	apolipoprotein A1 high-density lipoprotein
Hormones, hormone precursors, and signaling proteins	
parathyroid hormone insulin epidermal growth factor prolactin thyroglobin angiotensin II leptin	
Enzymes and enzyme-inhibitors	
plasminogen plasminogen activator inhibitor-type 1 plasminogen activator inhibitor-type 1-urokinase plasminogen activator inhibitor-type 1-tissue plasminogen activator pro-urokinase lipoprotein lipase α-amylase α_1-microglobulin cystatin lysozyme	
Immune- and stress-response related proteins	
immunoglobulin light chains pancreatitis-associated protein 1 advanced glycation end products β_2-microglobulin	immunoglobulin light chains Clara cell secretory protein
Receptors and transmembrane proteins	
cubilin heavy metallothionein	megalin Amnionless
Drugs and toxics	
aminoglycosides, polymyxin B aprotinin, trichosantin somatostatin analogues	
Others	
receptor-associated protein Ca^{++} cytochrom C	receptor-associated protein

Adapted from Christensen, 2002a

cells, resulting in impaired uptake of filtered LMW proteins (Leheste, 1999). Similar defects are observed in patients with inherited or acquired PT dysfunction. Moreover, numerous diseases with tubular proteinuria, including Dent's disease (see section 3.1.1.), have been associated with decreased urinary excretion of megalin itself (Norden, 2002). These clinical observations reflect the defective recycling of megalin to PT brush border, with subsequent impaired receptor-mediated reabsorption of urinary ligands (Christensen, 2003). Significant progress has been made in the identification of ligands that can interact with megalin (Christensen, 2002a). These include LMW plasma proteins, peptide hormones, vitamin-binding carriers, apolipoproteins, enzymes, Ca^{++}, and polybasic drugs such as aminoglycosides (Table 1.1). Although the affinity of megalin ligands varies from high to rather low, the abundant expression of megalin (and cubilin) receptors at PT brush border is regarded as a high-capacity system in constant and fast recycling that ensures the constitutive reabsorption of most filtered LMW proteins. Thus, megalin appears to play a key role in the homeostasis of distinct classes of molecules, ranging from ions to lipid carriers, hormones and vitamins.

1.3.2. Cubilin

Cubilin, also known as the intestinal intrinsic factor (IF)-B12 receptor, is a multiligand endocytic receptor that was originally identified as the target of teratogenic antibodies in rats (Brent, 1961).

Cubilin co-distributes with megalin in numerous absorptive epithelia, as mentioned above. In PT cells, cubilin has been located at the brush border and along the endocytic apparatus, including the coated pits, the endosomes and the dense apical tubule network that provides for the recycling of apical membrane and receptors (Christensen, 1998). Smaller amounts of cubilin have been also detected in lysosomal structures (Seetharam, 1997). The normal subcellular distribution of cubilin depends on its reciprocal interaction with the transmembrane protein amnionless (AMN, 45 kDa) identified as a key factor for mouse gastrulation (Figure 1.5) (Kalantry, 2001).

First AMN binds the EGF-type domains of cubilin, ensuring membrane attachment and export of the compound from the ER. The apical sorting of the cubilin-AMN (cubam) complex is then dependent on the correct glycosylation of cubilin extracellular domains. Cubam complexes are finally directed from the ER to the plasma membrane, where they participate in receptor-mediated endocytosis (Coudroy, 2005). Cubilin contributes ligand-binding regions of cubam complexes, whereas AMN ensures the membrane anchorage, biosynthetic processing, and recycling of the complexes at the plasma membrane (Fyfe, 2004). Indeed, defective apical insertion of cubilin has been reported in dogs with a mutation in *AMN* gene and in AMN-deficient mouse epithelial cells (He, 2005; Strope, 2004). Of note, although RAP has been demonstrated to bind cubilin, its role in cubilin processing and trafficking remains debated (Birn, 1997).

Cubilin is a highly conserved membrane glycoprotein of 460 kDa that contains 13-14% carbohydrates. Its structure consists of a N-terminal membrane anchoring domain followed by eight EGF-like repeats and 27 CUB domains, which encompass complement sub-components C1r/C1s, Uegf (EGF-related sea urchin protein), and bone morphogenic protein-1 domains (Figure 1.5) (Bork, 1993). CUB domains are frequently found in developmental proteins and are known for their ability to bind a variety of ligands. Interestingly, cubilin contains a cleavable signal sequence that allows the polypeptide chain to enter the ER, but it lacks a transmembrane domain or a glycosylphosphatidylinositol anchor. Its membrane association may involve a putative amphipathic helix as well as palmitoylation and myristoylation (Kristiansen, 1999). Recent biochemical and immunomorphological data support that AMN is essential not only for the trafficking and membrane anchoring of cubilin, but also for its internalization (Fyfe, 2004). In addition, high-affinity binding of purified megalin to cubilin N-terminal region (CUB domains 1 and 2) has been reported *in vitro*, suggesting that megalin also participates in the endocytosis and intracellular trafficking of cubam complexes (Moestrup, 1998).

The role of cubilin in PT function has been suggested by the investigations of an inbred strain of dogs with inherited intestinal cobalamin malabsorption due to a defective intracellular processing of cubilin, likely caused by the functional loss of AMN (Fyfe, 1991; He, 2003). These dogs have LMW proteinuria in addition to megaloblastic anaemia. Likewise, loss-of-function mutations in *CUBN* or *AMN* genes have been found in patients with Imerslund–Gräsbeck disease (also known as juvenile megaloblastic anemia, OMIM #261100), a rare autosomal recessive disorder characterized by selective intestinal malabsorption of vitamin B12 (Aminoff, 1999; Tanner, 2003). Most patients show an increased urinary excretion of LMW proteins, indicating a role of cubilin and AMN in protein reabsorption by PT cells. The variable severity of tubular proteinuria may reflect the functional consequences of *CUBN* mutations on its multiligand properties or only on its IF-B12 binding site. These observations indicating a role of cubilin in the renal handling of LMW proteins are further supported by the investigation of the *Clcn5* KO mouse model of Dent's disease. Indeed the absence of ClC-5 leads to impaired trafficking and enhanced degradation of cubilin (and megalin) in PT cells, resulting in the urinary loss of their ligands (Christensen, 2003). Of note, no mouse model deficient in cubilin has been reported so far. Genetic inactivation of cubilin in mice would probably lead to early embryonic lethality, as suggested by the role of cubilin in yolk-sac function and the severe fœtal malformations observed in rodents after the injection of anti-cubilin antibodies (Sahali, 1988). However, this limitation might be practically overcome in the near future by strategies based on conditional inactivation (e.g. Cre recombinase) of the *Cubn* gene in the kidney, similarly to what has been successfully achieved for the *megalin* gene (Leheste, 2003).

The comparison between megalin- and cubilin-ligands reveals that both receptors participate in the uptake of common peptides, such as albumin, hemoglobin, DBP, apolipoproteins, and immunoglobulin light chains (Table 1.1). In addition, cubilin-specific ligands have been identified and include the IF-vitamin B12, transferrin, apolipoprotein A-I, and Clara cell protein CC16. However, the *in vitro* uptake of these cubilin-specific ligands is inhibited by anti-megalin antibodies, as well as by megalin

antisense oligonucleotides (Birn, 2006). Conversely, the urinary excretion of megalin-specific ligands, such as α_1- and β_2-microglobulin, is increased in genetically well-defined patients with mutations in *CUBN* (Wahlstedt-Fröberg, 2003). These observations further support the functional interaction between cubilin and megalin necessary to its internalization and intracellular trafficking.

1.3.3. The V-ATPase

The V-ATPase is a ubiquitous multisubunit complex responsible for ATP-driven transport of H^+ across membranes (Nishi, 2002; Wagner, 2004). The V-ATPase belongs to the super-family of ATPases that is subdivided into three subgroups: (1) P-type ATPases, such as Na^+/K^+-ATPase, Ca^{++}-ATPases and H^+/K^+-ATPase; (2) mitochondrial F_1F_0-ATPase; and (3) V-type ATPase (http://www.gene.ucl.ac.uk/nomenclature/). The latter two sub-classes share many structural homologies, such as subunit composition and organization, although they function in an opposite way (Gruber, 2001). The mitochondrial F_1F_0-ATPase consumes H^+ gradients for ATP synthesis, whereas the V-ATPase uses ATP hydrolysis to generate pH gradient. Accordingly, structure and function of the V-ATPase have been mostly established from data obtained from either the F_1F_0-ATPase or the yeast vacuolar H^+-ATPase (Nelson, 1999).

The distribution of the V-ATPase includes a variety of intracellular compartments, such as endosomes, the Golgi/TGN apparatus, and lysosomes (Nelson, 1999). The function of these organelles depends on acidic intravesicular pH to maintain optimal enzyme activity. In the kidney, the V-ATPase is particularly found in the submicrovillar area of PT cells (Breton, 2000), where it ensures vesicular acidification along the endocytic pathway (Marshansky, 2002). Besides its intracellular distribution, the V-ATPase has also been located at the plasma membrane of specialized cells, where it mediates H^+ extrusion from the cell (Wagner, 2004). For example, osteoclasts and macrophages acidify their immediate environment to dissolve bone matrix and digest neighboring cells or pathogens, respectively. The epithelial

cells lining the inner ear and the epididymis regulate finely the extracellular pH of closed compartments. In the kidney, the V-ATPase is present at the surface of two cell types involved in urine acidification, i.e. PT cells and the IC of the CD (Giebisch, 2003b). In PT cells, the V-ATPase has been located at the base and on the microvilli of the brush border, where it participates in the reabsorption of ~70-80% of filtered HCO_3^- (Brown, 1988). The features of the V-ATPase present in the IC are detailed in section 2.3.

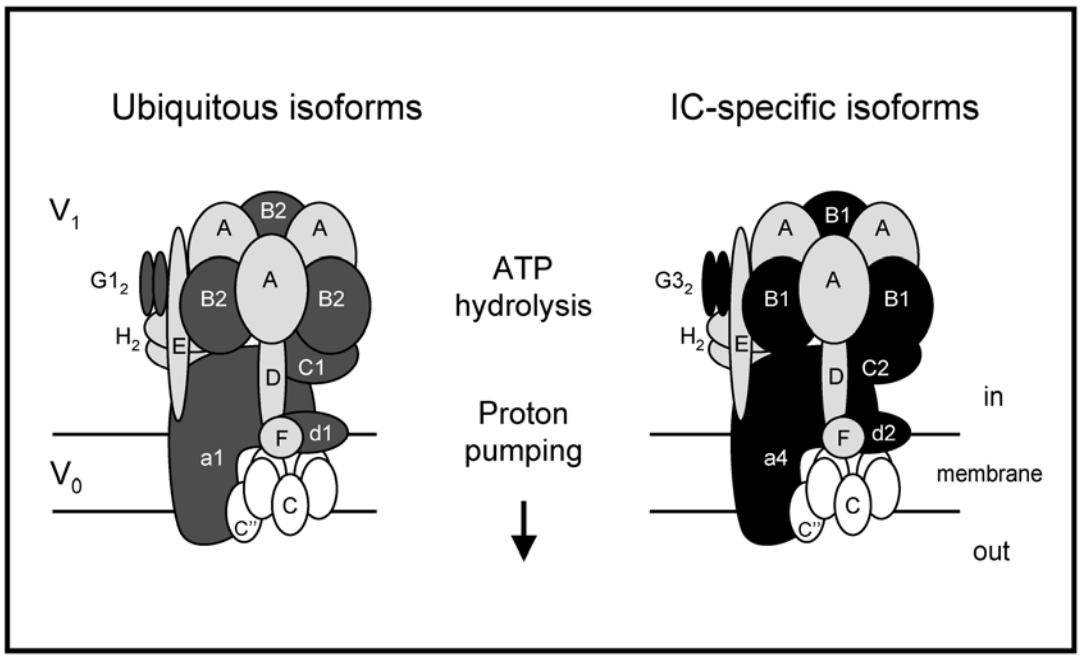

Figure 1.6. Structure of the vacuolar H+-ATPase

The transmembrane V0 domain of the mammalian V-ATPase is organized into a complex of $[a(c)_{4\text{-}5}c''d]$, whereas the cytosolic V1 domain has a stoichiometry of $[A_3B_3CDEFG_2H_2]$. The ubiquitous and the IC-specific alternate isoforms of V0 and V1 subunits are shaded. In the plasma membrane of murine IC, a4, d2, B1, C2, G3 substitute ubiquitous a1, d1, B2, C1 and G1, respectively. This model was modified from the yeast model to represent the mammalian V-ATPase complex. Note that the existence of the c' subunit in mammals is uncertain (Smith, 2002).

Adapted from Borthwick, 2002

The structure of the V-ATPase includes at least 13 different subunits forming two functional domains, V0 and V1 (Figure 1.6) (Wagner, 2004; Wilkens, 2004). According to quantitative amino acid analysis and single molecule electron microscopy imaging, the transmembrane V0 domain contains five different subunits

organized into a [a$(c)_{4-5}$c''d] channel responsible for H^+ translocation. The cytosolic V1 domain involves eight subunits with a stoichiometry of [$A_3B_3CDEFG_2H_2$], even though the exact number of copies of each E and G per V-ATPase remains debated. The A and B subunits are organized in an alternating manner to form a pseudo-hexagonal head-piece, which ensures ATP hydrolysis necessary for active H^+ transport. The other V1 subunits form the "stalk" that connects A and B subunits to the V0 domain. Interestingly, it is thought that ATP binding to B and subsequent hydrolysis by A lead to a rotation of the "stalk" structure relative to A_3B_3 domain, which may then induce the motion and the opening of the V0 channel (Nelson, 1999 ; Gruber, 2001). When located in the plasma membrane, the overall structure of V-ATPase is very similar but specific isoforms of V0 and V1 subunits are present (Figure 1.6) (Borthwick, 2002). These isoforms are encoded by distinct genes, with tissue-specific expression patterns (see section 2.3.).

The acidification of intracellular organelles along the endocytic pathway is a prerequisite for important processes in PT cells, such as ligand-receptor dissociation, receptor recycling and ligand degradation, storage, or intracellular targeting (Nelson, 1999). The mechanism by which the endosomal pH regulates trafficking processes remains unclear and may involve the vesicular recruitment of specialized coat proteins (COP), such as β-COP and small GTPases (Arf1, Arf6) of the ADP-ribosylation factor (ARF) family (Zeusem, 1992; Gu, 2000). Recent studies have demonstrated that functional interactions between coat proteins and particular V-ATPase V0 subunits regulate protein trafficking between early and late endosomes, indicating a pivotal role of the V-ATPase along the endocytic and degradative pathway (Hurtado-Lorenzo, 2006). Moreover, an endosomal pH-sensing machinery, not yet fully identified, has been suggested to initiate COP proteins recruitment in response to a V-ATPase-driven drop in luminal pH (Maranda, 2001).

At the plasma membrane of PT cells, the electrogenic V-ATPase participates in acid-base homeostasis by extruding H^+ from cytoplasm to lumen, in parallel with the

Na^+/H^+ exchanger NHE3 (Giebisch, 2003b). The secreted H^+ combine with luminal HCO_3^- under the influence of the membrane-bound carbonic anhydrase (CA) IV to form H_2O and CO_2. After diffusion into PT cell, CO_2 is reversibly hydrated by the cytosolic CAII isozyme, thereby generating H^+ for apical H^+ extrusion and HCO_3^- for basolateral exit via the co-transporter NBC1 (Figure 1.7). This process of HCO_3^- reabsorption in the PT is intricately linked to Na^+ and water homeostasis and thus finely modulated by hormones and metabolic status (Wagner, 1998). Thus, the V-ATPase plays pivotal roles in PT functions at both intracellular and plasma membrane locations. The severe PT cellular dysfunction observed in case of *in vitro* or *in vivo* disruption of the V-ATPase further highlights the importance of this pump in this segment.

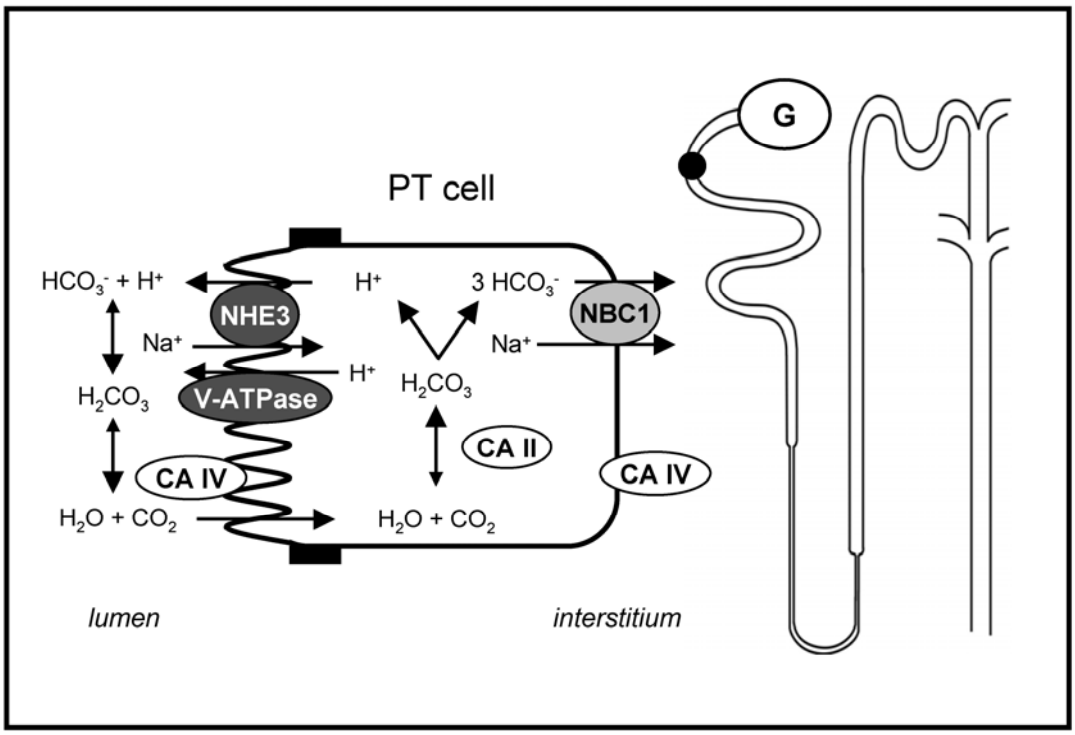

Figure 1.7. Schematic model of HCO_3^- reabsorption in PT cells

Protons are secreted via the apical Na^+/H^+ exchanger NHE3 and the vacuolar H^+-ATPase. The secreted H^+ combine with filtered HCO_3^- under the influence of a membrane-bound carbonic anhydrase (CAIV) to form H_2O and CO_2. After diffusion into PT cells, CO_2 is re-hydrated by the cytosolic CAII into H^+ that are secreted back to PT lumen, and HCO_3^- released into the interstitium via the basolateral Na^+/HCO_3^- co-transporter NBC1.

1.3.4. Lignac-de Toni-Debré-Fanconi syndrome

The Lignac - de Toni - Debré - Fanconi syndrome (renal Fanconi syndrome) is characterized by a generalized defect in PT reabsorption of filtered solutes, such as glucose, phosphate, calcium, uric acid, amino acids, as well as LMW proteins. Clinical features can also include a metabolic acidosis (Type 2 renal tubular acidosis due to HCO_3^- losses and impaired NH_4^+ generation), rickets and growth retardation in children and osteomalacia in adults (reduced vitamin D synthesis), nephrolithiasis related to increased urinary Ca^{++} excretion, hypocitraturia and impaired urine acidification, and progressive renal failure. The renal Fanconi syndrome can be inherited or acquired.

The list of acquired causes of renal Fanconi syndrome is largely heterogeneous and includes multiple myeloma, light chain deposition disease, and renal transplantation. In addition, various toxic compounds and drugs have been associated with PT defects, especially heavy metals (cadmium, uranium, lead and mercury), aminoglycoside antibiotics, as well as some anti-retroviral drugs (e.g. azidothymidine) and cytotoxics (e.g. ifosfamide, cisplatin). Most of these compounds affect the endocytic/lysosomal system and the mitochondrial function, which might explain their particular toxicity for the PT (Izzedine, 2003).

Inherited forms of the renal Fanconi syndrome are rare (approximately 1/40,000 births), transmitted as a recessive trait and mostly diagnosed during childhood (Table 1.2). Of note, the prevalence of cystinosis (OMIM #219800), the most frequent congenital PT disorder, has wide ranging estimates (from 0.03-0.4 per 10,000 live births) depending on the population studied. The genetic deficiencies affect cellular energy metabolism, membrane trafficking, or ion and solute transports (Bergeron, 1995). They include autosomal recessive disorders like cystinosis, tyrosinaemia, fructosaemia, galactosaemia, Type I glycogen storage disease, and cytochrome c oxidase deficiency; and X-linked recessive diseases like Dent's disease and Lowe oculocerebrorenal syndrome.

Table 1.2. Inherited causes of renal Fanconi syndrome

Disorder	OMIM	Gene	Protein	Inheritance
COX deficiency	#220110	*MTC01-03* *MTTS1* *COX10* *SC01-02*	Cytochrome c oxidase	AR
Cystinosis	#219800	*CTNS* (17p13)	Lysosomal cystine transporter	AR
Dent's disease (1)	#300009	*CLCN5* (Xp11.22)	H^+/Cl^- exchanger	XR
Dent's disease (2)	#300555	*OCRL* (Xq26.1)	PIP_2 5-phosphatase	XR
Fanconi-Bickel syndrome	#227810	*GLUT2* (3q26.1-3)	Glucose transporter GLUT2	AR
Fructosaemia	+229600	*ALDOB* (9q22.3)	Fructose-bisphosphate aldolase B	AR
Galactosaemia	#230400	*GALT* (9p13)	Galactose 1-phosphate uridylyltransferase	AR
Imerslund-Gräsbeck disease	#261100	*CUBN* (10p12.1) *AMN* (14q32)	Cubilin Amnionless	AR
Lowe syndrome	#309000	*OCRL* (Xq26.1)	PIP_2 5-phosphatase	XR
Tyrosinaemia	+276700	*FAH* (15q23-25)	Fumarylacetoacetase	AR
von Gierke disease	+232200	*G6PC* (17q21)	Glucose 6-phosphatase	AR
Wilson disease	#277900	*ATP7B* (13q14.3-21.1)	Copper-transporting ATPase 2	AR

A "number" symbol (#) indicates that the phenotype is not linked to a unique locus, whereas a "plus" sign (+) means that the entry associates a gene with a phenotype (AR: autosomal recessive; XR: X-linked recessive).

2. The intercalated cells of the collecting duct

2.1. Distribution and ultrastructure

The CD system has three segments designated after their distribution in kidney cortex, outer medulla or inner medulla, and continues the distal tubule of the nephron (Figure 1.1). The adult CD is composed of principal and intercalated cells that exhibit striking morphological and functional differences (Giebisch, 2003a). Principal cells represent about two thirds of CD cell population and mediate salt and water reabsorption under hormonal influence. They have a light cytoplasm with relatively few organelles and sparse mitochondria scattered randomly in the cytoplasm. Typically, principal cells show prominent infoldings of the basal membrane, no lateral interdigitations, and a single central cilium on the apical surface. In contrast, the IC are involved in acid-base transport and are characterized by a more electron dense cytoplasm and numerous dark staining mitochondria (hence, their previous name “dark cells”). The IC are the only cells along the urinary system that do not exhibit a primary cilium.

The IC can be further subdivided into two major groups, namely α- and β-type IC (Bastani, 1997). The existence of a non-α-non-β-type IC (also called γ-IC), which may represent an interconvertible state between α- and β-phenotypes, remains debated (Schwartz, 1985; Al-Awqati, 1996; Wagner, 2004). The α-type IC are present in all CD segments and have prominent apical micro-projections and typical tubulo-vesicular structures beneath the apical surface, both coated with studs on the cytoplasmic face. In contrast, the β-type IC are most frequently found in the cortical CD and show a fairly smooth apical surface, a zone free of organelles beneath the apical membrane, and abundant cytoplasmic vesicles. This distinction between α- and β-type IC is not only structural, but also (and mostly) functional as discussed hereafter.

2.2. Role in acid-base homeostasis

Together with the lungs, the kidneys play an essential role in acid-base homeostasis by reabsorbing virtually all filtered HCO_3^- and secreting H^+ into the urine (Giebisch, 2003b). The bulk of filtered HCO_3^- is taken up in the PT (and the thick

ascending limb, TAL), whereas the fine regulation of acid-base excretion and absorption occurs in the CD. The cortical CD either reabsorbs or secretes H^+ and HCO_3^-, while the outer medullary CD secretes only H^+. The average diet in the "Western" world is rich in proteins and generates daily 1-1.5 mmol hydrogen/kg body weight. The net urinary acid excretion is therefore essential and urine pH can drop as low as 4.5.

The IC are the main cells involved in acid-base transport along the CD. Both α- and β-type IC are characterized by high activity of cytosolic CAII (Figure 1.8). However, they differ by the selective polarity of the V-ATPase and the exclusive expression of a basolateral (α-IC) or apical anion-exchanger (β-IC) (Giebisch, 2003b). The α-type IC secrete H^+ into the urine *via* the V-ATPase that is present at high density on the luminal membrane. Studies in animal models have shown that the V-ATPase is also present within specialized intracellular tubulovesicles close to the membrane, allowing fast recruitment of additional pumps to the membrane in response to stimuli, like systemic acidosis (Penney, 1999; Brown, 2000a). Animal studies have also identified an additional P-type ATPase at the apical surface of α-IC that exchanges H^+ for K^+ (Wingo, 1990). However, the overall contribution of such pump in human acid-base physiology remains unclear. On the basolateral side, the α-IC are characterized by the expression of the kidney-specific truncated version of the band 3/AE1 (SLC4A1) Cl^-/HCO_3^- exchanger (Alper, 1989). In contrast, the β-type IC show a basolateral or bipolar expression of the V-ATPase and an apical anion exchanger different from AE1, whose molecular identity remains debated. Two Cl^-/HCO_3^- exchangers have been identified in β-IC: pendrin and AE4. Pendrin resides in the apical membrane of all non-α-type IC and is regulated by acid-base status (Wagner, 2002). However, the genetic loss of pendrin causes Pendred syndrome (OMIM #274600) of deafness and goiter in man and mouse, with no significant metabolic alkalosis at baseline (Royaux, 2001). AE4 is also expressed in non-α-type IC, but its subcellular localization seems to be species-specific (apical in rabbit, basolateral in mouse and rat) and its role remains, therefore, uncertain (Tsuganezawa, 2001).

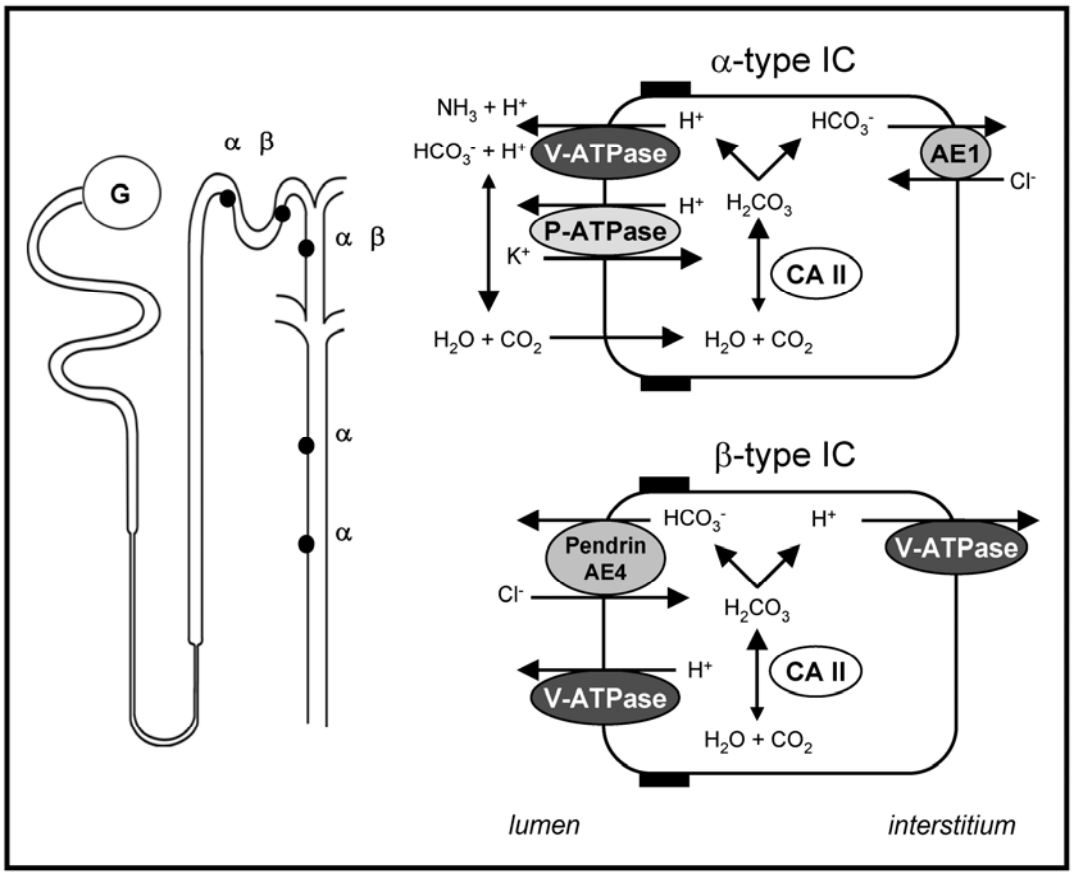

Figure 1.8. Schematic model of H^+ and HCO_3^- secretion in α- and β-type IC

The α-type IC are found in the connecting tubule (CNT), cortical collecting (CCD), and both outer and inner medullary CD, whereas the β-type IC are present only in the CNT and CCD.

The α-type IC are characterized by the expression of the basolateral Cl^-/HCO_3^- exchanger AE-1 and the apical V-ATPase. The cytosolic CAII generates H^+ and HCO_3^- that are secreted into the lumen and the interstitium, respectively. An apical H^+/K^+-ATPase has been identified in α-type IC of certain species.

The β-type IC are defined by the absence of the basolateral AE-1 exchanger, and the presence of the V-ATPase on both sides of the cell. The molecular identity of the apical Cl^-/HCO_3^- exchanger responsible for HCO_3^- secretion remains debated. Two putative anion exchangers, pendrin and AE4, have been proposed.

Apparent plasticity of molecular targeting according to ambient pH *in vitro* and/or acid and alkali load *in vivo* has suggested that α- and β-type IC may represent molecular mirror images of each other (Schwartz, 2005). Indeed, the various patterns of V-ATPase distribution observed in IC support the hypothesis that all IC are phenotypic variants of the same cell type, and that the precise cellular location of the V-ATPase is determined by the acid-base status. Moreover, the functional phenotype of cultured IC has been shown to be reversed by a novel matrix protein called hensin

(Schwartz, 1985). Hensin was proposed to induce terminal differentiation in IC, which was reflected by the α-cell phenotype. This change in functional activity of IC involves the concerted action of microtubules and microfilaments and requires *de novo* protein synthesis (Schwartz, 2002). It must be emphasized that the change in phenotype from α- to β-type involves more than a simple inversion of polarity of membrane transporters, as α-IC and β-IC have been distinguished by a differential expression of proteins, including the anion exchangers and NHE-RF (Na^+/H^+ exchanger regulatory factor) (Wagner, 2004). In any event, the daily acid load provided by an omnivorous human diet dictates that the majority of IC will be acid-secretory (α-type). The following sections address the specificity of the V-ATPase present in the IC and review the causes of inherited dysfunction of the IC resulting in distal renal tubular acidosis.

2.3. Kidney-specific isoforms of V-ATPase subunits

Tissue-specific isoforms of some V0 and V1 subunits, encoded by distinct genes, are present in the V-ATPase located at the plasma membrane of specialized cells, such as the IC of the CD (Figure 1.6) (Borthwick, 2002). The V1 B subunit was the first to be identified as such (Nelson, 1992). Although B2 is regarded as the ubiquitous isoform, B1 expression seems restricted to kidney, inner ear and male genital tract (Nelson, 1992; Breton, 2000). Three V1 G and two V1 C subunit isoforms have been identified in man, with G3 and C2 showing kidney-specific distribution (Smith, 2002). The V0 a subunit is even more complex, since four isoforms have been described in both man and mouse (Smith, 2001; Oka, 2001). All four a subunits are expressed in the kidney as detected by Northern blotting and RT-PCR analyses, with distribution patterns associated with various regions of the nephron (Wagner, 2004). The a4 isoform is particularly found in all subtypes of IC, as well as in the inner ear and along the epididymis (Smith, 2001). Finally the V0 d2 subunit isoform has been recently identified and located in kidney and bone (Smith, 2002).

Recent studies have addressed the roles of individual V-ATPase subunits, with a particular interest for those with tissue-specific expression. In contrast to the ubiquitous B2, the B1 subunit contains a C-terminal DTAL motif that may interact with the PDZ protein NHE-RF to generate, maintain or modulate the V-ATPase

polarity in β-IC, which are characterized by a highly variable pattern of intracellular localization of the V-ATPase (Breton, 2000). Whether PDZ proteins are involved in either the targeting, the trafficking, or the anchoring of the V-ATPase in specialized membrane domains remains to be determined. Of note, the α-IC that insert the V-ATPase uniquely into their apical domain contain little or no detectable NHE-RF. The distinct distribution of the V0 a isoforms also suggests that this subunit may be involved in the assembly and/or targeting of the V-ATPase. Indeed, the N-terminal domain of this subunit appears to play a major role in V-ATPase targeting to organelles and *in vivo* dissociation in yeast, whereas its C-terminal region controls the coupling of ATP hydrolysis and H^+ translocation (Kawasaki-Nishi, 2001). Altogether, these data support that particular isoforms of V-ATPase subunits interact with different proteins and/or confer specific sorting signals, resulting to a differential distribution of the pump in the cell.

2.4. Hereditary distal renal tubular acidosis

Renal tubular acidosis (RTA) refers to a group of tubular dysfunctions characterized by a hyperchloremic metabolic acidosis due to a failure of renal HCO_3^- reabsorption or H^+ excretion that is not related to a reduction in the glomerular filtration rate. These disorders may be inherited, with autosomal recessive or dominant modes of transmission, or acquired (Igarashi, 2002; Karet, 2002). The classification of RTAs is based on the perceived roles of the different nephron segments in the acid-base regulation. Proximal RTA (type 2 RTA) is due to an impaired reabsorption of HCO_3^- by the PT, often associated with other signs of PT dysfunction ("renal Fanconi syndrome"). The distal RTAs are due to a defective H^+ excretion by the distal tubule and CD. They are frequently associated with hypercalciuria and low urinary citrate excretion, leading to nephrocalcinosis and nephrolithiasis. They are further divided into the hypokalemic distal (type 1 RTA) and hyperkalemic distal (type 4 RTA). Finally, mutations in *CA2* gene cause Guibaud-Vainsel disease (type 3 RTA), an inherited syndrome characterized by renal tubular acidosis, osteopetrosis, and cerebral calcifications (Sly, 1985). In this case, the functional loss of CAII associates signs of both proximal and distal tubular dysfunction (Laing, 2005).

Type 1 distal RTAs are relatively rare in Western populations, but occur more commonly in regions where rates of parental consanguinity are high (Karet, 2002). The inheritance of type 1 RTA shows both autosomal recessive and dominant patterns, the most severe cases being inherited recessively (Table 1.3). Dominant Type 1a distal RTA is caused by mutations in *SLC4A1* gene encoding the Cl^-/HCO_3^- exchanger AE1 (Bruce, 1997; Karet, 1998). Both forms of recessive distal RTA are associated with defects in the IC-specific B1 and a4 subunits of the V-ATPase. The functional loss of B1, which is encoded by *ATP6V1B1* gene and present in both kidney and inner ear, causes Type 1b RTA with deafness (Karet, 1999). Type 1c RTA with preserved hearing in childhood is caused by inactivating mutations of *ATP6V0A4* (Smith, 2000). To note, some patients with distal RTA do not show linkage to either *SLC4A1*, *ATP6V1B1* or *ATP6V0A4* genes, suggesting that other distal RTA genes remain to be identified. These include (i) genes involved in IC differentiation; (ii) genes for V-ATPase subunit isoforms; (iii) genes with products that are required for trafficking of the V-ATPase in α-IC; (iv) and genes encoding molecules necessary for the generation of H^+, absorption of HCO_3^-, recycling of Cl^-, or maintenance of the electrochemical gradients across the epithelial barrier.

Table 1.3. Primary distal RTA: clinical and biochemical features

	Dominant dRTA	**Recessive dRTA**	**Type 3 RTA**
Age at diagnosis	Adulthood	Infancy/early childhood	Childhood
Symptoms/signs	None Nephrolithiasis Nephrocalcinosis Osteomalacia/rickets	Nephrocalcinosis Vomiting/dehydration Growth retardation Rickets Deafness (30% of cases)	Nephrocalcinosis Cerebral calcification Mental retardation Deafness Thickened bones
Hematology	Erythrocytosis		Anaemia
Blood chemistry	Mild hyperCl^- acidosis Normo/hypokalaemia	Severe hyperCl^- acidosis Hypokalaemia	HyperCl^- acidosis Hypokalaemia
Urine chemistry	pH > 5.5 Hypercalciuria Hypocitraturia Hypoammoniuria	pH > 5.5 Hypercalciuria Hypocitraturia Hypoammoniuria	pH > 5.5 Bicarbonaturia
***Gene* (protein)**	*SLC4A1* (AE1)	*ATP6V1B1* (V-ATPase B1) *ATP6V0A4* (V-ATPase a4) *SLC4A1* (AE1) - rare	*CA2* (CA II)

Adapted from Karet, 2002

A mouse model deficient in B1 V-ATPase subunit has been very recently engineered by homologous recombination-mediated targeting of exons 7-11 in *Atp6v1b1* gene (Finberg, 2005). In contrast to human distal RTA caused by *ATP6V1B1* mutations that presents in early infancy, *Atp6v1b1* KO mice appear healthy and grow normally. This phenotypic discrepancy is likely related to dietary differences. However, *Atp6v1b1* KO mice produce urine that is significantly more alkaline than that of wild-type littermates under standard diet and fail to acidify urine after oral acid challenge. Moreover, clearance studies performed after furosemide treatment have demonstrated that this defect in urine acidification results from IC dysfunction. Note that genetic inactivation of *Atp6v1b1* in mice was not associated with hypercalciuria and skeletal abnormalities, male infertility, or hearing loss as reported in patients. The compensatory role of B2 isoform in V-ATPase complexes in case of *Atp6v1b1* inactivation remains uncertain, but could provide a partial functional compensation in some organs in mice. Thus, these data demonstrate that plasma membrane V-ATPase represents the main pathway of urinary acidification in IC and propose a useful animal model to investigate *in vivo* its role in pH homeostasis.

Another mouse model of distal RTA has been recently reported (Blomqvist, 2004). These mice lack the forkhead transcription factor Foxi1 that plays a central role in IC differentiation during nephrogenesis. Accordingly, the epithelium lining the distal nephron in *Foxi1* KO mice show no typical IC, but a single population of cells positive for markers of both principal and intercalated cells. The importance of these observations on our knowledge about cell differentiation along the distal nephron is further detailed in section 4.3.2.

3. Chloride transporters in the kidney

Chloride is the most abundant anion in plants and animal tissues and Cl^- transport across cellular membranes is involved in the transepithelial transport of salt and water, membrane excitability, and regulation of cell volume and pH. In addition, Cl^- transporters participate in the acidification and ionic homeostasis of intracellular organelles (Jentsch, 2002). Over the last few years, numerous Cl^- transporters, including channels and exchangers, have been characterized in all segments of the nephron (Devuyst, 2002). Most of the Cl^- ions filtered by the glomeruli are reabsorbed through different mechanisms operating in the apical and basolateral membranes of tubular epithelial cells. Several Cl^- transporters use the energy generated by transmembrane gradients of other ions to move Cl^- against its electrochemical gradient, whereas passive diffusion of Cl^- through Cl^- channels is involved in cell volume regulation. Transport of Cl^- through Cl^- / HCO_3^- exchangers in IC, or through the Na^+-linked Cl^- / HCO_3^- exchanger operating in PT cells, participate in acid-base homesostasis. In addition, Cl^- ions are also important for acidification of intracellular vesicles by neutralizing the transmembrane potential generated by the electrogenic V-ATPase. The association of a large spectrum of human diseases affecting kidney function with mutations in distinct genes encoding Cl^- transporters, has provided new insights into the diverse roles ensured by Cl^- movement in cell physiology (Jentsch, 2005; Romero, 2005).

On one hand, two main families of Cl^- exchangers have been implicated in kidney function, namely the SLC4 and SLC26 transporters. The SLC4 HCO_3^- transporter family contains 10 members that move base equivalents (OH^- or HCO_3^-) across cell membranes to alter intracellular pH (Romero, 2005). There are at least 4 Cl^- / HCO_3^- exchangers in the SLC4 family: AE1-4 (also called SCL4A1-3 and SLC4A9). The kidney-specific truncated version of the band 3/AE1 is found in the basolateral membrane of the α-type IC of the CD and mutations in *SLC4A1* gene have been associated with distal RTA (see section 2.4). In addition, three isoforms of AE2 (SLC4A2a-c) have been located in the TAL and AE4 (SLC4A9) is present in the

apical membrane of rabbit β-type IC, where its role in acid-base homeostasis remains debated (see section 2.2). The SLC26 anion exchangers transport an expanding number of monovalent and divalent anions and play critical roles in skeletal development, synthesis of thyroid hormones, transepithelial Na^+, Cl^-, and HCO_3^- transport (Mount, 2004). The distribution of SLC26 members includes different segments of the nephron. SLC26A6 has been detected in the apical membrane of PT cells and may represent the long-elusive apical Cl^- entry site involved in PT Na^+-Cl^- reabsorption (Chernova, 2005). In addition, SLC26A4 (also called Pendrin) has been located in the luminal membrane of the β-type IC, which are known to secrete HCO_3^- via a Cl^- / HCO_3^- exchanger (see section 2.2).

On the other hand, several Cl^- channels have been identified along the nephron, based on single-channel properties and sensitivity to inhibitors. However, the molecular counterpart of many renal Cl^- channels remains debated (Devuyst, 2002). This section will focus on two structural classes of Cl^- transporters that have been extensively characterized: the CLC family and the CFTR (cystic fibrosis transmembrane conductance regulator). The emphasis will be particularly set on the role of the Cl^- transporter ClC-5 and the Cl^- channel CFTR in the pathophysiology of Dent's disease and cystic fibrosis, respectively.

3.1. Dent's disease and ClC-5

3.1.1. Dent's disease

In 1964, C.E. Dent and M. Friedman described two unrelated English boys with hypercalciuric rickets associated with renal tubular damage including tubular proteinuria, aminoaciduria, phosphaturia and hypercalciuria (Dent, 1964). The term *Dent's disease*, first introduced in early nineties, identifies a group of X-linked renal tubular disorders characterized by LMW proteinuria associated with hypercalciuria and nephrocalcinosis and/or nephrolithiasis (Wrong, 1994). This triad of manifestations has been variably named in the past as X-linked recessive nephrolithiasis, X-linked recessive hypophosphataemic rickets, and the idiopathic

LMW proteinuria of Japanese children. However, the three disorders were mapped to chromosome Xp11.22 (Scheinman, 1993; Fisher, 1994) and further associated with mutations in *CLCN5* gene (OMIM #300009) that encodes the renal Cl^- channel ClC-5 (Lloyd, 1996). The gene *CLCN5* is comprised of 12 exons that span between 25 and 30 kb of genomic DNA (Fisher, 1994).

Dent's disease usually presents in early childhood and tubular proteinuria has even been discovered in the first months of life (Nakazato, 1997). The LMW proteinuria, particularly of β_2-microglobulin and retinol-binding protein, represents the most consistent manifestation of Dent's disease, and is found in almost all affected males. The obligate carrier females also show, to a lower extent, a detectable LMW proteinuria, which is compatible with the Lyon hypothesis of the random inactivation of one X chromosome in females (Reinhart, 1995). In contrast, there is considerable inter- and intra-familial variability in other manifestations of the disease, including hypercalciuria, PT solute wasting, distal tubule disorders (urine acidification and concentrating ability), and rickets (Scheinman, 1998). In studies involving dietary deprivation and loading, about half of patients with Dent's disease were characterized by fasting hypercalciuria, but all patients showed an exaggerated calciuretic response to oral Ca^{++} loading (Reinhart, 1995). Urinary acidification defects were reported in half of patients (Wrong, 1994). Progression to end-stage renal failure occurs between the 3rd and the 5th decades of life in 30-80% of affected males.

So far, 85 mutations of *CLCN5* gene have been identified in more than 100 families (http://www.hgmd.cf.ac.uk/hgmd0.html). They consist of nonsense, missense, and donor splice site mutations and intragenic deletions that compromise the function of ClC-5, as well as microdeletions that lead to a total loss of ClC-5 (Lloyd, 1996; Igarashi, 1998). No evidence for a genotype-phenotype correlation has been reported so far in Dent's disease. Moreover, various mutations have been associated with clinical phenotypes ranging from slight biological abnormalities to the classical form of Dent's disease, even within the same family (Scheinman, 2000). Recent investigations provided evidence for genetic heterogeneity in Dent's disease and revealed that mutations in *OCRL1* gene encoding a phosphatidylinositol (4,5)

bisphosphate (PIP_2) 5-phosphatase were also responsible for Dent's disease (OMIM #30900). This topic is further discussed in section 3.1.4.

3.1.2. ClC-5

The ClC-5 is encoded by the gene *CLCN5* that belongs to the CLC family of voltage-gated chloride channels/transporters. The characterization of the founding ClC-0 in the electric organ of *Torpedo marmorata* by T.J. Jentsch led to the identification of a large molecular family, with isoforms expressed in nearly every cell in eukaryotes and many prokaryotes (Jentsch, 1990-2002). The human genome has nine CLC isoforms organized into two main classes according to their subcellular distribution. The isoforms ClC-1, -2, -Ka, and -Kb are preferentially expressed at the plasma membrane, whereas ClC-3, -4, -5, -6, and -7 are mainly located in intracellular vesicles, like endosomes and lysosomes (Table 1.4). In addition, some CLC channels require a β-subunit for intracellular trafficking, membrane stability, and activity. The functional expression of ClC-K channels depends on barttin, a rather small protein with 2 predicted transmembrane domains and a cytoplamsic C-terminus harbouring motifs involved in endocytosis (Estévez, 2001). Likewise, ClC-7 requires the β-subunit Ostm1 to support bone resorption and lysosomal function (Lange, 2006).

Most CLC isoforms (and β-subunits) have been associated with human disorders, such as myotonia (ClC-1 and –2), renal salt-losing Bartter syndrome (ClC-Kb), deafness (barttin subunit of ClC-Ka and -Kb), Dent's disease (ClC-5), and osteopetrosis (ClC-7, Ostm1) (Table 1.4) (Jentsch, 2005). The creation of transgenic mouse models with *CLC* gene deletion further helped figure out the role of these Cl^- transporters in the pathophysiology of human diseases. Of particular interest, the functional loss of ClC-5 in mice causes a generalized PT dysfunction, with LMW proteinuria and hypercalciuria, that mimics Dent's disease (Piwon, 2000; Wang, 2000).

Table 1.4. The CLC family of ClC channels in mammals

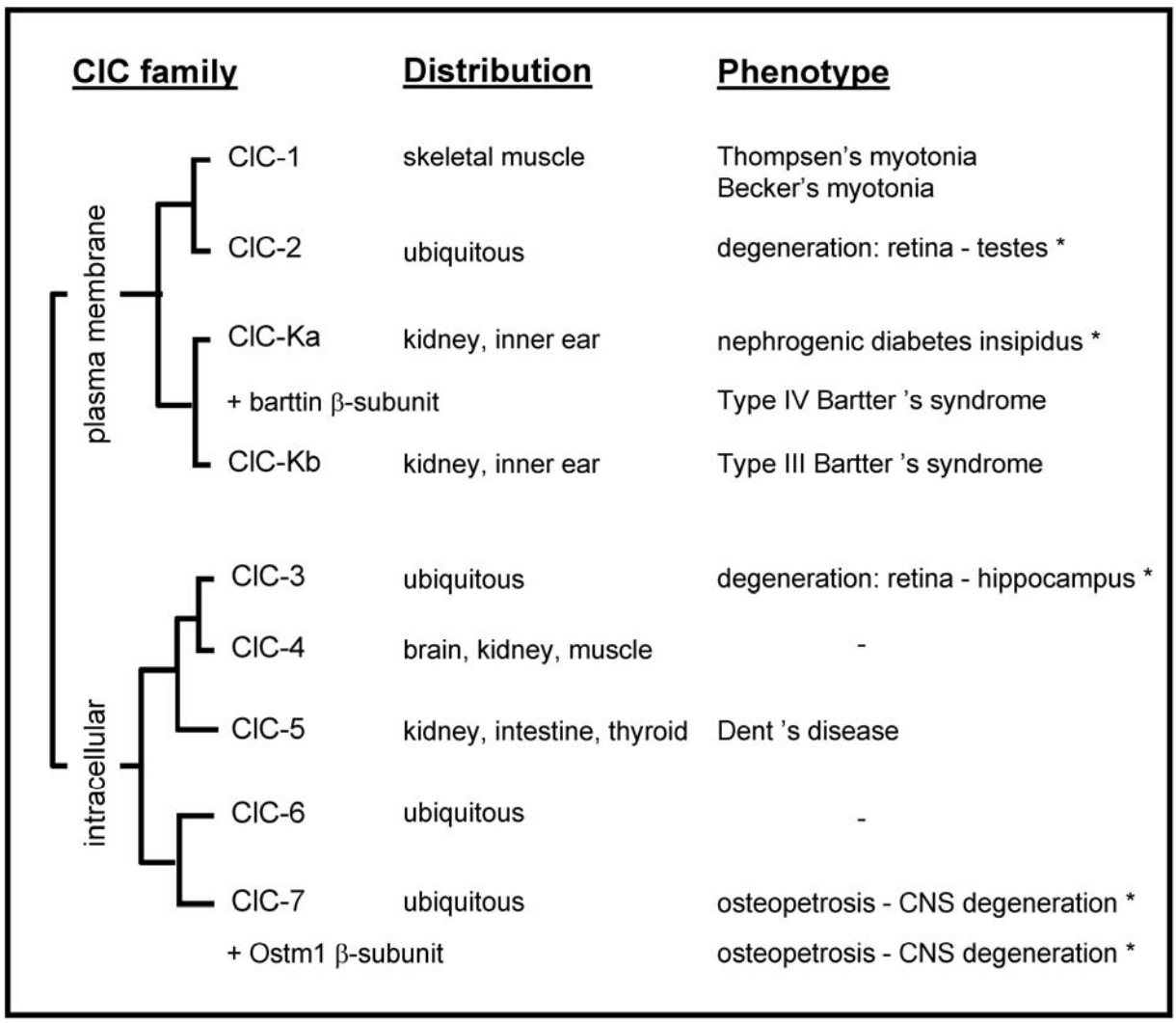

The nine mammalian CLC proteins can be grouped into two branches according to their subcellular distribution. In front of each ClC channel, the columns indicate the most important features of its tissue distribution, the human disease associated with its functional loss, and the phenotype of the corresponding knock-out mouse model, respectively. The asterisk * identifies the phenotype reported only in mice. In addition, β-subunits of certain ClC channels have been identified and associated with human disorders. Mutations in the β-subunit of ClC-Ka and ClC-kb, named barttin, cause Bartter syndrome with sensorineural deafness and kidney failure (Estévez, 2001). Likewise, mutations in Ostm1, recently identified as the β subunit of ClC-7, is associated with human osteopetrosis and central nervous system (CNS) degeneration in mice (Lange, 2006).

Adapted from Jentsch, 2002

Single channel analysis of ClC-0 supported - firstly - a model in "double-barrelled" configuration involving two identical Cl^- diffusion pathways, each with a voltage-dependent gate (Miller, 1982). Recently, the x-ray crystal structures of two bacterial CLC proteins at 3.0-Å resolution have confirmed the prediction that the CLC

channels form diamond-shaped homodimers (Dutzler, 2002). Each subunit has its own pore and 18 α-helices inserted into the plasma membrane, with an anti-parallel orientation that brings together residues that form the selectivity filter for the Cl^- anion (Jentsch, 2002). That pore stoechiometry resembles that of the water channels aquaporins (Murata, 2000), but differs from the K^+ channels in which four identical subunits encircle one central pore (Doyle, 1998). Based on these data, a three-dimensional model of the human ClC-5 has been established (Wu, 2003) (Figure 1.9). ClC-5 consists of 746 amino acids with a predicted molecular mass of 84 kDa and shares a high degree of homology (~78%) with ClC-3 and ClC-4 (Fisher, 1995). These homodimers are composed of two repeated halves that span the membrane in opposite orientations. Interestingly, non-truncating mutations causing Dent's disease mostly occur at the interface between the two subunits, emphasizing the importance of ClC-5 homodimerisation (Wu, 2003). Further evaluations of other naturally occurring mutants will help identify the roles of conserved domains in ClC-5 function and/or trafficking (Ludwig, 2005). Particularly, the intracellular C-terminal tail of ClC-5 harbours a pair of CBS (cystathionine β-synthase) domains that forms the so-called "Bateman" domain (Figure 1.9), which is considered as an energy-sensing module necessary for the allosteric control of ClC-5 gating (Bateman, 1997; Kemp, 2004). Between these two CBS domains is located an internalization motif (PPLPPY), resembling the PY motif that is essential for protein interaction with ubiquitin-protein ligases containing WW domains, like Nedd4-2 and WWP2 (Schwake, 2001). The disruption of this motif was shown to increase ClC-5 surface expression and currents by ~2-fold, suggesting a potential regulation of ClC-5 function by endocytosis like previously described for the epithelial Na^+ channel ENaC (Schild, 1996). Finally, the most distal residues (DSILFN) contain a putative PDZ domain that may be involved as a scaffold in the assembly, stabilization, and disassembly of the endocytic complex at the cell surface (Hryciw, 2006).

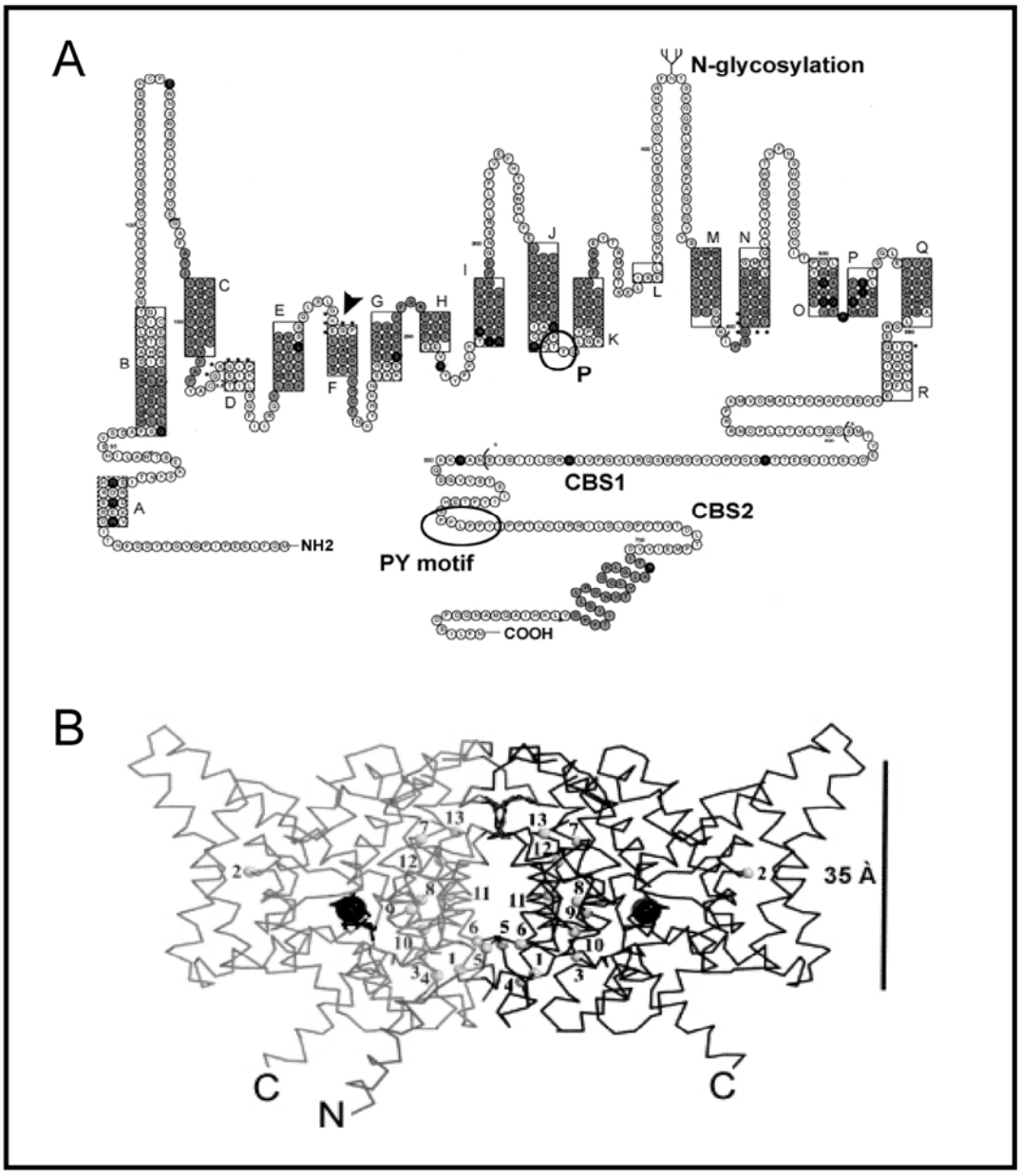

Figure 1.9. Structure of the Cl^- transporter hClC-5

Panel A. Motifs. The hCLC-5 consists of 18 α helices (boxed areas), with the cytoplasmic region below. Glutamate E211 (arrowhead), the consensus phosphorylation (P) sites at threonin 349 and 350, and the N-glycosylation (branch) site at position 408 are indicated. The C-terminal tail of hClC-5 harbours a pair of CBS (cystathionine b-synthase) domains ("Bateman" domain) and an internalization PY motif (PPLPPY).

Panel B. Three-dimensional model. The two subunits are differently contrasted with a Cl^- ion (black point) located in the pore of each. The approximate thickness of the plasma membrane is indicated, with the extracytoplasmic surface above. The numbers refer to missense mutations investigated by Wu, 2003. Note that most mutations cluster at the interface of the two subunits.

Adapted from Wu, 2003

Two recent studies (Picollo, 2005; Scheel, 2005) have demonstrated that the mammalian ClC-4 and ClC-5 isoforms, as well as most probably ClC-3, function as voltage-dependent Cl^-/H^+ exchangers, like the Escherichia Coli ClC-e1 homolog (Accardi, 2004), and are able to extrude H^+ against the electrochemical gradient. Two glutamate residues of ClC-e1 are required for H^+ transport – one at each side of the membrane (Figure 1.10). Similarly, neutralization of the glutamate residue at position 211 in ClC-5 (Figure 1.9) not only abolishes the steep voltage-dependence of transport, but also eliminates the coupling of anion flux to H^+ counter-transport (Picollo, 2005; Scheel, 2005). These observations support that intracellular CLC transporters could facilitate endosomal acidification by coupling vesicular pH gradients directly to Cl^- gradients, hence regulating also vesicular Cl^- concentration.

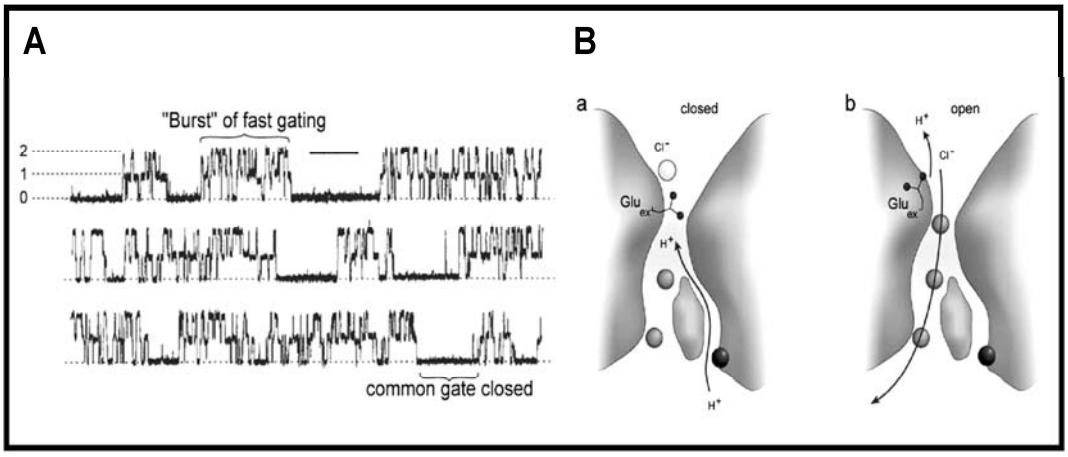

Figure 1.10. The Cl^-/H^+ exchange in ClC: relation structure-function

Panel A. Continuous single-channel recording of ClC-0. ClC channels open and close by two separate processes. "Fast gating" is characterized by rapid fluctuations among three activity levels corresponding to 0, 1 or 2 pores open independently. "Common gating" represents activity bursts, and requires communication between subunits of the ClC homodimer. Holding voltage is -100 mV, and single-channel current is 0.9 pA. The horizontal bar over the upper trace marks 1 second.

Panel B. Hypothetical model of Cl^-/H^+ exchange in one ClC subunit. The cytoplasmic region is below. In "closed state" (a), the side chain of Glu_{ex} is deprotonated, and blocks the pore. Intracellular H^+ transfer occurs, while allosteric Cl^- ion occupies hypothetical site external to Glu_{ex}. In "open state" (b), the side chain of Glu_{ex} becomes protonated, and Cl^- transport occurs. The black circle marks the position occupied by Glu_{in} in the ClC transporters, which is always substituted by a valine residue in the ClC channels.

Adapted from Miller, 2006

The kidney is the major site of ClC-5 expression, followed by the intestine (Steinmeyer, 1995; Fisher, 1995). Northern blotting and RT-PCR analyses also found tissue-specific mRNA variants of *CLCN5* in brain, lung, liver, prostate (Ludwig, 2003), and recent investigations located ClC-5 at the apical membrane of thyrocytes (van den Hove, 2006). In human kidney, immunoblotting analyses identified the ~80 kDa ClC-5 in both cortex and medulla (Devuyst, 1999). Immunohistochemistry on man and mouse kidneys revealed that ClC-5 distribution includes the epithelial cells lining the PT, the TAL of Henle's loop, and the α-type IC of the CD (Günther, 1998; Devuyst, 1999; Sakamoto, 1999). In PT cells, ClC-5 has been particularly localized right underneath the brush border. Moreover, studies of subcellular fractions of human kidney have indicated that ClC-5 co-distributes with markers of early endosomes (Rab 5a), as well as with the V-ATPase (Moulin, 2003). Confocal microscopy studies using opossum kidney (OK) cells as *in vitro* model for PT cells, revealed that ClC-5 co-localizes with albumin-containing endocytic vesicles that form part of the receptor-mediated endocytic pathway (Devuyst, 1999). In addition, surface biotinylation studies have recently demonstrated that ~8% of the total cellular pool of ClC-5 is located at the cell surface of PT cells, where it may participate in the formation/function of the endocytic complex (Wang, 2005; Hryciw, 2006).

The expression of ClC-5 in multiple nephron segments supports the complex phenotype of Dent's disease (Scheinman, 1998). The subcellular distribution of ClC-5 in PT cells points to an involvement in apical receptor-mediated endocytosis, which is consistent with the constant LMW proteinuria found in Dent's patients. The functional loss of ClC-5 in the TAL, which is the major site of regulated Na^+ and Ca^{++} reabsorption, may result in hypercalciuria and nephrocalcinosis, as well as the defective urinary concentration observed in a subset of patients. Finally, ClC-5 dysfunction in α-type IC may lead to impaired urine acidification, actually observed in half of patients with Dent's disease.

3.1.3. Mouse models of Dent's disease

Our group has collaborated to the generation and characterization of a *Clcn5* KO mouse model of Dent's disease by homologous recombination (Wang, 2000). Mice lacking ClC-5 are viable and fertile. They show renal tubular defects that mimic the phenotype of Dent's disease, including LMW proteinuria, aminoaciduria, glycosuria, phosphaturia, and polyuria (Figure 1.11, panel A). The urinary loss of LMW proteins includes both megalin- and cubilin-specific ligands, as well as lysosome enzymes. Mutant mice also develop hypercalciuria and nephrocalcinosis, whereas progressive renal failure is observed with aging (Cebotaru, 2005). Further investigations indicate that the hypercalciuria observed in *Clcn5* KO mice is of bone and renal origin, without significant increased intestinal calcium absorption – despite elevated levels of (1, 25)-dihydroxy vitamin D3 (Silva, 2003).

In order to address the LMW proteinuria associated with ClC-5 deficiency (Figure 1.11, panel B), mice were injected with peroxidase, a classical endocytic tracer that is filtered by the glomerulus and endocytosed by PT cells (Wang, 2000). Cytochemistry and electron microscopy showed a severe impairment of protein endocytosis by ClC-5-deficient PT cells, such that peroxidase bound to the brush border was poorly transferred into early endocytic vesicles (Figure 1.11, panel C). Moreover, quantification of kidney uptake of the LMW ^{125}I-β_2-microglobulin demonstrated a major dysfunction of PT receptor-mediated endosytosis, as well as delayed degradation, in *Clcn5* KO mice (Figure 1.11, panel D). This endocytic defect has been linked to a major and selective loss of megalin and cubilin at the brush border, reflecting a generalized trafficking defect in ClC-5-deficient PT cells (Christensen, 2003).

These data, which were essentially confirmed in another mouse model (Piwon, 2000), demonstrate that the impairment of receptor-mediated endocytosis in PT cells of ClC-5 deficient mice provides a basis for the defective uptake and increased urinary excretion of LMW proteins observed in patients with Dent's disease.

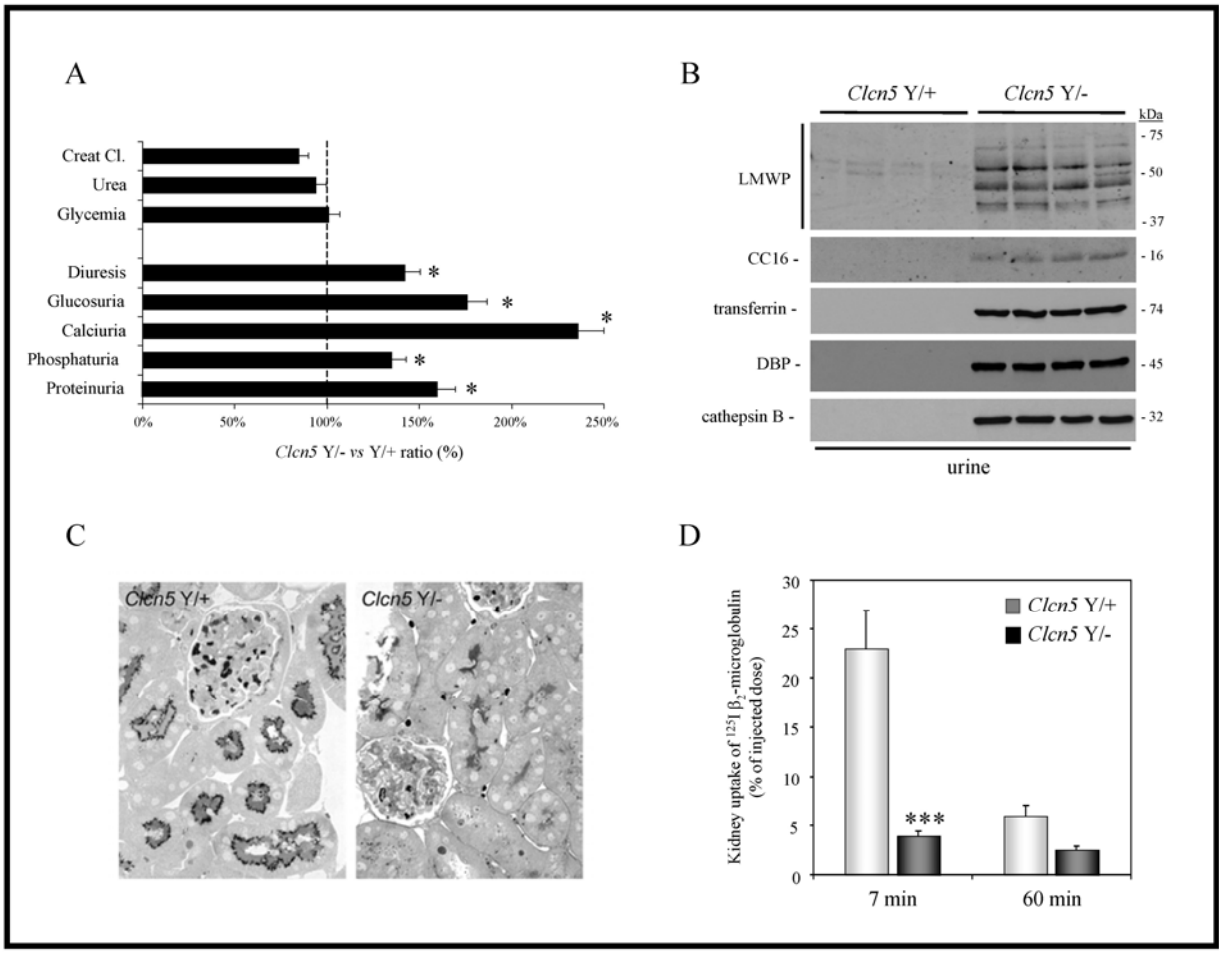

Figure 1.11. Phenotype of the *Clcn5* KO mouse

Panel A. Blood and urine biological parameters. In comparison to controls, *Clcn5*$^{Y/-}$ mice show a severe PT dysfunction, with polyuria, glucosuria, hyper-calciuria and phosphaturia, and proteinuria (n = 50, $p<0.05$).

Panel B. Characterization of the LMW proteinuria. Immunoblotting analyses on urine samples from *Clcn5*$^{Y/+}$ and *Clcn5*$^{Y/-}$ mice demonstrate a distinctive LMW proteinuria in *Clcn5*$^{Y/-}$ mice, including cubilin-specific ligands (CC16; transferrin), megalin-specific ligand (vitamin D-binding protein), and lysosome enzymes.

Panels C-D. Investigation of PT apical endocytosis in *Clcn5*$^{Y/+}$ and *Clcn5*$^{Y/-}$ mice. In control kidney, horseradish peroxydase (HRP) is detected, at 5min *post* iv injection, in numerous endocytic vesicles right beneath PT brush border (C). In contrast, HRP uptake is dramatically impaired in *Clcn5*$^{Y/-}$ kidney, with subsequent accumulation in PT lumen. Similarly, ^{125}I-β_2-microglobulin renal uptake at 7min *post* iv injection, is severely reduced in *Clcn5*$^{Y/-}$ mice (n=4; ***, $p<0.001$) (D). At 60 min postadministration, *Clcn5*$^{Y/-}$ kidneys are characterized by a delayed breakdown of ^{125}I-β_2-microglobulin.

Adapted from Wang, 2000, and Christensen, 2003

3.1.4. Evidence for genetic heterogeneity in Dent's disease

Scheinman SJ et al. reported 13 patients without mutations in the coding sequence and promoter regions of *CLCN5* among a series of 32 unrelated male patients meeting all the clinical criteria for Dent's disease [LMW proteinuria and

hypercalciuria in association with either nephrocalcinosis, kidney stones, hypophosphatemia, rickets, aminoaciduria, or positive familial history] (Hoopes, 2004). Among these 13 patients, linkage analysis identified candidate genes (*CLCN4, SLC9A6, OCRL1*) to a region located at Xq25-Xq27.1 (Hoopes, 2005). Direct sequencing of these genes found 5 mutations in the *OCRL1* gene (Xq26.1) that encodes the enzyme phospho-inositide (4,5) bisphosphate (PIP_2) 5-phosphatase (OMIM #300555). Of interest, mutations in *OCRL1* gene have been previously associated with the oculo-cerebro-renal syndrome of Lowe (OCRL, OMIM #30900), an X-linked disorder characterized by bilateral congenital cataract, severe mental retardation, and renal Fanconi syndrome (Lowe, 2005).

The enzyme PIP_2 5-phosphatase has been located in the trans-Golgi network (TGN), as well as on lysosome membranes, where it regulates the relative pools of $PI(4,5)P_2$ and PI(4)P responsible for correct intracellular vesicle trafficking (Pendaries, 2003). In addition, the OCRL protein may play a role in the dynamic regulation of actin polymerisation in the cytoskeleton and at the tight and adherent junctions. Interestingly, none of the 5 mutations in *OCRL1* found in patients with Dent's disease had been previously reported in OCRL syndrome (http://www.hgmd.cf.ac.uk/hgmd0.html). Moreover these patients with Dent's disease showed no mental retardation or cataract. The role of the enzyme (PIP_2) 5-phosphatase in the pathophysiology of PT dysfunction observed in both Dent's disease and OCRL syndrome and the possible interactions between ClC-5 and OCRL1 remain to be elucidated.

The absence of mutations in *CLCN5* and *OCRL1* genes in a subset of patients with Dent's disease strongly suggests that additional genes may be involved in Dent's disease (Hoopes, 2005). One could speculate that these genes may code for proteins involved in the complex endocytic machinery of PT cells, or interact directly with ClC-5 in endosomes. For instance, a physical interaction between the C-terminus of ClC-5 and cofilin, a protein involved in the depolymerization of actin in the vicinity of budding endosomes, has been documented in PT cells using a yeast two-hybrid screen and GST-fusion protein pulldown assay (Hryciw, 2003). In addition, recent studies

have demonstrated the role of β-subunits in the trafficking, stability, and functionality of several ClC channels. Mutations in *BSND* gene encoding the β-subunit of ClC-Ka and ClC-Kb, barttin cause Type IV Bartter syndrome with sensorineural deafness (OMIM #602522) (Estévez, 2001). The functional loss of Ostm1 impairs the trafficking and the stability of ClC-7 in lysosomes and causes osteopetrosis, lysosomal storage, and neurodegeneration in man and mouse (OMIM *607649) (Lange, 2006). Likewise, ClC-5 may require a β-subunit to exert its function along the endocytic pathway in PT cells.

3.2. Cystic fibrosis and CFTR

3.2.1. Cystic fibrosis

Cystic fibrosis (CF, OMIM #219700) is the most common lethal autosomal recessive disease in Caucasians. CF affects as many as one in 2,500 live births, a rate from which the carrier frequency can be estimated as one in 25 (Sheppard, 1999). The disorder primarily alters mucociliary clearance in various exocrine epithelia, in conjunction with excessive mucus production. Subsequent mucus accumulation in the airways and in the pancreatic and sweat ducts results in obstructive lung disease with chronic bacterial infection and inflammation, pancreatic insufficiency and high sweat Cl^- concentration (Rowe, 2005). In addition, the absence or obstruction of the vas deferens causes male infertility in most CF patients and altered cervical mucus production reduces significantly female fertility (Lyon, 2002). The airways manifestations represent the main cause of morbidity and mortality in the CF population. Nowadays improvement in medical care (physiotherapy, antibiotherapy, digestion enzyme supplements) often preserves life expectancy into adulthood, but the median lifetime remains only 30 years.

CF has been associated with loss-of-function mutations in the *CFTR* gene that encodes the Cl^- channel CFTR (Riordan, 1989). The *CFTR* gene, also named as *ABCC7*, is located on chromosome 7q31.2 and spans approximately 290 kb of

genomic DNA (27 exons) encoding a 1,480-amino acid protein (Ellsworth, 2000). Over 1,000 CF-associated mutations have been reported thus far in the *CFTR* gene (CF Genetic Analysis Consortium, http://www.genet.sickkids.on.ca/cftr/). These mutations are classified into five groups according to their structural or functional consequences on Cl^- conduction (Table 1.5). The in-frame deletion of three bases encoding a phenylalanine residue at position 508 (ΔF508), occurring in approximately 70% of CF patients, results in the misfolding and lack of maturation of the CFTR protein, with its subsequent degradation (Rowe, 2005). About 5 to 10 percent of *CFTR* mutations are due to premature truncation or non-sense alleles and are associated with the most severe CF phenotypes (Rowntree, 2003). The prevalence of such type I mutations is particularly high in the Ashkenazi Jewish population. Most other *CFTR* defects are unique to a particular family or to only a handful of cases across the world.

Table 1.5. Classification of *CFTR* mutations

Defect classification	**I**	**II**	**III**	**IV**	**V**
Defect result	No synthesis	Block in processing	Block in regulation	Altered conductance	Reduced synthesis
Types of mutations	Nonsense (G542X) Frameshift (394delT) (1717-1G→A)	Missense (N1303K) AA deletion (ΔF508)	Missense (G551D)	Missense (R117H) (R347P)	Missense (A445E) Alternative splicing (3849+10kbC→T)
Potential therapy	Gentamicin Gene transfer	Butyrate Curcumin; Gene transfer	Genistein Gene transfer	Milrinone Gene transfer	Gene transfer

Adapted from Zeitlin, 2000.

The type of *CFTR* mutations seems directly linked to the pancreatic phenotype, whereas the high variability in pulmonary complications among siblings carrying identical mutations strongly supports the influence of the environment and modifier genes in the disease severity (Rowntree, 2003). The feature of azoospermia identified

in 99% of male CF patients has no relation to any specific type of *CFTR* mutations and is even encountered in congenital bilateral absence of the vas deferens (CBAVD, OMIM #277180). CBAVD is caused by *CFTR* mutations on both alleles in approximately 80% of cases, with no other sign of CF (Claustres, 2005). Moreover subsets of patients with the CF phenotype have been reported with no or only one mutation in the *CFTR* gene (Groman, 2002). These cases exemplify the extremely broad clinical spectrum of *CFTR*-linked disease and support the existence of additional genes involved in the CF phenotype.

Although *CFTR* gene product has been identified in the developing and mature mammalian kidney (Crawford, 1991; Devuyst, 1996a), no overwhelming renal phenotype has been clearly associated with CF. Impaired salt and water homeostasis, with reduced renal NaCl excretion and decreased capacity to dilute and concentrate urine, has been reported in CF patients (Morales, 2000). However, this could result from a primary defect in kidney function, or simply reflect changes in the extracellular fluid volume caused by excessive losses of NaCl in sweat and feces. Microscopic nephrocalcinosis has also been detected in an autopsy series of CF patients ranging in age from birth to 36 years (Katz, 1988) and the incidence of kidney stones in CF patients may also be increased (Gibney, 2003). However, the relative contribution of lithogenic factors, such as hypocitraturia, hyper-oxaluria and -uricosuria, or impaired hydration remains elusive. Interestingly, CF patients show an enhanced renal clearance of many drugs including aminoglycosides (Samaniego-Picota, 1996), which may be due to impaired receptor-mediated endocytosis in PT cells (Schmitz, 2002). These data suggest that the functional loss of CFTR is probably balanced by alternative pathways for Cl^- conductance in the kidney (Devuyst, 2002). Further investigations of CF patients and mouse models will certainly help unravel the role of CFTR in specialized kidney functions, such as endocytosis and Ca^{++} and NaCl homeostasis. In addition, subtle abnormalities in kidney development, function and/or morphology may appear in later stages of CF or in association with other kidney diseases. For example, it has been demonstrated that CFTR is upregulated in the cells lining the cysts in autosomal

dominant polycystic kidney disease, the most common inherited nephropathy, suggesting that CFTR may play a role in cyst fluid accumulation and disease progression (Hanaoka, 1996; Devuyst, 1998).

3.2.2. Cystic Fibrosis Transmembrane conductance Regulator

The CFTR protein is a member of the ATP-binding cassette (ABC) superfamily of integral membrane transporters. The ABC transporters, also known as traffic ATPase, function as mediators of unidirectional organic solute transport and include the multidrug resistance proteins, such as MDR and P-glycoprotein and a number of prokaryotic and eukaryotic small nutrient and molecular transporters (Higgins, 1992). The CFTR is a Cl^- channel that is regulated by cAMP-dependent phosphorylation and ATP hydrolysis, which mediates Cl^- ion transport across epithelia (Fuller, 1992). In addition, CFTR interacts functionally with other proteins, including the outwardly rectifying Cl^- channels (ORCC) and the epithelium Na^+ channels (ENaC): hence, the name, CF transmembrane conductance regulator (Devidas, 1997). Of note, this name was “presciently” given at the time of *CFTR* gene identification, independently of any knowledge of the structure and functional interactions of CFTR (Riordan, 1989). The CFTR may participate in exocytosis and in the formation of macromolecular complexes at the plasma membrane, in close contact with receptors, signalling proteins and the cytoskeleton (Rowe, 2005). Therefore, the role of CFTR extends well beyond Cl^- permeability, as supported by its unique structure and its subcellular distribution in epithelial cells.

The CFTR protein is organized symmetrically in two transmembrane domains (TMD1 and TMD2) and two nucleotide binding domains (NBD1 and NBD2), separated by a large, polar, regulatory (R) domain unique within the ABC family (Figure 1.12) (Riordan, 1989). Each membrane-spanning domain contains six α helices, portions of which form the Cl^- pore. Both NBD domains regulate in concert Cl^- channel gating, whereas the activation of CFTR relies on the phosphorylation of the R domain, particularly by protein kinase A (Gadsby, 2006). The amino- and caboxy-termini of CFTR are both cytoplasmically oriented. The C-terminus of CFTR possesses a Type I PDZ domain-binding motif (D/E)TRL that is conserved among

species (Guggino, 2004). At least five PDZ-domain proteins have been shown to interact with the C-terminus of CFTR: the Na^+/H^+ exchange regulatory factors (NHE-RF1 and NHE-RF2), intestinal and kidney-enriched PDZ protein (IKEPP), and CFTR-associated protein-70 (CAP70) at the plasma membrane, and CFTR-associated ligand (CAL) in the Golgi. The hypothesis is that the dynamic regulation of CFTR binding to such scaffolding proteins determines its dimeric organization into macromolecular functional units containing regulatory molecules and other channels. Moreover, these functional interactions may increase CFTR efficiency by enhancing its activation by PKA, stabilizing its dimeric state at the plasma membrane and finally increasing channel gating (Li, 2005).

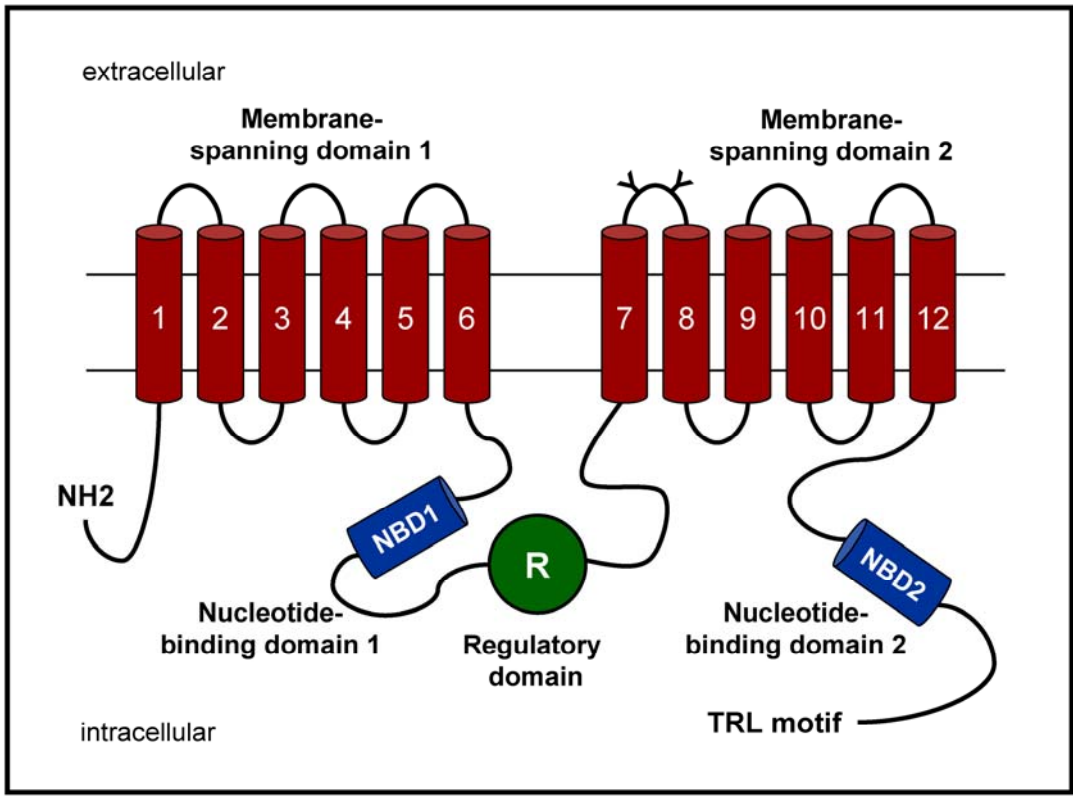

Figure 1.12. Structure of CFTR

The CFTR protein contains 1480 amino acids and is organized symmetrically into a number of discrete globular and transmembrane domains. Each membrane-spanning domain contains six α-helices, portions of which form a chloride-conductance pore. The loop between transmembrane segments 7 and 8 contains two possible glycosylation sites (Y) at asparagine residues. The regulatory domain (R) is a site of protein kinase A phosphorylation. The two nucleotide-binding domains (NBD) regulate Cl^- channel gating and activity. The carboxyl terminal tail of CFTR includes a TRL motif (threonine, arginine, and leucine) that anchors CFTR through PDZ-binding-type interactions with the cytoskeleton and macromolecular complexes.

Adapted from Rowe, 2005

The CFTR has been located primarily in the apical membrane of numerous secretory epithelia, including airways, colic crypts, pancreatic and sweat ducts, and male genital tract (Sheppard, 1999). In addition, several studies have demonstrated the presence of CFTR in the kidney (Morales, 2000). *CFTR* mRNA has been detected in all nephron segments by RT-PCR, but is particularly abundant in the cortex and outer medulla (Morales, 1996). Immunostaining analyses identified CFTR in the apical region of PT, distal tubule and cortical and outer medullary CD of the mature human kidney (Crawford, 1991), as well as in the branching ureteric bud (UB) during early nephrogenesis (Devuyst, 1996a). A functional truncated isoform (TNR-CFTR) made of the TMD1, NBD1 and R domains (Figure 1.12) has also been described in the kidney, with a distinct ontogeny pattern and a minor plasma membrane expression (Devuyst, 1996a; Huber, 1998). The specific function of TNR-CFTR variant that is particularly found in small intracellular vesicles in the renal medulla remains elusive, and may involve intracellular trafficking (Morales, 1996).

Besides its distribution in the plasma membrane, CFTR has been located in intracellular organelles along the endocytic and secretory pathways, in which it might act as a pH regulator by importing Cl^- in parallel to H^+ accumulation (Bradbury, 1999). Inhibition of the endocytic activity, as well as defective acidification in *trans*-Golgi and pre-lysosomal compartments has been reported in CF cells (Barasch, 1991). In turn, lysosomal enzyme deficiencies and abnormal trafficking and processing of newly synthesized polypeptides have been associated with the functional loss of CFTR (Bradbury, 1999). However the exact role of CFTR in regulating organelle pH remains controversial, with hyper- rather than hypo-acidification suggested to occur in CF respiratory epithelial cells (Poschet, 2002).

These observations demonstrate that CFTR is abundantly expressed in different segments of the mammalian kidney, where it may participate in Cl^- permeability and salt transport at the apical plasma membrane. In addition, by analogy to other

intracellular Cl^- channels such as ClC-5, CFTR may play a role in membrane recycling and/or vesicular pH regulation in kidney cells.

3.2.3. Mouse models of cystic fibrosis

Six knockout mouse models of CF have been generated in which the *Cftr* gene has been disrupted by insertion, duplication, or an in-frame stop codon (Table 1.6). In addition, four mutant models have been produced, with the deletion of phenlyalanine at position 508 (ΔF508) in three models and the G551D mutation in the fourth one (for a detailed review, see Grubb, 1999). We will focus on the CF strains used in our studies, i.e. the *Cftr*^{tm1Cam} KO (Ratcliff, 1993) and *Cftr*^{tm1Eur} (ΔF508) mice (van Doorninck, 1995).

Table 1.6. Mouse models of cystic fibrosis

	CF Mouse	Molecular Technique	Reference
CFTR			
knockout	*cftr*^{tm1Unc}	In-frame stop (exon 10)	Snouwaert J, *Science* 1992
	cftr^{tm1Hgu}	Insertion (exon 10)	Dorin JR, *Nature* 1992
	cftr^{tm1Cam}	Insertion (exon 10)	Ratcliff R, *Nature Genet* 1993
	cftr^{tm1Bay}	Duplication (exon 3)	O'neal WK, *Hum mol genet* 1993
	cftr^{tm3Bay}	In-frame stop (exon 2)	Hasty P, *Somat Cell Mol Genet* 1995
	cftr^{tm1Hsc}	Insertion (exon 1)	Rozmahel R, *Nature Genet* 1996
mutant	*cftr*^{tm1Kth}	Homologous recombination (ΔF508)	Zeiher BG, *J Clin Invest* 1995
	cftr^{tm1Eur}	Homologous recombination (ΔF508)	van Doorninck JH, *Embo J* 1995
	cftr^{tm2Cam}	Homologous recombination (ΔF508)	Colledge WH, *Nature Genet* 1996
	cftr^{TgHm1G551D}	Homologous recombination (G551D)	Delaney SJ, *Embo J* 1996

Computed from Grubb, 1999

The *Cftr*^{tm1Cam} KO mouse (C57BL/6J/129 background) was generated by targeted deletion of exon 10 of *Cftr* upon homologous recombination (Ratcliff, 1993). At birth, the expected mendelian distribution of the genotypes indicates that there is little, if any, prenatal lethality associated with homozygosity of the mutant allele. However, ~80% of *Cftr*^{tm1Cam} pups fail to thrive postnatally and die within five days from meconium ileus and severe peritonitis. A second period of high-mortality rate due to intestinal blockage manifests at the time of weaning (and first ingestion of solid food) (Hunton, 1966). Therefore CF mice have to be placed on a liquid diet that has been found to significantly prolong their life span (Eckman, 1995). In *Cftr*^{tm1Cam} pancreas, dilatation and blockage of small ducts, with occasional vacuolated acinar cells, were noted. Conversely, no pathological accumulation of mucus was found in *Cftr*^{tm1Cam} lung. Further electrophysiology studies showed that epithelial cells of both *Cftr*^{tm1Cam} trachea and caecum were unable to generate a Cl^- conductance in response to increased intracellular cAMP concentrations (forskolin stimulation). Thus, the *Cftr*^{tm1Cam} mouse is characterized by a severe CF phenotype caused by CFTR deficiency (Type I mutation) and represents a useful model to investigate the role of CFTR in distinct organs, such as the kidney.

The deletion of a phenylalanine residue at position 508 of the CFTR protein (ΔF508) represents the most common mutation in CF population. It is thought that 90% of Caucasian CF patients have at least one ΔF508 allele (Rowe, 2005). This mutation affects the correct processing and maturation of CFTR to its fully glycosylated form (Cheng, 1990), with retention of ΔF508-CFTR in the ER by molecular chaperones (Egan, 2002) and subsequent degradation via the ubiquitin-proteasome pathway (Ward, 1995). However, the ΔF508-CFTR can essentially function as a cAMP-regulated Cl^- channel, both in the ER and at the plasma membrane under distinct permissive conditions (Pasyk, 1995; French, 1996). The processing of ΔF508-CFTR has been particularly shown to revert to that of wild-type CFTR as the incubation temperature is reduced (Denning, 1992). A mouse model expressing the ΔF508 form of CFTR was generated by double homologous recombination (“Hit and Run”) procedure (van Doorninck, 1995). Of note, the mouse exon 10 amino acid

sequence is highly homologous to the human sequence, which suggests similar consequences of F508 deletion on CFTR properties in both species (Tata, 1991). Six-week-old mice homozygous for ΔF508 mutation (*Cftr*^{tm1Eur}) have abnormalities typical of CF, such as growth retardation, focal hypertrophy of goblet cells in the intestinal crypts, and higher basal nasal potential difference with reduced response to forskolin in trachea and intestine. However, the *Cftr*^{tm1Eur} tissues show a residual Cl^- conductance, suggesting that the mouse ΔF508-CFTR is partially processed and reaches the plasma membrane. Moreover, airway and gallbladder cells from *Cftr*^{tm1Eur} mutant mice show increased cAMP-induced Cl^- conductance when cultured at reduced temperature (27°C) (French, 1996). This may explain the minor phenotype of the *Cftr*^{tm1Eur} *versus* *Cftr*^{tm1Cam} mice (e.g. absence of lethal intestinal obstruction). Although such rescue phenomenon has not been clearly demonstrated thus far in man, residual Cl^- transport activity has also been observed in rectal biopsies of ΔF/ΔF patients with milder CF phenotype (Veeze, 1994). Moreover the expression of ΔF508-CFTR in man has been demonstrated tissue-specific, suggesting that the variable severity of CF in different organs may reflect heterogeneity of residual expression (Kalin, 1999). Thus, the ΔF508 mouse model represents a useful tool to decipher *in vivo* the complex pathophysiology of CF caused by CFTR processing defect (Type II mutation).

The discrete renal manifestations in CF patients have prompted only few investigations on kidney functions in CF mouse models (Devuyst, 2002). Renal Na^+ clearance studies were performed in control and *Cftr*^{tm2Cam} ΔF508 mice and showed similar results in both groups under basal conditions, as well as after acute extracellular volume expansion (Kibble, 2001). In addition, *Cftr*^{tm2Cam} ΔF508 mice were equally able to reduce Na^+ excretion under chronic dietary salt restriction, but displayed an increased amiloride sensitivity, compatible with a functional interaction between CFTR and the Na^+ channel ENaC in CD principal cells (Kibble, 2000; Letz, 1997). The use of isolated, microperfused TAL from the *Cftr*^{tm1Unc} KO mouse helped demonstrate that CFTR was not the molecular counterpart of the 9-pS Cl^- conductance

detected in this segment (Marvao, 1998; van Kuijck, 1996). In conclusion, although the role of CFTR in exocrine epithelia, including trachea and small intestine, has been studied extensively in CF mouse models (Grubb, 1999; Barriere, 2004), the issues of CFTR processing and function in the kidney remain largely debated.

The most striking phenotype in CF mouse models has been demonstrated in the intestine, including blockage and perforation, typical histological changes, and ion transport abnormalities (Grubb, 1999). This intestinal pathology closely mimics that observed in 10% of CF neonates and 3% of adult CF patients (Eggermont, 1991). In contrast, no pulmonary manifestations of the disease were observed in CF mouse models (Grubb, 1999), whereas ~95% of morbidity and mortality in CF patients is due to lung disease with mucus plugging and chronic bacterial infection (Rowe, 2005). Additional differences between CF mice and patients include the relatively low severity of pancreatic complications and the virtual absence of pathology in the male genital tract (Grubb, 1999). On a practical note, CF mice, like some patients, exhibit milky white and particularly fragile incisor teeth resulting from abnormal enamel development, which help distinguish them from their heterozygous and wild-type littermates (Wright, 1996).

An attractive explanation for the discrepancy between man and mouse CF lung phenotypes is that Cl^- channel(s) active in mouse airways may constitute an alternative pathway for Cl^- in the absence of CFTR (Devuyst, 2002). For instance, the tissue-specific expression of members of the Ca^{++}-activated Cl^- channels (CaCC or CLCA) family has been correlated inversely with the severity of organ-level disease in CF (Clarke, 1994; Grubb, 1994). Other putative candidates to provide apical membrane Cl^- transport in the absence of a functional CFTR include the ORCC channel (Gabriel, 1993) and volume-sensitive Cl^- channels (Strange, 1996). Of note, the ubiquitously expressed voltage-gated ClC-2 had been speculated to compensate for CFTR loss (Schwiebert, 1998). However, mice lacking both CFTR and ClC-2 showed a superimposition of the intestinal phenotype of *Cftr* KO mice and retinal and testicular

degeneration reported in ClC-2-deficient mice, without lung or pancreatic pathology (Jentsch, 2005). In contrast, recent studies have shown that ClC-5 was expressed at the apical surface of airways epithelial cells during lung ontogeny, suggesting that it may also participate in lung Cl^- secretion (Edmonds, 2002). As a whole, these observations suggest that the pathophysiological consequences of the loss of CFTR function can be partially compensated for by the induction of another Cl^- channel, as well as by the genetic modulation of modifier genes (Rozmahel, 1996; Rowntree, 2003). This possibility, which has been documented in the lung of CF mice, may apply to other epithelia expressing Cl^- channels, including the kidney.

4. Nephrogenesis

Most congenital disorders of kidney tubule function manifest in the first years of life. The severe infantile form of cystinosis, the most common inherited cause of renal Fanconi syndrome, presents fluid and electrolyte losses, aminoaciduria, glycosuria, phopshaturia, rickets, and growth retardation generally between 6 and 12 months of age (Kalatzis, 2003). The early onset of tubular proteinuria in infant cases of Dent's disease (Nakazato, 1997) and Imerslund-Gräsbeck disease (Christensen, 2003) further supports that PT function is essentially acquired at birth or during early infancy. Likewise, symptoms of recessive distal RTA manifest during infancy and early childhood, suggesting a rapid maturation of acid-base transporters along the distal nephron during pre- and post-natal nephrogenesis (Karet, 2002).

These clinical observations prompted us to investigate the differential expression, segmental distribution and maturation of tubular transporters (and transporter isoforms) along the nephron during nephrogenesis. This section summarizes the major steps of kidney development in mammals and provides further clinical and experimental evidences for a progressive tubular maturation *in utero* and during the first weeks of life. The emphasis is especially set on (i) the development of PT ability to reabsorb LMW proteins and (ii) the differentiation of the IC and the maturation of urine acidification processes.

4.1. Major steps in kidney organogenesis

Kidney development in mammals is characterized by three main ontogenic stages that develop from the intermediate mesoderm on the dorsal body wall: the pronephros, mesonephros and metanephros (Bard, 2003). The primitive pro- and mesonephroi degenerate rapidly during fœtal life, while the metanephros develops into the definitive adult kidney. Important events in human and mouse nephrogenesis are comparatively outlined in a timetable (Table 1.7) and schematically represented in Figure 1.13.

Table 1.7. Timetable for nephrogenesis : man *versus* mouse

	MAN	MOUSE
PRONEPHROS		
Development	22 d	9 d
Regression	25 d	10 d
MESONEPHROS		
Development	24 d	10 d
Regression	16 wks	14 d
METANEPHROS	28-32 d	11 d
Renal pelvis	33 d	12 d
Collecting tubules and nephrons	44 d	13 d
Glomeruli	8-9 wks	14 d
END OF NEPHROGENESIS	34-36 wks	7-10 d after birth
LENGTH OF GESTATION	40 wks	20-21 d

From Bard, 2003

The development of human metanephric kidney begins at day 28 after fertilization when the ureteric bud (UB) sprouts from the mesonephric Wolffian duct and penetrates the metanephric blastema. From that time, kidney organogenesis takes place by repetitive and reciprocal inductions between the UB and the metanephric mesenchyme (MM), with simultaneous development of renal vasculature (Gomez, 1997). The UB dichotomously branches into the renal mesenchyme and differentiates into the ureter, the pelvis, the calyces, and the CD system, while the MM condenses around the tips of the UB and aggregates into a vesicle, with subsequent mesenchyme-to-epithelium transformation and organization into comma- and S-shaped bodies.

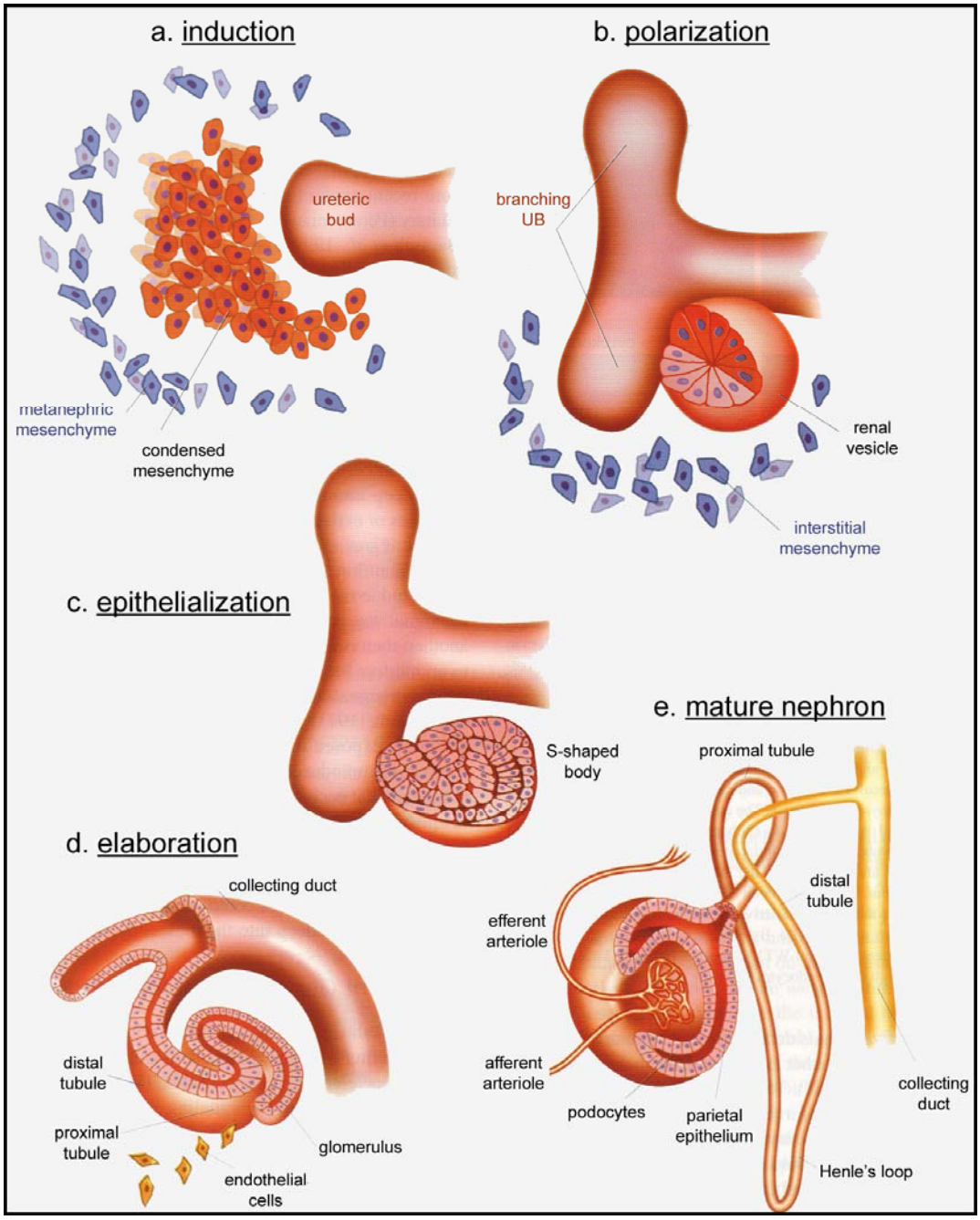

Figure 1.13. Morphogenesis of the nephron

Panel A. The penetration of the ureteric bud (UB) into the metanephric mesenchyme induces the aggregation of mesenchymal cells at the tips of UB.

Panels B-C. The aggregate becomes polarized into a renal vesicle, which remains closely associated with the UB. The UB grows and further branches dichotomously, and the next generation of nephron is induced. Mesenchymal cells around the bud constitute the stroma, with potential stem cells.

Panels D-E. At the S-shaped body stage, the renal vesicle elongates and forms two clefts, the most proximal of which becomes invaded by primitive endothelial cells to form the glomerular capillary tuft. The distal part of S shape differentiates into the proximal tubule, loop of Henle, and distal tubule, and connects with the collecting duct system originating from the UB.

Adapted from Cho, 2003

The distal portion of the S shape elongates and differentiates into the PT, the loop of Henle, and the distal tubule that fuses with the adjacent branch of the UB to form a continuous functional unit. Simultaneously, endothelial cells invade the proximal cleft of S-shaped bodies, giving rise to the glomerular capillary tuft. Glomerular filtration starts between the 9th and 12th GW in the human kidney and at E14 in mice. Thus, kidney organogenesis results from a centrifugal propagating wave of branching morphogenesis, tubulogenesis, glomerulogenesis, and differentiation starting in the renal pelvis and ending in the cortex. The developing kidney shows a clear delineation of the external cortex and the inner medullary region from E16.5 in mice. The glomeruli tend to be concentrated in the cortical area, whereas collecting ducts are more radially arranged in the medulla and drain to a primitive renal pelvis (Figure 1.14).

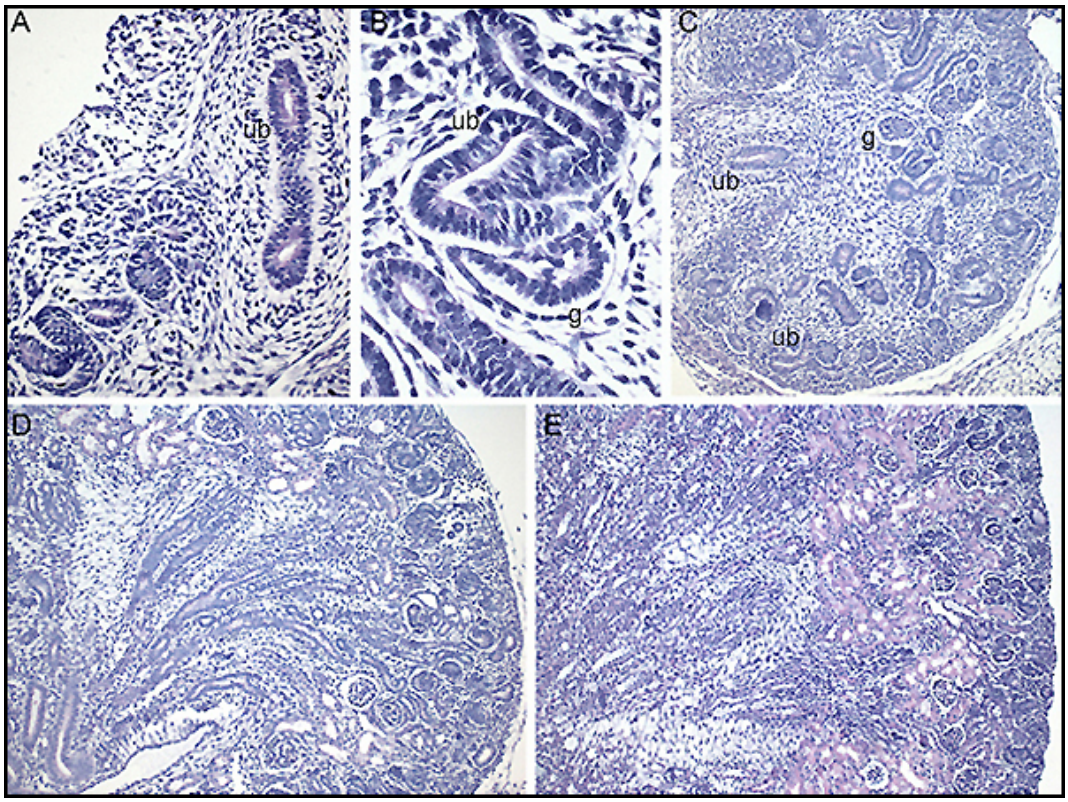

Figure 1.14. Mouse nephrogenesis

Hematoxylin-Eosin staining in the developing mouse kidney at E13.5 (A), E14.5 (B, C), E16.5 (D), E18.5 (E). By E13.5, the terminal part of the ureteric bud (ub) invades the metanephric mesenchyma and initiates its differentiation (A). The latter elongates and becomes an S-shaped body (B). At E14.5, the metanephros is divided into an outer primitive cortical region and an inner medullary region, containing few primitive glomeruli (g) (C). From E16.5, the developing kidney is well-subdivided into external cortical and inner medullary regions (D). At E18.5, kidney development is largely completed (E). Note that, at this stage, an outer thin band of differentiating mesenchyme remains visible under the renal cap.

Nephrogenesis ceases around 34 weeks of gestation in man and within the first week of life in mice. In contrast, the formation of new nephrons continues postnatally in premature infants of less than 35 GW like in rats and rabbits. The total number of nephrons per kidney, as assessed by counting glomeruli, varies widely between species and probably reflects the number of branches of the UB. It has been calculated that 9 to 10 rounds of UB branching occur in mice, thereby generating 10-20,000 nephrons per kidney, whereas 10 additional binary divisions occur during human nephrogenesis to give rise to approximately a million nephrons in each kidney (Ekblom, 1994). The cortical region of newborn kidney contains a large number of glomeruli and proximal and distal convoluted tubules, as well as an outer thin band of differentiating mesenchyme, whereas the medulla contains components of Henle's loop interspersed between collecting ducts.

The metanephric kidney begins to produce urine by 10 GW, which contributes to the formation of the amniotic fluid necessary for symmetrical fœtal growth and lung development (Rabinowitz R, 1989). Although water and electrolyte homeostasis is essentially achieved by the placenta during fœtal life, the *in utero* development of specialized nephron functions is an obvious prerequisite for the adaptation to extra-uterine conditions at birth. Recent high-density DNA array evidences in rat developing kidney have grouped gene expression during organogenesis in five typical clusters of temporally differentially regulated genes (http://organogenesis.ucsd.edu/). Particularly, the group of genes encoding transporters, ion-motive ATPases, and proteins involved in energy production, showed a progressive and relatively linear expression during late nephrogenesis (Stuart, 2001). A catalogue of gene expression in mouse developing kidney, based on microarrays and target amplification techniques, confirmed such clustering of gene regulation during organogenesis, with a preferential expression of transporters from E16.5 (Schwab, 2003). However one should emphasize that gene regulation only represents the first step of tissue differentiation and needs complementary studies at the protein level to integrate post-translational modifications, like complex N-glycosylation, in differentiation and organogenesis

cascades (Laitinen, 1987). Indeed further transport differentiation occurs during postnatal maturation in every nephron segment, including changes in the relative abundance of transporter isoforms, or in the intracellular signalling that regulates the transporters (Baum, 2003).

4.2. The handling of low-molecular-weight proteins in the developing kidney

The fœtal urine represents the most important component of the amniotic fluid (AF) during the second half of pregnancy (Wladimiroff, 1974). Changes in AF composition occur with gestation. They include decreased AF [electrolytes] and osmolarity, and increased $[creatinine]_{AF}$ and $[urea]_{AF}$ (Henneman, 1970). A wide range of proteins has been identified in human AF, with a dynamic temporal pattern characterized by a progressive increase of AF protein concentration from GW 7 to 20 and a subsequent decline during late gestation (Burdett, 1982). The AF concentration in LMW proteins has been particularly investigated as a potential marker of kidney tubule maturation. Indeed, the similarities in LMW protein contents (α_1- and β_2-microglobulin) in the first urine of pre-term and term neonates and the AF at the same gestational age support that these proteins are of fœtal origin. Healthy pregnancies show a significant decrease in AF [LMW proteins] between the 16^{th} and the 38^{th} GW (Burghard, 1987; Cagdas, 2000). In contrast, pregnancies carrying an OCRL syndrome fœtus have been associated with elevated AF concentration in the 70kDa α-fœtoprotein, reflecting fœtal renal tubular dysfunction (Miller, 1994).

These clinical observations indicate a progressive maturation in PT ability to reabsorb LMW proteins during the second half of pregnancy. Further experimental evidences support a progressive cell polarization in the PT during nephrogenesis, with the segmental distribution of receptor-mediated endocytosis partners acquired at the time of glomerular filtration (Biemesderfer, 1992).

4.2.1. Acquisition of cell polarity

The establishment of cell surface polarity during nephrogenesis is a multistage process involving cell-cell and cell-matrix interactions, as well as distinct proteins participating in intracellular transport (Karp, 2003). The polarization process starts at the time of mesenchyme-to-epithelium transition, as the forming tubular epithelium

develops specific transport functions (Figure 1.13). All epithelial cells are characterized by an apical domain that mediates specific and selective exchanges with the external milieu and a basolateral domain less specific responsible for cell-cell interactions and attachment to the basal membrane and the extracellular matrix. Surface membrane polarity is particularly important for nephron functions, since tubular epithelial cells represent the unique interface between the glomerular ultrafiltrate and the interstitium.

The cellular polarization is generated by differential protein and lipid sorting and maintained by the tight junctions that form a structural and functional barrier at the apex of the cell (Brown, 2000b; Aijaz, 2006). Most proteins involved in the development of the cytoskeleton and domain-specific membrane components, including the protein trafficking machinery, have been identified in early stages of kidney development (Lehtonen, 1999). In addition, the differential expression of specific surface membrane transporters has been demonstrated in defined morphogenic stages (Horster, 2000). Interestingly, the expression of alternative subunit isoforms within the same transporter class varies during kidney development, as described for the amiloride-sensitive ENaC, the CFTR, the Na^+/Pi co-transporter, and the Na^+/K^+-ATPase (Canessa, 1994; Devuyst, 1996a; Segawa, 2002; Burrow, 1999). As an example, the B2 isoform of Na^+/K^+-ATPase is expressed throughout nephrogenesis and the pump is found at both apical and basolateral domains. After birth, the B2 subunit is downregulated and replaced by the B1 isoform and the Na^+/K^+-ATPase is restricted to the basolateral domain (Burrow, 1999). These data support specific inductive signals that are temporally and spatially regulated and participate in the specialization of apical and basolateral domains (Baum, 2003).

These observations provide a basis on which to evaluate causal relations in morphogenesis, cell polarization, and functional differentiation. Any alteration that disrupts the polarity of surface membrane domains will indeed prevent normal cell function and result in organ dysfunction and potentially a disease state (Wagner, 1999).

4.2.2. Ontogeny of megalin and cubilin

Megalin has been identified in rat trophoectodermal cells as early as day-4 pre-implantation, and co-distributes with cubilin in coated pits of the first endoblastic cells in day-6 pre-implantation rat embryo (Sahali, 1993). Both receptors are present along the endocytic apparatus of the visceral yolk sac throughout gestation. Megalin has also been located at the surface of neurectodermal structures and later in the neural cavities. Megalin-deficient mice exhibit severe malformations of the forebrain similar to syndromes in man caused by insufficient supply of cholesterol during development, suggesting that megalin participates in the maternal-fœtal lipoprotein transport (Willnow, 1996). Most of megalin KO mice die within minutes after birth, apparently due to an inability to breath. Likewise, the importance of cubilin in organogenesis is strongly suggested by the severe fœtal malformations observed after injection of antibodies directed against cubilin during rat gestation (Sahali, 1988).

During renal development, megalin is found in the mesonephric tubules and in the early metanephric vesicles, whereas cubilin is first detected in S-shaped bodies (Sahali, 1993). Megalin is diffusely distributed in S-shaped bodies in the presumptive areas of the glomerulus, the proximal, and the distal tubules. In these cells, megalin is expressed on both apical and basolateral membranes, as well as intracellularly in the cisternae of the rough ER and in the perinuclear area. With nephron maturation, the expression of megalin and cubilin becomes progressively restricted to the epithelial cells of the PT, with a subcellular distribution compatible with clathrin-coated membrane domains and endosomes (Christensen, 2002b). The absence of gross kidney phenotype in megalin-deficient mice indicate that megalin is not required for nephrogenesis (Willnow, 1996). However, the loss of megalin induces a severe disruption of the endocytic apparatus of PT cells (Leheste, 1999). These data support that the complex maturation process of megalin and cubilin participates in the global organization of PT brush border during kidney development. Interestingly, the segmental distribution of both receptors coincides with the onset of glomerular filtration (Biemesderfer, 1992).

4.2.3. Ontogeny of V-ATPase subunits

The V-ATPase is ubiquitous in eukaryotic cell endomembranes, as well as in the plasma membrane of specialized cell types (Wagner, 2004). A growing body of evidence supports a role of the V-ATPase in cell proliferation and differentiation (Otani, 2000), as well as its participation in cell death regulation (Coakley, 2002). The intracellular compartments acidified by the V-ATPase are present from the one-cell stage of mouse pre-implantation embryo, with a polarized perinuclear distribution upon differentiation of the trophoblast and the inner cell mass at the blastocyst stage (Sun-Wada, 2000). Genetic inactivation of the V-ATPase 16-kDa proteolipid c subunit in mice causes a lack of post-implantation development (Inoue, 1999). When cultured *in vitro*, V0 c-null blastocysts grow significantly slower than controls, with swollen Golgi complexes and impaired endocytosis and most cells fail to survive for more than 4 days. These observations indicate that intracellular organelle acidification is essential for development after implantation (Sun-Wada, 2000). Similarly, the deletion of V-ATPase B subunit in *Drosophila* leads to early larval lethality, whereas point mutations cause defective phenotypes ranging from subvital to embryonic lethal (Davies, 1996). Moreover, the effect of the V-ATPase on pH and membrane potential may serve as one of the earliest signals for left-right asymmetry in *Xenopus* embryos, as well as in chicks and zebrafish (Adams, 2006). In later embryonic stages, the V-ATPase V0 c subunit is detected by northern blotting and *in situ* hydridization analyses from E14 in rat, especially at sites of mesenchymal differentiation and mesenchyme-epithelium interactions (Numata, 1995). Thus, the V-ATPase activity appears essential for both early and late phases of fœtal development.

The expression and distribution of V-ATPase subunits during nephrogenesis remains singularly unknown, although mutations in genes encoding kidney-specific V-ATPase subunits have been associated with infant cases of distal RTA (Karet, 2002). Mouse models with conditional null mutations of distinct V-ATPase subunits may be crucial to further evaluate V-ATPase importance in early and late kidney organogenesis. Moreover characterizing the developmental pattern of subunit isoforms

in comparison to established markers of nephron segments may help decipher the complex maturation of the nephron.

4.2.4. Ontogeny of the Cystic Fibrosis Transmembrane conductance Regulator

The cAMP-activated Cl^- channel CFTR is abundantly expressed in fœtal and postnatal lung, pancreas, and kidney in man, rat, and rabbit (Horster, 2000). *In situ* hybridization analysis of *CFTR* mRNA distribution in human fœtal tissues demonstrates temporal and tissue-specific patterns (Tizzano, 1993; Trezise, 1993). Most CFTR-positive sites in the fœtus are similar to those reported in adult tissues. However, the levels of *CFTR* mRNA expression in fœtal epithelia during the second trimester of human gestation are significantly higher than those in adults. CFTR is primarily detected in undifferentiated multipotent stem cells of pulmonary and pancreatic epithelia and gradually dissipates with epithelial differentiation (Hyde, 1997; Broackes-Carter, 2002). Cell differentiation is further associated with a significant shift from apolar to apical localization of CFTR (McGrath, 1993). The *in utero* overexpression of CFTR (adenovirus recombinant *CFTR* transgene) in normal rodents and primate fœtuses accelerates significantly the lung maturation (Larson, 2005). Conversely, the lack of functional CFTR during the fœtal period in CF patients disrupts the normal development of lung, intestine, and pancreas, with early sub-clinical inflammation and infection (Imrie, 1979; Ornoy, 1987). These findings prompted *in utero* gene therapy trials in *Cftr* KO mouse models that were proven to rescue the lethal phenotype of meconium ileus (Larson, 1997).

During human nephrogenesis, CFTR has been detected as early as 12 GW, with a segmental distribution including mostly the apical region of the branching UB (Devuyst, 1996a). This pattern of expression, also observed in rat developing kidney (Huber, 1998), is similar to that found during branching morphogenesis in pancreas and lung (Horster, 2000). Besides its relatively stable expression pattern in UB epithelial cells, CFTR abundance significantly increases in the cytoplasm of PT and loops of Henle from 15 to 24 GW. This increased immunoreactivity correlates with the morphological maturation of these segments and with the appearance of the water

channel aquaporin-1 in PT cells (Devuyst, 1996b). No glomerular staining for CFTR can be detected at any stage. In addition, a splice variant of CFTR (TNR-CFTR), that possesses only the TMD1, the NBD1 and the R domain (Figure 1.12), has been identified in man and rat developing kidney. This variant is predominantly present in intracellular compartments and shows distinct regulation during kidney organogenesis (Devuyst, 1996a; Huber, 1998). These observations show the complex regulation of CFTR during organogenesis and raise the question, still unsolved, of the respective roles of the full-length and the splice variant CFTR proteins in the developing and mature kidney. Indeed, CF patients do not show overt developmental abnormalities in the urinary excretory system, although CF-related changes in the male genital tract indicate that CFTR participates in the development of the mesonephrotic duct (Trezise, 1993).

4.3. Acid-base homeostasis during nephrogenesis

When analyzing the maturation of acid-base transport in the developing kidney, it is helpful to distinguish HCO_3^- reabsorption, primarily ensured by the PT, from net acid secretion occurring in the distal nephron. Both term and pre-term infants have a lower plasma [HCO_3^-] than adults do, which is thought to reflect a lower renal HCO_3^- threshold (intrinsic capacity of the PT to reabsorb HCO_3^-) and/or a state of relative volume expansion in early life (Edelmann, 1967). In addition, infants exhibit a larger fall in blood pH and [HCO_3^-] than older subjects in response to a comparable acid load, as well as a smaller and slower fall in urinary pH (Satlin, 2003). Such renal response to acid loading has been shown to increase with both gestational and postnatal ages, with a 50% increase in both $H_2PO_4^-$ and NH_4^+ excretion in the first 3 weeks of life (Svenningsen, 1974). These observations indicate that infants operate at close to their maximum rates of both HCO_3^- reabsorption and H^+ secretion. Therefore the expression, distribution, and maturation of acid-base transporters during pre- and postnatal nephrogenesis, appear essential to compensate the acid-generating processes of growth and diet changes at the time of weaning (Baum, 2003; Chan, 1974).

4.3.1. Maturation of acid-base transport in the proximal tubule

In acid-base homeostasis, PT cells are responsible for the reabsorption of ~80% of filtered HCO_3^-. For that purpose, PT cells are equipped with the apical Na^+/H^+ exchanger NHE3 and V-ATPase (H^+ secretion) and the Na^+/HCO_3^- co-transporter NBC1 on the basolateral membrane (HCO_3^- reabsorption). In addition, the cytosolic CAII and membrane-bound CAIV facilitate renal acidification by catalyzing the reversible hydration of CO_2 into $HCO_3^- + H^+$ (Figure 1.7). Most partners of this H^+ secretion and HCO_3^- recovery machinery have been investigated in the developing kidney. The activities of CAII and CAIV have been detected in the early human fœtal kidney, with primarily cytoplasmic distribution and progressive extension to plasma membrane with maturation (Larsson, 1985). The abundance of CAII and CAIV increases gradually after birth in rats and rabbits, which probably contributes to the three-fold increase in HCO_3^- reabsorption in the maturing PT (Karashima, 1998; Winkler, 2001). The NHE3 activity in PCT isolated from rabbit neonatal kidney represents only one third of that in adults, when assayed from the rate of recovery of cell pH after cell acidification (Baum, 2003). The participation of Na^+-independent H^+ secretion, presumably via the V-ATPase, in pH recovery from an acid load appears minor in neonatal *versus* adult PCT. However, the administration of glucocorticoids to rabbit and rat late in development accelerates PT maturation, with increased NHE3 abundance and HCO_3^- reabsorption to the adult level (Baum, 1995; Gupta, 2001). Recent studies in mice have further demonstrated massive and simultaneous changes in mRNA and protein expression levels of acid-base transporters during postnatal kidney maturation (Bonnici, 2004). Altogether these data demonstrate a significant postnatal increase in PT acidification ability that may reflect maturational changes of hormone levels, such as glucocorticoids.

4.3.2. Differentiation of the intercalated cells

The differentiation and maturation of the various cell types within the CD is poorly understood. Particularly, the embryologic origin of the IC has not been established. Studies in rats have shown that CAII and the V-ATPase are

simultaneously detected in IC of the metanephric nephron and the CD at the end of gestation (Kim, 1994). During the first weeks of life, IC continue their maturation, but are partially removed from specific parts of the CD by apoptosis (β-type) or luminal extrusion (α-type) (Kim, 1996). Recently the winged helix transcriptional factor, Foxi1, previously located in mouse fœtal distal nephron (Overdier, 1997), has been shown to play a crucial role in IC differentiation from epithelial precursor cells in the CD (Blomqvist, 2004).

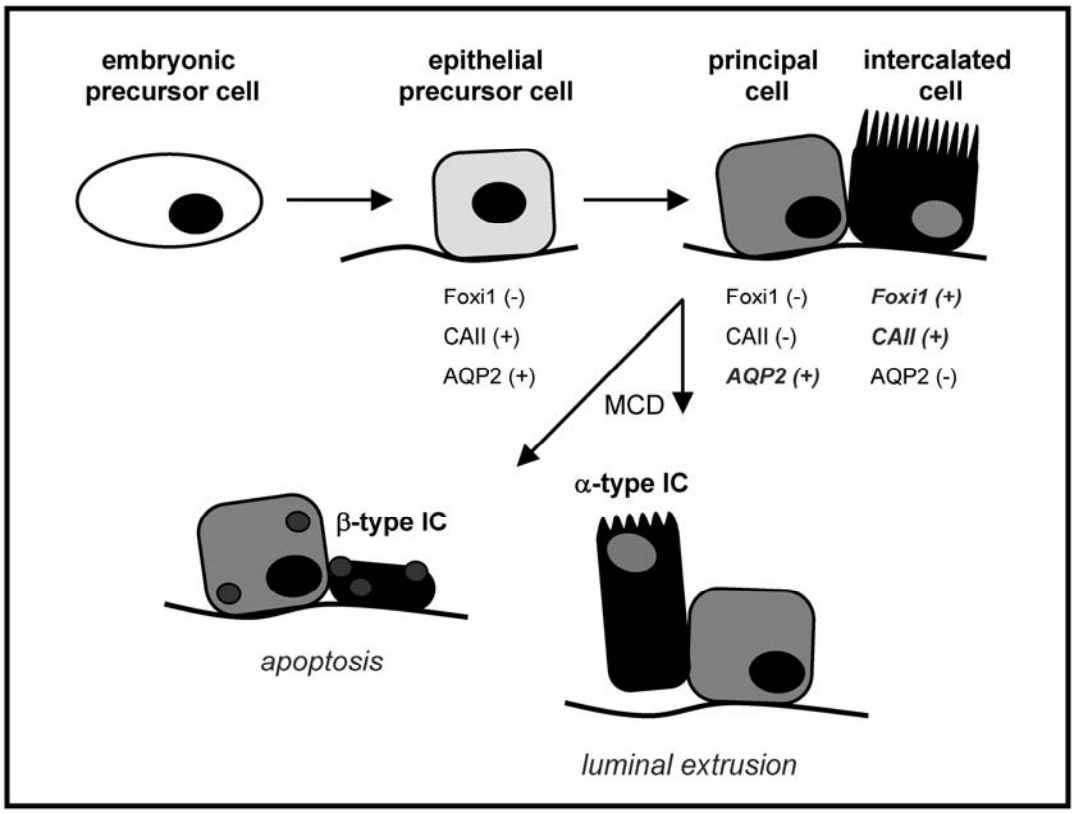

Figure 1.15. Differentiation scheme for intercalated cells of the collecting duct

Embryonic precursor cells of ureteric bud origin gradually acquire an epithelial phenotype. These cells constitute a transient cell population that expresses both type II carbonic anhydrase (CAII) and the water channel aquaporin-2 (AQP2). Activation of Foxi1 is required for this common progenitor to further develop into two separate specialized cell types: principal cells (Foxi1$^-$, CAII$^-$, AQP2$^+$) and intercalated cells (Foxi1$^+$, CAII$^+$, AQP2$^-$). During the first weeks of life, IC continue their maturation, but are partially removed from the medullary collecting duct (MCD) by apoptosis (β-type) or luminal extrusion (α-type).

Modified from Blomqvist, 2004

In silico studies (http://mordor.cgb.ki.se/cgi-bin/CONSITE/consite), coupled with cell-based reporter gene assays, indicate that gene promoters of IC-specific markers,

such as AE1, AE4, pendrin, and IC-specific V-ATPase subunits, exhibit Foxi1 DNA binding consensus sequence (Kurth, 2006). Interestingly, mice lacking Foxi1 have no IC as judged by electron microscopy and by the absence of IC-specific proteins. The entire CD of the mutant mice seems to be composed of one single cell type that expresses both IC (CAII) and principal cell (aquaporin-2) proteins. Consequently, *Foxi1* KO mice develop a typical phenotype of distal RTA, with overt metabolic acidosis, hypokalaemia, and decreased capacity to secrete protons (Blomqvist, 2004). These observations, as well as the role of Foxi1 in inner ear development (Hulander, 2003), led the authors to propose that Foxi1 activates a whole program of gene expression in epithelial precursor cells lining the UB, with a direct effect on IC determination (Figure 1.15). Moreover, mutations in *FOXI1* gene, located on chromosome 5q34, might prove to cause a sensorineural deafness syndrome with type 1b distal RTA, like mutations in *ATP6V1B1* gene.

In conclusion, the functional maturation of the metanephric kidney is a gradual process that lags behind anatomic maturation and is not completed *in utero*. The neonatal kidney plays a key role not only in water and electrolyte homeostasis, but also in the process of growth by maintaining a positive balance for most electrolytes, amino acids, (oligo-)peptides, and vitamins. Further studies of transporter abundance, distribution, and biophysical properties, as well as investigations of the differential expression of transporter isoforms during nephrogenesis, are essential to identify the factors that promote such developmental changes.

5. Aims of the study

The epithelial cells lining the PT have an extensive apical endocytic apparatus that is responsible for the reabsorption of filtered albumin and LMW proteins, as well as for the recycling of numerous functionally important plasma membrane proteins (Birn, 2006). The trafficking of internalized receptor-ligand complexes along the endocytic pathway depends on the progressive acidification of endocytic vesicles driven by the V-ATPase. Such translocation of H^+ from cytosol to endosomes is necessarily coupled with a parallel Cl^- conductance to neutralize the H^+ electrical gradient ($\Delta\Psi$) (Jentsch, 2005). Although the nature of this endosomal Cl^- conductance remains uncertain, recent studies performed in our laboratory on Dent's disease and ClC-5, as well as on CF and CFTR, have postulated a crucial role for Cl^- transporters in PT receptor-mediated endocytosis and intracellular trafficking (Devuyst, 2002; Christensen, 2003). In addition to PT cells, the V-ATPase and ClC-5 co-distribute in the IC of the CD which are mainly involved in acid-base homeostasis. At this location, the V-ATPase complex is located at the plasma membrane and is composed of specific subunits. Mutations in *ATP6B1B1* and *ATP6V0A4* genes encoding such IC-specific subunits of the V-ATPase cause distal RTA in infancy or early childhood (Karet, 2002). The comparative ontogeny of ubiquitous vs. IC-specific V-ATPase isoforms may help characterize the time course of IC differentiation along the developing nephron and the pathophysiology of inherited distal RTA.

In the first part of this work, we investigate the ontogeny of ClC-5 and the V-ATPase in man and mouse kidney development. Our data demonstrate that their segmental distribution in PT cells is essentially achieved during early nephrogenesis, in parallel with the onset of glomerular filtration (**Chapter II**). Conversely, the developmental pattern of the IC-specific V-ATPase subunit isoforms shows a progressive appearance in late nephrogenesis, following the induction of the forkhead transcription factor Foxi1 (**Chapter III**). We further characterize the tissue distribution of a novel V-ATPase subunit (V0 d2) in mice, and find that its segmental

distribution mostly includes the plasma membrane of the IC in both fœtal and adult kidney (**Chapter IV**).

In the second part, we assess the role of CFTR in kidney function (**Chapter V**). We demonstrate that the segmental expression of CFTR, at both the mRNA and protein levels, includes the straight part S3 of the PT, with a subcellular distribution compatible with endosomes. Taking advantage of *Cftr*^{tm1Cam} (KO) and *Cftr*^{tm1Eur} (ΔF508) mutant mice, we next characterize the role of CFTR in PT apical endocytosis, in comparison to the *Clcn5*$^{Y/-}$ mouse model of Dent's disease. Finally, we evaluate the renal handling of LMW proteins in a representative cohort of CF patients harbouring the ΔF508 mutation *vs*. age- and gender-matched controls.

In the last part of the project, we investigate the metabolic and functional consequences of PT dysfunction in ClC-5-deficient mice. Based on differential display results showing a consistent upregulation of the gene *Car3* encoding Type III CA isozyme in *Clcn5*$^{Y/-}$ kidneys, we further address the putative role of this cytosolic protein involved in cell oxidative defences using other mouse models of renal Fanconi syndrome and PT cell cultures (**Chapter VI**). In parallel, we demonstrate the feasibility and the benefits of a small-animal SPECT (single photon emission computed tomography) prototype developed in the Nuclear Medicine Department of our institution to explore PT functions in conscious mice (**Chapter VII**).

These studies provide new insights into the implication of the Cl^- transporters ClC-5 and CFTR and the V-ATPase in renal tubular maturation and in the pathophysiology of inherited tubular disorders.

***

CHAPTER II.

COMPARATIVE ONTOGENY, PROCESSING, AND SEGMENTAL DISTRIBUTION OF THE RENAL CHLORIDE CHANNEL CLC-5

François Jouret[(1)], Takashi Igarashi[(3)], Françoise Gofflot[(2)], Patricia D. Wilson[(4)], Fiona E. Karet[(5)], Rajesh V. Thakker[(6)], and Olivier Devuyst[(1)]

(1) Division of Nephrology and (2) Laboratory of Developmental Genetics, Université catholique de Louvain, Brussels, Belgium; (3) Department of Pediatrics, University of Tokyo, Tokyo, Japan; (4) Division of Nephrology, Mount Sinai Medical School, New York, USA; (5) Department of Medical Genetics, Cambridge University, Cambridge, UK; (6) Nuffield Department of Medicine, University of Oxford, Oxford, UK

***Kidney Int* 65: 198-208, 2004**

Kidney International, Vol. 65 (2004), pp. 198–208

Comparative ontogeny, processing, and segmental distribution of the renal chloride channel, ClC-5

FRANÇOIS JOURET, TAKASHI IGARASHI, FRANÇOISE GOFFLOT, PATRICIA D. WILSON, FIONA E. KARET, RAJESH V. THAKKER, and OLIVIER DEVUYST

Division of Nephrology and Laboratory of Developmental Genetics, Université Catholique de Louvain, Brussels, Belgium; Department of Pediatrics, University of Tokyo, Tokyo, Japan; Division of Nephrology, Mount Sinai Medical School, New York, New York, USA; Department of Medical Genetics, Cambridge University, Cambridge, UK; and Nuffield Department of Medicine, University of Oxford, Oxford, UK

Comparative ontogeny, processing, and segmental distribution of the renal chloride channel, ClC-5.

Background. The renal chloride channel ClC-5, which is responsible for Dent's disease, is coexpressed with the vacuolar H^+-ATPase in proximal tubules (PT) and α-type intercalated cells (IC) of the mature kidney. Neonatal cases of Dent's disease suggest that ClC-5 distribution must be acquired before birth. However, the ontogeny of ClC-5, and its processing and segmental distribution with respect to related proteins during nephrogenesis remain unknown.

Methods. Immunoblotting, real-time polymerase chain reaction (RT-PCR), immunostaining, and deglycosylation studies were used to investigate the expression, distribution, and maturation of ClC-5 during mouse and human nephrogenesis, in comparison with H^+-ATPase, type II carbonic anhydrase (CAII), and aquaporin-1 (AQP1).

Results. An early induction (E13.5-E14.5) of ClC-5 was observed in mouse kidney, with persistence at high levels through late nephrogenesis. This pattern contrasted with the progressive expression of H^+-ATPase and AQP1, and the postnatal upregulation of CAII. Immunostaining showed expression of ClC-5 in ureteric buds and, from E14.5, its location in developing PT. From E15.5, ClC-5 codistributed with H^+-ATPase in PT cells and α-type IC. In the human kidney, ClC-5 was detected from 12 gestation weeks; its distribution was similar to that observed in mouse, except for a later detection in IC. Although mouse and human ClC-5 proteins are glycosylated, biochemical differences between fetal and adult proteins were observed in both species.

Conclusion. The segmental expression of ClC-5 and H^+-ATPase is essentially achieved during early nephrogenesis, in parallel with the onset of glomerular filtration. These data give insight into PT and IC maturation, and explain early phenotypic variants of Dent's disease.

Key words: carbonic anhydrase, Dent's disease, endocytosis, H^+-ATPase, intercalated cells, proximal tubule.

Received for publication February 18, 2003
and in revised form May 31, 2003
Accepted for publication August 11, 2003

ClC-5 is an integral plasma membrane protein that belongs to the CLC family of voltage-gated chloride channels [1]. ClC-5 is encoded by the *CLCN5* gene, which is located on Xp11.22 and is predominantly expressed in the kidney [2]. Mutations in *CLCN5* are associated with Dent's disease, an X-linked renal tubular disorder characterized by low- molecular-weight proteinuria (LMWP) and renal Fanconi syndrome, associated with hypercalciuria, nephrocalcinosis, and nephrolithiasis [3, 4]. Studies in heterologous expression systems have shown that these mutations abolish or markedly reduce the outwardly rectifying chloride currents generated by ClC-5 [3].

The segmental expression of ClC-5 in the mature human and rat kidney includes the proximal tubule (PT), the thick ascending limb (TAL) of Henle's loop, and the α-type intercalated cells (IC) of the collecting duct (CD) [5–7]. The codistribution of ClC-5 with the vacuolar H^+-ATPase in endosomes suggests that both proteins could interact to regulate endosomal acidification [5, 7] and apical targeting [8] in PT cells. The interaction between ClC-5 and H^+-ATPase may also be important for the urinary acidification mediated by α-type IC [5–7]. These hypotheses are supported by the major defect in receptor-mediated endocytosis associated with PT dysfunction reported in ClC-5–deficient mice [9, 10], as well as by the alterations in polarity and expression of H^+-ATPase observed in PT cells and IC from patients with Dent's disease [8].

The clinical manifestations of Dent's disease, including hematuria, proteinuria, mild polyuria, and nephrolithiasis may often occur during childhood, and LMWP is a consistent feature of the disease [4]. In particular, the early onset of some cases [11, 12], in which tubular proteinuria was discovered in the first month of life, suggests that segmental expression of ClC-5 in PT must be acquired before birth. Developmental studies in rats have shown that assembly of brush border components coincides with the onset of glomerular filtration [13], but the

status of other components of the endocytic pathway in PT cells, such as ClC-5 and H^+-ATPase, is not known. Similarly, studies in rat kidney have shown that IC appear during late nephrogenesis and undergo postnatal maturation [14]. However, unlike rats, nephrogenesis in mouse and humans is essentially achieved at birth, and the pattern of appearance and differentiation of IC in these two species remains unclear.

In this study, we have investigated the renal ontogeny, processing, and distribution of ClC-5 during mouse and human nephrogenesis, in parallel with that of the vacuolar H^+-ATPase, which provides the driving force for endosomal acidification in PT cells [15], type II carbonic anhydrase (CAII), which is essential for Na^+ reabsorption and urinary acidification in PT cells [16], and the water channel aquaporin-1 (AQP1) as an ontogeny marker for PT cells [17]. These studies provide new insights into the maturation of PT and IC during nephrogenesis and help to understand the role of ClC-5 and the early phenotypic variants of Dent's disease.

METHODS

Human and mouse kidney samples

Human fetal kidneys from therapeutic abortion were procured by the International Institute for Advancement of Medicine (Philadelphia, PA, USA), the Anatomic Gift Foundation (Woodbine, GA,USA), and the Necker Hospital (Paris, France). Eighteen human fetal kidneys, ranging from 12 to 25 weeks of gestation (GW), were used for immunoblotting and immunostaining studies. For comparison and additional studies, we also used 3 newborn or infant human kidneys ranging in age from 4 months to 2 years. These normal kidneys were obtained directly at surgery and perfused with ice-cold neutral buffered salt solutions before processing for fixation and/or protein extraction [7, 17]. The use of these samples conformed to local ethical guidelines and were approved by the University of Louvain Ethical Review Board.

Mouse kidney samples were obtained from CD-1 mice (Iffa Credo, Brussels, Belgium). Pregnant mice were sacrified by cervical dislocation, and embryos were dissected under a binocular to isolate kidneys. An average of 12 embryos from 4 different litters were collected every day from embryonic day 13.5 (E13.5) until day 5 after birth (newborn). Comparative studies were performed with 4 adult male kidneys. Kidney samples from wild-type versus *ClC-5* knockout (KO) mice [10] and adult male Wistar rats were also used.

Antibodies

Affinity-purified polyclonal antibodies (SB499) directed against the N-terminus of human ClC-5 have been characterized previously [10]. Other antibodies included a monoclonal antibody against the 31 kD E subunit (V1 domain) of the vacuolar H^+-ATPase (a gift of Dr. S. Gluck, Washington University, St. Louis, MO, USA), a rabbit polyclonal antibody against the 116 kD a4 subunit (V0 domain) of the vacuolar H^+-ATPase [18], a monoclonal antibody against β-actin (Sigma, St. Louis, MO, USA), a rabbit polyclonal antibody against AQP1 (Chemicon, Temecula, CA, USA), and sheep polyclonal antibodies against CAII (Serotec, Oxford, UK) and Tamm-Horsfall protein (Biodesign International, Kennebunk, ME, USA).

Immunoblot analyses and deglycosylation studies

Membrane extracts were prepared as previously described [7, 10]. Briefly, kidney samples were homogenized in ice-cold buffer (300 mmol/L sucrose and 25 mmol/L N-2-hydroxyethylpiperazine-N′-2-ethanesulfonic acid made to pH 7.0 with 1 mol/L tris (hydroxymethyl)aminomethane [Tris]) containing Complete™ protease inhibitors (Roche, Vilvoorde, Belgium). The homogenate was centrifuged at 1000*g* for 15 minutes at 4°C, and the resulting supernatant was centrifuged at 100,000*g* for 120 minutes at 4°C. The pellet ("membrane" fraction) was suspended in ice-cold homogenization buffer before determination of protein concentration and storage at –80°C.

Deglycosylation studies were performed on human and mouse kidney extracts and control glycoproteins (Roche). The samples (15 µg total protein) were incubated for 60 to 90 minutes at 37°C with 12 units of N-glycosidase F, as recommended by the manufacturer.

Immunoblotting was performed as previously described [7, 10]. After blocking, membranes were incubated overnight at 4°C with primary antibodies, washed, incubated for 1 hour at room temperature with appropriate peroxidase-labeled antibodies (Dako, Glostrup, Denmark), washed again, and visualized with enhanced chemiluminescence. Normalization for β-actin was obtained after stripping the blots and reprobing with the anti-β-actin antibody. Specificity of the immunoblot was determined by incubation with: (*1*) preimmune rabbit serum; (*2*) nonimmune rabbit or mouse immunoglobulin (Ig)G (Vector Laboratories, Burlingame, CA, USA) or control ascites fluid (Sigma); and (*3*) anti-ClC5 antibody preadsorbed with a 5-fold (w/w) excess of immunogenic peptide. Determination of the molecular mass was obtained by comparison with different precision standards (MBI Fermentas, Vilnius, Lithuana; Bio-Rad, Hercules, CA, USA). Densitometry analysis of the specific bands was performed with a Hewlett Packard Scanjet model IVC using the National Institutes of Health (NIH) Image V1.60 software, and optical densities normalized to β−actin density in the corresponding sample. All immunoblots were at least performed in duplicate.

RT-PCR and semiquantitative RT-PCR

Mouse kidney samples were homogenized in Trizol (Invitrogen, Merelbeke, Belgium) in order to extract total RNA. Total RNA samples (2.7 µg) were treated with DNase I (Invitrogen) and reverse-transcribed into cDNA using SuperScript II Rnase H Reverse Transcriptase (Invitrogen). The following primers were designed using Beacon Designer 2.0 (Premier Biosoft International, Palo Alto, CA, USA): ClC-5 (exon 6) sense 5′AAGTGG ACCCTTGTCATCAA 3′ and antisense 5′ACAAG ATGTTCCCACAGCAG 3′, AQP1 (exons 1–2) sense 5′ GCTGTCATGTATATCATCGCCCAG 3′ and antisense 5′ AGGTCATTTCGGCCAAGTGAGT 3′, GAPDH (exon 1) sense 5′ TGCACCACCAACTGCTTAGC 3′ and antisense 5′ GGATGCAGGGATGATGTTCT 3′. The predicted lengths of the resulting PCR fragments were 115 bp (ClC-5), 107 bp (AQP1), and 176 bp (GAPDH). RT-PCR reactions were performed with 200 nmol/L of both sense and antisense primers in a final volume of 25 µL using 1 unit of Platinum Taq DNA polymerase, 2 mmol/L $MgCl_2$, 400 µmol/L dNTP. PCR conditions were 94°C for 5 minutes followed by 35 (ClC-5), 36 (AQP1), and 30 (GAPDH) cycles of 30 seconds at 95°C, 30 seconds at 61°C, and 1 minute at 72°C. The PCR products were size-fractionated on 1.5% agarose gel and then stained with ethidium bromide. Negative controls confirmed that the samples were not cross-contaminated (sterile water instead of RNA) or polluted by genomic DNA (not reverse-transcribed RNA samples). The expression of ClC-5 was also verified using another set of primers (exons 8–9), sense 5′ TCC GCACAAACATTGCCTG 3′ and antisense 5′ AGGC AGCAGCCCCAACCAT 3′ (predicted length of the fragment: 519 bp).

Real-time PCR analyses were performed in duplicate with 200 nmol/L of both sense and anti-sense primers in a final volume of 25 µL using 1 U of Platinum Taq DNA Polymerase, 2 mmol/L MgSO4, 400 µmol/L dNTP, and SYBR Green I (Molecular Probe, Leiden, The Netherlands) diluted to $1/10^5$. PCR mixture contained 10 nmol/L fluorescein for initial well to well fluorescence normalization. PCR conditions were settled as incubation at 94°C for 3 minutes followed by 40 cycles of 30 seconds at 95°C, 30 seconds at 61°C, and 1 minute at 72°C. The melting temperature of PCR product was checked at the end of each PCR by recording SYBR green fluorescence increase upon slowly renaturating DNA. For each assay, standard curves were prepared by serial 4-fold dilutions of mouse adult kidney cDNA. The mRNA levels of ClC-5 and AQP1 were adjusted to GAPDH mRNA level at each stage, and relative changes in mRNA levels during ontogeny were determined by comparison to the adult mRNA level using the following formula: Ratio = $(E_{target})^{\Delta Ct(Adult-Sample)}/(E_{GAPDH})^{\Delta Ct(Adult-Sample)}$ [19].

Immunostaining

Kidney samples were fixed in 4% paraformaldehyde (Boehringer Ingelheim, Heidelberg, Germany) in 0.1 mol/L phosphate buffer, pH 7.4, prior to embedding in paraffin as described [7, 10, 17]. Six µm sections were incubated for 30 minutes with 0.3% hydrogen peroxide to block endogenous peroxidase. For ClC-5 and H^+-ATPase immunostaining, antigen retrieval was performed by incubating sections in 0.01 mol/L citrate buffer, pH 5.8, for 75 minutes, in a water bath heated at 97°C, before cooling down and rinsing. Following incubation with 10% normal serum for 20 minutes, sections were incubated for 45 minutes with the primary antibodies diluted in phosphate-buffered saline (PBS) containing 2% bovine serum albumin (BSA). After washing, sections were successively incubated with biotinylated secondary anti-immunoglobulin (Ig)G antibodies, avidin-biotin peroxidase, and aminoethylcarbazole (Vectastain Elite, Vector Laboratories). Sections were viewed under a Leica DMR coupled to a Leica DC300 digital camera (Leica, Heerbrugg, Switzerland). The specificity of immunostaining was tested by incubation: (*1*) in absence of primary antiserum; (*2*) with preimmune rabbit serum; (*3*) with non-immune rabbit serum or control rabbit or mouse IgG (Vector Laboratories); and (*4*) with the anti-ClC-5 antibody preadsorbed with the immunogenic peptide. The intensity of immunostaining was graded by an observator unaware of the embryonic stage and the antibody used, in comparison with the intensity observed in adult samples.

RESULTS

Comparative ontogeny of ClC-5 in the mouse kidney

ClC-5 was detected as a broad band at ~80 kD in the adult mouse kidney (Fig. 1A). The band was not detected in kidney extracts from *Clcn5* KO mouse (left panel), or when the blot was incubated with anti-ClC-5 antibodies preadsorbed with the immunogenic peptide (right panel). The signal for ClC-5 observed in embryonic samples was different from the adult (right panel); it included two bands at ~90 kD and ~75 kD, respectively, separated by a smear of diffuse immunoreactive bands. With the exception of the upper band at ~90 kD, all the immunoreactive bands were abolished when using preadsorbed antibodies (right panel).

The expression of ClC-5 in the developing kidney was already detected at E13.5 (Fig. 1B). At this early stage, the immunoreactive pattern was characterized by the non-specific upper band at ~90 kD, and the diffuse specific bands including the ~75 kD band. The signal intensity for ClC-5 peaked early (E14.5), and remained quite stable to E16.5. From E16.5 to the newborn stage, the immunoreactivity pattern for ClC-5 showed a progressive decrease

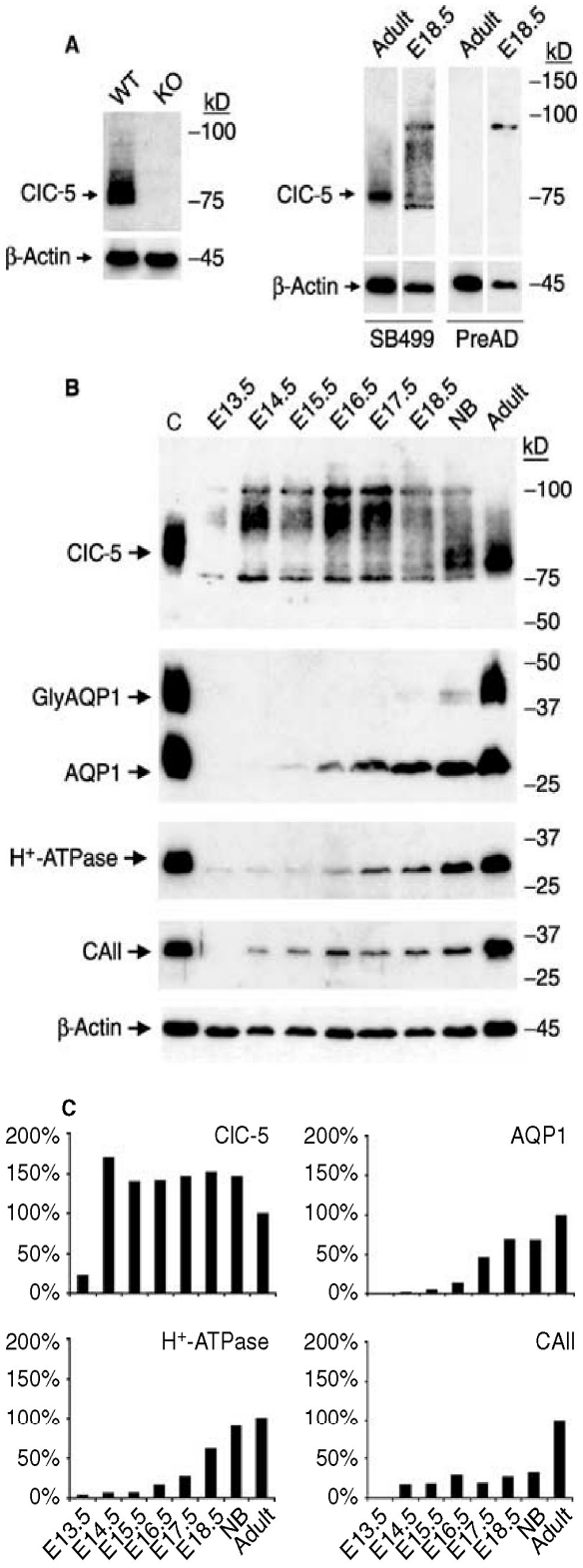

Fig. 1. Comparative ontogeny of ClC-5 in mouse kidney. (*A*) Characterization of the SB499 anti-ClC-5 antibodies. *Left*: Kidney extracts (30 μg/lane) from wild-type (WT) and knockout (KO) *ClCn5* mice were run on 7.5% PAGE and transferred to nitrocellulose. The blot was probed with SB499 anti-ClC-5 antibodies (1:1000). The diffuse band corresponding to ClC-5 at ~80 kD is absent in KO mice. The membranes were stripped and reincubated with a monoclonal antibody against β-actin (1:10,000). *Right*: Adult and fetal (E18.5) mouse kidney extracts (20 μg/lane) were run on 7.5% PAGE and transferred to nitrocellulose. Identical strips were probed with control (SB499; 1:1000) or preadsorbed (PreAd; 1:1000) SB499 anti-ClC-5 antibodies. With the exception of the nonspecific upper band at ~90 kD detected in fetal samples, the distinct signal corresponding to ClC-5 in mature and developing kidney is abolished when incubation is performed with preadsorbed antibodies. Reprobing for β-actin was performed as above. (*B*) Representative immunoblots for ClC-5 in extracts from adult rat (positive control, C) and mouse at different stages—from E13.5 to E18.5, neonates (NB) and adults. Twenty μg of protein were loaded in each lane, and blots were probed with antibodies against ClC-5 (1:1000), AQP1 (1:20,000), H^+-ATPase (1:100), CAII (1:1000), and after stripping, β-actin (1:10,000). ClC-5 is detected at E13.5, upregulated at E14.5, and then sustained during ontogeny. The immunoreactive pattern is also clearly different in the early (higher molecular mass bands) and late stages (focused immunoreactive bands around 75–80 kD) of maturation. The expression of AQP1 and H^+-ATPase gradually increases from E16.5 and during late ontogeny, whereas CAII expression is characterized by post-natal upregulation. (*C*) Expression of ClC-5, AQP1, H^+-ATPase, and CAII during mouse nephrogenesis: densitometry analyses of immunoblots. Values were obtained from duplicate blots and, after normalization over β-actin in each lane, compared with the adult kidney taken as the 100% reference. The early induction of ClC-5 contrasts with the progressive increase in AQP1 and H^+-ATPase, and with the postnatal upregulation of CAII. The densitometry analyses of ClC-5 included all bands detected below the upper, nonspecific band at ~90 kD (see A).

in the higher molecular mass isoforms and apparition of a more focused signal around 75 to 80 kD. Adult samples were characterized by concentrated immunoreactive bands around 80 kD, as described above.

The expression of AQP1 in the kidney is characterized by two isoforms—the core AQP1 (28 kD) and the glycosylated AQP1 (GlyAQP1, 35 to 50 kD). The core AQP1 was detected at E15.5 and it gradually increased during late ontogeny. The GlyAQP1 was detected only at E18.5 and in the newborn kidney, probably reflecting the increased amount of AQP1 [17]. The 31 kD band corresponding to the E1 subunit of the H^+-ATPase was detected at low level from E13.5 and showed a gradual increase from E16.5 to birth. A progressive induction of the 116 kD a4 subunit of the H^+-ATPase from E16.5, in parallel with the E subunit, was observed in developing mouse kidney (data not shown). The CAII band at 30 kD was detected at E14.5, remained stable during all ontogeny, and showed a dramatic increase postnatally (Fig. 1B). Densitometry analysis (Fig. 1C) confirmed the different expression patterns of ClC-5, which peaked at E14.5 (170% of adult level), remained high (140% to 150% of adult level) during ontogeny, and decreased after birth, AQP1 and H^+-ATPase, which showed a gradual increase from E16.5, and CAII, with low expression levels (15% - 30% of adult level) during all ontogeny and a significant postnatal increase.

Quantification of ClC-5 mRNA expression in the developing mouse kidney

Semiquantitative (Fig. 2A) and real-time PCR analyses (Fig. 2B) confirmed the early induction of ClC-5 at

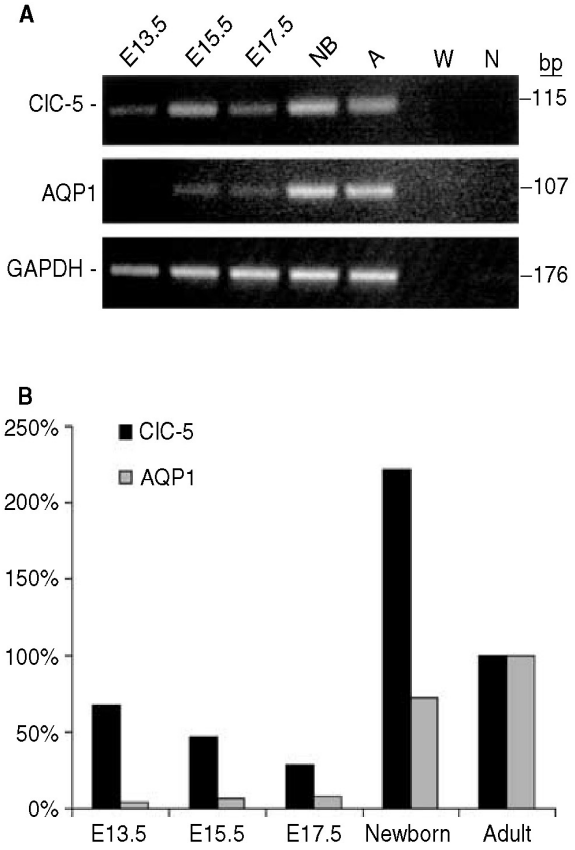

Fig. 2. Differential expression of ClC-5 and AQP1 in the developing mouse kidney: semi-quantitative and real-time PCR analysis. (*A*) Representative semiquantitative RT-PCR analysis of the expression of ClC-5, AQP1, and GAPDH during embryogenesis (E13.5, E15.5, E17.5) and in newborn (NB) and adult (A) mouse kidneys. Negative controls with water (W) and in absence of RT product (N) are shown. (*B*) Quantitative RT-PCR of ClC-5 and AQP1 mRNA expression during mouse nephrogenesis. The primers for ClC-5, AQP1, and GAPDH were similar to those used above. The ClC-5 and AQP1 mRNA levels were adjusted to GAPDH for each stage. The relative changes in expression during ontogeny were determined by comparison to the adult mRNA level taken as 100%. ClC-5 mRNA is significantly expressed at E13.5 (70% of the adult value), with a subsequent decrease until E17.5 (30%) and a major 2-fold upregulation at birth. This expression pattern contrasts with the low level of AQP1 at E13.5 (4% of the adult value) and its gradual increase from E15.5 (6%) to nearly reach the adult level at birth (73%).

E13.5, with a slight decrease of expression during late ontogeny, and a dramatic 2-fold increase in newborns. This expression pattern contrasted with that of the water channel AQP1, which showed a later induction at the end of nephrogenesis to nearly reach the adult level at birth.

Processing of ClC-5 during mouse nephrogenesis: Deglycosylation studies

Sequence analysis predicted that ClC-5 is a glycoprotein with N-glycans linked to Asn at position 408 [3]. Deglycosylation studies with N-glycosidase F were performed in control glycoproteins and developing and adult mouse kidney samples (Fig. 3). Digestion of transferrin (65 to 60 kD), α1-acid glycoprotein (45 to 22 kD), and ribonuclease B (17 to 15 kD) demonstrated the efficiency of deglycosylation (data not shown). Immunoblot analysis showed that untreated embryonic samples (Fig. 3A) are characterized by diffuse immunoreactive ClC-5 bands (asterisk) located below the nonspecific 90 kD band and a specific, core band at ~75 kD (arrow). The latter is above a nonspecific immunoreactive band at 60 kD (arrowhead), which results from incubation in reaction buffer. Untreated adult samples (Fig. 3B) showed the mature ClC-5 band at ~80 kD (asterisk) in addition to the nonspecific band at 60 kD (arrowhead), but not the 75 kD core band (arrow). Treatment with N-glycosidase F yielded a shift of the specific ClC-5–positive bands to a lower apparent molecular weight, indicating the existence of Asn-linked glycan chains in both embryonic and adult samples. To note, the molecular weight of the deglycosylated form of ClC-5 was slightly higher in developing than in mature kidney samples.

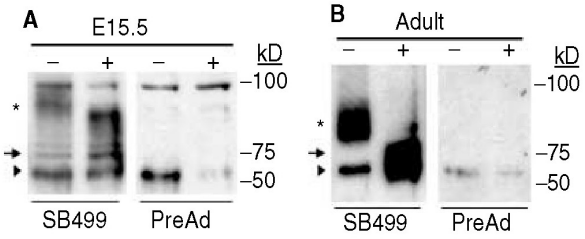

Fig. 3. Processing and glycosylation of ClC-5 in mouse kidney. The samples [(*A*) E15.5; (*B*) adult] were incubated with the reaction buffer containing (+) or not (–) N-glycosidase F, separated (7.5 μg protein/lane) on 7.5% PAGE and probed with anti-ClC5 antibodies alone (SB499) or preadsorbed (PreAd) (both diluted 1:1000). Untreated embryonic samples (A) are characterized by diffuse immunoreactive ClC-5 bands (asterisk), located below the nonspecific 90 kD band, and by a 75 kD band (arrow). Incubation in the reaction buffer yielded a nonspecific immunoreactive band at 60 kD (arrowhead) in all samples. Untreated adult samples (B) do not show the 75 kD band (arrow), but are characterized by a focused band at ~80 kD (asterisk), in addition to the nonspecific band at 60 kD (arrowhead). The shift of ClC-5-positive bands to a lower molecular weight after N-glycosidase F treatment indicates the existence of Asn-linked glycan chains in both embryonic and adult samples. It must be noted that embryonic samples differ from adult by the existence of a 75 kD, PGNase F-insensitive band, as well as by the higher molecular mass of the PGNase F-sensitive proteins in control and treated conditions.

Ontogeny and glycosylation of ClC-5 in the human kidney

The broad immunoreactive band corresponding to ClC-5 was detected by immunoblotting in the developing human kidney at 12GW (Fig. 4A). The intensity of ClC-5 expression was sustained during all nephrogenesis, similar to that observed in the infant kidney. Treatment with N-glycosidase F induced a significant shift of

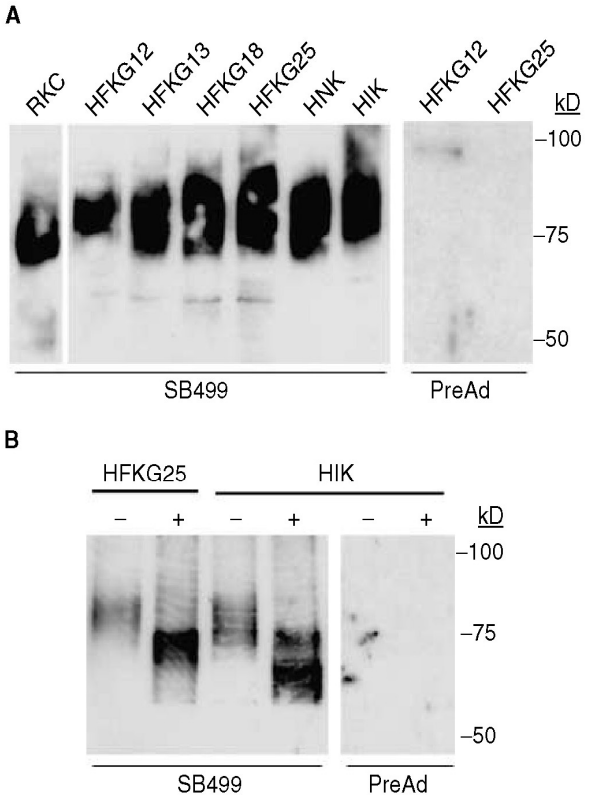

Fig. 4. Ontogeny and glycosylation of ClC-5 in the human kidney. (*A*) Representative immunoblot for ClC-5 in membrane extracts from rat kidney (positive control, RKC), human fetal kidney (HFK) at 12, 13, 18, and 25 GW, newborn (HNK) and infant (HIK) human kidney. Thirty µg of protein were loaded in each lane, and the blot was probed with the anti-ClC-5 antibodies alone (SB499) or preadsorbed (PreAd) (both diluted 1:1000). The broad band corresponding to ClC-5 is detected at 12 GW, and its expression is sustained during nephrogenesis. The ClC-5 signal is abolished when incubation is performed with preadsorbed antibodies. Discrete bands below 60 kD are also detected with nonimmune IgG. (*B*) Deglycosylation with N-glycosidase F in human kidney samples (25 GW, HFK25; infant, HIK). The samples were incubated with the reaction buffer containing (+) or not (–) N-glycosidase F, separated (7.5 µg protein/lane) on 7.5% PAGE and probed with anti-ClC-5 antibodies (SB 499 lanes). The shift of ClC-5 bands to a lower molecular weight confirms the existence of Asn-linked glycan chains. As in mouse, the molecular mass of the PGNase F-sensitive ClC-5 proteins is higher in fetal than in postnatal samples. The pattern observed in HIK samples (more diffuse immunoreactive bands including lower mass isoforms) suggests that they may include residual embryonic isoforms. The signal is abolished when a similar blot is incubated with preadsorbed anti-ClC-5 antibodies (PreAd).

ClC-5–positive bands to a lower molecular weight (Fig. 4B), indicating the existence of Asn-linked glycan chains in developing and mature human kidney samples. As described in mouse, the molecular weight of the deglycosylated form of ClC-5 was higher in fetal than in postnatal samples.

Segmental distribution of ClC-5 during mouse nephrogenesis

ClC-5 was detected in the developing mouse kidney at E13.5 (Fig. 5A). The signal was located in branching

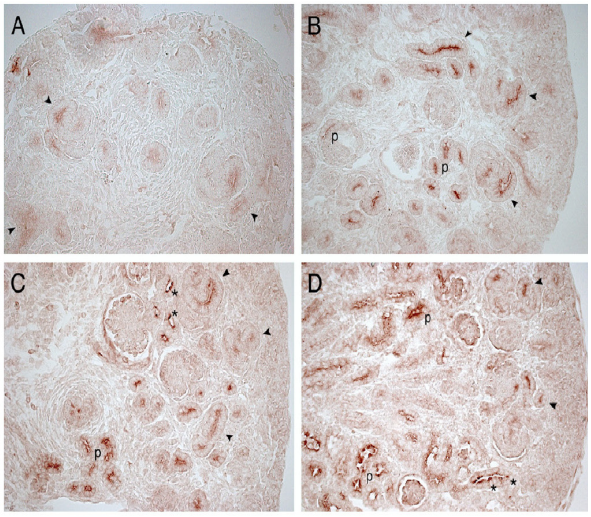

Fig. 5. Immunodetection of ClC-5 in the developing mouse kidney. (A) The staining for ClC-5 is first detected in the ureteric buds (arrowheads) located in the inner part of the primitive cortex at E13.5. (*B*) The staining intensity markedly increases at E14.5, with ClC-5 being located primarily in the ureteric buds (arrowheads) and developing PT (p). (*C*) ClC-5 staining at E15.5 and (*D*) E18.5 is observed in ureteric buds (arrowheads), and its intensity increases in developing PT (p); IC are detected from E15.5 (asterisks). Glomeruli, condensates, comma- and S-shaped bodies are negative (Original magnification A-D, × 150).

ureteric buds within the inner part of the primitive cortex, whereas the undifferentiated metanephric cap tissue, the condensates, and the inner mesenchyme, were negative. Staining intensity for ClC-5 markedly increased at E14.5, by which dispersed primitive glomeruli were identified (Fig. 5B). The staining was stronger in the ureteric buds and also appeared in developing PT. Glomeruli, as well as comma- and S-shaped bodies, were all negative. From E15.5 (Fig. 5C) to E18.5 (Fig. 5D), ClC-5 staining persisted in ureteric buds, became more apparent in developing PT, and gradually appeared in the IC.

At higher magnification (Fig. 6), staining for ClC-5 within the primitive cortex of E14.5 kidneys was identified in the apical area of the tips of ureteric buds (Fig. 6A). A similar staining was observed within branching ureteric buds in the outer part of the primitive medulla (Fig. 6B), whereas an apical staining restricted to a subpopulation of ureteric buds cells was observed in the inner medulla (Fig. 6C). At E15.5, ClC-5 was identified in PT originating from recently formed glomeruli, and scattered CD cells (Fig. 6D and inset). The latter were also stained for apical H^+-ATPase, indicating that they correspond to α-type IC (see below). At E16.5, ClC-5 showed an homogeneous, subapical staining in cells lining developing PT, and a strong apical staining in IC (Fig. 6E). To note, codistribution of ClC-5 (Fig. 6F) and Tamm-Horsfall protein (Fig. 6G) was observed in some juxtaglomerular tubules at E16.5 and later. Distribution of ClC-5 in E18.5 kidneys included the apical area of PT cells and IC of the cortical CD (Fig. 6H), exactly like in newborn mouse (Fig. 6I). Codistribution of ClC-5 (Fig. 6J) and CAII (Fig. 6K)

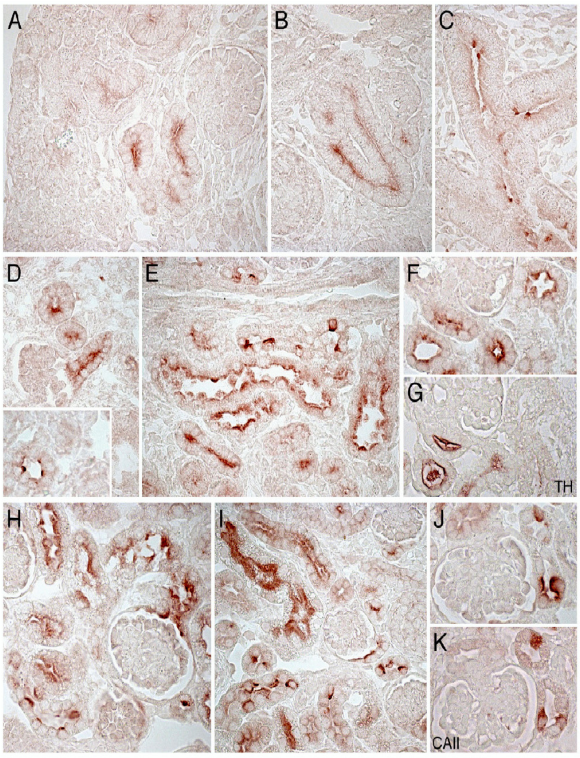

Fig. 6. Segmental distribution of ClC-5 during mouse nephrogenesis. (*A*, *B*, *C*, *D*, *E*, *F*, *H*, *I*, *J*) Immunostaining for ClC-5, (*G*) Tamm-Horsfall protein, and (*K*) CAII in the developing mouse kidney at (A–C) E14.5, (D) E15.5, (E–G) E16.5, (H) E18.5 (H), (I–K) and newborn kidney. At E14.5, staining for ClC-5 is restricted to the apical area of the (A, B) ureteric buds, and in a subpopulation of ureteric buds cells in the (C) inner medulla. At E15.5, ClC-5 is located in developing PT and scattered cells within developing CD in the (D) outer cortex. At (E) E16.5, linear apical ClC-5 staining is detected in PT cells, paralleled by a strong apical staining in IC within CD. Staining on serial sections from E16.5 kidneys shows codistribution of (F) ClC-5 and (G) Tamm-Horsfall protein in juxtaglomerular tubules. The distribution of ClC-5 in PT and IC is exactly similar in (H) E18.5 and (I) newborn kidneys. Staining on serial sections shows the codistribution of (J) ClC-5 and (K) CAII in postnatal IC. (Original magnification: A–C, E, H, I, × 310; D, F, G, J, K, ×410).

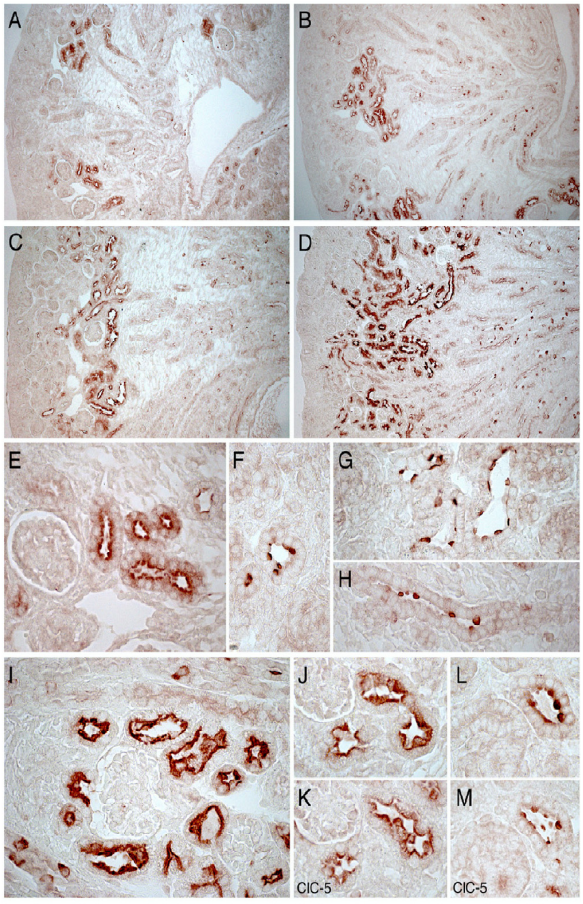

Fig. 7. Segmental distribution of H^+-ATPase in the developing mouse kidney. (*A–L*) Immunostaining for H^+-ATPase, and (*K*, *M*) ClC-5 in the developing mouse kidney at (A, E, F) E15.5 (B, G, H) E16.5 (C, J–M) E18.5, and (D, I) newborn kidney. (A) Staining for H^+-ATPase is detected in developing tubules in the inner cortex at E15.5. (B) A progressive increase in staining is then observed at E16.5, (C) E18.5, and further in the (D) newborn, with a distribution that includes developing PT in the cortex and scattered IC within cortical and medullary CD. (E, F) At E15.5, H^+-ATPase is located in the subapical area of developing (E) PT cells and scattered IC in (F) cortical CD. Numerous positive IC are also detected in the (G) cortical and (H) inner-medullary CD at E16.5. The H^+-ATPase distribution during late ontogeny is similar to that observed in the (I) newborn kidney, including linear, subapical staining in PT cells and focal, apical staining in α-type IC. Staining on serial sections confirmed the colocalization of (K, M) ClC-5 with (J, L) H^+-ATPase in (J, K) PT and (L, M) α-type IC. (Original magnification: A–D, × 80; E, F, I–M: ×330; G, H, × 385).

was observed in postnatal IC. The specificity of ClC-5 staining was demonstrated with preadsorbed SB499 antibodies (data not shown). In comparison with ClC-5, CAII was first identified in IC at E15.5 and PT cells at E16.5, whereas AQP1 was detected in PT cells from E16.5 (data not shown). The distribution of ClC-5 and tubular markers during mouse nephrogenesis is summarized in Table 1.

Segmental distribution of H^+-ATPase during mouse nephrogenesis

Staining for H^+-ATPase was detected in the developing mouse kidney at E15.5 (Fig. 7A). The signal was located in the subapical area of developing PT in the inner cortex (Fig. 7E), whereas ureteric buds, glomeruli and undifferentiated structures were negative. Apical staining for H^+-ATPase was also identified in scattered IC (Fig. 7F). A significant increase in H^+-ATPase expression was detected at E16.5 (Fig. 7B), with staining of developing PT and IC in the cortex and inner medulla (Fig. 7G and H). The IC in the medulla were characterized by apical protrusion into the lumen (Fig. 7H), unlike those observed in the cortex (Fig. 7G). The distribution of H^+-ATPase at E18.5 (Fig. 7C) was similar to that observed in the newborn mouse kidney (Fig. 7D and I) and included PT cells (linear, subapical staining) and IC (punctuated, apical staining). H^+-ATPase (Fig. 7J and L) and ClC-5 (Fig. K and M) colocalized in the developing PT and IC as early as E15.5 (see Table 1 for summary).

Table 1. Distribution of ClC-5, H^+-ATPase, AQP1, and CAII in the developing mouse kidney: Summary

		E13.5	E14.5	E15.5	E16.5	E17.5	E18.5	Newborn
PT	ClC-5	(–)	(+)	(++)	(+++)	(+++)	(+++)	(+++)
	H^+-ATPase	(–)	(–)	(+)	(++)	ND	(+++)	(+++)
	AQP1	(–)	(–)	(–)	(+)	(++)	(+++)	(+++)
	CA II	(–)	(–)	(–)	(+)	ND	(++)	(+++)
CCD	ClC-5	(+)UB tips	(++) UB tips	(++)UB tips Rare IC	(++) UB tips Numerous IC	(++) UB tips Numerous IC	Rare (++) UB tips Numerous IC	Rare (+) UB tips Numerous IC
	H^+-ATPase	(–)	(–)	Rare IC	Numerous IC	ND	Numerous IC	Numerous IC
	AQP1	(–)	(–)	(–)	(–)	(–)	(–)	(–)
	CA II	(–)	(–)	Rare IC	Rare IC	ND	Numerous IC	Numerous IC
MCD	ClC-5	(–)	Rare UB cells	Rare IC	Numerous IC	Numerous IC	Numerous IC	Numerous IC
	H^+-ATPase	(–)	(–)	Rare IC	Numerous IC	ND	Numerous IC	Numerous IC
	AQP1	(–)	(–)	(–)	(–)	(–)	(–)	(–)
	CA II	(–)	(–)	(–)	Rare IC	ND	Numerous IC	Numerous IC

Abbreviations are: PT, proximal tubule; CCD, cortical collecting duct; MCD, medullary collecting duct; UB, ureteric bud; IC, intercalated cells; ND, not done. Intensity of staining was graded as (–), absent; (+), weak; (++), moderate; (+++), strong.

Segmental distribution of ClC-5 and H^+-ATPase in the developing human kidney

Diffuse staining for ClC-5 was identified in 13GW kidneys, located in developing PT from juxtamedullary nephrons (Fig. 8A and C). No specific staining was detected in condensates, comma and S-shaped bodies, and glomeruli. At 19 GW, a slightly more intense staining for ClC-5 was detected in maturing PT (Fig. 8B and D), whereas no specific staining was detected with preadsorbed SB499 antibodies (Fig. 8E). The distribution of ClC-5 in developing PT was confirmed in serial sections stained for AQP1; to note, the staining for AQP1 was more polarized than ClC-5 at that stage (Fig. 8F and G). In juxtamedullary nephrons, ClC-5 was also located in juxtaglomerular tubule profiles that were positive for Tamm-Horsfall protein (Fig. 8H and I). In contrast with CAII (15GW) and H^+-ATPase (19GW), ClC-5 could not be clearly identified in IC until the 24 GW (data not shown). Identification of ClC-5 staining in IC was ascertained postnatally by colocalization with CAII (Fig. 8J and K).

A faint signal for H^+-ATPase (Fig. 9) was detected at 13 GW in the apical area of developing PT in the outer cortex, whereas glomeruli and ureteric buds were negative (Fig. 9A). From 15 GW to 24 GW (Fig. 9B), a progressive increase in H^+-ATPase expression was detected in the subapical area of PT cells. Isolated cells positive for H^+-ATPase (Fig. 9B) were also identified in the CD as early as 19 GW (inset of Fig. 9B). The reactivity for H^+-ATPase after birth included a strong signal in the apical area of PT cells and IC of the CD (Fig. 9C).

DISCUSSION

Our studies show that ClC-5 undergoes a rapid induction at an early stage of mouse nephrogenesis, followed by a progressive maturation during late nephrogenesis. This ontogeny pattern is distinct from the progressive increase of H^+-ATPase and AQP1 expression, and the postnatal induction of CAII. Studies with PGNase F confirm the early N-linked glycosylation of ClC-5, and the progressive maturation of the core protein during nephrogenesis. The distribution of ClC-5 in PT and α-type IC, and its colocalization with H^+-ATPase in these locations, are already achieved at E15.5 (see Table 1 for summary). In human nephrogenesis, ClC-5 is detected early during the second trimester, with a distribution that includes developing PT cells and later, IC.

Nephrogenesis in mouse and humans is characterized by a repetitive and reciprocal induction between the ureteric bud and the metanephric mesenchyme, resulting in the formation of a mature kidney before birth. In other species, such as rat or rabbit, nephrogenesis continues after birth ([20] for review). Glomerular filtration starts at E14 in mouse [21], and between the 9th and 12th GW in the human kidney [22]. The molecular events that take place in renal tubular cells following the onset of glomerular filtration remain partially unknown. The reabsorption of LMW proteins that are freely filtered is confined to PT cells, which are characterized by an intense endocytic activity followed by transport and degradation into the acidic vacuolar-lysosomal system [23]. Indirect evidence in rats [24] and humans [25] suggests that the PT endocytic activity is effective during nephrogenesis or immediately after birth. Furthermore, an increase of transporting membrane area and CA activity, as well as the upregulation of AQP1, has been documented in PT cells during nephrogenesis [17, 22, 26]. In contrast, the ontogeny and distribution of intracellular transporters such as ClC-5 and H^+-ATPase during nephrogenesis have not been characterized to date. The issue is particularly relevant for PT maturation, since several lines of evidence suggest that ClC-5 interacts with the vacuolar H^+-ATPase [8] and plays an essential role in the megalin receptor-mediated endocytic pathway [5, 7, 9, 10].

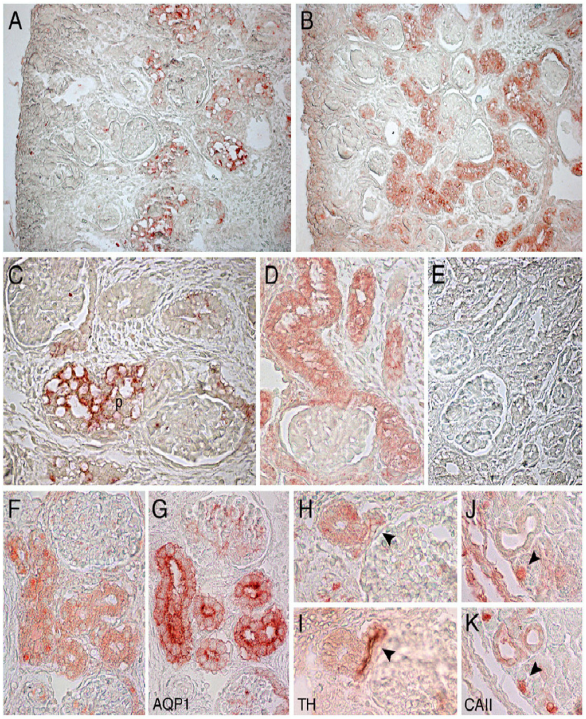

Fig. 8. Segmental distribution and co-localization of ClC-5 in the developing human kidney. Immunostaining for (*A–F*, *H*, *J*) ClC-5, (*G*) AQP1, (*I*) Tamm-Horsfall protein, and (*K*) CAII in the developing human kidney at (A, C) 13 GW, (E) 17 GW, (B, D) 19 GW, (F–I) 24 GW, and in a (J, K) 4-month infant kidney. Diffuse staining for ClC-5 is identified in developing PT (p) from juxtamedullary nephrons at 13GW, whereas (A, C) glomeruli are negative. A similar pattern is observed at 19 GW, with a slightly more intense staining for ClC-5 in maturing (B, D) PT. No specific staining is observed when using preadsorbed SB499 antibodies on similar sections (E). Staining on serial sections from 24 GW human kidneys demonstrated the colocalization of (F) ClC-5 and (G) AQP1 in PT. ClC-5 is also located in juxtamedullary tubule profiles (H, arrowheads) positive for (I) Tamm-Horsfall protein. Identification of ClC-5 staining in IC (J, arrowhead) is confirmed by colocalization with (K) CAII in serial sections from a 4-month-old kidney. (Original magnification: A, B, × 150; C, J, K, × 300; D, E, H, I, ×320; F, G, × 280).

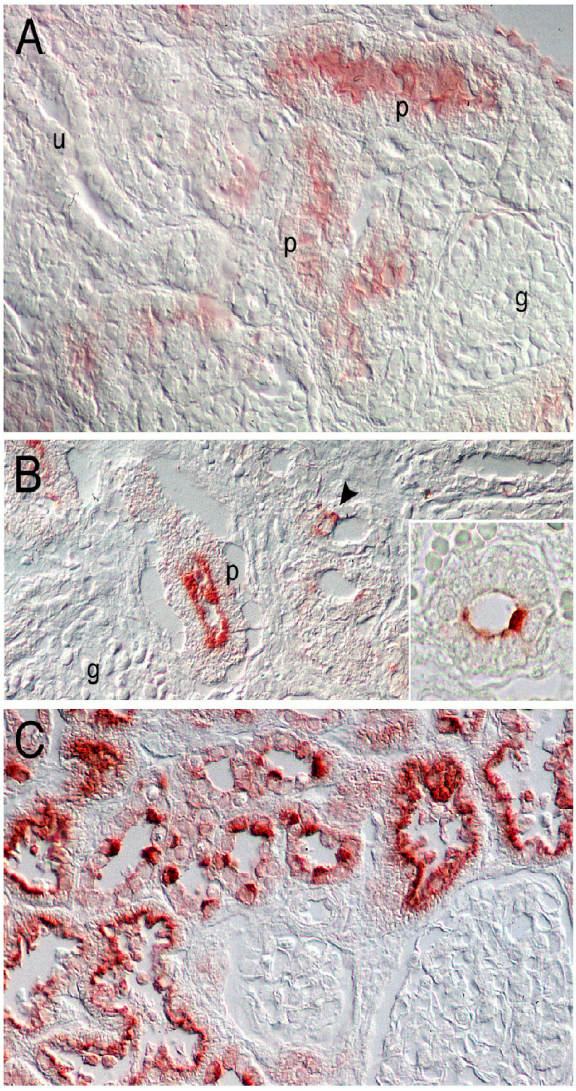

Fig. 9. Segmental distribution of H^+-ATPase during human nephrogenesis. (*A*) At 13 GW, a faint signal for H^+-ATPase is detected in the apical region of the developing PT (p) in the outer cortex. Glomeruli (g) and ureteric buds (u) are negative. (*B*) At 24 GW, H^+-ATPase is located in PT cells (p) and IC (arrowhead). To note, the latter are already positive for H^+-ATPase at 19 GW (inset). (*C*) Typical staining for H^+-ATPase in a 2-year-old kidney includes PT cells and α-type IC within CD. (Original magnification: A, × 225; B–D, × 425).

Immunoblotting and RT-PCR analyses show that ClC-5 undergoes a rapid induction in the developing mouse kidney, followed by progressive maturation during late ontogeny and a marked induction just after birth (Figs. 1 and 2). Thus, the developmental pattern of ClC-5 expression in mouse clearly differs from that of another glycoprotein such as AQP1, or the co-expressed H^+-ATPase. Studies with PGNase F not only confirmed the early N-glycosylation of ClC-5 [30] but also demonstrated biochemical differences between embryonic and adult ClC-5 proteins. These differences include the higher molecular mass of the PGNase F-sensitive proteins in embryonic versus adult samples, as well as the specific expression in mouse embryonic samples of a ClC-5 isoform (~75 kD) that is resistant to PGNase F treatment and that may correspond to the "core" ClC-5 protein (Fig. 3). By analogy with other members of the CLC family, the complex maturation of ClC-5 may result from alternative splicing [27, 28], post-translational modifications [29], or covalent binding to proteins that are expressed during nephrogenesis [20]. It is tempting to hypothesize that the transient expression of immature ClC-5 isoforms during ontogeny may correspond to the signal observed in ureteric buds, where there is no colocalization with H^+-ATPase, whereas a progressive increase in mature ClC-5 isoforms may actually parallel the induction of H^+-ATPase during late nephrogenesis. These results, and the postnatal regulation of CAII (Fig. 1C), confirm recent evidence showing that differentially regulated genes, including transporters, ion-motive ATPases, and enzymes, can be grouped in clusters that participate in different steps of kidney organogenesis [31].

As summarized in Table 1, the segmental expression of ClC-5 and H^+-ATPase in PT cells is already detected at

E15.5 in mouse (Figs. 5 to 7), and essentially achieved during the second trimester of gestation in humans (Fig. 8). These results complete early observations that the apical expression of brush border components and the distribution of megalin to the apical clathrin-coated membrane domains and endosomes coincide with the onset of glomerular filtration in rats [13, 32]. The coexpression of ClC-5 and H^+-ATPase in PT cells immediately after initiation of glomerular filtration could thus indicate the progressive maturation of renal tubular function and explain the decrease in the concentration of LMW proteins in the amniotic fluid during gestation [25]. These data also help to understand the pathophysiology of early phenotypic variants of Dent's disease, in which LMWP has been identified during the first weeks of life [11, 12].

In addition to PT cells, ClC-5 and H^+-ATPase are codetected from E15.5 in the apical area of isolated cells within the CD. The apical polarity of both markers allow to identify these cells as α-type IC, which, in the mature kidney, are primarily involved in urinary acidification. Studies in rat have shown that α-type IC simultaneously express H^+-ATPase and CAII at the end of the gestation, mature and increase in number during the first weeks of life, and are then partially removed from the CD [14, 33]. Our results provide additional informations on IC maturation in mouse and human nephrogenesis. In mouse nephrogenesis, isolated cells of the medullary ureteric buds, positive for ClC-5, are detected as early as E14.5. IC positive for ClC-5, H^+-ATPase, and CAII are observed in the cortical CD at E15.5. In human nephrogenesis, isolated cells positive for CAII are identified within ureteric buds and medullary CD at 15 GW, and rare, isolated cells positive for H^+-ATPase are identified at 19 GW. In contrast, ClC-5 could not be identifed in IC before 24 GW. The colocalization of ClC-5 with CAII and/or H^+-ATPase in IC was only observed postnatally, confirming data obtained in mature kidney [5, 7]. These results suggest species differences in the maturation of IC [14, 33] and support the hypothesis that, in humans, the differentiation of IC occurs later than that of the principal cells of the CD [17]. Finally, ClC-5 is also located in tubules positive for Tamm-Horsfall protein, a marker of maturation of the TAL of Henle's loop [34]. The location of ClC-5 in maturing TAL confirms observations in mature human and rat kidney [6, 7]. It has been speculated that ClC-5 could play a role in the regulated Ca^{2+} reabsorption that occurs in TAL [35], providing a potential explanation for the hypercalciuria observed both in Dent's disease [4] and *ClCn5* KO mice [10].

CONCLUSION

Our data demonstrate that the segmental distribution of ClC-5 and H^+-ATPase is essentially achieved during early nephrogenesis in mouse and the second trimester of gestation in humans. These data provide new insights in the maturation of renal tubules and help to understand the pathophysiology of early phenotypic variants of Dent's disease.

ACKNOWLEDGMENTS

We are grateful to P.J. Courtoy, N.Y. Loh, M-Cl. Gubler, R. Rezsohazy, and F. Wu for helpful discussions and material, and to Ph. Camby, Y. Cnops, H. Debaix, and L. Wenderickx for excellent technical assistance. The *Clcn5* KO mice were kindly provided by W.B. Guggino (Dept. of Physiology, Johns Hopkins University Medical School, Baltimore, MD, USA). This work was supported by the Belgian agencies FNRS and FRSM, the Foundation Alphonse et Jean Forton, the Action de Recherches Concertées 00/05-260, and the Wellcome Trust (UK) and MRC (UK). F.J. is a Research Fellow of the FNRS.

Reprint requests to Olivier Devuyst, M.D., Ph.D., Division of Nephrology, Université catholique de Louvain, 10 Avenue Hippocrate, B-1200 Brussels, Belgium.
E-mail: devuyst@nefr.ucl.ac.be

REFERENCES

1. JENTSCH TJ, STEIN V, WEINREICH F, ZDEBIK AA: Molecular structure and physiological function of chloride channels. *Physiol Rev* 82:503–568, 2002
2. FISHER SE, BLACK GC, LLOYD SE, *et al*: Isolation and partial characterization of a chloride channel gene which is expressed in kidney and is a candidate for Dent's disease (an X-linked hereditary nephrolithiasis). *Hum Mol Genet* 3:2053–2059, 1994
3. LLOYD SE, PEARCE SH, FISHER SE, *et al*: A common molecular basis for three inherited kidney stone diseases. *Nature* 379:445–449, 1996
4. SCHEINMAN SJ: X-linked hypercalciuric nephrolithiasis: Clinical syndromes and chloride channel mutations. *Kidney Int* 53:3–17, 1998
5. GÜNTHER W, LÜCHOW A, CLUZEAUD F, *et al*: ClC-5, the chloride channel mutated in Dent's disease, co-localizes with the proton pump in endocytotically active kidney cells. *Proc Natl Acad Sci USA* 95:8075–8080, 1998
6. LUYCKX VA, GODA FO, MOUNT DB, *et al*: Intrarenal and subcellular localization of rat ClC-5. *Am J Physiol* 275:F761–F769, 1998
7. DEVUYST O, CHRISTIE PT, COURTOY PJ, *et al*: Intra-renal and subcellular distribution of the human chloride channel, CLC-5, reveals a pathophysiological basis for Dent's disease. *Hum Mol Genet* 8:247–257, 1999
8. MOULIN P, IGARASHI T, VAN DER SMISSEN P, *et al*: Altered polarity and expression of H^+-ATPase without ultrastructural changes in kidneys of Dent's disease patients. *Kidney Int* 63:1285–1295, 2003
9. PIWON N, GÜNTHER W, SCHWAKE M, *et al*: ClC-5 Cl^-channel disruption impairs endocytosis in a mouse model for Dent's disease. *Nature* 408:369–373, 2000
10. WANG SS, DEVUYST O, COURTOY PJ, *et al*: Mice lacking renal chloride channel, CLC-5, are a model for Dent's disease, a nephrolithiasis disorder associated with defective receptor-mediated endocytosis. *Hum Mol Genet* 9:2937–2945, 2000
11. NAKAZATO H, HATTORI S, FURUSE A, *et al*: Mutations in the ClCN5 gene in Japanese patients with familial idiopathic low molecular weight proteinuria. *Kidney Int* 52:895–900, 1997
12. BOSIO M, BIANCHI ML, LLOYD SE, THAKKER RV: A familial syndrome due to Arg648Stop mutation in the X-linked renal chloride channel gene. *Pediatr Nephrol* 13:278–283, 1999
13. BIEMESDERFER D, DEKAN G, ARONSON P, FARQUHAR MG: Assembly of distinctive coated pit and microvillar microdomains in the renal brush border. *Am J Physiol* 262:F55–F67, 1992
14. KIM J, TISHER CC, MADSEN KM: Differentiation of intercalated cells in developing rat kidney: An immunohistochemical study. *Am J Physiol* 266:F977–F990, 1994
15. MELLMAN I, FUCHS R, HELENIUS A: Acidification of the endocytic and exocytic pathways. *Annu Rev Biochem* 55:663–700, 1986

16. HAMM LL, ALPERN RJ: Cellular mechanisms of renal tubular acidification, in *The Kidney: Physiology and Pathophysiology*, edited by Seldin DW, Giebisch G, Philadelphia, Lippincott Williams & Wilkins, 2000, pp 1935–1979
17. DEVUYST O, BURROW CR, SMITH BL, *et al*: Expression of aquaporins-1 and -2 during nephrogenesis and in autosomal dominant polycystic kidney disease. *Am J Physiol* 271: F169–F183, 1996
18. SMITH AN, SKAUG J, CHOATE KA, *et al*: Mutations in ATP6N1B, encoding a new kidney vacuolar proton pump 116-kD subunit, cause recessive distal renal tubular acidosis with preserved hearing. *Nat Genet* 26:71–75, 2000
19. PFAFFI MW: A new mathematical model for relative quantification in real-time RT-PCR. *Nucleic Acids Research* 29:2004–2007, 2001
20. KUURE S, VUOLTEENAHO R, VAINIO S: Kidney morphogenesis: Cellular and molecular regulation. *Mech Develop* 92:31–45, 2000
21. LOUGHNA S, LANDELS E, WOOLF AS: Growth factor control of developing kidney endothelial cells. *Exp Nephrol* 4:112–118, 1996
22. BAUM M, QUIGLEY R: Postnatal renal development, in *The Kidney: Physiology and Pathophysiology*, edited by Seldin DW, Giebisch G, Philadelphia, Lippincott Williams & Wilkins, 2000, pp 703–725
23. CHRISTENSEN EI, NIELSEN S: Structural and functional features of protein handling in the kidney proximal tubule. *Semin Nephrol* 11:414–439, 1991
24. SMAOUI H, SCHAEVERBEKE M, MALLIE JP, SCHAEVERBEKE J: Transplacental effects of gentamicin on endocytosis in rat renal proximal tubule cells. *Pediatr Nephrol* 8:447–450, 1994
25. MUSSAP M, FANOS V, PICCOLI A, *et al*: Low molecular mass proteins and urinary enzymes in amniotic fluid of healthy pregnant women at progressive stages of gestation. *Clin Biochem* 29:51–56, 1996
26. LÖNNERHOLM G, WISTRAND PJ: Carbonic anhydrase in the human fetal kidney. *Pediatr Res* 17:390–397, 1983
27. BORSANI G, RUGARLI EI, TAGLIALATELA M, *et al*: Characterization of a human and murine gene (CLCN3) sharing similarities to voltage-gated chloride channels and to a yeast integral membrane protein. *Genomics* 27:131–145, 1995
28. LAMB F, GRAEFF RW, CLAYTONGH, *et al*: Ontogeny of CLCN3 chloride channel gene expression in human pulmonary epithelium. *Am J Respir cell Mol Biol* 24:376–381, 2001
29. SHAILUBHAI K, SAXENA ES, BALAPURE AK, VIJAY IK: Developmental regulation of glucosidase I, an enzyme involved in the processing of asparagine-linked glycoproteins in rat mammary gland. *J Biol Chem* 265:9701–9706, 1990
30. ROTH J: Protein n-glycosylation along the secretory pathway: Relationship to organelle topography and function, protein quality control, and cell intercations. *Chem Rev* 102:285–303, 2002
31. STUART RO, BUSH KT, NIGAM SK: Changes in global gene expression patterns during development and maturation of the rat kidney. *Proc Natl Acad Sci USA* 98:5649–5654, 2001
32. SAHALI D, MULLIEZ N, CHATELET F, *et al*: Comparative immunochemistry and ontogeny of two closely related coated pit proteins. The 280-kd taget of teratogenic antibodies and the 330-kd taget of nephritogenic antibodies. *Am J Pathol* 142:1654–1667, 1993
33. NARBAITZ R, VANDORPE D, LEVINE DZ: Differentiation of renal intercalated cells in fetal and postnatal rats. *Anat Embryol (Berl)* 183:353–361, 1991
34. ZIMMERHACKL LB, ROSTASY K, WIEGELE G, *et al*: Tamm-Horsfall protein as a marker of tubular maturation. *Pediatr Nephrol* 10: 448–452, 1996
35. RICCARDI D, LEE WS, LEE K, *et al*: Localization of the extracellular Ca^{2+}-sensing receptor and PTH/PTHrH receptor in rat kidney. *Am J Physiol* 271:F951–F956, 1996

CHAPTER III.

UBIQUITOUS AND KIDNEY-SPECIFIC SUBUNITS OF THE V-ATPASE ARE DIFFERENTIALLY EXPRESSED DURING NEPHROGENESIS

François Jouret[(1)], Céline Auzanneau[(2)], Huguette Debaix[(1)], Ge-Hong Sun Wada[(3)], Chrystel Pretto[(2)], Etienne Marbaix[(2)], Fiona E. Karet[(4)], Pierre J. Courtoy[(2)] and Olivier Devuyst[(1)]

(1) Division of Nephrology and (2) Christian de Duve Institute of Cellular Pathology, CELL Unit, Université catholique de Louvain, Brussels, Belgium; (3) Doshisha University, Kyoto, Japan; (4) Department of Medical Genetics, Cambridge University, Cambridge, UK.

***J Am Soc Nephrol* 16: 3235-46, 2005**

Ubiquitous and Kidney-Specific Subunits of Vacuolar H^+-ATPase Are Differentially Expressed during Nephrogenesis

François Jouret,* Céline Auzanneau,† Huguette Debaix,* Ge-Hong Sun Wada,‡ Chrystel Pretto,† Etienne Marbaix,† Fiona E. Karet,§ Pierre J. Courtoy,† and Olivier Devuyst*

*Division of Nephrology and †ICP Cell Unit, Université catholique de Louvain, Brussels, Belgium; ‡Doshisha University, Kyoto, Japan; and §Department of Medical Genetics, Cambridge University, Cambridge, United Kingdom

The vacuolar H^+-ATPase (V-ATPase) is a ubiquitous multisubunit pump that is responsible for acidification of intracellular organelles. In the kidney, a particular form of V-ATPase, made of specific subunits isoforms, has been located at the plasma membrane of intercalated cells (IC). Mutations in genes encoding IC-specific subunits cause infant distal renal tubular acidosis (dRTA), suggesting that the segmental distribution of these subunits is acquired at birth or during early infancy. However, the comparative ontogeny of the IC-specific *versus* the ubiquitous subunits of V-ATPase and the mechanisms involved in their segmental expression remain unknown. Real-time reverse transcription–PCR, *in situ* hybridization, immunoblotting, immunostaining, and subcellular fractionation analyses characterized the expression and distribution of V-ATPase subunits, transcription factors, and differentiation markers during mouse nephrogenesis. Ubiquitous A, E1, B2, G1, and C1 subunits showed an early (embryonic day 13.5 [E13.5]) and stable expression throughout nephrogenesis, followed by a slight increase around birth. The developmental pattern of a1 was bimodal, with early induction, gradual decrease during organogenesis, and neonatal increase. These patterns contrasted with the later (from E15.5) and progressive expression of IC-specific a4, B1, G3, and C2 subunits, after the induction of the forkhead transcription factor Foxi1. From E15.5, Foxi1 mRNA was detected in IC, where it co-distributed with B1 in late nephrogenesis. Immunostaining showed that the distribution of ubiquitous E1 and B2 was acquired from E15.5, whereas a4 was located in IC during late nephrogenesis. Subcellular fractionation showed that in both fetal and mature (cortex and medulla) kidneys, E1 and a4 were located in endosomes. These data demonstrate a differential expression and a coordinate regulation of IC-specific *versus* ubiquitous V-ATPase subunits during nephrogenesis. They provide new insights into the complex regulation of V-ATPase subunits, the maturation of IC along the nephron, and the pathophysiology of hereditary dRTA.

J Am Soc Nephrol 16: 3235–3246, 2005. doi: 10.1681/ASN.2004110935

The vacuolar-type proton ATPase (V-ATPase) is a ubiquitous multisubunit pump that is essential for the acidification of intracellular organelles by coupling ATP hydrolysis to transmembrane proton transport (1). The V-ATPase has been located in a variety of intracellular compartments, including clathrin-coated vesicles, endosomes, and lysosomes. Acidification of these intracellular organelles is a prerequisite for a number of important intracellular processes, such as ligand-receptor dissociation, receptor recycling and ligand degradation, storage, or intracellular targeting (2). In addition to its intracellular distribution, V-ATPase has been located in the plasma membrane of specialized epithelial cells of the kidney and epididymis, as well as in the ruffled border membrane of osteoclasts, where it functions in urinary or semen acidification and in bone resorption, respectively (3).

The structure of V-ATPase includes at least 13 different subunits that form two functional domains, V0 and V1 (Figure 1) (3,4). According to quantitative amino acid analysis, the transmembrane V0 domain contains five different subunits that are organized into a complex that is responsible for proton translocation. The cytosolic V1 domain, which involves eight subunits, catalyzes ATP hydrolysis and provides the energy necessary for active proton transport. When located to the plasma membrane, the overall structure of V-ATPase is very similar, but specific isoforms of V0 and V1 subunits are present (5).

The subunit isoforms of the V-ATPase are encoded by distinct genes, with tissue-specific expression patterns. In the kidney, the V-ATPase is essentially distributed in two cell types that are involved in acid–base homeostasis: the proximal tubule cells (PTC) and the intercalated cells (IC) of the collecting duct (CD) (5,6). In PTC, the V-ATPase has been located on the apical side, where it participates in HCO_3^- reabsorption (7). In addition, V-ATPase is responsible for correct vesicular acidification along

Received November 12, 2004. Accepted July 26, 2005.

Published online ahead of print. Publication date available at www.jasn.org.

Address correspondence to: Dr. Olivier Devuyst, Division of Nephrology, Université catholique de Louvain, 10 Avenue Hippocrate, Brussels, Belgium B-1200. Phone: +32-2-764-1855; Fax: +32-2-764-5455; E-mail: devuyst@nefr.ucl.ac.be

ISSN: 1046-6673/1611-3235

3236 Journal of the American Society of Nephrology J Am Soc Nephrol 16: 3235–3246, 2005

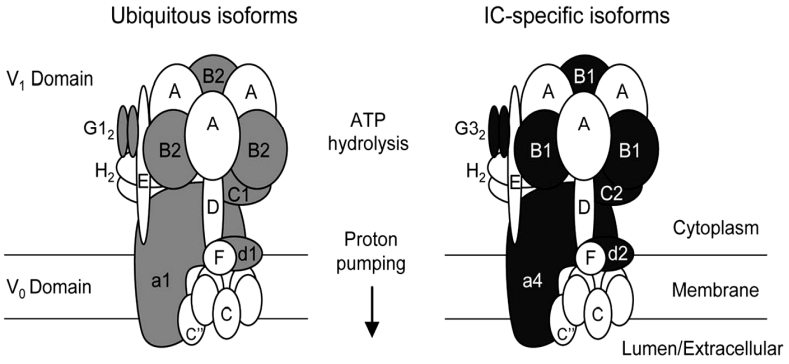

Figure 1. Structural model of the vacuolar type H^+-ATPase (V-ATPase). The transmembrane V0 domain of the mammalian V-ATPase is organized into a complex of $a(c)_{4\text{ to }5}\,c''d$, whereas the cytosolic V1 domain has a stoichiometry of $A_3B_3CDEFG_2H_2$. The ubiquitous and the intercalated cell (IC)-specific alternate isoforms of V0 and V1 subunits are colored. In the plasma membrane of murine IC, a4, d2, B1, C2, and G3 substitute ubiquitous a1, d1, B2, C1, and G1, respectively. This model was modified from the yeast model to represent the mammalian V-ATPase complex (adapted with permission from reference 5). Note that the presence of up to three copies of each E and G per V-ATPase complex has been suggested from analysis of Coomassie staining (4) and that the existence of the c′ subunit in mammals is uncertain (42).

the endocytic pathway, which is essential for receptor-mediated endocytosis and proper intracellular membrane targeting (8). In IC, a specialized form of V-ATPase, made of tissue-specific V0 and V1 subunits isoforms, mediates transepithelial proton transport, ensuring correct urinary acidification (7).

Despite the pivotal role of V-ATPase in acid–base homeostasis, the ontogeny of its subunits in the nephron remains unknown. During pre- and postnatal nephrogenesis, the expression and maturation of several transporters implicated in acid–base homeostasis is tightly regulated to compensate the acid-generating process of growth (9,10). Term neonates are indeed characterized by lower values of blood pH than adults, reflecting an incomplete kidney maturation to reabsorb HCO_3^- (11). The targeted disruption of the V0 c subunit in mouse leads to early fetal lethality by lack of postimplantation development (12). By contrast, mutations in *ATP6V0A4* and *ATP6V1B1* genes, encoding IC-specific V0 a4 and V1 B1 subunits, respectively (13–15), have been associated with early-onset cases of distal renal tubular acidosis (dRTA), which suggests that the segmental distribution of IC-specific isoforms of V-ATPase could be acquired during early infancy.

In this study, we used real-time reverse transcription–PCR (RT-PCR) and *in situ* hybridization, coupled with immunoblotting and immunostaining analyses, to establish the comparative ontogeny of ubiquitous *versus* IC-specific subunits of V-ATPase during mouse nephrogenesis. In addition, on the basis of the structural model of V-ATPase (4), we assessed the relative mRNA expression of alternate isoforms in the adult mouse kidney. Finally, the subcellular distribution of V-ATPase subunits in the developing and mature kidney was compared with endosomal and lysosomal markers by analytical subcellular fractionation.

Materials and Methods

Mouse Kidney Samples

All samples were obtained from CD-1 mice (Iffa Credo, Brussels, Belgium), in accordance with National Institutes of Health guidelines for the care and use of laboratory animals and with the approval of the Committee for Animal Rights of the Université catholique de Louvain. Fetuses were removed and microdissected to isolate kidneys. Embryos from four different litters (average 12 embryos per litter) were collected daily from embryonic day 13.5 (E13.5) until day 5 after birth (newborn). Comparative studies were performed with eight 12-wk-old male kidneys.

Real-Time RT-PCR

Mouse kidney samples were homogenized in Trizol (Invitrogen, Merelbeke, Belgium) to extract total RNA. Total RNA samples (2.7 μg) were treated with DNase I (Invitrogen) and reverse-transcribed into cDNA using SuperScript II RNase H Reverse Transcriptase (Invitrogen). Specific primers for V-ATPase subunits, Foxi1, Pendrin (PDS), glyceraldehyde-3-phosphate dehydrogenase (GAPDH), cyclophilin, and hypoxanthine guanine phosphoribosyl transferase (HPRT1) were designed using Beacon Designer 2.0 (Premier Biosoft International, Palo Alto, CA) and are summarized in Table 1. Real-time PCR analyses were performed in duplicate with 200 nM of both sense and antisense primers in a final volume of 25 μl using 1 unit of Platinum TaqDNA Polymerase, 2 mM $MgSO_4$, 400 μM dNTP, and SYBR Green I (Molecular Probe, Leiden, The Netherlands) diluted to $1:10^5$. The PCR mixture contained 10 nM fluorescein for initial well-to-well fluorescence normalization. PCR conditions were settled as incubation at 94°C for 3 min followed by 40 cycles of 30 s at 95°C, 30 s at 61°C, and 1 min at 72°C. The melting temperature of PCR product was checked at the end of each PCR by recording SYBR green fluorescence increase upon slowly renaturating DNA. For each assay, standard curves were prepared by serial four-fold dilutions of mouse adult kidney cDNA. The efficiencies of the amplifications with each primer set were calculated from the slope of the standard curve [efficiency = $(10^{-1/\text{slope}}) - 1$] and were close to 100% (Table 1).

The relative mRNA expression of the various isoforms (A, a1, B2, E1, G1, C1, a4, B1, G3, and C2) was investigated in adult male kidneys (n = 8), after normalization to HPRT1, cyclophilin, and GAPDH [Ratio = $2^{\Delta Ct\,(\text{Reporter} - \text{Target Gene})}$]. The relative changes in mRNA levels of these alternate isoforms during ontogeny were determined by comparison with the adult mRNA level, after adjustment to GAPDH [Ratio = $(\text{Efficiency}_{\text{target gene}})^{\Delta Ct(\text{Adult} - \text{Sample})} / (\text{Efficiency}_{\text{GAPDH}})^{\Delta Ct\,(\text{Adult} - \text{Sample})}$]

Table 1. Primers used for real-time RT-PCR[a]

Primer Pair	Forward	Reverse	Length (bp)	Efficiency
V-ATPase				
Atp6v0a1	5′-GCTTGGGAAGGTCCAATTTC-3′	5′-GGCACCTCTGGGTTTTCACCG-3′	174	1.02 ± 0.01
Atp6v0a4	5′-CCCTGTATGGACATCAGCAA-3′	5′-GATTTCTGGTGCTTGGCTCT-3′	115	1.02 ± 0.04
Atp6v1e1	5′-GGCGCTCAGCGATGCAGATGT-3′	5′-CAAGGCGACCTTTCTCAATG-3′	134	1.05 ± 0.01
Atp6v1a1	5′-CGTCAGTATGATGGCCGACT-3′	5′-ACTCTGCCTGCTCGCTCATA-3′	147	0.99 ± 0.01
Atp6v1b1	5′-TGGACCAGGTCAAGTTTGC-3′	5′-CCCTGAAGTCCCTTCAAACA-3′	134	1.05 ± 0.02
Atp6v1b2	5′-TGAGCCGGAACTACCTATCCCA-3′	5′-GTGCCATCTGGTAATGTCAAGTGG-3′	136	1.01 ± 0.01
Atp6v1c1	5′-GGAAGTTTGCTAACGCGAAG-3′	5′-TACCATTTCTGCGAGCGTTT-3′	150	1.01 ± 0.01
Atp6v1c2	5′-GAAGGCCAACCTGGAGAACT-3′	5′-AAGCTTGACTTGGGGACGAT-3′	144	1.05 ± 0.03
Atp6v1g1	5′-TGAAGCAGGCCAAAGAAGAA-3′	5′-GTCATCTTCTCCCGGGTCT-3′	148	1.04 ± 0.02
Atp6v1g3	5′-CATGGTGTGCGACATGAAAC-3′	5′-CATCAGGTGCACAGTTGCAG-3′	140	1.03 ± 0.01
Foxi1	5′-CCTCTCCACCATGACAGCAT-3′	5′-TCCCATGGCTACTGAGGTTG-3′	155	1.06 ± 0.05
Pendrin	5′-TTTGGAGGTTTGCAGATTGG-3′	5′-TAATGGAGAGGATGCCGTTG-3′	154	1.07 ± 0.06
GAPDH	5′-TGCACCACCAACTGCTTAGC-3′	5′-GGATGCAGGGATGATGTTCT-3′	176	1.04 ± 0.03
Cyclophilin	5′-CGTCTCCTTCGAGCTGTTTG-3′	5′-CCACCCTGGCACATGAATC-3′	139	1.02 ± 0.02
HPRT1	5′-ACATTGTGGCCCTCTGTGTG-3′	5′-TTATGTCCCCCGTTGACTGA-3′	162	0.99 ± 0.01

[a]V-ATPase, vacuolar H+-ATPase; GAPDH, glyceraldehyde-3-phosphate dehydrogenase; HPRT1, hypoxanthine guanine phosphoribosyl transferase.

(16). Real-time RT-PCR results were confirmed by using another set of primers for each of V-ATPase subunits.

In parallel with the relative quantification described above, we cloned DNA plasmids for each subunit and GAPDH to determine copy numbers of V-ATPase subunits transcripts. The PCR products were cloned into a pTZ57R vector (Fermentas GmbH, Vilnius, Lithuania) and transformed in JM 107 Competent Cells (MBI Fermentas). LB-broth cultures (150 ml) of single colonies were grown up overnight skating at 200 rpm at 37°C. Plasmid purification was performed with the High Purity Plasmid Systems (Gentaur, Brussels, Belgium) according to the manufacturer's recommendations. Standard curves were generated from serial 10-fold dilutions of the purified plasmid that contained the appropriate cDNA, and regression analyses of the threshold cycle (Ct) values of standard dilution series were used to determine the amplification efficiency (data not shown). The absolute amount of mRNA molecules of V-ATPase subunits in mouse adult kidneys ($n = 8$) was determined by extrapolating the Ct values from the standard curves, according to the molecular weight of the plasmid (1.9×10^6 g/mol) and the Avogadro's number (1 mol = 6.022×10^{23} molecules), and then normalized to the GAPDH level in each sample. Each experiment was run in duplicate, with highly reproducible results.

In Situ *Hybridization*

Kidney samples were fixed in 4% formaldehyde (Boehringer Ingelheim, Heidelberg, Germany) in 0.1 M phosphate buffer (pH 7.4) before embedding in paraffin as described (17). Five-micrometer-thick sections were deparaffinized, rehydrated. and treated for 45 min at 37°C with 1 mg/ml proteinase-K (Sigma, St. Louis, MO) in 100 mM Tris-HCl (pH 8.0) and 50 mM EDTA. Sections then were acetylated for 10 min in 0.25% acetic anhydride and 0.1 M triethanolamine (pH 8.0) and prehybridized for 1 h at 52°C (Foxi1) or 56°C (B1) in the hybridization mixture that contained 40% (vol/vol) formamide, 50% (wt/vol) dextran sulfate, 2% (vol/vol) Denhardt's solution, and 2× SSC (1× SSC = 150 mM NaCl and 15 mM sodium citrate) in a humidified chamber. A mixture of two Foxi1- or B1-specific oligonucleotide probes (Foxi1 5′-AGGCTGGGTGACCTTCGAAGGCTGGATAAAGGGAACCGGG-3′, 5′-GAGTGGCTGTGAGCACAGCCTCTGGCACTGCTCGCTCCTCT-3′; B1 5′-AACATGGGTTCAAGCCATAAAGGAGAAGGCTGCAGCTGG-3′, 5′-TCCATTTCAGTTACATCTTTGGAGGCGGGGCTTCTATAAT-3′) or of two control oligonucleotides with the complementary sequence was prepared by fluorescein-dUTP labeling of the 3′ ends (Amersham Biosciences, Piscataway, NJ). The sections then were hybridized overnight at 52°C (Foxi1) or 56°C (B1) with the hybridization mixture supplemented with 1.5 ng/ml labeled probes and washed with decreasing concentrations of SSC (4×, 2×, and 1×). All washes were carried out at room temperature for 2 × 10 min. The detection of hybridized fluorescein-labeled probes was performed according to the immunostaining procedure, described below.

Antibodies

Immunoblotting and immunostaining analyses were performed with well-characterized antibodies, including mAb against the E1 subunit of the V-ATPase (a gift of Dr. S. Gluck, University of California, San Francisco, CA) (6); β-actin (Sigma); fluorescein (Dako, Glostrup, Denmark); α1 Na^+/K^+-ATPase (Upstate Biotechnology Inc., Waltham, MA); rabbit polyclonal antibodies against a4 subunit (13); B1, B2, G1, and G3 subunits (17); A subunit (Wako Chemicals GmbH, Neuss, Germany); C1 subunit (Santa Cruz Biotechnology, Santa Cruz, CA); Rab5a (Santa Cruz Biotechnology); aquaporin-2 (AQP2; Sigma); podocin (a gift from C. Antignac, Inserm U574, Necker Hospital, Paris, France) (18); sheep polyclonal antibodies against megalin (a gift from P.J. Verroust, Saint-Antoine Medical Faculty, Paris, France) (8); type II carbonic anhydrase (CAII; Serotec, Oxford, UK); goat polyclonal antibodies against cathepsin D (Santa Cruz Biotechnology); and chicken polyclonal antibodies against pendrin (a gift from P. Kopp, Northwestern University, Chicago, IL).

Analytical Subcellular Fractionation

Kidneys from approximately 40 fetuses at E16.5 and dissected cortex and medulla from five adult mice were minced in 0.25 M sucrose and 3 mM imidazole buffer (pH 7.4) that contained Complete protease inhibitors (Roche, Vilvoorde, Belgium) and homogenized in a Potter-Elvehjem tissue homogenizer (Thomas Scientific, Swedesboro, NJ). A low-speed "nuclear" fraction was pelletted at 700 × *g* for 10 min and extracted twice by resuspension sedimentation. Pooled postnuclear supernatants were sedimented further at 100,000 × *g* for 60 min in a 50Ti fixed-angle rotor (Beckman, Palo Alto, CA). The supernatant (S), which represents the cytosolic fraction, was collected for further char-

acterization. The high-speed pellet (MLP fraction of postnuclear particles) was resuspended in 1 ml of homogenization buffer, mixed with 7 ml of 16% (vol/vol) Percoll (average final density 1.048 g/ml), layered over a 250-μl Percoll cushion, and centrifuged at 60,000 × *g* for 30 min in a 50Ti rotor into a self-generating gradient, after which 10 fractions of approximately 750 μl each, excluding the packed cushion, were collected from the bottom. Each fraction was analyzed for density (refractometry), total protein content (Lowry assay), and amount of the indicated antigens (immunoblotting).

Immunoblotting

Membrane extraction and immunoblotting were performed as described previously (19). Briefly, kidney samples were homogenized in ice-cold buffer [300 mM sucrose and 25 mM N-2-hydroxyethylpiperazine-N′-2-ethanesulfonic acid made to pH 7.0 with 1 M tris(hydroxymethyl)aminomethane (Tris)] that contained Complete protease inhibitors (Roche). The homogenate was centrifuged at 1000 × *g* for 15 min at 4°C, and the resulting supernatant was centrifuged at 100,000 × *g* for 120 min at 4°C. The pellet was suspended in ice-cold homogenization buffer, before determination of protein concentration and storage at −80°C. After resolution by SDS-PAGE and blotting on nitrocellulose, the membranes were incubated overnight at 4°C with primary antibodies, washed, incubated for 1 h at room temperature with appropriate peroxidase-labeled antibodies (Dako), washed again, and visualized with enhanced chemiluminescence. Normalization for β-actin was obtained after stripping the blots and reprobing with the anti–β-actin antibody. Specificity of the immunoblot was determined by incubation with nonimmune rabbit or mouse IgG (Vector Laboratories, Burlingame, CA) or control ascites fluid (Sigma). Densitometry analysis was performed with a Canon CanoScan8000F using the NIH Image V1.60 software. All immunoblots were performed at least in duplicate.

Immunostaining

After blocking endogenous peroxidase for 30 min with 0.3% hydrogen peroxide, sections were incubated with 10% normal goat serum for 60 min, before incubation with the primary antibodies diluted in PBS that contained 2% BSA for 60 min. After washing in 50 mM Tris-HCl, sections were incubated successively with biotinylated secondary anti-IgG antibodies, avidin-biotin peroxidase, and diaminobenzidine or aminoethylcarbazole (Vector Laboratories). For immunofluorescence studies, secondary antibodies were detected with Texas red–conjugated and FITC-conjugated avidin (Vector Laboratories). Sections were viewed under a Leica DMR coupled to a Leica DC300 digital camera (Leica, Heerbrugg, Switzerland). The specificity of immunostaining was tested by incubation (*1*) in the absence of primary antiserum and (*2*) with nonimmune rabbit serum or control rabbit or mouse IgG (Vector Laboratories).

Results

Relative Expression of V-ATPase Subunits in Adult Mouse Kidney

The recently updated structure of the V-ATPase contains at least 13 different subunits that form two functional domains, V0 and V1 (Figure 1). Before considering the expression of isoforms during mouse nephrogenesis, we performed comparative real-time RT-PCR quantification, with different reporter genes, to establish the relative mRNA expression of ubiquitous and IC-specific subunits in adult mouse kidney (Figure 2). These data were essentially confirmed by absolute real-time RT-PCR using standard curves of cloned DNA plasmids for the V-ATPase subunits and GAPDH (data not shown). These studies revealed striking differences in terms of relative expression

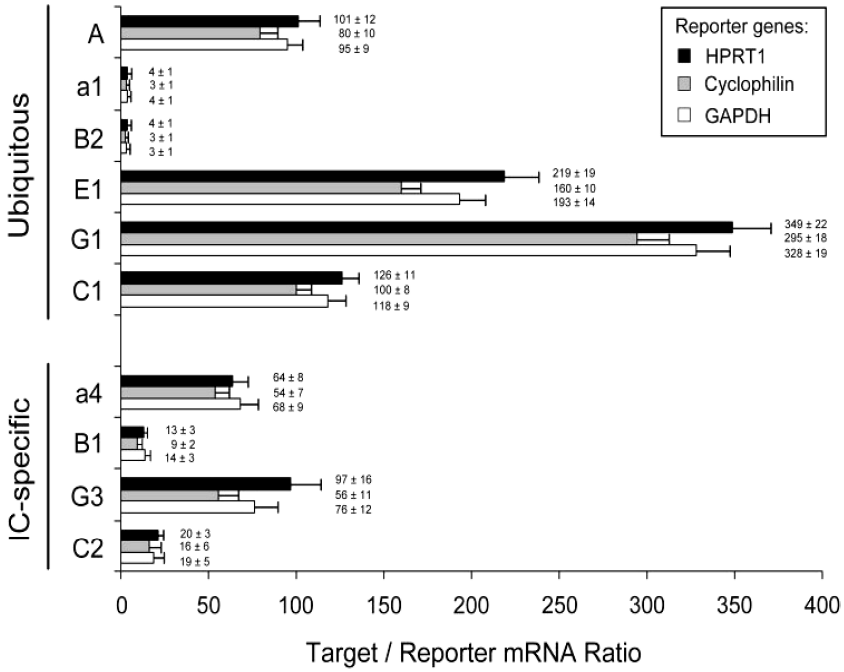

Figure 2. mRNA quantification of V-ATPase subunits. Real-time reverse transcription–PCR (RT-PCR) quantification of ubiquitous (A, a1, B2, E1, G1, and C1) and IC-specific (a4, B1, G3, and C2) subunits in mouse adult kidney (n = 8). The mRNA expression levels (mean ± SEM) were compared after adjustment to HPRT1 (×50), cyclophilin (×10^3), or glyceraldehyde-3-phosphate dehydrogenase (GAPDH; ×2.10^3) as reporter genes. HPRT1, hypoxanthine guanine phosphoribosyl transferase.

at the mRNA level that could not be explained by the structural stoichiometry of the V-ATPase complex shown in Figure 1. For instance, the A subunit was 20-fold more abundant than B2, although these subunits are considered to form the A3B3 catalytic core of the V1 domain. Moreover, comparative analysis of alternate isoforms inside ubiquitous (a1, B2, C1, and G1) or IC-specific (a4, B1, C2, and G3) pumps did not show a constant stoichiometry. These results suggest that the assembly of the V-ATPase complex results from important posttranscriptional modifications and/or reflects significant differences in the turnover of its various components.

Expression of V-ATPase Subunits mRNA in Developing Mouse Kidney

The differential expression patterns of ubiquitous and IC-specific V-ATPase subunits during mouse nephrogenesis were investigated using real-time RT-PCR analyses (Figure 3). The ubiquitous A, B2, E1, G1, and C1 subunits showed an early (E13.5) and stable expression (approximately 40% of the adult level) throughout nephrogenesis, reaching the adult level at birth (Figure 3A). Of note, the a1 isoform showed an earlier induction at E13.5 (approximately 135%) followed by a gradual decrease during late ontogeny and a second increase around birth. This particular developmental pattern is similar to that described for the endosomal kidney-specific chloride channel, ClC-5, and for the V0 d1 V-ATPase subunit (19,20). In contrast, the corresponding IC-specific B1, G3, C2, and a4 subunits were barely detected at E15.5 and showed a progressive induction during late ontogeny, like the anion transporter pendrin (Figure 3B). It must be noted that the forkhead transcription factor Foxi1, which is a member of the HFH/winged helix family, was detected from E15.5 (Figure 3B). These data show that the early expression of ubiquitous subunits of V-ATPase definitively contrasts with the later and more progressive appearance of Foxi1, pendrin, and IC-specific subunits.

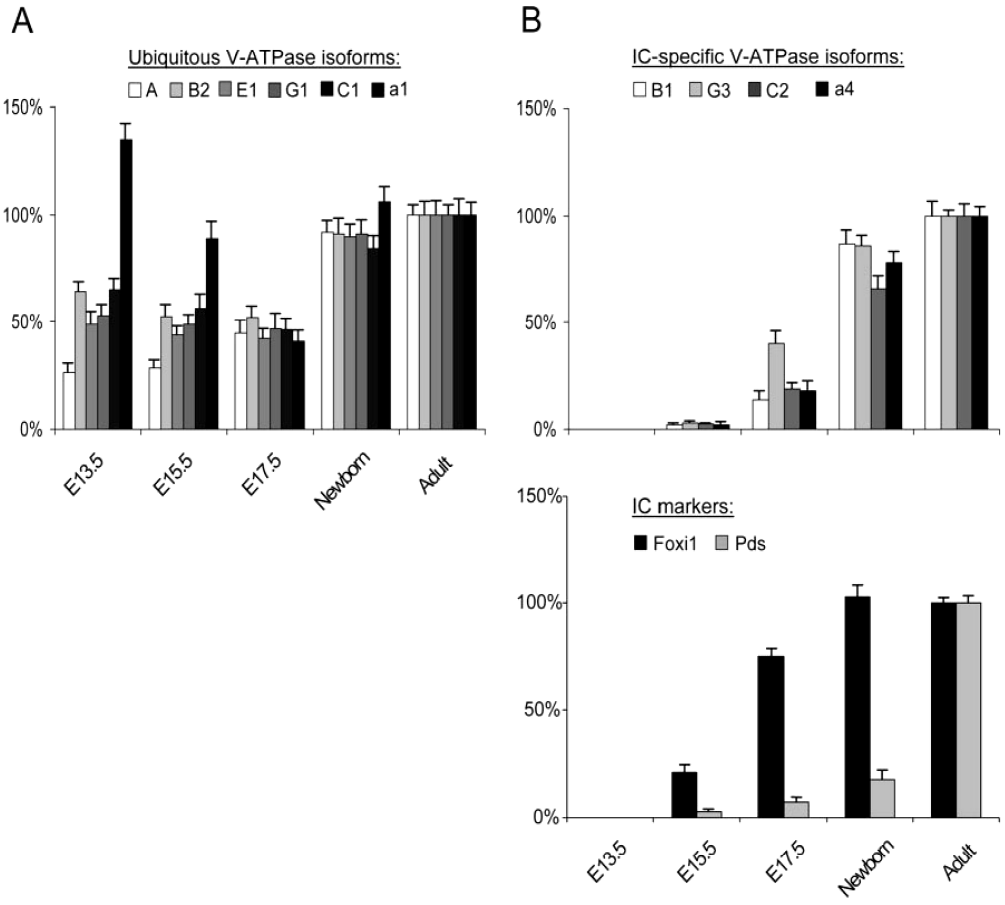

Figure 3. Expression of V-ATPase subunits in mouse developing kidney. Real-time RT-PCR quantification for mRNA expression of ubiquitous A, B2, E1, G1, C1, and a1 subunits (A) and IC-specific B1, G3, C2, and a4 isoforms, as well as Foxi1 and pendrin (pds) (B), during mouse nephrogenesis. The mRNA levels were first adjusted to GAPDH at every developmental stage, then normalized to the adult level set at 100% using the following formula: [Ratio = $(\text{Efficiency}_{\text{target}})^{\Delta Ct\,(\text{Adult} - \text{Sample})}$/ $(\text{Efficiency}_{\text{GAPDH}})^{\Delta Ct\,(\text{Adult} - \text{Sample})}$]. The early (embryonic day 13.5 [E13.5]) and stable expression of ubiquitous subunits during nephrogenesis clearly contrasts with the later and progressive appearance of IC-specific isoforms and pds, which follows the induction of the transcription factor Foxi1 at E15.5. Note that the a1 subunit is characterized by a bimodal developmental pattern.

Distribution of Forkhead Transcription Factor Foxi1 in Developing Mouse Kidney

The winged helix transcriptional activator Foxi1 has been located to the distal part of the nephron from E16.5 during mouse nephrogenesis (21) and recently implicated in IC differentiation along the CD (22). To investigate the putative link between Foxi1 and IC-specific V-ATPase isoforms expression, we performed *in situ* hybridizations on mouse developing kidney with fluorescein-labeled oligonucleotides directed against Foxi1 or B1 (Figure 4). At E15.5, Foxi1 was detected in some scattered cells of the medullary CD, whereas no signal was found in glomeruli, PT, and differentiating structures in the cortex (Figure 4A). At later stages, Foxi1 mRNA was identified in a subset of cells within distinct tubules in cortex and medulla (Figure 4C). In these cells, Foxi1 co-distributed with the IC-specific B1 V-ATPase subunit (Figure 4D). Altogether, the real-time RT-PCR and *in situ* hybridization data during mouse nephrogenesis strongly support the role of Foxi1 in the differentiation of IC along the CD.

Expression of V-ATPase Subunits in Developing Mouse Kidney

Well-characterized antibodies were used to evaluate the expression of ubiquitous and IC-specific V-ATPase subunits in mature and developing kidney (Figure 5). Postnuclear particles and high-speed supernatant, resolved by differential centrifugation of adult kidney samples, were analyzed by immunoblotting. In the adult kidney, approximately 20% of V1 subunits, *i.e.*, A, B2, E1 and G1, were detected in the cytosolic fraction, whereas the transmembrane a4, as well as the V1 C1 subunit, was associated only with membranes (Figure 5A). During nephrogenesis (Figure 5B), ubiquitous V-ATPase subunits (A, B2, E1, G1, and C1) were detected as early as E13.5 and gradually increased from E16.5 until birth. In contrast, the IC-specific subunit isoforms (a4, B1, and G3) and the anion exchanger pendrin were detected only from E16.5 and increased progressively during late nephrogenesis.

Segmental Distribution of V-ATPase Subunits in Developing Mouse Kidney

The segmental distribution of ubiquitous and IC-specific subunits in the developing mouse kidney was investigated using well-characterized antibodies against E1, B2, and a4 (Figure 6). No immunostaining for the IC-specific a4 subunit was detected at E14.5, by which time dispersed glomeruli and developing PT were observed in the inner cortex (Figure 6A). At E15.5, the immunoreactive signal was located in the apical area of scattered cells along the cortical (Figure 6B) and medullary CD (Figure 6C), whereas PT, ureteric buds, glomeruli, and differentiating structures remained unlabeled. By contrast, at this fetal stage, the distribution of ubiquitous E1 and B2 was acquired in PTC (Figure 6, D and I), as well as the distribution of E1 in IC (Figure 6D, inset). From E16.5, apical staining for a4 was detected in scattered IC (Figure 6, E, G, and H), clearly identified by co-distribution with CAII (Figure 6, F and G) but negative staining for AQP2 (Figure 6H). The distribution pattern of a4 in mouse developing kidney was restricted to IC (Figure 6J), similar to that observed in adult kidney (Figure 6K). The specificity of a4 staining was demonstrated with preimmune rabbit antibodies (Figure 6L). These results show that, in mouse developing kidney, the a4 subunit is detected progressively during IC differentiation, whereas the distribution of ubiquitous E1 and B2 includes both PTC and IC of the CD at an early stage.

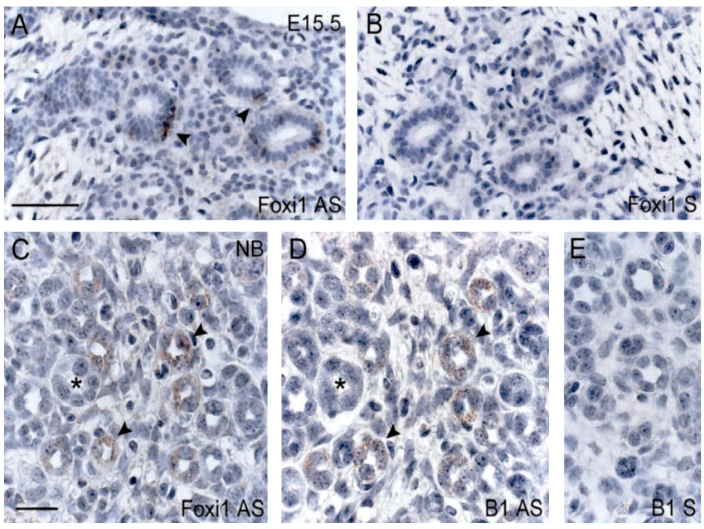

Figure 4. Distribution of Foxi1 and V-ATPase B1 subunit mRNA in mouse developing kidney. *In situ* hybridization for Foxi1 (A and C: antisense probe; B: sense); B1 V-ATPase subunit (D: antisense probe; E: sense) in the developing mouse E15.5 (A and B) and neonatal (C through E) kidney. At E15.5, Foxi1 mRNA is specifically detected in scattered cells within medullary collecting ducts (CD; A, arrowheads). In the newborn kidney, Foxi1 and B1 co-distribute in distinct cells within cortical CD (C and D, arrowheads on serial sections). No signal was detected when sense probes were used on consecutive sections (E). Bars = 50 μm in A and B; 20 μm in C through E.

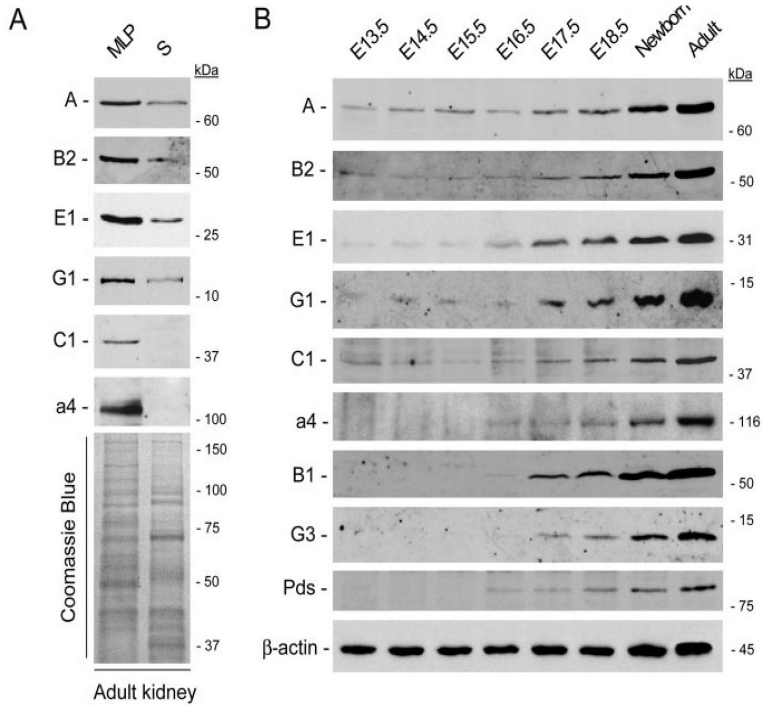

Figure 5. Expression of V-ATPase subunits in mouse developing kidney. (A) Relative expression of V1 A, B2, E1, G1, and C1, and V0 a4 in membrane (MLP) and cytosolic (S) compartments of adult mouse kidney. Equal loads (20 μg) of postnuclear particles (MLP 37% of total homogenate proteins) and high-speed supernatant (S 29% of total homogenate proteins) were analyzed. Densitometry analyses show that approximately 20% of V1 subunits are not associated with membranes at steady state. The transmembrane V0 a4 subunit, as well as the V1 C1, are not detected in the cytosolic fraction. (B) Representative immunoblots for ubiquitous A, B2, E1, G1, C1, and IC-specific a4, B1, and G3 V-ATPase subunits and pds in fetal (from E13.5 to E18.5), newborn, and adult mouse kidneys. A total of 20 μg of protein was loaded in each lane. Blots were probed with antibodies against A (1:1000), B2 (1:1000), E1 (1:100), G1 (1:500), C1 (1:1000), a4 (1:5000), B1 (1:1000), and G3 (1:500) subunits; pendrin (1:2000); and, after stripping, β-actin (1:10,000). Ubiquitous subunits are detected as early as E13.5 and gradually increase during late nephrogenesis, whereas the developmental pattern of IC-specific isoforms and pendrin is characterized by a later expression from E16.5.

Subcellular Fractionation in Percoll Gradients

In addition to its intracellular location where it mediates vesicle acidification, the V-ATPase is located at the cell surface of renal IC. We investigated the subcellular distribution of ubiquitous E1 and IC-specific a4 subunits in the mature and developing mouse kidney (Figure 7). Adult kidneys were dissected into cortex and medulla, and appropriate markers were analyzed by immunoblotting to validate the dissection (Figure 7A). Podocin and pendrin, as well as E1 and a4, were considerably enriched in the cortex, whereas AQP2 was detected mostly in the medulla (Figure 7B). These results confirm that the two parts of adult kidneys were purified adequately, as indicated by an enrichment ratio >30 (podocin *versus* AQP2). Next, the subcellular distribution of E1 and a4 in fetal kidney and adult cortex and medulla was compared (Figure 7C). Percoll gradients resolved a low-density peak (fractions 2 to 4) that comprised all (fetus) or the bulk (adult) of the early endosomal marker Rab5a from a high-density peak (fractions 9 and 10), including most of the lysosomal marker cathepsin D. In the three tissue samples, both V-ATPase subunits peaked in the low-density fractions, suggesting their major association with endosomes and not with lysosomes.

Discussion

In this study, we showed that ubiquitous and IC-specific isoforms of V-ATPase subunits are differentially expressed in mature kidney and during mouse nephrogenesis. The early expression of the ubiquitous A, B2, E1, G1, C1, and a1 subunits contrasts with the later and more progressive appearance of the IC-specific isoforms B1, G3, C2, and a4. The forkhead transcription factor Foxi1 mRNA was detected in IC from E15.5, with co-distribution with the B1 subunit in late nephrogenesis. The segmental distribution of E1 and B2 was acquired in PTC at E15.5, whereas a4 co-distributed with CAII in the IC during late nephrogenesis. Subcellular fractionation studies indicated a preferential location of both ubiquitous and IC-specific subunits to endosomes in both developing and mature kidneys.

The subunit composition of the bovine V-ATPase, previously determined by quantitative amino acid studies (1), was updated recently using electron microscopy and single-molecule image analysis (4). These investigations led to a structural model of the mammalian V-ATPase, which seems to be similar to the F_1F_0-ATP synthase in yeast (4). As a preliminary to the ontogeny analysis, real-time RT-PCR analyses in the adult kidney showed that the

3242 Journal of the American Society of Nephrology J Am Soc Nephrol 16: 3235–3246, 2005

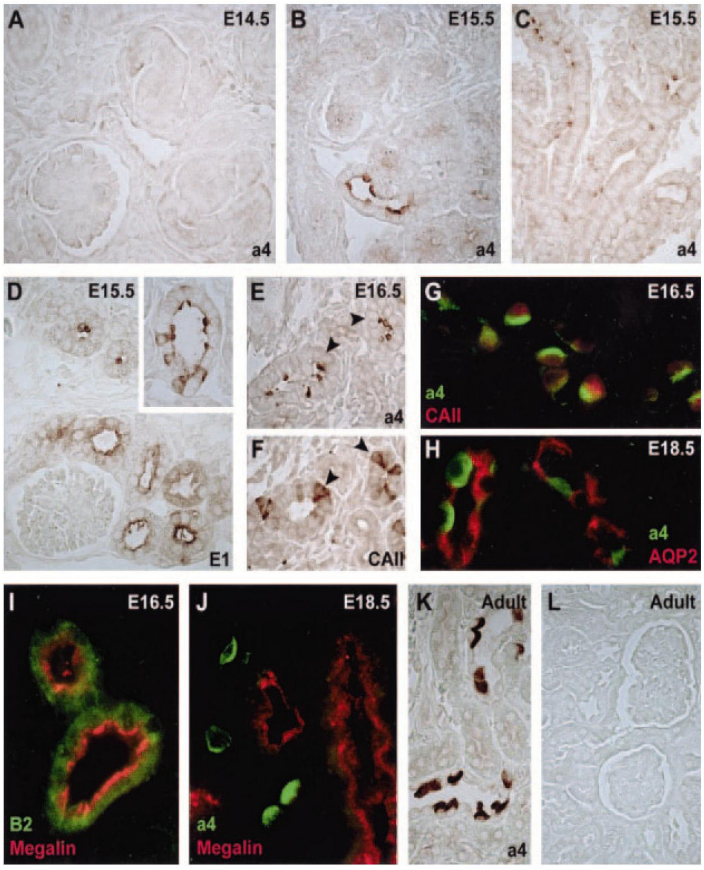

Figure 6. Segmental distribution of E1 and a4 V-ATPase subunits in mouse developing kidney. Immunostaining for a4 (all panels except D, F, I, and L), E1 (D), B2 (I), type II carbonic anhydrase (F and G), aquaporin 2 (AQP2; H), megalin (I and J), and negative control (L) in developing mouse kidney at E14.5 (A), E15.5 (B through D), E16.5 (E through G and I), and E18.5 (H and J) and in adult mouse kidney (K and L). No specific staining for a4 is observed at E14.5 (A). From E15.5, a4 is detected in the apical area of scattered cells of cortical (B) and medullary (C) CD, whereas proximal tubule cells (PTC) remain unstained. At this stage, the ubiquitous E1 and B2 are already expressed in developing PTC (D and I) and in IC of the medullary and cortical (D, inset) CD. At E16.5, apical staining for a4 is still present in scattered IC of the CD (E, arrowheads), clearly identified by co-staining positive for type II carbonic anhydrase (CAII; F, arrowheads, and G) but negative for AQP2 (H). This segmental distribution restricted to IC in mouse fetal kidney (J) is similar to that observed in the adult kidney (K). No staining for a4 subunit was observed with preimmune rabbit serum (L). Magnification, ×300 in A through F, K, and L; ×450 in G through J.

relative mRNA expression of V-ATPase subunits does not correspond to the expected stoichiometry. These results were confirmed by absolute mRNA quantification using standard curves from serial dilution of purified plasmids (data not shown). The ratio between the two methods varied between 0.8 and 1.8 according to the subunits, in agreement with previous comparative studies (23). This variability is attributed to distinct primer efficiency and, overall, cumulative errors introduced by the additional steps of the absolute mRNA quantification (spectrophotometry, calculations of molecular weight) (24). Thus, the relative method, using primer sets of similar efficiency (Table 1) and three distinct internal standards, was preferred to compare the abundance of V-ATPase subunit transcripts in one single kidney sample. The comparative mRNA quantification of subunits demonstrates a variable expression from ubiquitous to IC-specific V-ATPase complexes. Although minimal and/or limited correlation between the mRNA and protein levels is most often reported, the degree of correlation could vary according to subcellular localization or functional category (25). In the case of the renal V-ATPase complex, a first hypothesis could be significant variations in the turnover of the subunits that compose the complex, as well as a differential regulation of subunit mRNA stability (26). Because *in vivo* regulation of V-ATPase, which involves the reversible dissociation of V1 from V0 domain (27), does not require new protein synthesis but an efficient microtubular system (28), a second hypothesis could be posttranscriptional modifications during subunit synthesis and V-ATPase assembly. For instance, rearrangements during the formation of V0 and V1 domains might stabilize each of these subunits by tight interactions and/or mutual chaperoning. Of interest, a selective posttranscriptional control of protein expression levels among loci of the V-ATPase complex has been shown to operate in *Saccharomyces cerevisiae* (29).

The molecular events that occur in renal tubular cells after the onset of glomerular filtration, which starts at E14 in mouse

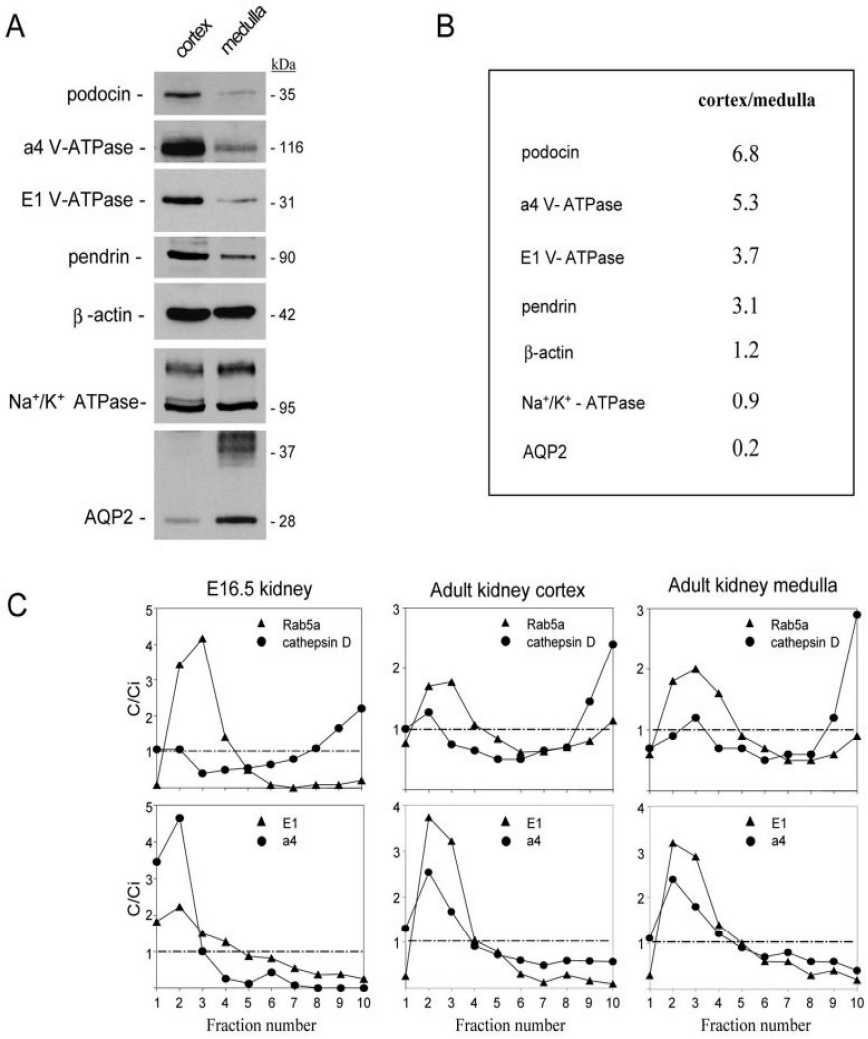

Figure 7. Localization and subcellular distribution of V-ATPase subunits in fetal and adult (cortex and medulla) mouse kidneys. (A) Representative immunoblots for podocin, IC-specific a4 and ubiquitous E1 V-ATPase subunits, pendrin, β-actin, Na^+/K^+-ATPase, and AQP2 in cortex and medulla of adult mouse kidney. Thirty micrograms of protein were loaded in each lane. Podocin (1:5000), a4 (1:5000), E1 (1:100), and pendrin (1:1000) are highly enriched in the dissected cortex and depleted in the dissected medulla; β-actin (1:10,000) and Na^+/K^+-ATPase (1:5000) are equally expressed in both tissues; AQP2 (1:2000) is detected mostly in the dissected medulla. (B) The relative enrichment of these markers, based on densitometry. (C) Percoll gradients of total fetal (E16.5) and adult (cortex and medulla) mouse kidneys. Distributions after centrifugation are presented in comparison with the initial concentration (C/Ci) so that values >1 reflect organelle enrichment and values <1 reflect organelle depletion. For immunoblotting analyses, equal volumes were loaded in each lane. The gradients resolve a low-density peak (fractions 2 to 4), including early endosomes (Rab5a), from a high-density peak (fractions 9 and 10), enriched in lysosomes (cathepsin D). The two V-ATPase subunits peak in the low-density fractions, which suggests their major association with endosomes and not with lysosomes in both developing and adult (cortex and medulla) kidneys.

(30), remain incompletely elucidated. Recent evidence suggests that different steps of kidney organogenesis are reflected by clusters of differentially regulated genes, including transporters and ions-motive ATPases, under the control of specific transcription activators (9,31). In rats (32) and humans (33), PT endocytic activity is effective during nephrogenesis or immediately after birth. Both the receptor-mediated endocytic pathway and the apical targeting within PTC (8) depend on a correct vacuolar acidification, which is mediated by V-ATPase in PTC. Our real-time RT-PCR and immunoblotting analyses show an early and stable expression of ubiquitous isoforms of V-ATPase subunits during nephrogenesis, which is in keeping with its essential role for early mouse development (12). It is interesting that the endosomal a1 subunit shows an early induction, a progressive decrease during late ontogeny, and a novel induction around birth. Such a biphasic developmental pattern is also described for the renal chloride channel ClC-5 that co-locates with V-ATPase in PT endosomes (34), as well as

for the V0 d1 subunit (20). ClC-5 is mutated in Dent's disease, an X-linked renal tubular disorder characterized by a major and early defect in the PT endocytic pathway (35). Thus, besides the stable expression of ubiquitous subunits, ClC-5 and a1 isoform, which are considered to target correctly V-ATPase complex to appropriate intracellular compartments (36), both are expressed simultaneously in PTC as early as the glomerular filtration starts. These essential components of the endocytotic process, responsible for the reabsorption of amino acids, vitamins, and minerals, may indeed be required early for correct growth and development. Analytical subcellular fractionation clearly resolved the two V-ATPase subunits from lysosomes, as assessed by the cathepsin D distribution, and rather pointed to a primary endosomal location, as shown by co-distribution with Rab5a. This low-density pattern is identical to what we recently reported for ClC-5 (8). Thus, kidney endosomes seem to be well equipped with electrogenic proton pumps and a chloride conductance, both in the adult and the fetus.

The IC constitute approximately one third of the cells that line the mouse CD (37). Although both α- and β-IC are characterized by high CAII activity, they differ by the selective polarity of V-ATPase and type 1 anion exchanger, allowing them to participate in proton (α type) or bicarbonate (β type) urinary secretion (7). The differentiation and maturation of the various cell types within the CD is poorly understood. Studies in the rat have shown that V-ATPase and CAII are detected simultaneously in IC at the end of gestation (38). During the first weeks of life, IC continue their maturation but are partially removed from specific parts of the CD by apoptosis or luminal extrusion (39). Recently, the winged helix transcriptional factor Foxi1, previously located in mouse fetal distal nephron (21), was shown to play an essential role in IC differentiation from epithelial precursor cells in the CD (22). In addition, Foxi1 is regarded as an upstream regulator of the anion transporter pendrin during inner ear development (40). Indeed, mice that lack Foxi1 showed a lack of differentiation of the distal nephron, leading to dRTA (22), as well as a sensorineural deafness resembling that of Pendred syndrome (40). Our description of the developmental expression of Foxi1, IC-specific V-ATPase isoforms, and pendrin provides additional information on CD maturation in mouse. Real-time RT-PCR showed that IC-specific subunits B1, G3, C2, and a4, as well as pendrin, are expressed later than the ubiquitous isoforms, with a progressive induction after Foxi1 appearance (E15.5). *In situ* hybridization showed that at E15.5, Foxi1 is expressed in scattered cells of the medullary CD. At later stages, Foxi1 is identified in distinct cells within tubules in the cortex and outer medulla, in which it co-distributes with the IC-specific B1 subunit. *In silico* studies (http://mordor.cgb.ki.se/cgi-bin/CONSITE/consite) indicate that gene promoters of IC-specific markers, such as type 1 anion exchanger, AE4, pendrin, or IC-specific V-ATPase subunits, exhibit Foxi1 DNA binding consensus sequence (21,22). Immunoblot studies showed a coordinate expression of the IC-specific subunits and pendrin at approximately E16.5, with immunolocalization of a4 and CAII in IC. Of note, subcellular fractionation showed that, in both fetal (E16.5) and adult kidneys, a4 and E1 subunits are located mostly in endosomes. This observation corroborates a dynamic process that occurs in IC, which involves regulated exocytic insertion of V-ATPase from a vesicular pool to the plasma membrane (41). Taken together, the mRNA and protein data support the case for a differential but coordinate regulation of IC-specific *versus* ubiquitous V-ATPase subunits during kidney development.

The comparative ontogeny of V-ATPase subunits helps us understand the pathophysiology of inherited renal disorders such as Dent's disease and dRTA. Dent's disease, which is due to inactivating mutations in *CLCN5* that presumably lead to impaired endosomal acidification in PTC, is characterized by low molecular weight proteinuria that can be detected within the first weeks of life (35). These clinical findings, which suggest that the molecular mechanisms that ensure endosomal acidification must be acquired at birth (19), have their counterpart in our demonstration of a parallel induction of the endosomal a1 isoform and ClC-5 that culminates at birth. Given the essential role of V-ATPase in early embryogenesis and its large tissue distribution, no mutation of any ubiquitous V-ATPase subunits has ever been reported, being definitively not compatible with life (12). In contrast, mutations in IC-specific isoforms have been associated with human dRTA (13–15). Some well-documented patients show clinical manifestations of dRTA during infancy, which suggests that the segmental expression of these IC-specific isoforms of V-ATPase must be acquired early, as indeed documented here.

In conclusion, our data demonstrate that ubiquitous and IC-specific isoforms of V-ATPase subunits are differentially expressed during mouse nephrogenesis. These results provide new insights into the segmental distribution of V-ATPase complexes in the kidney and represent a useful tool to investigate further any newly discovered subunit isoforms. The deciphering of the complex maturation of PTC and IC along the distal nephron also helps us understand the pathophysiology of renal tubular disorders.

Acknowledgments

These investigations were supported by the Université catholique de Louvain, the Fonds National de la Recherche Scientifique (FNRS), the Forton Foundation, Concerted Research Actions, Inter-University Attraction Poles, and the EuReGene integrated project of the European Community (FP6). F.J. is a research fellow of the FNRS, and C.P. is a research fellow of the FRIA.

We are grateful to Y. Cnops, M. Leruth, L. Wenderickx, and P. Henriet for excellent technical help and discussion and to M. Futai, P. Gailly, A. Goffinet, N. Tajeddine, and M.-F. van den Hove for material.

References

1. Nishi T, Forgac M: The vacuolar H+-ATPases: Nature's most versatile proton pumps. *Nat Rev Mol Cell Biol* 3: 94–103, 2002
2. Nelson N, Harvey WR: Vacuolar and plasma membrane proton-adenosinetriphosphatases. *Physiol Rev* 79: 361–385, 1999
3. Wagner CA, Finberg KE, Breton S, Marshansky V, Brown D, Geibel JP: Renal vacuolar H+-ATPase. *Physiol Rev* 84: 1263–1314, 2004
4. Wilkens S, Takao I, Forgac M: Three-dimensional structure of the vacuolar ATPase—Localization of subunit H by difference imaging and chemical cross-linking. *J Biol Chem* 279: 41942–41949, 2004

5. Borthwick KJ, Karet FE: Inherited disorders of the H+-ATPase. *Curr Opin Nephrol Hypertens* 11: 563–568, 2002
6. Brown D, Hirsch S, Gluck S: Localization of a proton-pumping ATPase in rat kidney. *J Clin Invest* 82: 2114–2126, 1988
7. Giebisch G, Windhager E: Transport of acids and bases. In: *Medical Physiology*, edited by Boron WF, Boulpaep EL, Philadelphia, Saunders, 2004, pp 845–860
8. Christensen EI, Devuyst O, Dom G, Nielsen R, Van der Smissen P, Verroust P, Leruth M, Guggino WB, Courtoy PJ: Loss of chloride channel, ClC-5, impairs endocytosis by defective trafficking of megalin and cubilin in kidney proximal tubules. *Proc Natl Acad Sci U S A* 100: 8472–8477, 2003
9. Schwab K, Patterson LT, Aronow BJ, Luckas R, Liang HC, Potter SS: A catalogue of gene expression in the developing kidney. *Kidney Int* 64: 1588–1604, 2003
10. Bonnici B, Wagner CA: Postnatal expression of transport proteins involved in acid-base transport in mouse kidney. *Pflugers Arch* 448: 16–28, 2004
11. Satlin LM, Woda CB, Schwartz GJ: Development of function in the metanephric kidney. In: *The Kidney, from Normal Development to Congenital Disease*, edited by Vize PD, Woolf AS, Bard JBL, Orlando, Academic Press (Elsevier), 2003, pp 267–326
12. Inoue H, Noumi T, Nagata M, Murakami H, Kanazawa H: Targeted disruption of the gene encoding the proteolipid subunit of mouse vacuolar H+-ATPase leads to early embryonic lethality. *Biochem Biophys Acta* 1413: 130–138, 1999
13. Smith AN, Skaug J, Choate KA, Nayir A, Bakkaloglu A, Ozen S, Hulton SA, Sanjad SA, Al-Sabban EA, Lifton RP, Scherer SW, Karet FE: Mutations in ATP6N1B, encoding a new kidney vacuolar proton pump 116-kDa subunit, cause recessive distal renal tubular acidosis with preserved hearing. *Nat Genet* 26: 71–75, 2000
14. Karet FE, Finberg KE, Nelson RD, Nayir A, Mocan H, Sanjad SA, Rodriguez-Soriano J, Santos F, Cremers CW, Di Pietro A, Hoffbrand BI, Winiarski J, Bakkaloglu A, Ozen S, Dusunsel R, Goodyer P, Hulton SA, Wu DK, Skvorak AB, Morton CC, Cunningham MJ, Jha V, Lifton RP: Mutations in the gene encoding B1 subunit of H+-ATPase cause renal tubular acidosis with sensorineural deafness. *Nat Genet* 21: 84–90, 1999
15. Stover EH, Borthwick KJ, Bavalia C, Eady N, Fritz DM, Rungroj N, Giersch AB, Morton CC, Axon PR, Akil I, Al-Sabban EA, Baguley DM, Bianca S, Bakkaloglu A, Bircan Z, Chauveau D, Clermont MJ, Guala A, Hulton SA, Kroes H, Li Volti G, Mir S, Mocan H, Nayir A, Ozen S, Rodriguez Soriano J, Sanjad SA, Tasic V, Taylor CM, Topaloglu R, Smith AN, Karet FE: Novel ATP6V1B1 and ATP6V0A4 mutations in autosomal recessive distal renal tubular acidosis with new evidence for hearing loss. *J Med Genet* 39: 796–803, 2002
16. Pfaffi MW: A new mathematical model for relative quantification in real-time RT-PCR. *Nucleic Acids Res* 29: 2004–2007, 2001
17. Sun-Wada GH, Murata Y, Namba M, Yamamoto A, Wada Y, Futai M: Mouse proton pump ATPase C subunit isoforms (C2-a and C2-b) specifically expressed in kidney and lung. *J Biol Chem* 278: 44843–44851, 2003
18. Roselli S, Gribouval O, Boute N, Sich M, Benessy F, Attie T, Gubler MC, Antignac C: Podocin localizes in the kidney to the slit diaphragm area. *Am J Pathol* 160: 131–139, 2002
19. Jouret F, Igarashi T, Gofflot F, Wilson PD, Karet FE, Thakker RV, Devuyst O: Comparative ontogeny, processing, and segmental distribution of the renal chloride channel, ClC-5. *Kidney Int* 65: 198–208, 2004
20. Smith AN, Jouret F, Bord S, Borthwick KJ, Al-Lamki RS, Wagner CA, Ireland DC, Cormier-Daire V, Frattini A, Villa A, Kornak U, Devuyst O, Karet FE: Vacuolar H+-ATPase d2 subunit: Molecular characterization, developmental regulation, and localization to specialized proton pumps in kidney and bone. *J Am Soc Nephrol* 16: 1245–1256, 2005
21. Overdier DG, Ye H, Peterson RS, Clevidence DE, Costa RH: The winged helix transcriptional activator, HFH-3, is expressed in the distal tubules of embryonic and adult mouse kidney. *J Biol Chem* 272: 13725–13730, 1997
22. Blomqvist SR, Vidarsson H, Fitzgerald S, Johansson BR, Ollerstam A, Brown R, Persson AE, Bergstrom GG, Enerback S: Distal renal tubular acidosis in mice that lack the forkhead transcription factor, Foxi1. *J Clin Invest* 113: 1560–1570, 2004
23. Rose'Meyer RB, Mellick AS, Garnham BG, Harrison GJ, Massa HM, Griffiths LR: The measurement of adenosine and estrogen receptor expression in rat brains following ovariectomy using quantitative PCR analysis. *Brain Res Brain Res Protoc* 11: 9–18, 2003
24. Freeman WM, Walker SJ, Vrana KE: Quantitative RT-PCR: Pitfalls and potential. *Biotechniques* 26: 112–122, 1999
25. Greenbaum D, Colangelo C, Williams K, Gerstein M: Comparing protein abundance and mRNA expression levels on a genomic scale. *Genome Biol* 4: 117, 2003
26. Wang SP, Krits I, Bai S, Lee BS: Regulation of enhanced vacuolar H+-ATPase expression in macrophages. *J Biol Chem* 277: 8827–8834, 2002
27. Kane PM: Disassembly and reassembly of the yeast vacuolar H+-ATPase in vivo. *J Biol Chem* 270: 17025–17032, 1995
28. Xu T, Forgac M: Microtubules are involved in glucose-dependent dissociation of the yeast vacuolar H+-ATPase in vivo. *J Biol Chem* 276: 24855–24861, 2001
29. Washburn MP, Koller A, Oshiro G, Ulaszek RR, Plouffe D, Deciu C, Winzeler E, Yates JR 3rd: Protein pathway and complex clustering of correlated mRNA and protein expression analyses in *Saccharomyces cerevisiae*. *Proc Natl Acad Sci U S A* 100: 3107–3112, 2003
30. Loughna S, Landels E, Woolf AS: Growth factor control of developing kidney endothelial cells. *Exp Nephrol* 4: 112–118, 1996
31. Stuart RO, Bush KT, Nigam SK: Changes in global gene expression patterns during development and maturation of the rat kidney. *Proc Natl Acad Sci U S A* 98: 5649–5654, 2001
32. Smaoui H, Schaeverbeke M, Mallie JP, Schaeverbeke J: Transplacental effects of gentamicin on endocytosis in rat renal proximal tubule cells. *Pediatr Nephrol* 8: 447–450, 1994
33. Mussap M, Fanos V, Piccoli A, Zaninotto M, Padovani EM, Plebani M: Low molecular mass proteins and urinary enzymes in amniotic fluid of healthy pregnant women at progressive stages of gestation. *Clin Biochem* 29: 51–56, 1996
34. Devuyst O, Christie PT, Courtoy PJ, Beauwens R, Thakker RV: Intra-renal and subcellular distribution of the human chloride channel, ClC-5, reveals a pathophysiological basis for Dent's disease. *Hum Mol Genet* 8: 247–257, 1999
35. Scheinman SJ: X-linked hypercalciuric nephrolithiasis: Clinical syndromes and chloride channel mutations. *Kidney Int* 53: 3–17, 1998
36. Manolson MF, Wu B, Proteau D, Taillon BE, Roberts BT, Hoyt MA, Jones EW: STV1 gene encodes functional homo-

logue of 95-kDa yeast vacuolar H+-ATPase subunit Vph1p. *J Biol Chem* 269: 14064–14074, 1994
37. Teng-umnuay P, Verlander JW, Yuan W, Tisher CC, Madsen KM: Identification of distinct subpopulations of intercalated cells in the mouse collecting duct. *J Am Soc Nephrol* 7: 260–274, 1996
38. Kim J, Tisher CC, Madsen KM: Differentiation of intercalated cells in developing rat kidney: An immunohistochemical study. *Am J Physiol* 266: F977–F990, 1994
39. Kim J, Cha JH, Tisher CC, Madsen KM: Role of apoptotic and nonapoptotic cell death in removal of intercalated cells from developing rat kidney. *Am J Physiol* 270: F575–F592, 1996
40. Hulander M, Kiernan AE, Blomqvist SR, Carlsson P, Samuelsson EJ, Johansson BR, Steel KP, Enerback S: Lack of pendrin expression leads to deafness and expansion of the endolymphatic compartment in inner ears of Foxi1 null mutant mice. *Development* 130: 2013–2025, 2003
41. Brown D, Breton S: H+-ATPase-dependent luminal acidification in the kidney collecting duct and the epididymis/vas deferens: Vesicle recycling and transcytotic pathways. *J Exp Biol* 203: 137–145, 2000
42. Smith AN, Borthwick KJ, Karet FE: Molecular cloning and characterization of novel tissue-specific isoforms of the human vacuolar H(+)-ATPase C, G and d subunits, and their evaluation in autosomal recessive distal renal tubular acidosis. *Gene* 297: 169–177, 2002

CHAPTER IV.

VACUOLAR H^+-ATPASE d2 SUBUNIT:

MOLECULAR CHARACTERIZATION, DEVELOPMENTAL REGULATION, AND LOCALIZATION TO SPECIALIZED PROTON PUMPS IN KIDNEY AND BONE

Annabel N. Smith[(1)], François Jouret[(2)], Sharyn Bord[(3)], Katherine J. Borthwick[(1)], Rafia S. Al-Lamki[(3)], Carsten A. Wagner[(4)], Deborah C. Ireland[(3)], Valerie Cormier-Daire[(5)], Annalisa Frattini[(6)], Anna Villa[(6)], Uwe Kornak[(7)], Olivier Devuyst[(2)], and Fiona E. Karet[(1,8)]

(1) Departments of 1Medical Genetics, (3) Medicine, and (8) Division of Renal Medicine, University of Cambridge, Cambridge, United Kingdom; (2) Division of Nephrology, Université catholique de Louvain, Brussels, Belgium; (4) Institute of Physiology, University of Zurich, Zurich, Switzerland; (5) Department of Medical Genetics, Hôpital Necker, Paris, France; (6) Istituto di Tecnologie Biomediche, Milan, Italy; (7) Institute for Medical Genetics, Charité University Hospital, Berlin, Germany.

***J Am Soc Nephrol* 16: 1245-56, 2005**

Vacuolar H$^+$-ATPase d2 Subunit: Molecular Characterization, Developmental Regulation, and Localization to Specialized Proton Pumps in Kidney and Bone

Annabel N. Smith,* François Jouret,‖ Sharyn Bord,† Katherine J. Borthwick,* Rafia S. Al-Lamki,† Carsten A. Wagner,¶ Deborah C. Ireland,† Valerie Cormier-Daire,# Annalisa Frattini,** Anna Villa,** Uwe Kornak,†† Olivier Devuyst,‖ and Fiona E. Karet*§

*Departments of *Medical Genetics and †Medicine and §Division of Renal Medicine, University of Cambridge, Cambridge, United Kingdom; ‖Division of Nephrology, Université catholique de Louvain, Brussels, Belgium; ¶Institute of Physiology, University of Zurich, Zurich, Switzerland; #Department of Medical Genetics, Hôpital Necker, Paris, France; **Istituto di Tecnologie Biomediche, Milan, Italy; and ††Institute for Medical Genetics, Charité University Hospital, Berlin, Germany*

The ubiquitous multisubunit vacuolar-type proton pump (H$^+$- or V-ATPase) is essential for acidification of diverse intracellular compartments. It is also present in specialized forms at the plasma membrane of intercalated cells in the distal nephron, where it is required for urine acidification, and in osteoclasts, playing an important role in bone resorption by acid secretion across the ruffled border membrane. It was reported previously that, in human, several of the renal pump's constituent subunits are encoded by genes that are different from those that are ubiquitously expressed. These paralogous proteins may be important in differential functions, targeting or regulation of H$^+$-ATPases. They include the d subunit, where d1 is ubiquitous whereas d2 has a limited tissue expression. This article reports on an investigation of d2. It was first confirmed that in mouse, as in human, kidney and bone are two of the main sites of d2 mRNA expression. d2 mRNA and protein appear later during nephrogenesis than does the ubiquitously expressed E1 subunit. Mouse nephron-segment reverse transcription–PCR revealed detectable mRNA in all segments except thin limb of Henle's loop and distal convoluted tubule. However, with the use of a novel d2-specific antibody, high-intensity d2 staining was observed only in intercalated cells of the collecting duct in fresh-frozen human kidney, where it co-localized with the a4 subunit in the characteristic plasma membrane-enhanced pattern. In human bone, d2 co-localized with the a3 subunit in osteoclasts. This different subunit association in different tissues emphasizes the possibility of the H$^+$-ATPase as a future therapeutic target.

J Am Soc Nephrol 16: 1245–1256, 2005. doi: 10.1681/ASN.2004090761

The multisubunit vacuolar-type proton pump (H$^+$- or V-ATPase) is essential for acidification of diverse intracellular compartments in eukaryotic cells, including endosomes, lysosomes, clathrin-coated and synaptic vesicles, chromaffin granules, and the central vacuoles of plants and fungi. In addition, H$^+$-ATPases function to pump protons across the plasma membrane of certain cell types, one such example being the H$^+$-ATPases present at high density at the apical surface of α-intercalated cells in the collecting duct of the distal nephron, where vectorial proton transport is required for urinary acidification and the maintenance of acid-base homeostasis (1).

Plasma membrane H$^+$-ATPases also play an important role in bone resorption by osteoclasts (2). Osteoclasts form a sealed extracellular compartment (resorption lacuna) between the plasma membrane (ruffled border) and the bone surface. Large numbers of H$^+$-ATPases present in the ruffled border acidify this resorption lacuna, facilitating mineral solubilization and the hydrolysis of bone matrix by proteolytic enzymes such as cathepsin K (3).

The general structure of H$^+$-ATPases comprises two functional sectors, V_1 and V_0. The peripheral V_1 domain binds and hydrolyzes ATP, providing the energy for H$^+$ translocation across the integral membrane V_0 domain. The complete identity of all of the pump components has yet to be elucidated, but the structural model put forward by Nishi and Forgac (4), based mostly on studies of the bovine clathrin-coated vesicle and yeast H$^+$-ATPases, suggests that there are at least 13 different subunits. In this model (Figure 1), the V_1 domain (640 kD) comprises subunits A through H, in a proposed stoichiometry of $A_3B_3C_1D_1E_1F_1G_2H_1$, whereas V_0 (260 kD) contains five subunits in a possible complex of $a_1d_1c''_1(c, c')_{5-6}$, although whether the c′ subunit is present in all species is currently unclear. Another integral membrane protein, the e subunit, also referred to as M9.7 or M9.2, was recently shown to be essential for H$^+$-ATPase activity in yeast and is probably a functionally essential part of all eukaryotic H$^+$-ATPases (5).

Received September 13, 2004. Accepted February 15, 2005.

Published online ahead of print. Publication date available at www.jasn.org.

Address correspondence to: Dr. Fiona Karet, Cambridge Institute for Medical Research, Box 139 Addenbrooke's Hospital, Cambridge, CB2 2XY, UK. Phone: +44-1223-762617; Fax: +44-1223-331206; E-mail: fek1000@cam.ac.uk

ISSN: 1046-6673/1605-1245

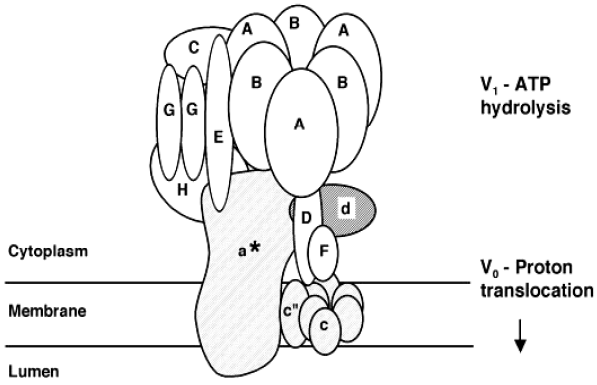

Figure 1. Schematic model of the H^+-ATPase. Adapted from reference 4. The peripheral V_1 domain subunits A through H are indicated by open symbols, and the integral membrane V_0 domain subunits a, c, and c″ are shown as gray hatched symbols, with the subject of this study, the d subunit, being indicated by darker hatching. The c′ subunit is not shown because it may not be present in all H^+-ATPases, and the e subunit was not included in this model. *The a-subunit has four different isoforms; those most relevant to this study are a3 and a4, which are present in the proton pumps found at the ruffled border of osteoclasts and the cell surface of renal intercalated cells, respectively.

The precise function(s) of many of the proton pump's subunits and the interactions between them remain undetermined. Moreover, in higher eukaryotes, several H^+-ATPase subunits have recently been shown to have multiple isoforms encoded by different genes and with differing tissue expression patterns, as summarized in Table 1. These include the B, C, E, G, a, d, and e subunits (6–12). The existence of different subunit isoforms may play an important role in the localization and activity of proton pumps in specific cell types and subcellular compartments. In support of this hypothesis, we showed previously that in human, mutations in the genes encoding B1 and a4, isoforms of the B and a-subunits that are predominantly expressed in the apical proton pumps of α-intercalated cells in the kidney, cause autosomal recessive distal renal tubular acidosis (RTA) (13,14). Similarly, autosomal recessive osteopetrosis (ARO) can be caused by mutations in a3 (15,16), a different isoform of the a-subunit that is chiefly expressed in proton pumps at the ruffled border of osteoclasts. These observations suggest that the normal functioning of some specialized types of H^+-ATPase is dependent on the presence of particular subunit isoforms, which cannot be substituted fully by a different isoform of the same subunit.

We showed previously that in human, the d2 subunit gene is expressed predominantly in kidney and osteoclasts, whereas d1 is ubiquitously expressed (10). We now report an investigation into the distribution of d2 in kidney and bone. We also analyzed the expression of the d2 subunit during mouse and human nephrogenesis and compared this with expression of the ubiquitously expressed d1 and E1 subunits, as well as with a3.

Materials and Methods

Ethical Approval

All tissues were procured with appropriate institutional ethical approval (Addenbrooke's Hospital Local Research Ethics Committee, Université catholique de Louvain Ethical Review Board).

Reverse Transcription–PCR

Total RNA was prepared from freshly harvested mouse tissues using TRIzol Reagent (Invitrogen, San Diego, CA) by standard methods. Two micrograms each of kidney, liver, testis, bone, brain, heart, skeletal muscle, lung, spleen, and thymus RNA was treated with RQ1 RNase-free DNase I (Promega, Madison, WI) and then reverse-transcribed using Super RT (HT Biotechnology Ltd, Cambridge, UK) and oligo $p(dT)_{18}$ (New England BioLabs, Beverly, MA) as primer according to the manufacturer's protocol. An aliquot of each cDNA preparation was used as template for PCR with the following primers: *Atp6v0d1*, AGCAGATGGAGGCTGTGAACATC and ACACCAAAATGGAACTGGTTCAGG; *Atp6v0d2*, CAGAGATGGAAGCTGTCAACATTG and ACACCATAATGGAATTGCCTGTTG. These primers lie in exons 3 and 8 of both *Atp6v0d1* and *Atp6v0d2*, and the expected products are 535 and 532 bp in size, respectively. For confirming successful reverse transcription, a 540-bp fragment of β-actin was amplified in parallel using the primers GTGGGCCGCCCTAGGCAC and CTCTTTGATGTCACGCACGATTTC. In each experiment, sterile water was used as template to provide a negative control. Reverse transcription reactions performed in the absence of enzyme provided a negative control sample for each tissue (data not shown). PCR fragments were resolved by electrophoresis in a 2% agarose gel.

Nephron Segment Isolation and Reverse Transcription–PCR

C57BL/6J mice (male, 25 to 30 g; Jackson Laboratory, Bar Harbor, ME) were anesthetized with ketamine and perfused through the left ventricle with PBS that contained 250 μg/ml collagenase (Sigma, St. Louis, MO). The kidneys were rapidly removed, and coronal slices 2 to 3 mm thick were cut and incubated in PBS/collagenase at 37°C for 15 min. After rinsing with ice-cold PBS, nephron segments were hand-dissected and placed in TRIzol. Total RNA was extracted and reverse-transcribed as described above. An aliquot of each cDNA preparation was amplified by PCR using the *Atp6v0d2* primers shown above. A 452-bp fragment of glyceraldehyde-3-phosphate dehydrogenase (G3PDH) was amplified in parallel using the primers ACCACAGTCCATGCCATCAC and TCCACCACCCTGTTGCTGTA. In each experiment, sterile water was used as template to provide a negative control.

Polyclonal Antisera

Two peptides, one containing 13 internal residues of human d2 (amino acids 67 to 79; VSKIDTEMRKRLC, peptide 1) and one corresponding to the C terminal 17 residues (amino acids 334 to 350; CISQRHRTKINSYIPIL, peptide 2) were synthesized, conjugated to keyhole limpet hemocyanin, and used to raise a guinea pig polyclonal antiserum, designated SK20 (Eurogentec, Seraing, Belgium).

Western Blot Analysis

Western blot analysis was carried out by standard methods, using nonfat dried milk as the blocking agent, and SK20 antiserum, either at 1:1000 dilution or 1:50, after affinity purification against peptide 2. Preimmune serum from the same animal was used as a control. Extracts of human renal cortex, rat and mouse whole kidney, and mouse brain were prepared by grinding up 0.5 to 1.0 g of snap-frozen tissue under liquid nitrogen, transferring to homogenization buffer (10 mM Tris, 150 mM NaCl, 2 mM PMSF, 1 mM EGTA, 1 mM EDTA, and 1 mM DTT,

Table 1. Mammalian H^+-ATPase subunits expressed at specialized sites in kidney and bone[a]

Subunit	Tissue	Species	mRNA	Protein	Evidence for Presence in Specialized H^+-ATPase		References
					Technique	Site	
B1	Kidney	Human	√	√	IL	IC plasma membrane (co-localizes with a4)	13,14,35
		Mouse	√	√	IL	IC plasma membrane	26,29
					Co-IP (C2, G3, a4, d2)	Kidney membranes	26
		Bovine	√	√			6
		Rat		√	IL	IC plasma membrane	6
	Inner ear	Human	√				13
		Mouse		√	IL	Endolymphatic sac/ cochlea	13
	Placenta	Human	√				35
	Male genital tract	Mouse	√	√	IL	Epididymis	29
		Rat		√	IL	Epididymis/vas deferens	36
	Eye	Rat		√	IL	Ciliary epithelium	37
		Rabbit		√	IL	Ciliary epithelium	37
C2	Kidney	Human	√				10
		Mouse (C2b)	√	√	IL	IC plasma membrane	11,26
					Co-IP (B1)	Kidney membranes	26
	Placenta	Human	√				10
	Lung	Mouse (C2a)	√	√	IL	Type II alveolar cells	11,26
G3	Kidney	Human	√				10
		Mouse	√	√	IL	IC plasma membrane	11,26
					Co-IP (B1)	Kidney membranes	26
a3[b]	Bone	Human	√	√	IL	Osteoclasts (co-localizes with d2[c])	15,24,38
		Mouse	√	√	IL	Osteoclasts	22,25,39,40
		Rabbit	√		ISH	Osteoclasts	41
a4	Kidney	Human	√	√	IL	IC plasma membrane (co-localizes with B1, d2[c])	14,21
		Mouse	√	√	IL	IC plasma membrane	7,8,21,26
					Co-IP (B1, B2)	Kidney membranes	26
	Inner ear	Human	√				42
		Mouse		√	IL	Endolymphatic sac	43
	Male genital tract	Mouse		√	IL	Epididymis/vas deferens	8,21
d2[b]	Kidney	Human	√	√	IL	IC plasma membrane (co-localizes with a4[c])	10
		Mouse	√ [c]	√	IL	IC plasma membrane	11,26,33
					Co-IP (B1)	Kidney membranes	26
	Bone	Human	√	√	IL	Osteoclasts (co-localizes with a3[c])	10
		Mouse	√ [c]				
	Lung	Human	√				10
		Mouse	√ [c]				33

[a]Co-IP, co-immunoprecipitation; IL, immunolocalization; ISH, *in situ* hybridization; IC, intercalated cells.
[b]mRNA has been observed at low levels in more widespread distribution.
[c]This study.

with one Complete Mini EDTA-free Protease Inhibitor Cocktail tablet [Roche, Lewes, UK] per 10 ml of buffer), homogenizing at 15,000 rpm with a Polytron homogenizer (Kinematica, Basel, Switzerland) for 1 min, and centrifuging at 1000 × *g* for 10 min at 4°C. For separating membrane and cytosolic fractions, supernatants were centrifuged further at 100,000 × *g* for 1 h at 4°C. Extracts of human cancellous bone were prepared by shaking fragments of bone tissue, snap-frozen in liquid nitrogen, at 2500 rpm for 2 min using a Mikro-Dismembranator S homogenizer (B. Braun Biotech, Melsungen, Germany). The crushed bone was resuspended in homogenization buffer and centrifuged as above. Protein concentrations were determined using the BioRad Protein Assay kit (Hercules, CA), and 30 or 40 μg of each was used for PAGE.

Osteoclast Culture

CD14-positive monocytes were isolated from peripheral blood of normal volunteers by magnetic bead sorting (Millenyi Biotec, Sunnyvale, CA) according to the manufacturer's protocol. For generating osteoclasts, cells were cultured in α-MEM supplemented with 10% FCS (Invitrogen), human recombinant M-CSF (25 ng/ml; R&D Systems, Abingdon, UK), and human recombinant soluble RANKL (50 ng/ml; Insight Biotechnology, Wembley, UK) on Osteologic calcium phosphate–coated slides (BD Biosciences, Oxford, UK) for 7 d at 37°C in 5% CO_2. Cells then were either prepared for immunofluorescence analysis by washing in PBS; fixing in 4% paraformaldehyde; permeabilizing using 0.1% Triton X-100; and staining for a3, d2, and vitronectin receptor (VNR) as described below or stained using Diffquik (Baxter, McGaw Park, IL) to identify osteoclasts and resorption pits. Diffquik-stained cells were visualized on a Nikon E800 microscope, and images were captured using a Basler camera.

Immunolocalization

Samples of normal human kidney were obtained from the unaffected portions of nephrectomy specimens removed for renal tumors. Samples were snap-frozen in Tissue-Tek O.C.T Compound (Sakura FineTek Europe, Zoeterwoude, The Netherlands), using isopentane cooled over liquid nitrogen. Serial 7-μm frozen cryostat-cut sections were placed on poly-L-lysine-coated (BDH) (Dagerham, UK) slides and stored at −80°C until use.

Neonatal ribs were collected post mortem from infants who were born at full term with no evidence of growth retardation or skeletal abnormalities. Ribs were immediately placed on ice and then embedded in 5% polyvinyl alcohol (Sigma) and snap-frozen in liquid nitrogen. Serial 9-μm frozen sections were cryostat-cut and picked off onto 2% 3-aminopropyltriethoxysilane–coated (Sigma) slides, air dried for 15 min, and stored at −80°C until use.

Sections were permeabilized with 100% methanol for 5 min at −20°C and washed twice with PBST (1× PBS, 0.01% Tween 20). Sections were incubated in 0.5% BSA/PBST for 15 min at room temperature, before primary antibody was applied overnight at 4°C. Primary antibodies were diluted in 0.5% BSA/PBST as follows: Guinea pig anti-human d2 (SK20) or preimmune serum 1:100; affinity-purified SK20 1:3; rabbit anti-human a3 1:1000 (gift of Jan Mattsson, AstraZeneca, Mölndal, Sweden); rabbit anti-human a4 (RA2922 [14]) 1:3000; rabbit anti-rat/mouse aquaporin-2 1:100 (Chemicon International, Temecula, CA); rabbit anti-OKP cell (opossum) megalin 1:500 (gift of Daniel Biemesderfer, Yale University); and mouse monoclonal 23C6 anti-human VNR 1:5 (gift of Mike Horton, University College London). Sections were washed three times with PBST before the following secondary antibodies (Molecular Probes, Eugene, OR) were applied at 1:250 dilution in 0.5% BSA/PBST for 1 h at room temperature: Goat anti-guinea pig Alexa 488, goat anti-rabbit Texas Red, and goat anti-mouse Alexa 568. After sections were washed three times with PBST, they were mounted with VECTASHIELD Mounting Medium with DAPI (Vector Laboratories, Burlingame, CA) and viewed using either a Zeiss Axiovert 200M fluorescence microscope and Improvision Openlab Volume Deconvolution software or a Zeiss LSM510 META confocal microscope.

Nephrogenesis Studies

Samples from human fetal kidneys, ranging from 12 to 25 wk of gestation, neonatal kidney at 4 mo, and adult kidney were obtained from the International Institute for Advancement of Medicine (Philadelphia, PA) and the Anatomic Gift Foundation (Woodbine, GA). Mouse kidney samples were obtained from CD-1 mice (Iffa Credo, Brussels, Belgium). Pregnant mice were killed by cervical dislocation. Embryos were removed and microdissected to isolate kidneys. Embryos from four different litters (average 12 embryos/litter) were collected every day from embryonic day 13.5 (E13.5) until day 5 after birth (newborn). Comparative studies were performed with four adult male kidneys.

Mouse kidney samples were homogenized in TRIzol, and total RNA was extracted and reverse-transcribed as described above. For semi-quantitative reverse transcription–PCR (RT-PCR), cDNA preparations were amplified using the following primers: *Atp6v0d2*, CTTGAGTTTGAGGCCGACAG and TTGAGCTAACAACCGCAACC; *Atp6v0d1*, GCCAGCTTCCTGGACTTCAT and ACAGCCTCCATCTGCTCAAA; *Atp6v1e1*, GGCGCTCAGCGATGCAGATGT and CAAGGCGACCTTTCTCAATG; and *Atp6v0a3*, TGCTCATGGGTCTGTTCTCC and CATGGAGTGCTGGGACAGAT, which give products of 138, 143, 134, and 149 bp, respectively. A 177-bp fragment of G3PDH was amplified in parallel using primers TGCACCACCAACTGCTTAGC and GGATGCAGGGATGATGTTCT. PCR conditions were 94°C for 5 min followed by 35 (d2 subunit), 32 (d1 subunit), 33 (E1 subunit), 35 (a3 subunit), and 30 (G3PDH) cycles of 30 s at 95°C, 30 s at 61°C, and 1 min at 72°C. Negative controls included non–reverse-transcribed RNA samples and sterile water.

Real-time PCR analyses (iCycler iQ System; BioRad) were performed in duplicate using the primers shown above and iQ SYBR Green Supermix as described previously (17). PCR mixtures contained 10 nM fluorescein for initial well-to-well fluorescence normalization. PCR conditions were as follows: 94°C for 3 min followed by 40× (30 s at 95°C, 30 s at 61°C, and 1 min at 72°C). The melting temperature of each PCR product was established by recording SYBR Green fluorescence increase upon slowly renaturing DNA at the end of PCR. For each assay, standard curves were prepared by serial four-fold dilutions of mouse adult kidney cDNA. Relative mRNA expression of the d2, d1, E1, and a3 subunits was investigated in four adult male kidneys, after normalization to G3PDH: Ratio = $2^{\Delta Ct\,(G3PDH-Target\,Gene)}$. At each embryonic stage, mRNA levels of the different subunits were adjusted to the G3PDH mRNA level, and relative changes in mRNA levels during ontogeny were determined by comparison to the adult level (taken as 100%) using the following formula: Ratio = $(Efficiency_{target})^{\Delta Ct(Adult-sample)}/(Efficiency_{G3PDH})^{\Delta Ct\,(Adult-sample)}$ (18).

Kidney membrane extracts were prepared for Western blot analysis as described previously (19). Immunoblotting was carried out by standard methods, using a mouse mAb against the bovine E1 subunit (gift of Stephen Gluck, Gainesville, FL) at a 1:100 dilution and guinea pig anti-human d2 (SK20) at a 1:1000 dilution. Normalization for β-actin was obtained after stripping the blots and reprobing with a mouse monoclonal anti–β-actin antibody (Sigma). All immunoblots were performed at least in duplicate.

Screening of ARO Kindreds

With appropriate local ethical approval, genomic DNA from the affected index cases of 25 ARO kindreds and one with coexistent osteopetrosis and RTA was prepared from whole blood by standard procedures (20). All exons of the *ATP6V0D2* gene were individually amplified by PCR, using primers designed from intronic sequences flanking each exon. PCR products were sequenced using BigDye Terminator v3.1 Cycle Sequencing (Applied Biosystems, Foster City, CA).

Results

Expression Profile of the Murine d2 Subunit

We first used RT-PCR analysis to assess the gene expression profiles of the d1 and d2 subunit isoforms in a panel of 10 mouse tissues (Figure 2A). This demonstrated that the d1 isoform is ubiquitously expressed, whereas d2 is predominantly expressed in kidney, bone, and lung. The d2 isoform is also expressed at apparently lower levels in thymus, skeletal muscle, heart, and liver, although it must be noted that the assay is not quantitative. These findings are broadly in agreement with those seen previously in human, where d2 was expressed chiefly in kidney and osteoclasts (10).

Mouse Nephron Segment–Specific RT-PCR

To investigate the renal distribution of d2, we used RT-PCR to examine d2 expression in defined tubule segments prepared from mouse kidney as described previously (21). As shown in Figure 2B, d2 mRNA is present in proximal tubule, cortical collecting duct, outer medullary collecting duct, inner medullary collecting duct, and papilla. It does not seem to be expressed in the thin loop of Henle or the distal convoluted tubule.

Antibody SK20 Specifically Recognizes the d2 Subunit

We wished to confirm the localization of d2 in kidney at the protein level and also look at the distribution of this subunit in bone. We therefore raised a polyclonal antibody (SK20) in guinea pig, directed against two regions of the human d2 protein: An internal peptide of 13 residues and one corresponding to the C terminal 17 residues. We first confirmed specificity by ELISA using SK20 with and without separate affinity purification against the immunizing peptides. Immunoblotting extracts from kidney and brain showed that SK20 recognizes a protein of approximately 40 kD, corresponding to the predicted size of d2, in human kidney membrane extract but not kidney cytosol (Figure 3A). No d2 signal was seen using preimmune serum from the same animal (data not shown). Both crude and affinity-purified SK20 also cross-reacted with d2 in mouse and rat kidney membrane (Figure 3B). No band corresponding to d2 was seen in mouse brain membrane extract (data not shown). This is consistent with the RT-PCR analysis and, importantly, indicates that SK20 does not cross-react with the ubiquitously expressed d1 isoform.

Immunolocalization of d2 in Human Kidney

SK20 was used to localize d2 in unfixed frozen human kidney sections. High-intensity d2 staining was seen at the apical surface of intercalated cells in both cortical and medullary collecting ducts, with some appearing intracellularly. This appearance of d2 co-localized completely with a4 staining (Figure 4, A and B), confirming the cell type. No d2 staining was seen in cells that were positive either for the principal cell marker aquaporin-2 (Figure 4D) or for the proximal tubule marker megalin (Figure 4E). Specificity of the d2 staining was confirmed by its absence when preimmune serum from the same animal was substituted (Figure 4C).

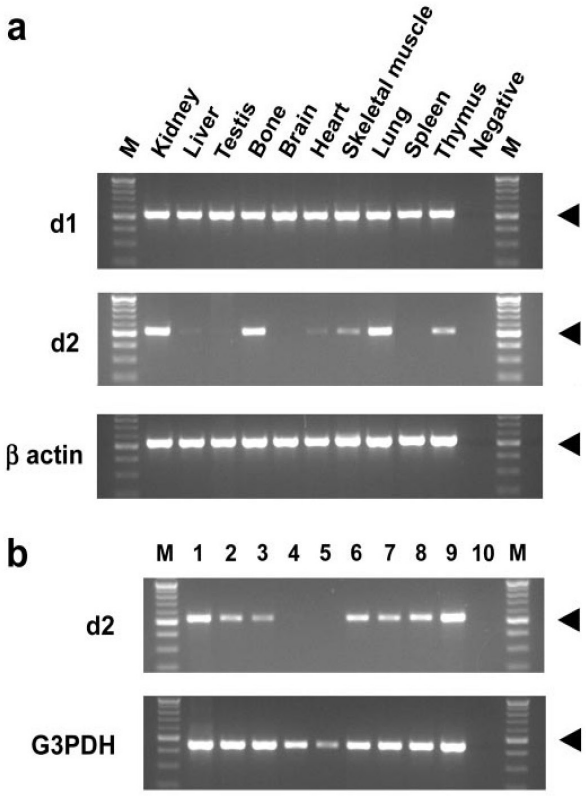

Figure 2. Reverse transcription–PCR (RT-PCR) amplification of d1 and d2 subunit mRNA from mouse tissues. (A) PCR amplification of cDNA from 10 mouse tissues was performed using gene-specific primers. *Atp6v0d1* (535-bp product) is expressed in all tissues. In contrast, *Atp6v0d2* (532 bp) is expressed chiefly in kidney, bone, and lung. β-Actin–specific primers generated a 540-bp product in all tissues, confirming successful reverse transcription. Water replaced cDNA as a negative control. Size markers (M) are in increments of 100 bp; arrowheads indicate the 500-bp band. (B) PCR amplification of *Atp6v0d2* was performed using cDNA prepared from defined segments of the mouse nephron: Total kidney (lane 1), proximal tubule S1 with glomerulus (lane 2), proximal tubule S1-S3 (lane 3), thin loop of Henle (lane 4), distal tubule (lane 5), cortical collecting duct (lane 6), outer medullary collecting duct (lane 7), inner medullary collecting duct (lane 8), papilla (lane 9), and negative control (lane 10). *Atp6v0d2* mRNA (532-bp product) is present in all of the segments studied except the thin limb of Henle's loop and distal tubule. Glyceraldehyde-3-phosphate dehydrogenase (G3PDH)-specific primers generated a 452-bp product in all tubule segments, confirming successful reverse transcription. Size markers (M) are in increments of 100 bp; arrowheads indicate the 500-bp band.

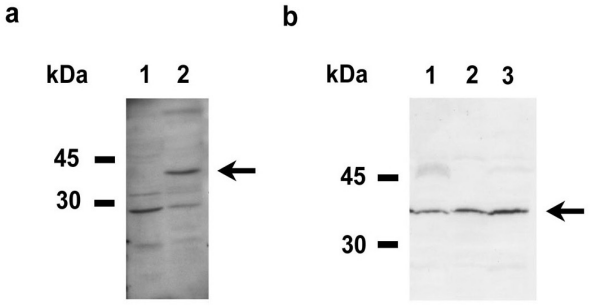

Figure 3. Western blot analysis of d2 expression in kidney extracts. (A) immunoblotting of human kidney cytosol (lane 1) and human kidney membrane (lane 2). The guinea pig polyclonal antibody SK20 recognizes a protein of approximately 40 kD (indicated by the arrow), corresponding to the predicted size of d2, in human kidney membrane extract but not in kidney cytosol. (B) Immunoblotting, using affinity-purified SK20, of human kidney membrane (lane 1), rat kidney membrane (lane 2), and mouse kidney membrane (lane 3). SK20 cross-reacts with d2 in rat and mouse kidney membrane (indicated by the arrow).

Immunolocalization of d2 in Cultured Human Osteoclasts and Human Neonatal Rib Bone

We studied d2 expression in bone both *in vitro* and *ex vivo*. Primary osteoclasts that were cultured on a synthetic resorbable substrate were used to demonstrate sites of localization of d2, the H^+-ATPase a3 subunit, and the VNR (integrin $\alpha V\beta 3$), a marker of osteoclast activity. Areas of lysis of the substrate were always associated with large multinucleated cells, indicating active resorption (Figure 5A). By confocal microscopy, these large cells were identified as osteoclasts, first by their intense staining for VNR and second by their multinuclearity seen with DAPI staining (Figure 5B). VNR was widely localized in the plasma membrane, again indicative of resorptive activity. There was less VNR staining within a basal area, within which, in these same cells, a3 and d2 co-localized, adjacent to the substrate (Figure 5C). a3 is known to be present at the ruffled border of osteoclasts and in late endosomes and lysosomes (22).

The *in vivo* localization of d2 in unfixed frozen human neonatal rib bone sections was also studied using SK20. Staining was confined to osteoclasts, as confirmed by positive staining of VNR (Figure 5D). d2 signal fully co-localized with staining for a3 in these cells (Figure 5E). No specific staining was seen when preimmune serum from the same animal was substituted (Figure 5F).

Thus, d2 is co-expressed with the a4 subunit in kidney and the a3 subunit in bone. However, Northern blot and RT-PCR (23–25) have demonstrated a3 mRNA in human and mouse kidney, and immunoprecipitation data have suggested that a3 protein is expressed in mouse kidney (26). We therefore sought to determine whether d2 is also co-expressed with the a3 subunit in human renal tissue, but on no occasion did the anti-a3 antibody show a staining pattern in human kidney sections. This does not necessarily exclude low levels of a3 protein expression in kidney but suggests that it may be present only at levels that are undetectable using this antibody. Conversely, a4 immunofluorescence was not detectable in bone sections (data not shown), confirming our previous negative RT-PCR findings from both mouse and human (8 and Smith *et al.*, unpublished data).

Comparative Quantification of d2 mRNA in Adult and Developing Mouse Kidney

We conducted real-time RT-PCR studies to establish the relative expression of d2 with respect to several other H^+-ATPase subunits (d1, E1, and a3) both during mouse nephrogenesis and in adult mouse kidney. As might be expected from its limited distribution pattern, these studies showed that in mature kidney, the d2 subunit mRNA was approximately 20-fold less prevalent than was message for the E1 subunit (Figure 6, A and B) and approximately 10-fold less abundant than d1 mRNA, both of which are ubiquitously expressed. a3 subunit mRNA was also less well expressed, by approximately the same fractions.

In the developing kidney, semiquantitative (Figure 6C) and real-time (Figure 6D) PCR analyses showed detectable d2 mRNA expression at E15.5 (approximately 10% of the adult level), with a progressive increase during late ontogeny (E17.5; approximately 45%) to reach the adult level at birth. By contrast, the ubiquitous d1 and E1 subunits were characterized by earlier (E13.5) expression, but whereas E1 levels seemed stable (approximately 50% of the adult level) throughout nephrogenesis followed by a significant increase at birth, as previously observed (17), the d1 isoform gradually decreased during late ontogeny before a neo-induction at birth. Although overall levels of a3 were low in the adult kidney (Figure 6B), its ontogeny pattern was characterized by an early and stable expression at a relatively higher level (approximately 150% of the adult level), with no significant change until after birth.

We also investigated the ontogeny pattern of d2 at the protein level. Immunoblotting (Figure 6E) confirmed the later detection of d2 expression at E15.5 compared with E1, but in contrast to the mRNA data, expression of E1 was seen to increase gradually from E16.5 until birth. However, there was only a negligible increase in d2 protein expression levels during late ontogeny, which contrasts with the semiquantitative and real-time PCR analyses. Of note, the d2 immunoreactive pattern was seen as a doublet in the fetal and newborn samples, whereas only the lower molecular weight band was present in the adult sample.

Expression of the d2 Subunit during Human Nephrogenesis

The expression of the d2 subunit of the H^+-ATPase during human nephrogenesis was also investigated using immunoblotting (Figure 6F). This subunit was detected from 12 gestational weeks and showed stable expression throughout kidney organogenesis. As in mouse, d2 was detected in fetal samples as a doublet, with increasing prominence of the larger band, which was noted to persist in infancy, whereas only a single band was observed in adult kidney, corresponding to the lower molecular weight band as in mouse. The significance of this doublet and the apparent switch in size are unclear at present.

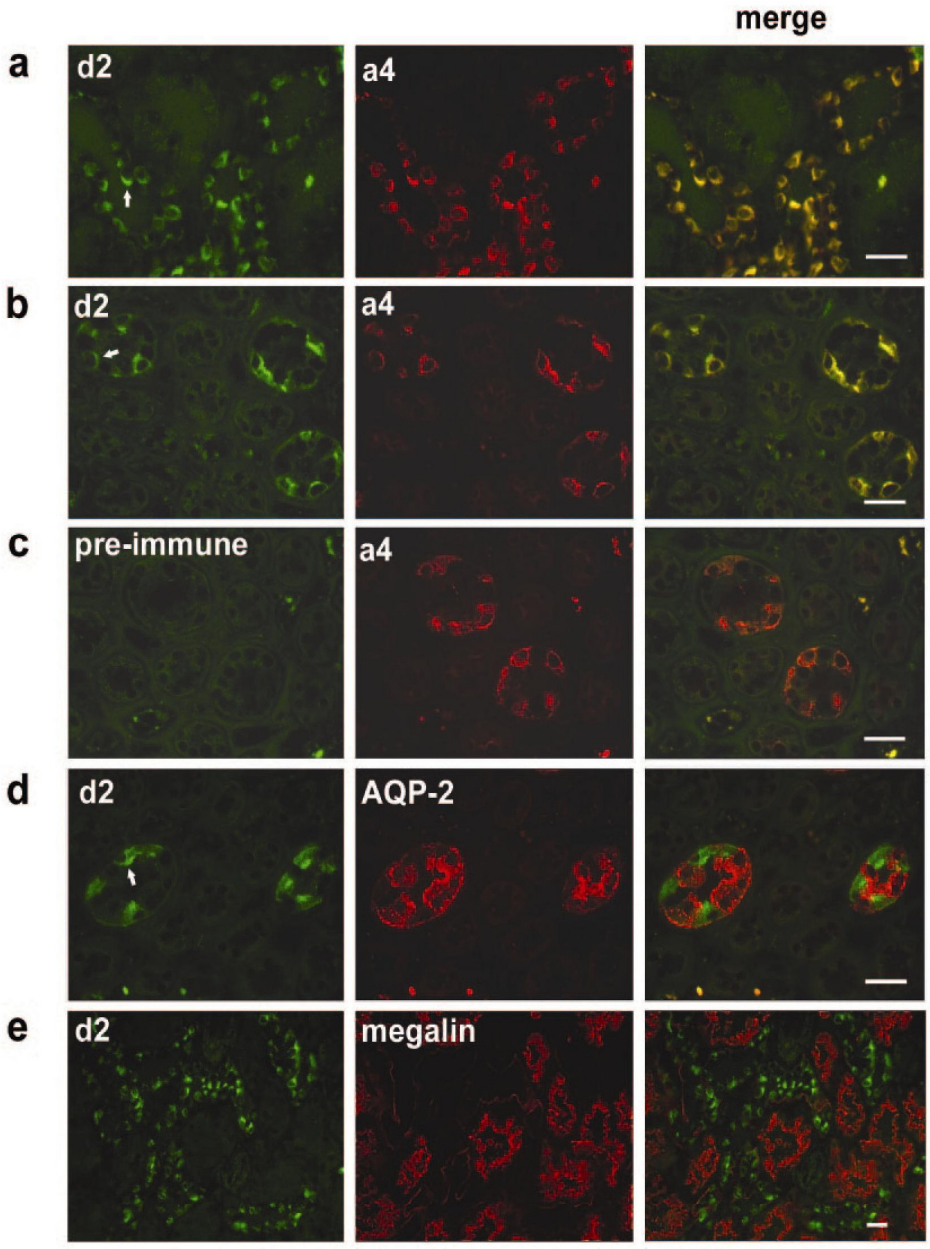

Figure 4. Immunolocalization of d2 in human kidney. SK20 was used to localize d2 in 7 μm unfixed frozen human kidney sections. Cortex (A) and medulla (B) incubated with SK20 (green) and the anti-a4 antibody RA2922 (red) reveal high-intensity d2 staining, co-localizing with a4 staining (yellow), at the apical surface of intercalated cells in the collecting duct (examples indicated by arrows). The specificity of d2 staining was confirmed by its absence when preimmune serum from the same animal was substituted (medulla; C). Confirmation of the collecting duct intercalated cell localization of d2 was provided by the absence of co-localization with either the principal cell marker aquaporin-2 (AQP-2; medulla; D) or the proximal tubule marker megalin (cortex; E). All scale bars = 25 μm.

Screening ARO Patients

Having found co-localization of d2 and a3 in osteoclasts, we proceeded to assess the candidacy of the *ATP6V0D2* gene encoding the d2 subunit as a causative gene of autosomal recessive osteopetrosis. We obtained genomic DNA from a 39-yr-old white woman who had osteopetrosis accompanied by a urine acidification defect, hypokalemia, and nephrocalcinosis and in whom normal carbonic anhydrase II levels have been found. Direct sequencing of coding exons and exon-intron boundaries of *ATP6V0D2* revealed no departures from wild-type sequence.

We also screened the gene in a cohort of 25 patients from 23 kindreds that either do not have potential disease-associated mutations in genes that are known to cause ARO, namely *TCIRG1*, *CLCN7*, and *OSTM1*, which encode the H^+-ATPase a3 subunit,

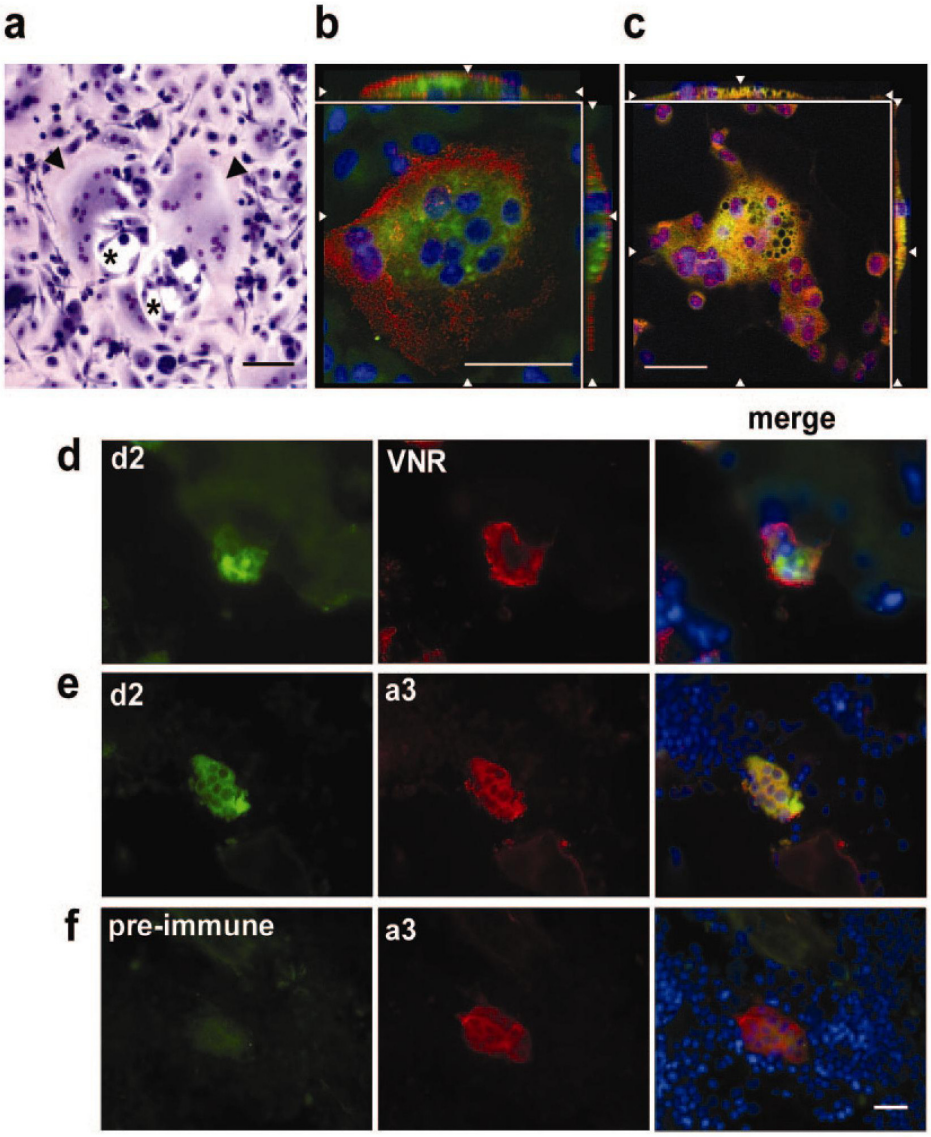

Figure 5. Immunolocalization of d2 in human cultured osteoclasts and neonatal rib bone. (A through C) Primary human osteoclasts cultured on a synthetic resorbable substrate. (A) Light microscopy reveals two large multinucleated osteoclasts (arrowheads) and associated areas of substrate lysis (*). (B and C) Merged confocal images of single osteoclasts stained for d2 (green) and one of two osteoclast markers (red): Vitronectin receptor (VNR; B) or the H^+-ATPase a3 subunit (C). Nuclei were stained using DAPI (blue). (B) VNR staining localizes to the plasma membrane, and d2 staining is seen intracellularly and in the ruffled border region, adjacent to the substrate. (C) d2 staining co-localizes with a3 (yellow). White arrowheads indicate planes of cross section. (D through F) 9-μm human frozen neonatal rib bone sections, stained for d2 and either VNR (D) or a3 (E) as above. DAPI staining demonstrates the presence of one multinucleated osteoclast per panel. As seen with cultured osteoclasts, d2 and a3 co-localize (E), with VNR staining present mainly at the cell surface (D). Specificity of d2 staining was confirmed by its absence when preimmune serum was substituted (F). All scale bars = 50 μm.

ClC-7 chloride channel, and grey-lethal protein, respectively (13 patients), or in whom only one disease-causing allele has been identified (12 patients). The affected subjects all met the clinical and biochemical criteria for the disease. RTA was absent in this group. Twenty of these patients have been previously reported (16,27,28). No potential disease-causing sequence alterations were found. This sequence analysis did identify a heterozygous single-nucleotide polymorphism (SNP), 814G→A, in exon 6 in one patient, which results in a missense alteration (G272R). As this SNP was also found heterozygously in both unaffected parents, it cannot be disease causing in isolation in the heterozygous state. We subsequently found that this SNP has recently been entered into the NCBI dbSNP database. In addition, we identified two novel intronic SNP (IVS4–12C→T and IVS5+42C→T) that were common, each being present in five patients.

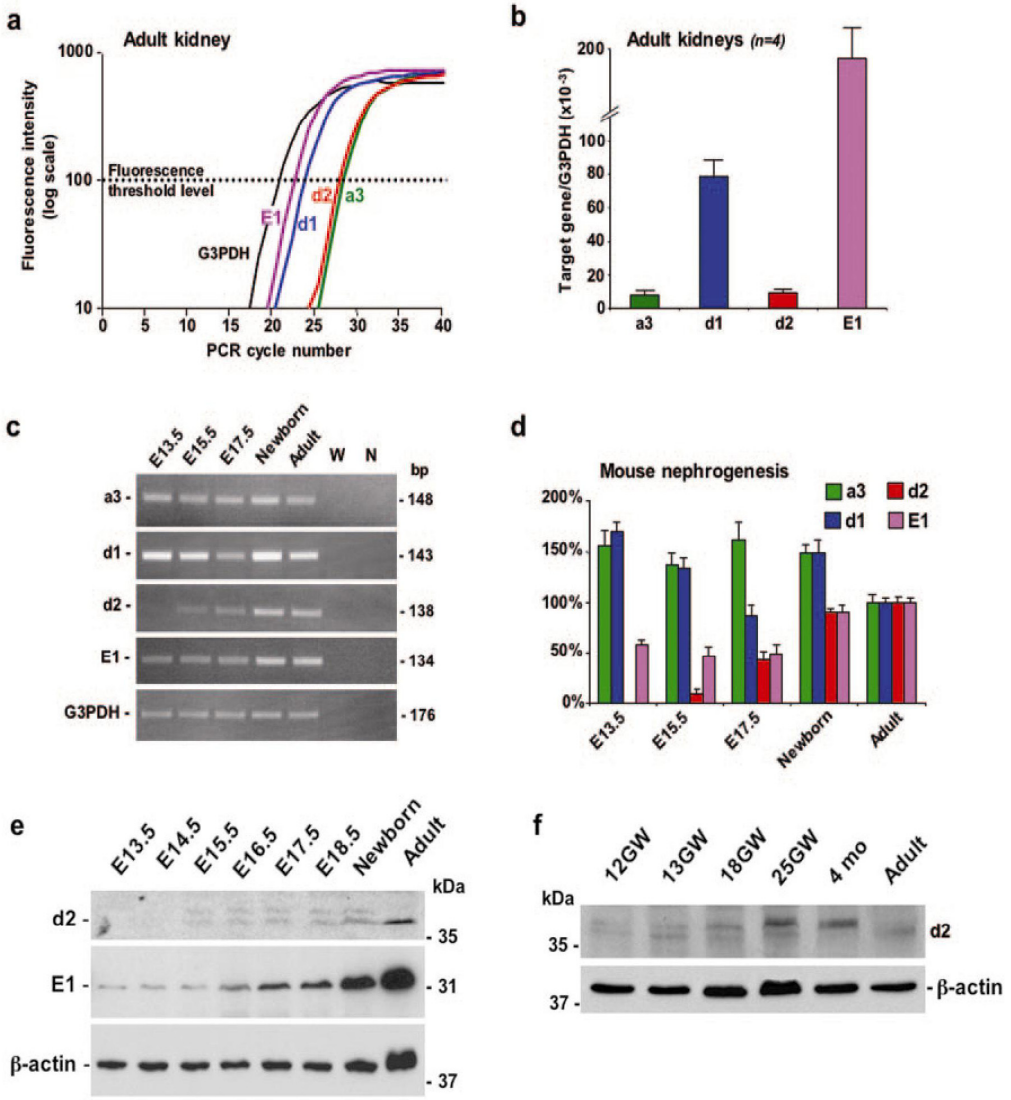

Figure 6. Comparative ontogeny of the d2, d1, E1, and a3 subunits during mouse and human nephrogenesis. (A) Representative tracings of G3PDH, a3, d1, d2, and E1 mRNA amplification by real-time RT-PCR in adult mouse kidney. (B) Comparative mRNA quantification by real time RT PCR of a3, d1, d2, and E1 subunits in adult mouse kidney ($n = 4$). After normalization to G3PDH, d2 and a3 were each approximately 20- and 10-fold less abundant than E1 and d1, respectively (one-way ANOVA, $P < 0.001$). (C) Representative semiquantitative PCR analysis of the expression of d2, d1, a3, E1, and G3PDH during embryogenesis (E13.5, E15.5, E17.5) and in neonatal and adult mouse kidneys. Negative controls with water (W) and non–reverse-transcribed product (N) are shown. The size of the PCR products is shown in bp. (D) Quantitative real-time RT-PCR of d2, d1, a3, and E1 mRNA expression during mouse nephrogenesis. mRNA levels were adjusted to G3PDH for each stage. The relative changes in expression during ontogeny were determined by comparison with the adult mRNA level taken as 100%. d2 mRNA is first detected at E15.5 (approximately 10% of the adult value), with a progressive increase during late ontogeny (E17.5; approximately 45%) to reach the adult expression level at birth. By contrast, ontogeny of d1 is characterized by early expression followed by a slight decrease and a neo-induction at birth, whereas E1 mRNA expression starts early during nephrogenesis and remains stable (approximately 50% of the adult value) throughout ontogeny, with a subsequent upregulation at birth. a3 shows an early (E13.5) and stable fetal expression at higher levels (approximately 150% of the adult level), without significant changes until after the neonatal period. (E) Representative immunoblots for d2, E1, and β-actin in extracts from embryonic (E13.5 to E18.5), neonatal, and adult mouse kidneys. Thirty micrograms of protein was loaded in each lane, and blots were probed with antibodies against d2, E1, and, after stripping, β-actin. The d2 subunit is detected from E15.5, with a slight increase during late ontogeny. In embryonic samples, d2 appears as a doublet, which is not found in mature kidneys. The E1 subunit is detected early during nephrogenesis and gradually increases from E16.5 until birth. (F) Representative immunoblots of d2 and β-actin in human fetal (from 12 to 25 wk gestation [GW]), 4-mo-old, and adult kidneys. The d2 subunit was detected early during human nephrogenesis at 12 wk gestation, again as a doublet. d2 expression was present throughout development, with a postnatal maturation as in the mouse.

Discussion

Our investigations of the H^+-ATPase d2 subunit confirm its limited tissue expression in mouse as well as in human. Notably, we demonstrate here that this subunit coexists with different a-subunit isoforms in the different specialized proton pumps that occur at the plasma membrane in distinct cells in kidney and in bone. This supports the idea that the existence of H^+-ATPase subunit isoforms is important for allowing the development of diverse and often specialized functions of proton pumps. Apart from G2, which is brain specific, and the a-subunit, which had already been shown to exist in a paralogous form in bone, the variance of subunit isoforms in different tissues has to date been limited to epithelia, whether in kidney, inner ear, lung, or male genital tissue. The d2 and a3 subunits are now revealed to co-localize in osteoclasts, which are of very different embryologic origin.

The polyclonal SK20 antiserum used here specifically recognizes d2 in human, mouse, and rat kidney, and it is detectable only in the membrane fraction. Our immunolocalization results in human kidney showed that d2 is present at high density at the apical pole of intercalated cells in both cortical and medullary collecting ducts, co-localizing with a4, but it is not seen in the proximal tubule. This distribution parallels previous findings for other subunits, specifically B1 in both human and rodent kidney, human a4, and the C2-b isoform in mouse (6,14,26,29). In these cases, no significant signal was observed in glomeruli or proximal and distal convoluted tubules. However, there is some discrepancy with regard to a4, where proximal staining was observed in mouse kidney (8), and it is also reported in both human and mouse renal tissue subjected to antigen retrieval techniques (21). This could be due to technical differences in fixation and retrieval and/or species-specific expression patterns. Our d2 results also show a difference between protein and nephron segment RT-PCR expression patterns, but the detection of d2 mRNA in proximal tubule by this particularly sensitive technique does not necessarily suggest the presence of d2 protein.

The murine d2 isoform can be co-immunoprecipitated from renal tissue with the B1 but not the ubiquitously expressed B2 subunit (26). Because under normal conditions it is the B1 rather than the B2 subunit that participates in the surface-destined luminal and basolateral proton pumps of α- and β-intercalated cells, respectively (6), this suggests that d2 is present only in these particular specialized proton pumps of the kidney, which in rodents also contain a4, C2-b, and G3 (7,8,26).

In contrast, further immunoprecipitation studies using mouse kidney have revealed an association between a3 and the B2 but not the B1 subunit (26). Because there is evidence to suggest that a3 mRNA is detectable in kidney in human as well as in mouse (24), we were interested to know whether a3 protein could be observed in the human kidney as well. In the event, a3 could not be seen. This suggests either a species difference or that if a3 is translated in the human kidney, it is present only at levels that are too low to permit detection.

In human bone, we observed d2 expression only in osteoclasts. These cells are more prevalent in developing bone than in adult cancellous bone, where they represent at most 1% of the cells. This explains why the signal was too weak to be visualized when SK20 was used in immunoblots of adult bone extracts (data not shown).

The presence of d2 together with a3 at the ruffled membrane and within osteoclasts may make either of these subunits attractive drug targets for the treatment of osteoporosis, but in the case of d2, this will inevitably depend on the consequences for the kidney as well. In principle, there is great potential for using H^+-ATPase inhibitors as antiresorptive therapeutics, with the caveat that compounds directed at subunits with widespread expression patterns are unlikely to be useful—such as the pharmacologically active antagonist bafilomycin used in *in vitro* studies to inhibit proton pump function. Instead, the possibility of specifically targeting the osteoclast membrane H^+-ATPase is much more attractive, as long as any therapeutic agent could be delivered efficiently to the desired site of action. Indeed, a recent publication described a compound that can discriminate between osteoclast vacuolar ATPase and lysosomal vacuolar ATPase (30).

As with the a4 subunit (17), we have found that d2 subunit expression differs temporally from the ubiquitously expressed d1 and E1 subunits during nephrogenesis in that it first appears later. This may well represent differences in the rate of maturation of different segments of the developing nephron, in that even at birth, collecting duct morphology and function are still immature. Similarly, a postnatal increase in mRNA and protein for the B1 and a4 subunits, both of which are important for collecting duct function, was reported recently (31).

We also observed a d2 doublet in fetal samples. This might be due to differential protein processing, for example by glycosylation or phosphorylation. Another possibility is that of alternative mRNA splicing, but we have observed only a single PCR product when amplifying from various cDNA.

Given the specificity of d2 expression, we regarded it as a good candidate gene for inherited osteopetrosis. We reasoned that the likeliest phenotype would include both bone thickening and a urine acidification defect, as is seen in those with *CA2* mutations (32), but also screened ARO patients who harbor one or no mutations in the known ARO genes. We have not found any disease-causing mutations in the patients who are available to us, whether with or without accompanying RTA. In view of the uncertainty about renal a3 expression in the human kidney, it is notable that no renal phenotype is reported in recessive osteopetrosis caused by *ATP6V0A3* mutations, although it is unlikely that this has been systematically sought.

The d subunit is classified as a component of the V_0 domain through protein–protein interactions rather than by integration into the membrane itself and is proposed to be present at the cytoplasmic side of the membrane. Its precise contribution to H^+-ATPase function remains unclear, although Forgac *et al.* (33) suggested that the d subunit may play a role in the coupling of ATP hydrolysis to proton transport. Recently, the crystallization of *Thermus thermophilus* subunit C, which is homologous to the eukaryotic d subunit, was reported (34). Solution of the crystal structure and its superposition onto the low-resolution electron micrograph structure of the holoenzyme, using data from cross-linking experiments, suggest that

this subunit serves as a socket to attach V_1 central stalk subunits onto the phospholipid ring of the V_0 domain, which would couple the two domains, in agreement with Forgac's model.

Acknowledgments

This work was supported by the Wellcome Trust (K.J.B., S.B., D.C.I., F.E.K., A.N.S.) and Medical Research Council (R.A.); the Swiss National Science Foundation (grant 31-68318.02 to C.A.W.); the Belgian agencies FNRS (research fellowship to F.J.) and FRSM; the Fondation Alphonse et Jean Forton and the Action de Recherches Concertées (00/05-260); and MIUR-FIRB (grant RBNE019J9W to A.V.).

Parts of this work were presented in abstract form at the American Society of Nephrology (San Diego, CA, November 14 to 17, 2003) and the UK Bone and Tooth Society (Oxford, UK, June 29 to 30, 2004).

We are grateful to Y. Cnops, H. Debaix, and Mark Bowen for excellent technical assistance. We thank Dr. S. Misler and Dr. Gul Shah (Washington University, St. Louis, MO) for provision of clinical details and for preparing DNA.

References

1. Gluck SL, Underhill DM, Iyori M, Holliday LS, Kostrominova TY, Lee BS: Physiology and biochemistry of the kidney vacuolar H+-ATPase. *Annu Rev Physiol* 58: 427–445, 1996
2. Blair HC, Teitelbaum SL, Ghiselli R, Gluck S: Osteoclastic bone resorption by a polarized vacuolar proton pump. *Science* 245: 855–857, 1989
3. Bossard MJ, Tomaszek TA, Thompson SK, Amegadzie BY, Hanning CR, Jones C, Kurdyla JT, McNulty DE, Drake FH, Gowen M, Levy MA: Proteolytic activity of human osteoclast cathepsin K. Expression, purification, activation, and substrate identification. *J Biol Chem* 271: 12517–12524, 1996
4. Nishi T, Forgac M: The vacuolar (H+)-ATPases—Nature's most versatile proton pumps. *Nat Rev Mol Cell Biol* 3: 94–103, 2002
5. Sambade M, Kane PM: The yeast vacuolar proton-translocating ATPase contains a subunit homologous to the *Manduca sexta* and bovine e subunits that is essential for function. *J Biol Chem* 279: 17361–17365, 2004
6. Nelson RD, Guo XL, Masood K, Brown D, Kalkbrenner M, Gluck S: Selectively amplified expression of an isoform of the vacuolar H+-ATPase 56-kilodalton subunit in renal intercalated cells. *Proc Natl Acad Sci U S A* 89: 3541–3545, 1992
7. Oka T, Murata Y, Namba M, Yoshimizu T, Toyomura T, Yamamoto A, Sun-Wada GH, Hamasaki N, Wada Y, Futai M: a4, a unique kidney-specific isoform of mouse vacuolar H+-ATPase subunit a. *J Biol Chem* 276: 40050–40054, 2001
8. Smith AN, Finberg KE, Wagner CA, Lifton RP, Devonald MA, Su Y, Karet FE: Molecular cloning and characterization of *Atp6n1b*: A novel fourth murine vacuolar H+-ATPase a-subunit gene. *J Biol Chem* 276: 42382–42388, 2001
9. Imai-Senga Y, Sun-Wada GH, Wada Y, Futai M: A human gene, *ATP6E1*, encoding a testis-specific isoform of H+-ATPase subunit E. *Gene* 289: 7–12, 2002
10. Smith AN, Borthwick KJ, Karet FE: Molecular cloning and characterization of novel tissue-specific isoforms of the human vacuolar H+-ATPase C, G and d subunits, and their evaluation in autosomal recessive distal renal tubular acidosis. *Gene* 297: 169–177, 2002
11. Sun-Wada GH, Yoshimizu T, Imai-Senga Y, Wada Y, Futai M: Diversity of mouse proton-translocating ATPase: Presence of multiple isoforms of the C, d and G subunits. *Gene* 302: 147–153, 2003
12. Ueda T, Ugawa S, Shimada S: A novel putative M9.2 isoform of V-ATPase expressed in the nervous system. *Neuroreport* 14: 25–30, 2003
13. Karet FE, Finberg KE, Nelson RD, Nayir A, Mocan H, Sanjad SA, Rodriguez-Soriano J, Santos F, Cremers CW, Di Pietro A, Hoffbrand BI, Winiarski J, Bakkaloglu A, Ozen S, Dusunsel R, Goodyer P, Hulton SA, Wu DK, Skvorak AB, Morton CC, Cunningham MJ, Jha V, Lifton RP: Mutations in the gene encoding B1 subunit of H+-ATPase cause renal tubular acidosis with sensorineural deafness. *Nat Genet* 21: 84–90, 1999
14. Smith AN, Skaug J, Choate KA, Nayir A, Bakkaloglu A, Ozen S, Hulton SA, Sanjad SA, Al-Sabban EA, Lifton RP, Scherer SW, Karet FE: Mutations in *ATP6N1B*, encoding a new kidney vacuolar proton pump 116-kD subunit, cause recessive distal renal tubular acidosis with preserved hearing. *Nat Genet* 26: 71–75, 2000
15. Frattini A, Orchard PJ, Sobacchi C, Giliani S, Abinun M, Mattsson JP, Keeling DJ, Andersson AK, Wallbrandt P, Zecca L, Notarangelo LD, Vezzoni P, Villa A: Defects in TCIRG1 subunit of the vacuolar proton pump are responsible for a subset of human autosomal recessive osteopetrosis. *Nat Genet* 25: 343–346, 2000
16. Kornak U, Schulz A, Friedrich W, Uhlhaas S, Kremens B, Voit T, Hasan C, Bode U, Jentsch TJ, Kubisch C: Mutations in the a3 subunit of the vacuolar H+-ATPase cause infantile malignant osteopetrosis. *Hum Mol Genet* 9: 2059–2063, 2000
17. Jouret F, Igarashi T, Gofflot F, Wilson PD, Karet FE, Thakker RV, Devuyst O: Comparative ontogeny, processing, and segmental distribution of the renal chloride channel, ClC-5. *Kidney Int* 65: 198–208, 2004
18. Pfaffl MW: A new mathematical model for relative quantification in real-time RT-PCR. *Nucleic Acids Res* 29: e45, 2001
19. Devuyst O, Christie PT, Courtoy PJ, Beauwens R, Thakker RV: Intra-renal and subcellular distribution of the human chloride channel, CLC-5, reveals a pathophysiological basis for Dent's disease. *Hum Mol Genet* 8: 247–257, 1999
20. Bell GI, Karam JH, Rutter WJ: Polymorphic DNA region adjacent to the 5′ end of the human insulin gene. *Proc Natl Acad Sci U S A* 78: 5759–5763, 1981
21. Stehberger PA, Schulz N, Finberg KE, Karet FE, Giebisch G, Lifton RP, Geibel JP, Wagner CA: Localization and regulation of the ATP6V0A4 (a4) vacuolar H+-ATPase subunit defective in an inherited form of distal renal tubular acidosis. *J Am Soc Nephrol* 14: 3027–3038, 2003
22. Toyomura T, Murata Y, Yamamoto A, Oka T, Sun-Wada GH, Wada Y, Futai M: From lysosomes to the plasma membrane: Localization of vacuolar-type H+-ATPase with the a3 isoform during osteoclast differentiation. *J Biol Chem* 278: 22023–22030, 2003
23. Nishi T, Forgac M: Molecular cloning and expression of three isoforms of the 100-kDa a subunit of the mouse vacuolar proton-translocating ATPase. *J Biol Chem* 275: 6824–6830, 2000
24. Scott BB, Chapman CG: The putative 116 kDa osteoclast

specific vacuolar proton pump subunit has ubiquitous tissue distribution. *Eur J Pharmacol* 346: R3–R4, 1998
25. Toyomura T, Oka T, Yamaguchi C, Wada Y, Futai M: Three subunit a isoforms of mouse vacuolar H^+-ATPase. Preferential expression of the a3 isoform during osteoclast differentiation. *J Biol Chem* 275: 8760–8765, 2000
26. Sun-Wada GH, Murata Y, Namba M, Yamamoto A, Wada Y, Futai M: Mouse proton pump ATPase C subunit isoforms (C2-a and C2-b) specifically expressed in kidney and lung. *J Biol Chem* 278: 44843–44851, 2003
27. Frattini A, Pangrazio A, Susani L, Sobacchi C, Mirolo M, Abinun M, Andolina M, Flanagan A, Horwitz EM, Mihci E, Notarangelo LD, Ramenghi U, Teti A, Van Hove J, Vujic D, Young T, Albertini A, Orchard PJ, Vezzoni P, Villa A: Chloride channel ClCN7 mutations are responsible for severe recessive, dominant, and intermediate osteopetrosis. *J Bone Miner Res* 18: 1740–1747, 2003
28. Ramirez A, Faupel J, Goebel I, Stiller A, Beyer S, Stockle C, Hasan C, Bode U, Kornak U, Kubisch C: Identification of a novel mutation in the coding region of the grey-lethal gene *OSTM1* in human malignant infantile osteopetrosis. *Hum Mutat* 23: 471–476, 2004
29. Finberg KE, Wagner CA, Stehberger PA, Geibel JP, Lifton RP: Molecular cloning and characterization of Atp6v1b1, the murine vacuolar H^+-ATPase B1-subunit. *Gene* 318: 25–34, 2003
30. Niikura K, Takano M, Sawada M: A novel inhibitor of vacuolar ATPase, FR167356, which can discriminate between osteoclast vacuolar ATPase and lysosomal vacuolar ATPase. *Br J Pharmacol* 142: 558–566, 2004
31. Bonnici B, Wagner CA: Postnatal expression of transport proteins involved in acid-base transport in mouse kidney. *Pflugers Arch* 448: 16–28, 2004
32. Sly WS, Hewett-Emmett D, Whyte MP, Yu YS, Tashian RE: Carbonic anhydrase II deficiency identified as the primary defect in the autosomal recessive syndrome of osteopetrosis with renal tubular acidosis and cerebral calcification. *Proc Natl Acad Sci U S A* 80: 2752–2756, 1983
33. Nishi T, Kawasaki-Nishi S, Forgac M: Expression and function of the mouse V-ATPase d subunit isoforms. *J Biol Chem* 278: 46396–46402, 2003
34. Iwata M, Imamura H, Stambouli E, Ikeda C, Tamakoshi M, Nagata K, Makyio H, Hankamer B, Barber J, Yoshida M, Yokoyama K, Iwata S: Crystal structure of a central stalk subunit C and reversible association/dissociation of vacuole-type ATPase. *Proc Natl Acad Sci U S A* 101: 59–64, 2004
35. van Hille B, Richener H, Schmid P, Puettner I, Green JR, Bilbe G: Heterogeneity of vacuolar H^+-ATPase: Differential expression of two human subunit B isoforms. *Biochem J* 303: 191–198, 1994
36. Breton S, Tyszkowski R, Sabolic I, Brown D: Postnatal development of H^+ ATPase (proton-pump)-rich cells in rat epididymis. *Histochem Cell Biol* 111: 97–105, 1999
37. Wax MB, Saito I, Tenkova T, Krupin T, Becker B, Nelson N, Brown D, Gluck SL: Vacuolar H^+-ATPase in ocular ciliary epithelium. *Proc Natl Acad Sci U S A* 94: 6752–6757, 1997
38. Li YP, Chen W, Stashenko P: Molecular cloning and characterization of a putative novel human osteoclast-specific 116-kDa vacuolar proton pump subunit. *Biochem Biophys Res Commun* 218: 813–821, 1996
39. Li YP, Chen W, Liang Y, Li E, Stashenko P: *Atp6i*-deficient mice exhibit severe osteopetrosis due to loss of osteoclast-mediated extracellular acidification. *Nat Genet* 23: 447–451, 1999
40. Deng W, Stashenko P, Chen W, Liang Y, Shimizu K, Li YP: Characterization of mouse *Atp6i* gene, the gene promoter, and the gene expression. *J Bone Miner Res* 16: 1136–1146, 2001
41. Manolson MF, Yu H, Chen W, Yao Y, Li K, Lees RL, Heersche JN: The a3 isoform of the 100-kDa V-ATPase subunit is highly but differentially expressed in large ($\geq$10 nuclei) and small ($\leq$5 nuclei) osteoclasts. *J Biol Chem* 278: 49271–49278, 2003
42. Stover EH, Borthwick KJ, Bavalia C, Eady N, Fritz DM, Rungroj N, Giersch AB, Morton CC, Axon PR, Akil I, Al-Sabban EA, Baguley DM, Bianca S, Bakkaloglu A, Bircan Z, Chauveau D, Clermont MJ, Guala A, Hulton SA, Kroes H, Li Volti G, Mir S, Mocan H, Nayir A, Ozen S, Rodriguez Soriano J, Sanjad SA, Tasic V, Taylor CM, Topaloglu R, Smith AN, Karet FE: Novel *ATP6V1B1* and *ATP6V0A4* mutations in autosomal recessive distal renal tubular acidosis with new evidence for hearing loss. *J Med Genet* 39: 796–803, 2002
43. Dou H, Xu J, Wang Z, Smith AN, Soleimani M, Karet FE, Greinwald JH Jr, Choo D: Co-expression of pendrin, vacuolar H^+-ATPase a4-subunit and carbonic anhydrase II in epithelial cells of the murine endolymphatic sac. *J Histochem Cytochem* 52: 1377–1384, 2004

CHAPTER V.

CYSTIC FIBROSIS IS ASSOCIATED WITH A DEFECT IN APICAL RECEPTOR-MEDIATED ENDOCYTOSIS IN MOUSE AND HUMAN KIDNEY

François Jouret[(1)], Alfred Bernard[(2)], Cédric Hermans[(3)], Geneviève Dom[(4)], Sara Terryn[(5)], Patrick Lebecque[(6)], Jean-Jacques Cassiman[(7)], Bob J. Scholte[(8)], Hugo R. De Jonge[(8)], Pierre J. Courtoy[(4)], and Olivier Devuyst[(1)]

(1) Division of Nephrology, (2) Unit of Industrial Toxicology and Occupational Medicine, (3) Haemostasis and Thrombosis Unit, (4) Christian de Duve Institute of Cellular Pathology, CELL Unit, and (6) Department of Pneumology–Paediatrics, Université catholique de Louvain, B-1200 Brussels, Belgium; (5) Laboratory of Cell Physiology, Centrum voor Milieukunde, Universiteit Hasselt, B-3590 Diepenbeek, Belgium; (7) Center for Human Genetics, University of Leuven, B-3000 Leuven, Belgium; (8) Departments of Biochemistry/Cell Biology, Erasmus University Medical Center, 3015 GD Rotterdam, The Netherlands.

J Am Soc Nephrol, submitted

Summary

Inactivation of the chloride channel CFTR causes CF. Although CFTR is expressed in the PT of the kidney, no renal phenotype has been documented in CF patients. Here, we investigated the expression, subcellular distribution, and processing of CFTR in the kidney; used different mouse models to assess the role of CFTR in PT function; and tested the relevance of these findings in CF patients.

The level of CFTR mRNA in mouse kidney approached that found in lung. CFTR was located in the apical area of PT cells, with a maximal intensity in the straight part (S3) of the PT. Subcellular fractionation showed that CFTR co-distributed with the chloride/proton exchanger ClC-5 in PT endosomes. Two CF mouse models were used to assess the role of CFTR in PT endocytosis. *Cftr*$^{-/-}$ mice showed impaired ^{125}I-β_2-microglobulin uptake, together with a decreased amount of the multi-ligand receptor cubilin and a significant loss of LMW cubilin ligands in the urine. Defective receptor-mediated endocytosis was less consistently found in *Cftr*$^{\Delta F/\Delta F}$ mice, characterized by a large phenotypic heterogeneity, and moderate *vs.* mice lacking ClC-5. The defective PT endocytosis, evidenced by increased urinary excretion of LMW ligands, was confirmed in a cohort of CF patients *vs.* controls.

In conclusion, CFTR inactivation leads to a moderate defect in receptor-mediated PT endocytosis, associated with a significant LMW proteinuria in mouse and man. The magnitude of the endocytosis defect caused by CFTR *vs.* ClC-5 loss likely reflects functional heterogeneity along the PT.

5.1. Introduction

Cystic fibrosis (CF, OMIM #219700), the most common autosomal recessive disease in Caucasians, is caused by mutations in the *CFTR* gene that encodes the chloride channel and conductance regulator, CFTR (1,2). CFTR is a 1480 amino acid protein that belongs to the ABC family of integral membrane proteins. It is located mainly in the apical membrane area of secretory epithelia, where it functions as a cAMP-dependent chloride channel and as a conductance regulator via interactions with other ion channels (2). Mutations in *CFTR* are classified into five groups according to their structural or functional consequences on the protein. The deletion of three bases encoding a phenylalanine residue at position 508 (ΔF508), occurring in approximately 70% of CF patients, results in the misfolding and lack of maturation of the CFTR protein (3). Most of the clinical features observed in CF patients originate from mucosal obstruction of exocrine glands, such as the respiratory system, pancreas, intestine, gallbladder and sweat glands (1-3).

Besides exocrine epithelia, CFTR has been located in the mammalian kidney, which primarily ensures reabsorptive functions (4). During human nephrogenesis, CFTR is expressed in the apical membrane of the branching ureteric bud and, later, in the apical pole of PT cells in the cortex where it remains detected after birth (5,6). A functional truncated isoform (TNR-CFTR) has also been described in the kidney, with a distinct ontogeny pattern and a minor plasma membrane expression than full-length CFTR (7,8). Despite the high level of CFTR expression in the developing and mature kidney, no documented renal phenotype has been clearly associated with CF, except for enhanced clearance of some drugs including aminoglycosides (4,9). The incidence of kidney stones in CF patients may also be increased, but the relative contribution of lithogenic factors or impaired hydration remains elusive (4,10). In addition to its location in the apical membrane, CFTR is distributed in intracellular organelles along the endocytic and secretory pathways (11,12). Inhibition of endocytic activity, as well as defective acidification in *trans*-Golgi and pre-lysosomal compartments has been reported in CF cells (13). However the exact role of CFTR in regulating organelle pH

remains controversial, with hyper- rather than hypo-acidification suggested to occur in CF respiratory epithelial cells (14).

Recent findings about the endosomal protein, ClC-5, which belongs to the CLC family of Cl^- channels/exchangers, have provided insights into the role of anion transporters in PT cells (15). In normal conditions, LMW proteins as well as albumin and transferrin in some species are ultrafiltered by the glomerular membrane, but almost entirely reabsorbed by receptor-mediated endocytosis at the apical side of PT cells (16). The loss of ClC-5, which co-distributes with the V-ATPase in PT endosomes, causes a major defect in receptor-mediated endocytosis and a LMW proteinuria in *Clcn5* KO mice (17,18) like in patients with Dent's disease, which is caused by inactivating mutations in *CLCN5* (19). By analogy, other intracellular anionic transporters such as CFTR might play a role in the endocytic reabsorption of LMW proteins by the kidney (4,15).

In this study, we describe the segmental and subcellular distribution of CFTR in the kidney, at both the mRNA and protein levels. Taking advantage of $Cftr^{-/-}$ and $Cftr^{\Delta F/\Delta F}$ mutant mice, we characterize the role of CFTR in PT apical endocytosis, in comparison to the $Clcn5^{Y/-}$ mouse model. Finally, we evaluate the renal handling of LMW proteins in a representative cohort of CF patients harbouring the ΔF508 mutation *vs*. age- and gender-matched controls.

5.2. Patients, materials and methods

CF mouse models. Experiments were conducted on 12-week-old, gender-matched $Cftr^{+/+}$ and $Cftr^{-/-}$ mice (129/C57Bl/6 background), generated by targeted deletion of exon 10 of *Cftr* (20); and gender-matched $Cftr^{N/N}$ and mutated $Cftr^{\Delta F/\Delta F}$ mice (FVB background), generated by double homologous recombination (21). All animals had free access to appropriate standard diet (Carfil Quality, Oud-Turnhout, Belgium) and water enriched with Kleanprep solution™ (Helsinn Birex Pharmaceuticals, Dublin, Ireland). The renal phenotype of CF mice was compared to $Clcn5^{Y/-}$ mice, an established model of Dent's disease (18,22). The experiments were conducted in accordance with the National Institutes of Health Guide for the Care and Use of Laboratory Animals and were approved by the Ethics Committee of the Université catholique de Louvain.

Real-time RT-PCR analyses. Total RNA from mouse kidney samples was extracted by Trizol (Invitrogen, Merelbeke, Belgium), treated with DNase I (Invitrogen) and reverse-transcribed into cDNA using SuperScript II Rnase H (Invitrogen). Specific mouse primers were designed using Beacon Designer 2.0 (Premier Biosoft International, Palo Alto, CA; see Table 5.1). Real-time RT-PCR analyses were performed in duplicate with 200 nM of both sense and anti-sense primers in a final volume of 25 µl of iQ SYBR Green Supermix (Bio-Rad, Nazareth, Belgium). The PCR mixture contained 10 nM fluorescein for initial well-to-well fluorescence normalization. PCR conditions were settled as incubation at 94°C for 3 min followed by 40 cycles of 30 sec at 95°C, 30 sec at 61°C and 1 min at 72°C. The melting temperature of PCR product was checked at the end of each PCR by recording SYBR green fluorescence increase upon slowly renaturating DNA. For each assay, standard curves were prepared by serial 4-fold dilutions of mouse adult kidney cDNA, and primers efficiencies were calculated [efficiency = $(10^{-1/slope}) - 1$] (Table 5.1). CFTR mRNA expression was investigated in 4 adult male lungs and kidneys, after normalization to HPRT1: Ratio = $2^{\Delta Ct\ (Lung\text{-}Kidney)\ CFTR}$ / $2^{\Delta Ct\ (Lung\text{-}Kidney)\ HPRT1}$. CFTR mRNA expression was further quantified in S1 *versus* S3 PT samples: Ratio = $2^{\Delta Ct\ (GAPDH\text{-}CFTR)}$. Real-time PCR results were confirmed with two sets of primers for CFTR and ClC-5, and using two reporter genes, HPRT1 and GAPDH.

Table 5.1. Primers used for semi-quantitative and real-time RT-PCR.

	Forward	Reverse	Length *(bp)*	Efficiency
Cftr	5' GATTTTGGGAGAACTGGAAGC 3'	5' GTTGGCAAGCTTTGACAA 3'	166	1.05 ± 0.03
	5' GATGGTGTCTCATGGAATTCA 3'	5' GAGCTGTCCAGGAAACTGCT 3'	193	1.02 ± 0.01
Clcn5	5' TGGAGGAGCCAATCCCTGGTGT 3'	5' CAGTGTGAGCGATGCTTTCT 3'	156	0.95 ± 0.07
	5' AAGTGGACCCTTGTCATCAA 3'	5'ACAAGATGTTCCCACAGCAG 3'	115	1.04 ± 0.02
podocin	5' GTCTAGCCCATGTGTCCAAA 3'	5' CCACTTTGATGCCCCAAATA 3'	162	0.96 ± 0.02
Aqp1	5' GCTGTCATGTATATCATCGCC 3'	5' AGGTCATTTCGGCCAAGTGA 3'	102	1.03 ± 0.04
Clcnkb	5' GGCTACCAGCAAACCCTTGT 3'	5' CATCAGTGCCCAGGAGTTGT 3'	151	0.99 ± 0.04
Aqp2	5' TCACTGGGTCTTCTGGATCG 3'	5' CGTTCCTCCCAGTCAGTGT 3'	147	1.03 ± 0.04
tnAP	5' CGTTTTCACATTCGGTGGAT3'	5' TGGAGACATTTTCCCGTTCA 3'	155	0.96 ± 0.07
GAPDH	5' TGCACCACCAACTGCTTAGC 3'	5' GGATGCAGGGATGATGTTCT 3'	176	1.04 ± 0.03
HPRT1	5' ACATTGTGGCCCTCTGTGTG 3'	5' TTATGTCCCCCGTTGACTGA 3'	162	1.01 ± 0.01

Microdissection studies. Renal cortices from male C57/Bl6 mice were dissected and minced, before incubation with 0.1% (w/v) type-2 collagenase solution containing 100 μg/ml soybean trypsin inhibitor for 30 min at 37°C. After digestion, the supernatant was sieved through 250 μm and 80 μm nylon filters. Nephron fragments remained in the 80 μm sieve and were resuspended by flushing. Distinct segments (glomeruli, S1 and S3 PT, thick ascending limbs (TAL) and CD) were isolated upon their morphological features (23), and preserved in RNA later™ (Westburgh, Leusden, The Netherlands). Four distinct collections were snap-frozen in liquid nitrogen and conserved at –80°C. The extraction of total RNA was performed using RNAqueous-Micro™ kit, following the manufacturer's recommendations (Ambion, Huntingdon, UK).

Antibodies. The following antibodies were used : affinity-purified rabbit polyclonal antibodies (MD1314) against the C-terminus of rodent CFTR (24, Dr. C.R. Marino, V.A. Medical Center, The University of Tennessee, Memphis, TN, USA); the N-terminus of human ClC-5 (18); AQP1 (Chemicon, Temecula, CA); cubilin (Dr. P. Verroust, INSERM, Paris, France); Rab5a (Santa Cruz Biotechnology, Santa Cruz, CA); villin (Dr. D. Louvard and S. Robine, Institut Curie, Paris, France); and transferrin (Dako, Glostrup, Denmark); goat polyclonal antibodies against cathepsin D (Santa Cruz Biotechnology); sheep polyclonal antibodies against megalin (Dr. P. Verroust); mouse monoclonal antibodies (E11) against the E1 subunit of V-ATPase (Dr. S. Gluck, University of California, San Francisco, CA); and β-actin (Sigma, St Louis, MO).

Western blotting and deglycosylation studies. Membrane extracts were prepared as described (25). Kidney samples were homogenized in ice-cold sucrose buffer containing Complete™ protease inhibitors (Roche, Vilvoorde, Belgium) and centrifuged at 1,000 *g* for 15 min at 4°C. The supernatant was centrifuged at 100,000 *g* for 120 min at 4°C. The resulting pellet ("membrane" fraction) was suspended in ice-cold homogenization buffer and stored at –80°C. Protein concentrations were determined with the bicinchoninic acid protein assay using BSA as standard. Deglycosylation studies using N-glycosidase F (Roche) and SDS-PAGE and immunoblotting were performed as described (25). Equal loading was verified by reprobing against β-actin. All immunoblots were performed at least in duplicate.

Immunostaining. Kidney samples were fixed in 4% formaldehyde (Boehringer Ingelheim, Heidelberg, Germany) in 0.1 M phosphate buffer, pH 7.4, prior to embedding in paraffin as described (25). Six-μm sections were first incubated in 0.01 M citrate buffer, pH 5.8, for 75 min, in a water bath heated at 97°C, before cooling down and rinsing. After blocking endogenous peroxidase for 30 min with 0.3% hydrogen peroxide, sections were incubated with 10% normal serum, then with the primary antibodies diluted in PBS containing 2% BSA. After washing, sections were successively incubated with

biotinylated secondary anti-IgG antibodies, avidin-biotin peroxidase, and aminoethylcarbazole (Vector Laboratories, Brussels, Belgium). Sections were viewed under a Leica DMR coupled to a Leica DC300 digital camera (Leica, Heerbrugg, Switzerland).

Analytical subcellular fractionation. Kidneys were homogenized in 0.25 M sucrose, 3 mM imidazole buffer, pH 7.4, containing Complete^{TM} protease inhibitors (Roche), in a Potter-Elvehjem tissue homogenizer (Thomas Scientific, Swedesboro, NJ) (26). A low-speed "nuclear" fraction was pelletted at 700 x *g* for 10 min and extracted twice by resuspension/sedimentation; pooled postnuclear supernatants were further sedimented at 100,000 x *g* for 60 min in a 50Ti fixed-angle rotor (Beckman, Palo Alto, CA). This high-speed pellet was resuspended in 1 ml of homogenization buffer, mixed with 7 ml of 16 % (vol/vol) Percoll (average final density: 1.048 g/ml), layered over a 250-µl Percoll cushion, and centrifuged at 60,000 x *g* for 30 min in a 50Ti rotor into a self-generating gradient. Ten fractions (750 µl each) were collected from the bottom and numbered from 1 (light) to 10 (dense).

Measurement of endocytic tracer uptake. Mice were anaesthetized under anesketin (Eurovet, Brussels, Belgium) and rompun (Bayer, Brussels, Belgium), and injected i.v. with 620 ng/g body weight of radiolabeled ^{125}I-β_2-microglobulin (Sigma). After 7 min, kidneys were exsanguinated *in situ*. One kidney was fixed for 6 h at 4°C in 4% formaldehyde for immunostaining and autoradiography. The contralateral kidney and the liver were homogenized and analyzed biochemically as previously reported (22).

Urine and plasma analyses in mice. Animals were kept in metabolic cages for 24 h with *ad libitum* access to food and drinking water. Urine was collected on ice-cold Complete^{TM} protease inhibitors (Roche). Blood was obtained by aorta puncture at the time of sacrifice. Plasma and urine levels of electrolytes, urea and creatinine were measured by standard methods (Eastman Kodak Company, Rochester, NY), whereas CC16 concentration, a 16 kDa marker for PT dysfunction, was determined in duplicate by latex immunoassay (18).

CF patients and controls. Thirty unselected CF patients (range: 3 to 39 year-old) were investigated during their routine follow-up at the St-Luc Academic Hospital, Brussels, Belgium, and compared to age- and gender-matched controls. The diagnosis of CF was based on clinical characteristic findings and a positive sweat testing (3). Genotyping identified the ΔF508 mutation in all patients (homozygous in 25/30; heterozygous with N1303K, G542X, or 3849 10 kb C→T in 3/30; second mutation not identified in 2/30). Second-morning urine samples were analyzed routinely for creatinine, albumin, CC16, β_2-microglobulin, transferrin and calcium. The protocol was approved by the Université catholique de Louvain Ethical Review Board. All patients and controls gave informed consent.

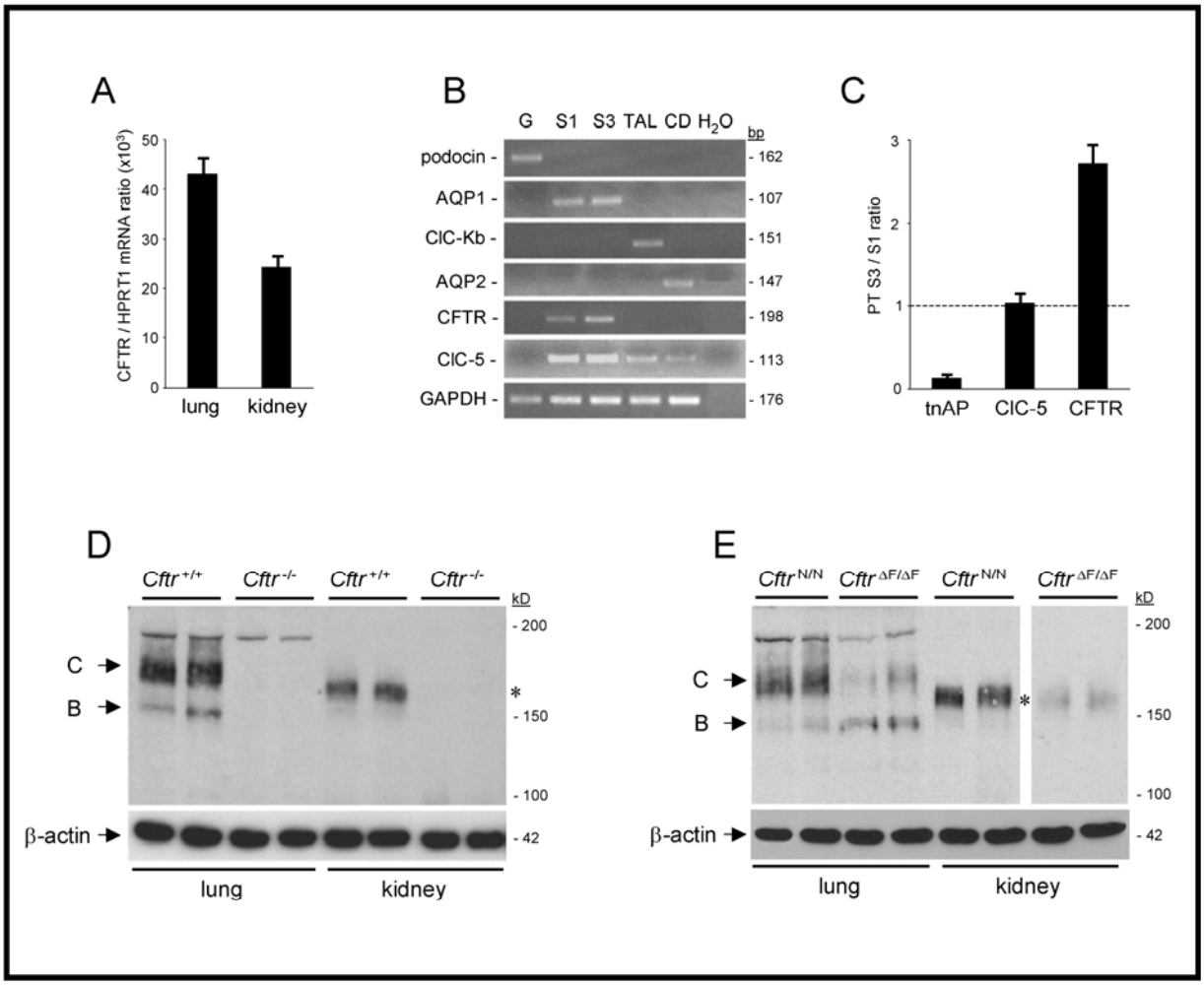

Figure 5.1. Expression of CFTR in mouse kidney: mRNA and protein studies

Panel A. Comparative expression levels of CFTR mRNA in mouse lung and kidney. Quantitative real-time RT-PCR shows that the abundance of CFTR mRNA in kidney reaches ~60% of that in lung, considered as reference organ. Results are presented as ratios ($x10^3$) to the reporter gene HPRT1 *(n=4 kidneys/lungs from 4 different mice).*

Panels B - C. Differential expression of CFTR in microdissected nephron segments. (B) Semi-quantitative RT-PCR for segment-specific markers confirms the purity of fractions, with glomeruli (podocin), PT (AQP1), TAL (ClC-Kb) and CD (AQP2). RT-PCR products (20 μl per lane) were size-fractionated on 1.5% agarose gel. (C) Real-time RT-PCR quantification demonstrates that the abundance of tissue-nonspecific alkaline phosphatase mRNA (tnAP) is ~8-fold greater in S1 than in S3 PT segments. ClC-5 mRNA is equally abundant in S1 and S3 samples, whereas CFTR expression is ~ 3-fold more abundant in S3 than in S1 segments (*n=4*).

Panel D. Representative immunoblots for CFTR in lung and kidney from *Cftr*$^{+/+}$ and *Cftr*$^{-/-}$ mice. Membrane extracts (30 μg/lane) were run on 5% PAGE and transferred to nitrocellulose. The blot was probed with MD1314 anti-CFTR antibodies (1/500) and, after stripping, β-actin (1/10.000). In lung, both B (150 kDa) and C bands (180 kDa) are present, whereas, in kidney, CFTR is detected as a single large band at ~160 kDa (asterisk). In both tissues, immunoreactive bands for CFTR are absent in *Cftr*$^{-/-}$ extracts.

Panel E. Representative immunoblots for DF508-CFTR in lung and kidney. In *Cftr*$^{DF/DF}$ lung, the fully glycosylated protein (C band) strongly decreases whereas the B band increases. In the *Cftr*$^{DF/DF}$ kidney, there is a strong reduction in the CFTR immunodetection signal at 160 kDa (asterisk), requiring longer film exposure (60 min vs. 1 min) for visualization.

Statistical analyses. Unless specified otherwise, data are given as mean ± SEM. Non-normally distributed human parameters were compared after log-transformation, using SPSS V11.5.1 software (Chicago, IL). A multivariate model using stepwise regression was performed to assess the influence of previous aminoside treatment on LMW proteinuria.

5.3. Results

5.3.1. Expression and distribution of CFTR mRNA and protein in mouse kidney

Real-time RT-PCR analyses showed that the level of CFTR mRNA in adult mouse kidney reached ~60% of that found in lung, considered as reference organ (Figure 5.1.A). The segmental distribution of CFTR mRNA in mouse nephron was investigated using tubular fractions obtained by microdissection. These fractions were characterized for segment-specific markers, such as podocin (glomeruli), aquaporin-1 (AQP1) (PT), ClC-Kb (TAL) and aquaporin-2 (AQP2) (CD) (Figure 5.1.B). The tissue-nonspecific alkaline phosphatase (tnAP) was ~ 8-fold enriched in samples from the convoluted (S1-S2) part of the PT, allowing to distinguish them from the straight (S3) PT segment (Figure 5.1.C) (27). In these tubular fractions, CFTR mRNA was ~3-fold more abundant in the S3 than in the S1-S2 PT fragments, in contrast with the comparable mRNA abundance of ClC-5 (Figure 5.1.C). Note that CFTR was not detected in glomeruli, TAL and CD fractions.

Immunoblotting demonstrated a distinct pattern for CFTR in mouse kidney and lung (Figure 5.1.D). In lung samples, both the partially glycosylated precursor (B band at ~150 kDa) and the fully glycosylated (C band at ~180 kDa) CFTR were clearly distinguished. In the kidney, CFTR was detected as a single, ~160 kDa band. Deglycosylation studies using N-glycosidase F demonstrated the same shift to the ~150 kDa band in both kidney and lung (data not shown). In contrast to various antibodies, the MD1314 antibodies used here did not detect any specific bands at these positions in tissue extracts from *Cftr*$^{-/-}$ mice (Figure 5.1.D). The ΔF508 mutation is known to alter CFTR processing in lung (2). As shown in Figure 5.1.E, the fully glycosylated C band was markedly reduced in *Cftr*$^{\Delta F/\Delta F}$ lung samples, whereas the B band was increased. In *Cftr*$^{\Delta F/\Delta F}$ kidney, a residual expression of ΔF508-CFTR was

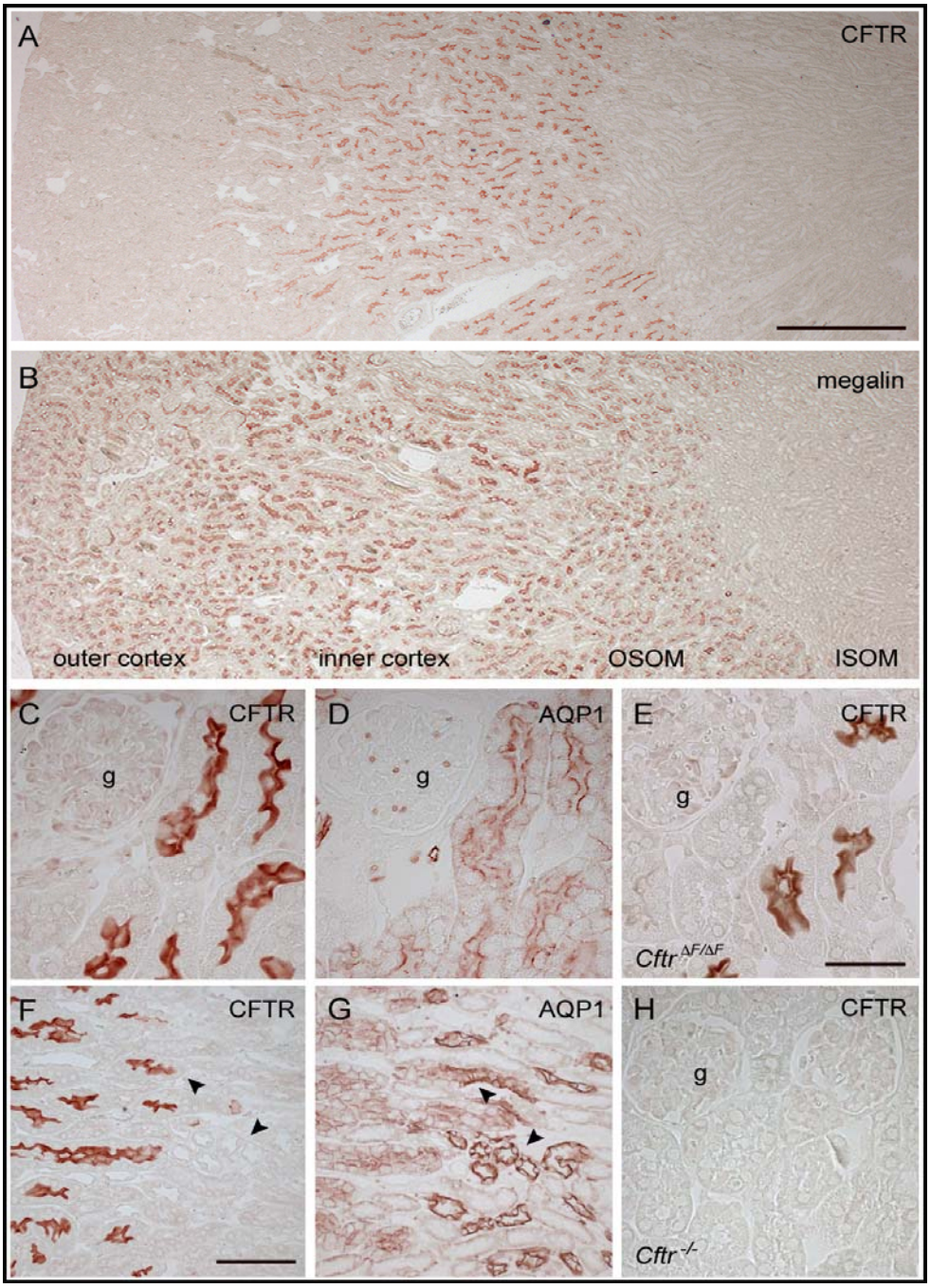

Figure 5.2. Localization of CFTR in mouse kidney

Immunoperoxidase labeling for CFTR (panels A, C, E, F, H), megalin (B) and AQP1 (D, G) in mouse *Cftr*$^{+/+}$ (A-D; F-G), *Cftr*$^{\Delta F/\Delta F}$ (E) and *Cftr*$^{-/-}$ (H) kidney. In control kidney, CFTR is preferentially detected at the cortico-medullary junction, whereas megalin encompasses both inner and outer cortices and the outer stripe of the outer medulla (OSOM) (compare panels A, B). The segmental co-localization of CFTR and AQP1 (C-D, F-G) indicates that CFTR is particularly abundant in the apical area of the distal S3 segment of PT, just before the transition with the descending thin limb in the inner stripe of the outer medulla (ISOM) (F-G arrowheads). No specific staining is observed in *Cftr*$^{-/-}$ kidney (panel H), whereas DF508-CFTR is detected with a lower intensity (requiring longer chromogenic reaction) in the S3 segment of PT (panel E).
Bars: 500 μm (panels A-B); 100 μm (panels F-G); 50 μm (panels C-D, E, H); *g, glomerulus*

detected as a faint specific band at ~160 kDa. These results validate the specificity of anti-CFTR antibodies used in this study, and suggest a tissue-specific processing of CFTR. They also show that the defect of CFTR biosynthesis and/or stability caused by the ΔF508 mutation, previously documented in lung, also occurs in the kidney.

5.3.2. Segmental localization and subcellular distribution of CFTR

Immunostaining performed on mouse kidney showed that CFTR is strongly detected at the cortico-medullary junction, whereas the distribution of the PT multi-ligand receptor, megalin, includes both inner and outer cortices, as well as the outer stripe of the outer medulla (Figure 5.2.A-B). The co-localization of CFTR with AQP1 indicated that CFTR was detected in the apical area of PT cells. The signal was faint in S1-S2 segments and stronger in the S3 segment of PT, close to the transition to the descending thin limb of Henle's loop (Figure 5.2.C-D, F-G). The segmental location of the ΔF508-CFTR was similar to that of normal CFTR, including the apical region of the distal part of PT, although the immunoreactive signal was weaker than in control kidneys (Figure 5.2.E). No specific signal for CFTR was detected in *Cftr*$^{-/-}$ kidneys (Figure 5.2.H).

The subcellular distribution of CFTR in the kidney was further investigated by fractionation in Percoll gradients (Figure 5.3). These gradients resolved a low-density peak (fractions 2–5), including the early endosomal marker, Rab5a, an intermediate density peak (fractions 7-9), including the brush border marker, villin, and a bottom peak enriched in lysosomes (cathepsin D marker). The bulk of CFTR was detected in the endosomal fractions 3-4, where it co-localized with the vacuolar proton pump, V-ATPase (E1 subunit), and ClC-5.

As a whole, these data support that, in mouse kidney, CFTR is particularly abundant in the S3 PT cells, with a subcellular distribution similar to ClC-5 and the V-ATPase in PT endosomes. Despite a weaker expression, the segmental location of the ΔF508-CFTR was preserved in mouse kidney.

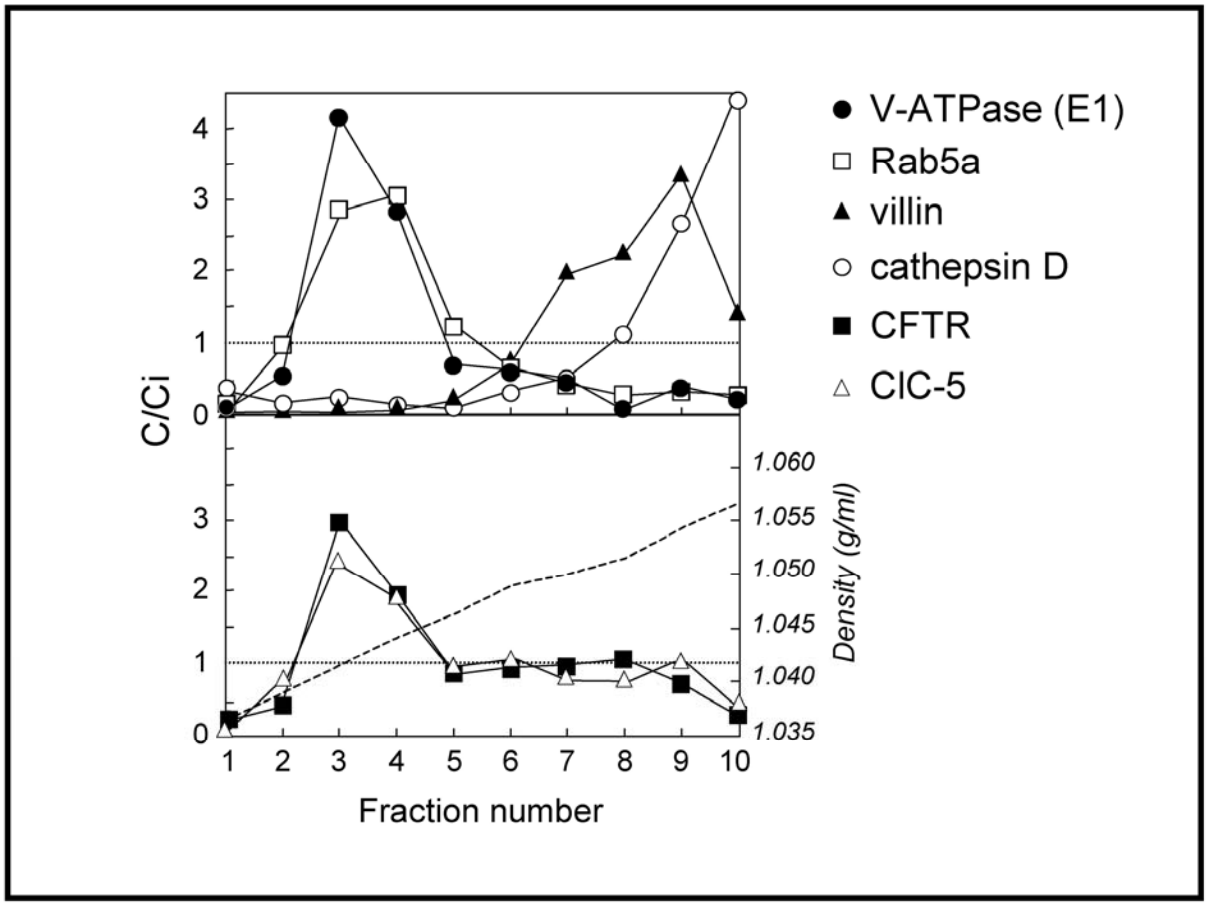

Figure 5.3. Subcellular distribution of CFTR in mouse kidney

Percoll gradients of total mouse *Cftr*$^{+/+}$ kidney resolve a low-density peak (fractions 2-4), including the early endosomal maker, Rab5a; an intermediate density peak (fractions 7-9), including the brush border component, villin; and a bottom peak enriched in lysosomes (cathepsin D).

Distributions after centrifugation are presented by comparison with the initial concentration as C/Ci (values >1 reflect organelle enrichment and values <1 reflect organelle depletion). Typical densities are indicated by a broken line in the lower panel.

CFTR co-distributes with ClC-5 and the vacuolar H^+-ATPase (E1 subunit) in endosomal fractions 3-4.

5.3.3. Evaluation and characterization of PT function in CF mouse models

Having established the segmental distribution of CFTR in the kidney, we investigated whether its disruption (*Cftr*$^{-/-}$ mice) or altered processing (*Cftr*$^{\Delta F/\Delta F}$ mice) influenced renal and PT function in mice. Plasma and urine analyses (Table 5.2) revealed that the renal function was normal in both *Cftr*$^{-/-}$ and *Cftr*$^{\Delta F/\Delta F}$ mice. However, the significant increase in the urinary excretion of the LMW Clara Cell protein (CC16, 16 kDa) in *Cftr*$^{-/-}$ animals *vs.* controls, contrasting with similar plasma levels, suggested a deficient PT handling of LMW proteins in *Cftr*$^{-/-}$ mice.

Table 5.2. Clinical and biological parameters in control and CF mice

Genotype	Weight	Plasma			Urine			
	(g)	Creat (mg/dL)	Urea (mg/dL)	CC16 (μg/L)	Diuresis (nl/min.g)	Urea (g/L)	Na^+ (mEq/L)	Ratio CC16/Cr
Cftr $^{+/+}$ **(n=5)**	28 ± 5	0.6 ± 0.1	19.1 ± 1.8	57.8 ± 6	26 ± 4	161.7 ± 16.1	280 ± 21	5 ± 2
Cftr $^{-/-}$ **(n=5)**	27 ± 2	0.6 ± 0.1	17.8 ± 1.5	59.6 ± 4	24 ± 3	144.1 ± 5.2	270 ± 22	39 ± 13 *
Cftr $^{N/N}$ **(n=6)**	25 ± 1	0.7 ± 0.1	21.1 ± 0.9	53.9 ± 3	28 ± 2	159.2 ± 13.2	316 ± 19	17 ± 4
Cftr $^{\Delta F/\Delta F}$ **(n=6)**	24 ± 1	0.6 ± 0.1	19.6 ± 1.2	52.1 ± 4	28 ± 3	142.7 ± 15.3	346 ± 16	18 ± 4

Values are means ± SEM. Values were compared by non-parametric Mann-Whitney test, and differences regarded as significant at $p<0.05$, *. (Creat: creatinine; CC16: Clara cell protein)

CF and control mice were next injected i.v. with ^{125}I-β_2-microglobulin, a LMW protein that is freely filtered by the glomerulus and taken up by receptor-mediated endocytosis in PT cells (22). After 7 min, renal uptake of ^{125}I-β_2-microglobulin was significantly decreased (by ~50%) in *Cftr*$^{-/-}$ mice *vs.* their matched controls (Figure 5.4.A). Liver uptake of ^{125}I-β_2-microglobulin, which was used as internal control since CFTR is not expressed in hepatocytes, was similar in both groups (data not shown). The *Cftr*$^{\Delta F/\Delta F}$ population showed a ~30% decrease of ^{125}I-β_2-microglobulin uptake,

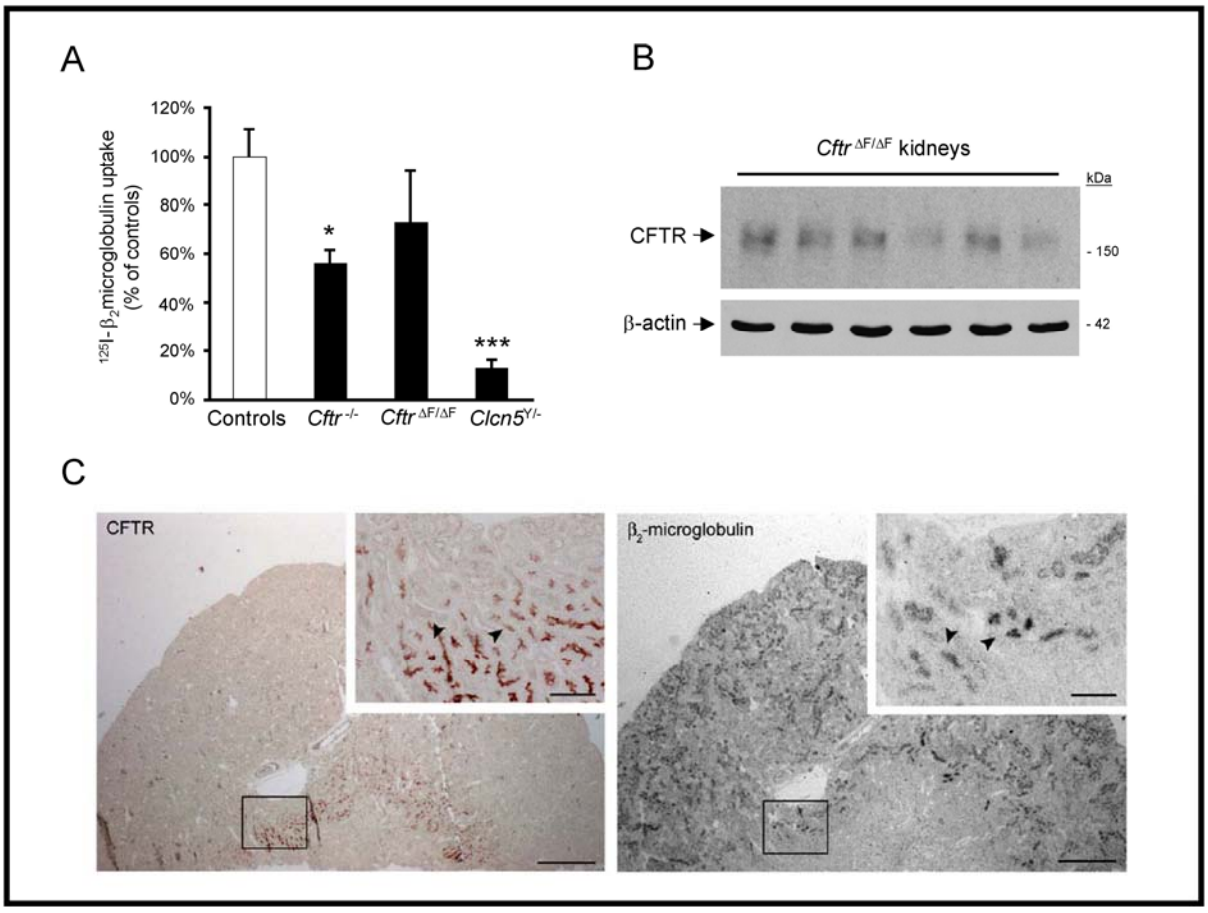

Figure 5.4. Investigation of PT apical endocytosis in CF and control kidneys

Panel A. Quantification of ^{125}I-$\beta_2$microglobulin uptake in *Cftr*$^{-/-}$ and in *Cftr*$^{\Delta F/\Delta F}$ *versus* control kidneys. Seven min after iv injection, radioactivity was measured from bleached kidneys. Uptake of ^{125}I-β_2-microglobulin uptake in the *Cftr*$^{-/-}$ kidneys is significantly decreased in comparison to age- and gender-matched kidneys (*, $p < 0.05$); the decrease is less consistent in the ΔF508 population, characterized by a large phenotypic heterogeneity. The severe reduction of ^{125}I-β_2-microglobulin uptake in *Clcn5*$^{Y/-}$ kidneys (***, $p < 0.001$) is indicated for comparison (derived from Ref. 22).

Panel B. Representative immunoblot for ΔF508-CFTR in *Cftr*$^{\Delta F/\Delta F}$ kidneys. Membrane extracts from 6 individual *Cftr*$^{\Delta F/\Delta F}$ kidneys (40 μg/lane) were run on 5% PAGE and transferred to nitrocellulose. The blot was probed with MD1314 anti-CFTR antibodies (1/500) and, after stripping, β-actin (1/10.000). The residual expression of ΔF508-CFTR is highly variable between *Cftr*$^{\Delta F/\Delta F}$ kidney samples.

Panel C. Comparative localization of CFTR and endocytosed ^{125}I-β_2-microglobulin in mouse kidney. CFTR immunodetection and autoradiography were performed on serial kidney sections. CFTR is preferentially expressed at the cortico-medullary junction, whereas endocytosed ^{125}I-β_2-microglobulin (7 min) is detected in both inner and outer cortices and in the outer stripe of the outer medulla. The CFTR-positive tubules that are positive for ^{125}I-β_2-microglobulin (insets, arrowhead) provide a molecular explanation for the defect in receptor-mediated endocytosis observed in CF mice.
Bars: 500 μm; 100 μm (inset)

with a phenotype heterogeneity probably reflecting the variable, residual expression of ΔF508-CFTR in kidney (Figure 5.4.B). The renal phenotype of *Cftr*$^{-/-}$ mice was mild in comparison to *Clcn5*$^{Y/-}$ mice, characterized by a major defect (~85%) in ^{125}I-β_2-microglobulin renal uptake (Figure 5.4.A).

To assess the role of CFTR in the segmental reabsorption of LMW proteins in the PT, we correlated the distribution of CFTR (immunostaining) and ^{125}I-β_2-microglobulin (autoradiography) on adjacent serial sections (Figure 5.4.C). These studies showed that ^{125}I-β_2-microglobulin uptake occurred mostly in S1-S2 PT segments expressing megalin and ClC-5, whereas only a residual reabsorption was observed in the S3 PT segments with high CFTR immunoreactivity (Figure 5.4.C, arrowheads). We next evaluated the total content of endocytic actors (megalin, cubilin, ClC-5), in CF versus control kidneys (Figure 5.5). Although no deficit was found at the mRNA level (data not shown), a specific ~two-fold decrease of cubilin expression was consistently observed in *Cftr*$^{-/-}$ kidney (Figure 5.5.A-B). Moreover the intensity of cubilin staining in PT cells at the cortico-medullary junction was weaker in *Cftr*$^{-/-}$ than in *Cftr*$^{+/+}$ kidneys, suggesting an enhanced degradation and/or a trafficking defect of this specific receptor in S3 PT cells (Figure 5.5.C). Furthermore, the cubilin defect was reflected by the urinary loss of its ligand transferrin (73 kDa) in the *Cftr*$^{-/-}$ mice (Figure 5.5.D). Conversely, no significant changes were observed in the kidneys from *Cftr*$^{\Delta F/\Delta F}$ mice (data not shown).

These data suggest that in *Cftr*$^{-/-}$ mice, the complete loss of CFTR induces a significant defect of apical receptor-mediated endocytosis in PT cells, with increased urinary excretion of LMW ligands of megalin (β_2-microglobulin) and cubilin (CC16, transferrin). This phenotype is less consistently observed in *Cftr*$^{\Delta F/\Delta F}$ mice, which may be explained by a variable functionality of the mutated ΔF508-CFTR in the *Cftr*$^{\Delta F/\Delta F}$ kidneys (21,28).

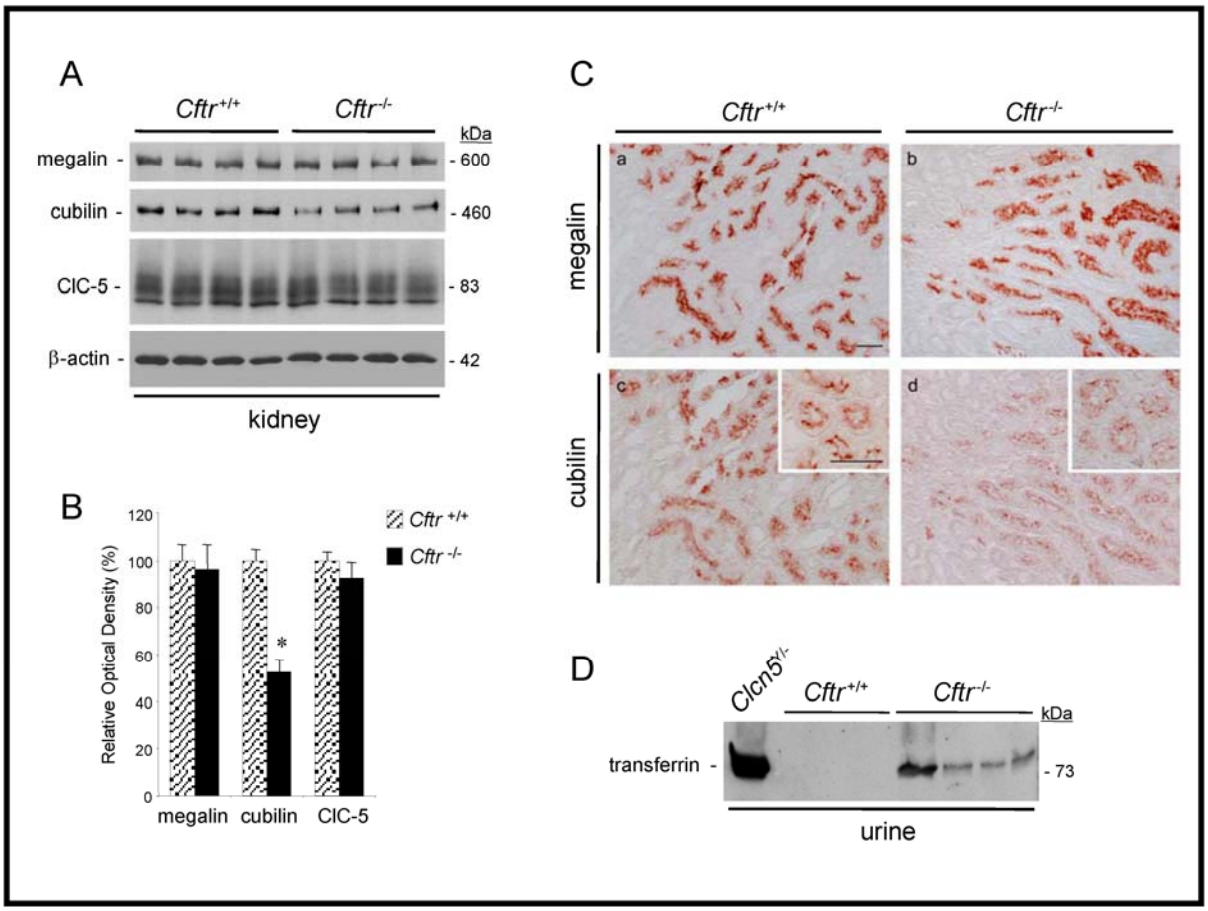

Figure 5.5. Total content of endocytic receptors and ClC-5 in *Cftr*$^{+/+}$ and *Cftr*$^{-/-}$ kidneys

Panels A and B. Representative immunoblots for megalin, cubilin and ClC-5 in *Cftr*$^{-/-}$ *versus* *Cftr*$^{+/+}$ kidneys. (A) Membrane extracts (30 μg/lane) were run on 5% PAGE and transferred to nitrocellulose. The blots were probed with anti-megalin (1/20.000), anti-cubilin (1/10.000) or anti-ClC-5 (1/1000) antibodies and, after stripping, β-actin (1/10.000). (B) Densitometry analyses were obtained from duplicate blots, after normalization to β-actin in each lane and comparison to *Cftr*$^{+/+}$ samples regarded as the 100 % reference. In *Cftr*$^{-/-}$ extracts, the expression of megalin and ClC-5 is not modified, whereas cubilin abundance is reduced by ~50% (*, $p<0.05$).

Panel C. Immunoperoxidase labeling for the multi-ligand receptors megalin (a-b) and cubilin (c-d) in *Cftr*$^{+/+}$ (a-c) and *Cftr*$^{-/-}$ (b-d) kidney. Both receptors are located at the apical surface of straight S3 PT segments (a, c) at the cortico-medullary junction of control kidneys. In *Cftr*$^{-/-}$ kidneys, the expression of cubilin is much weaker than in *Cftr*$^{+/+}$ samples, without changes in megalin signal. Immunostaining experiments were performed strictly in parallel on two distinct *Cftr*$^{+/+}$ and *Cftr*$^{-/-}$ paired samples.
Bars: 50 μm.

Panel D. Urinary excretion of transferrin in *Cftr*$^{+/+}$ and *Cftr*$^{-/-}$ mice. Urine samples were loaded on 7.5% PAGE, blotted to nitrocellulose and incubated with rabbit antibody anti-transferrin (1/1000). Loading volume was normalized to urine creatinine concentration; urine from *Clcn5*$^{Y/-}$ mouse was used as positive control. Transferrin, a specific ligand of cubilin, is detected in the urine from *Cftr*$^{-/-}$ mice, but not in the *Cftr*$^{+/+}$ samples.

5.3.4. Evaluation of PT function in patients with CF

In order to substantiate the renal phenotype found in CF mouse models, we analyzed the urinary excretion of LMW proteins in a series of non-selected, 30 clinically stable CF patients and controls matched for age and gender (Table 5.3). All CF patients harboured the ΔF508 mutation (homozygous in 25/30; heterozygous with N1303K, G542X, or 3849 10 kb C→T in 3/30; second mutation not identified in 2/30). There was a major increase in the urinary excretion of transferrin, as well as a two-fold increase in the urinary excretion of albumin and β_2-microglobulin in CF patients *vs.* controls. In contrast, the increase in CC16 was not significant and the urinary concentration of calcium was similar in both groups. A multivariate model using stepwise regression showed that urinary excretion of LMW proteins was independent of previous treatment with aminosides.

Table 5.3. Clinical and urinary parameters in 30 CF patients and controls.

	Controls (n=30)	**CF patients (n=30)**	***p value***
age (years)	17.8 ± 10	17.8 ± 10	
gender (M/F)	17/13	17/13	
albumin / creatinine (mg/g)	5.5 (2.6)	10.3 (2.5)	0.012
CC16 / creatinine (μg/g)	2.0 (3.9)	4.2 (4.6)	0.054
β_2-microglobulin / creatinine (μg/g)	27.7 (4.2)	65.1 (4.3)	0.034
transferrin / creatinine (mg/g)	0.70 (2.7)	20.69 (4.8)	0.001
calcium / creatinine (mg/g)	75.2 (2.1)	69.0 (3.2)	0.73

Except for age (arithmetic mean ± SD), values are given as the geometric mean with (SD). Non-normally distributed parameters were log-transformed before the application of Student's unpaired t-test. (CC16: Clara cell protein)

5.4. Discussion

The spectrum of CF, which was previously considered as a respiratory and digestive disease associated with a rapidly fatal outcome, has broadened considerably over the last decade. The disease includes many milder cases, which are associated with a longer survival and a potential for developing complications in multiple organs (2,3). Based on recent insights into the role of chloride transporters in the kidney (4,15), we analyzed the consequences of a functional loss of CFTR and showed it to be associated with an impaired receptor-mediated endocytosis in renal PT cells, leading to LMW proteinuria in both mouse and man. Both CFTR and the renal chloride/proton exchanger ClC-5 preferentially associate with the endosomal marker, Rab5a, and the V-ATPase in PT cells. The striking contrast between the severe PT dysfunction associated with ClC-5 loss and the mild renal phenotype of CF probably reflects the uneven segmental distribution of these transporters in the PT.

Although the role of CFTR in exocrine epithelia, including trachea and small intestine, has been studied extensively (2,3), the issues of CFTR distribution, processing and function in the kidney remain debated (4-9). In rat kidney, immunostaining for CFTR was shown at the apical surface of both proximal and distal tubules, but was not detected in the outer medullary CD (5). In the human kidney, CFTR protein expression was found in the PT, thin limbs of Henle's loop, distal tubules and collecting ducts (5-7). Our studies in mouse kidney (using antibodies of strict specificity) show that CFTR is expressed in the apical area of PT cells, with a maximal intensity in the S3 part of the PT, and that the electrophoretic mobility of N-glycosylated CFTR is slightly different in kidney *vs.* lung. The established relationship between CFTR glycosylation and its stability/function at the plasma membrane (29) suggests that the distinct CFTR maturation in the kidney may reflect distinct trafficking/targeting, and possibly different channel activity, within tubular cells (30).

In parallel to its role in regulating chloride permeability across the apical membrane, CFTR could also affect the acidification of intracellular organelles along the endocytic pathway (12). An acidification defect was indeed reported in *trans*-Golgi

and pre-lysosomal compartments in immortalized respiratory epithelial cells and nasal polyps from CF patients (13). More recently, however, enhanced rather than decreased acidification was reported in endosomes of CF respiratory epithelial cells (14). Our fractionation data show that, in mouse kidney, CFTR co-distributes with ClC-5 and the V-ATPase in PT endosomes, pointing to a possible involvement in apical endocytosis. The endocytic uptake of LMW proteins is mediated by the multi-ligand receptors, megalin and cubilin, which are expressed at the apical surface of cells lining the PT (16). Recently, the vesicular Cl^-/H^+ exchanger ClC-5 has clearly been involved in renal endocytosis (17-19). Mutations of *CLCN5* gene that encodes ClC-5 cause Dent's disease, a tubulopathy essentially characterized by a generalized dysfunction of the PT associated with LMW proteinuria, hypercalciuria, and nephrolithiasis (19). Studies in *Clcn5*$^{Y/-}$ mice demonstrated that the loss of ClC-5 induces a defect in intracellular trafficking and membrane recycling in PT cells (17,18,22), confirming the essential role of vesicular chloride transporters along the endocytic pathway (4,15). Likewise, the moderate but significant alteration of LMW proteins handling observed in *Cftr*$^{-/-}$ mice and CF patients suggests that CFTR may similarly participate in PT endocytosis. The selective decrease of cubilin expression in the S3 PT segment of *Cftr*$^{-/-}$ mice, without significant changes observed at the mRNA level, indicates an enhanced degradation and/or a trafficking defect of this receptor in PT cells, similar to what has been reported in *Clcn5*$^{Y/-}$ mice (22). A similar decrease in cubilin has been observed in the small intestine of the CFTR null (*Cftr*^{tmlUNC}) mice, which may explain a reduced vitamin B12 absorption in CF patients (31). The defect reported here may also explain why the renal clearance of aminoglycosides, which accumulate in PT cells following uptake by receptor-mediated endocytosis (32), is enhanced in CF patients (33).

Several explanations may account for the milder renal phenotype observed in *Cftr*$^{-/-}$ mice and CF patients in comparison to *Clcn5* KO mice and patients with Dent's disease (17-19). First, it could reflect the more distal distribution of CFTR as compared with ClC-5 along the PT. Indeed, although ClC-5 is evenly distributed in the S1 to S3 parts of the PT, CFTR appears to be most abundant in the S3 segment of the

PT, which displays lower endocytic activity (34). Second, CFTR functions as a cAMP-regulated, ATP-dependent chloride channel, whereas the flux of chloride through ClC-5 depends constitutively on transmembrane Cl^- and H^+ concentration gradient, together with the membrane voltage (15). The number of active CFTR channels is also known to be regulated by cAMP-dependent vesicle trafficking, as well as by correct glycosylation (2,30). Third, the discrete nature of renal manifestations in CF might be due to tissue-specific protective mechanisms, such as the occurrence of functional CFTR splice variants (7,8), or alternative pathways for chloride (4). For instance, a Ca^{++}-activated Cl^- channel is upregulated in the nasal mucosa of *Cftr*^{tmlUNC} mice (35). Although ClC-5 might represent a CFTR surrogate, comparative analysis performed on *Cftr*$^{-/-}$ *vs.* *Cftr*$^{+/+}$ kidneys did not show any changes in ClC-5 expression (Figure 5.5).

The CF patients examined here, all harbouring at least one ΔF508 mutation, showed a mild LMW proteinuria *vs.* controls. The phenotype was less consistent in the *Cftr*$^{\Delta F/\Delta F}$ mice, which showed either unchanged or increased urinary excretion of LMW proteins. The mutant ΔF508-CFTR shows defective glycosylation and impaired trafficking from the ER to the plasma membrane (2,3). However, ΔF508-CFTR can function as a cAMP-regulated chloride channel, both in the plasma membrane and intracellularly (24,36). Previous studies demonstrated a residual chloride permeability in intestine and gallbaldder of the *Cftr*$^{\Delta F/\Delta F}$ mice used here (21); and the electrolyte and water handling is preserved in the PT of *Cftr*^{tm2cam} ΔF508 mice (37). We documented a ~2 fold reduction in ΔF508-CFTR mRNA abundance in *Cftr*$^{\Delta F/\Delta F}$ *vs.* *Cftr*$^{N/N}$ kidneys (data not shown), and a large individual variability in the residual expression of ΔF508-CFTR protein (Figure 5.4). The expression of ΔF508-CFTR in man is strikingly tissue-specific, suggesting that the variable severity of CF in different organs reflects heterogeneity of residual expression (28,38). Taken together, these data suggest that, in mouse kidney, the ΔF508-CFTR is variably processed into its mature form, reaching the plasma membrane and ensuring correct function in some *Cftr*$^{\Delta F/\Delta F}$ mice.

In conclusion, the functional loss of CFTR is associated with a moderate but significant defect in LMW protein handling in mouse and man, supporting a role of CFTR within intracellular organelles along the endocytic pathway in renal PT cells. These data give new insights into the tissue-specific processing of wild-type and mutant CFTR, and the pathophysiology of chloride transporters in the kidney. The PT renal phenotype, which can trigger interstitial renal disease (39), must be integrated in the multi-systemic complications increasingly observed in CF patients.

Acknowledgements

We are grateful to R. Beauwens, S.E. Guggino, W.B. Guggino, T. Leal, P. Nguyen and P. Verroust for helpful discussions and material, and to Y. Cnops, H. Debaix, X. Dumont M. Leruth, T. Lac, P. Van der Smissen and L. Wenderickx for excellent technical assistance. This work was supported by the Belgian agencies FNRS and FRSM, the Foundation Alphonse et Jean Forton, Concerted Research Actions, Inter-University Attraction Poles, the Association Belge de Lutte contre la Mucoviscidose, Amgen, and the EuReGene integrated project of the European Community (FP6).

References

1. Riordan JR, Rommens JM, Kerem B, Alon N, Rozmahel R, Grzelczak Z, Zielenski J, Lok S, Plavsic N, Chou JL, et al.: Identification of the cystic fibrosis gene: cloning and characterization of complementary DNA. *Science* 245: 1066-1073, 1989

2. Sheppard DN, Welsh MJ: Structure and function of the CFTR chloride channel. *Physiol Rev* 79: S23-S45, 1999

3. Rowe SM, Miller S, Sorscher EJ: Cystic fibrosis. *N Engl J Med* 352: 1992-2001, 2005

4. Devuyst O, Guggino WB: Chloride channels in the kidney: lessons learned from knockout animals. *Am J Physiol Renal Physiol* 283: F1176-F1191, 2002

5. Crawford I, Maloney PC, Zeitlin PL, Guggino WB, Hyde SC, Turley H, Gatter KC, Harris A, Higgins CF: Immunocytochemical localization of the cystic fibrosis gene product CFTR. *Proc Natl Acad Sci USA* 88: 9262-9266, 1991

6. Devuyst O, Burrow CR, Schwiebert EM, Guggino WB, Wilson PD: Developmental regulation of CFTR expression during human nephrogenesis. *Am J Physiol* 27: F723-F735, 1996

7. Morales MM, Carroll TP, Morita T, Schwiebert EM, Devuyst O, Wilson PD, Lopes AG, Stanton BA, Dietz HC, Cutting GR, Guggino WB: Both the wild type and a functional isoform of CFTR are expressed in kidney. *Am J Physiol* 270: F1038-F1048, 1996

8. Huber S, Braun G, Burger-Kentischer A, Reinhart B, Luckow B, Horster M: CFTR mRNA and its truncated splice variant (TRN-CFTR) are differentially expressed during collecting duct ontogeny. *FEBS Let* 423: 362-366, 1998

9. Stanton BA: Cystic fibrosis transmembrane conductance regulator (CFTR) and renal function. *Wien Klin Wochenschr* 109: 457-464, 1997

10. Gibney EM, Goldfarb DS : The association of nephrolithiasis with cystic fibrosis. *Am J Kidney Dis* 42 : 1-11, 2003

11. Crawford IT, Maloney PC: Identification of cystic fibrosis transmembrane conductance regulator in renal endosomes. *Methods Enzymol* 292: 652-663, 1998

12. Bradbury NA: Intracellular CFTR: localization and function. *Physiol Rev* 79: S175-191, 1999

13. Barasch J, Kiss B, Prince A, Saiman L, Gruenert D, al-Awqati Q: Defective acidification of intracellular organelles in cystic fibrosis. *Nature* 352: 70-73, 1991

14. Poschet JF, Skidmore J, Boucher JC, Firoved AM, Van Dyke RW, Deretic V: Hyperacidification of cellubrevin endocytic compartments and defective endosomal recycling in cystic fibrosis respiratory epithelial cells. *J Biol Chem* 277: 13959-13965, 2002

15. Jentsch TJ, Maritzen T, Zdebik AA: Chloride channel diseases resulting from impaired transepithelial transport or vesicular function. *J Clin Invest* 115: 2039-2046, 2005

16. Christensen EI, Birn H: Megalin and cubilin: multifunctional endocytic receptors. *Nat Rev Mol Cell Biol* 3: 256-266, 2002

17. Piwon N, Gunther W, Schwake M, Bosl MR, Jentsch TJ: ClC-5 Cl- -channel disruption impairs endocytosis in a mouse model for Dent's disease. *Nature* 408: 369-373, 2000

18. Wang SS, Devuyst O, Courtoy PJ, Wang XT, Wang H, Wang Y, Thakker RV, Guggino S, Guggino WB: Mice lacking renal chloride channel, CLC-5, are a model for Dent's disease, a nephrolithiasis disorder associated with defective receptor-mediated endocytosis. *Hum Mol Genet* 9: 2937-2945, 2000

19. Lloyd SE, Pearce SH, Fisher SE, Steinmeyer K, Schwappach B, Scheinman SJ, Harding B, Bolino A, Devoto M, Goodyer P, Rigden SP, Wrong O, Jentsch TJ, Craig IW, Thakker RV: A common molecular basis for three inherited kidney stone diseases. *Nature* 379: 445-449, 1996

20. Ratcliff R, Evans MJ, Cuthbert AW, MacVinish LJ, Foster D, Anderson JR, Colledge WH: Production of a severe cystic fibrosis mutation in mice by gene targeting. *Nat Genet* 4: 35-41, 1993

21. van Doorninck JH, French PJ, Verbeek E, Peters RH, Morreau H, Bijman J, Scholte BJ: A mouse model for the cystic fibrosis delta F508 mutation. *EMBO J* 14: 4403-4411, 1995

22. Christensen EI, Devuyst O, Dom G, Nielsen R, Van der Smissen P, Verroust P, Leruth M, Guggino WB, Courtoy PJ: Loss of chloride channel, ClC-5, impairs endocytosis by defective trafficking of megalin and cubilin in kidney proximal tubules. *Proc Natl Acad Sci USA* 100: 8472-8477, 2003

23. Wagner CA, Lukewille U, Valles P, Breton S, Brown D, Giebisch GH, Geibel JP: A rapid enzymatic method for the isolation of defined kidney tubule fragments from mouse. *Pflugers Arch* 446: 623-632, 2003

24. French PJ, van Doorninck JH, Peters RH, Verbeek E, Ameen NA, Marino CR, de Jonge HR, Bijman J, Scholte BJ: A delta F508 mutation in mouse cystic fibrosis transmembrane conductance regulator results in a temperature-sensitive processing defect in vivo. *J Clin Invest* 98: 1304-1312, 1996

25. Jouret F, Igarashi T, Gofflot F, Wilson PD, Karet FE, Thakker RV, Devuyst O: Comparative ontogeny, processing, and segmental distribution of the renal chloride channel, ClC-5. *Kidney Int* 65: 198-208, 2004

26. Jouret F, Auzanneau C, Debaix H, Sun Wada GH, Pretto C, Marbaix E, Karet FE, Courtoy PJ, Devuyst O: Ubiquitous and kidney-specific subunits of the vacuolar H^+-atpase are differentially expressed during nephrogenesis. *J Am Soc Nephrol* 16: 3235-3246, 2005

27. Nouwen EJ, De Broe ME: Human intestinal versus tissue-nonspecific alkaline phosphatase as complementary urinary markers for the proximal tubule. *Kidney Int* 47: S43-S51, 1994

28. Kalin N, Claass A, Sommer M, Puchelle E, Tummler B: DeltaF508 CFTR protein expression in tissues from patients with cystic fibrosis. *J Clin Invest* 103: 1379-1389, 1999

29. Denning GM, Anderson MP, Amara JF, Marshall J, Smith AE, Welsh MJ: Processing of mutant cystic fibrosis transmembrane conductance regulator is temperature sensitive. *Nature* 358: 761-764, 1992

30. O'Riordan CR, Lachapelle AL, Marshall J, Higgins EA, Cheng AH: Characterization of the oligosaccharide structures associated with the cystic fibrosis transmembrane conductance regulator. *Glycobiology* 10: 1225-1233, 2000

31. Norkina O, Kaur S, Ziemer D, De Lisle RC: Inflammation of the cystic fibrosis mouse small intestine. *Am J Physiol Gastrointest Liver Physiol* 286: G1032-G1041, 2004

32. Schmitz C, Hilpert J, Jacobsen C, Boensch C, Christensen EI, Luft FC, Willnow TE: Megalin deficiency offers protection from renal aminoglycosides accumulation. *J Biol Chem* 277: 618-622, 2002

33. Samaniego-Picota MD, Whelton A: Aminoglycosides-induced nephrotoxicity in cystic fibrosis: a case presentation and review of the literature. *Am J Therapeutics* 3: 248-257, 1996

34. Mori K, Lee HT, Rapoport D, Drexler IR, Foster K, Yang J, Schmidt-Ott KM, Chen X, Li JY, Weiss S, Mishra J, Cheema FH, Markowitz G, Suganami T, Sawai K, Mukoyama M, Kunis C, D'Agati V, Devarajan P, Barasch J: Endocytic delivery of lipocalin-siderophore-iron complex rescues the kidney from ischemia-reperfusion injury. *J Clin Invest* 115: 610-621, 2005

35. Grubb BR, Vick RN, Boucher RC: Hyperabsorption of Na^+ and raised Ca^{++}-mediated Cl^- secretion in nasal epithelia of CF mice. *Am J Physiol Cell Physiol* 266: C1478-C1483, 1994

36. Pasyk EA and Foskett JK: Mutant (delta F508) cystic fibrosis transmembrane conductance regulator Cl- channel is functional when retained in endoplasmic reticulum of mammalian cells. *J Biol Chem,* 270: 12347-12350, 1995

37. Kibble JD, Balloch KJ, Neal AM, Hill C, White S, Robson L, Green R, Taylor CJ: Renal proximal tubule function is preserved in Cftr(tm2cam) deltaF508 cystic fibrosis mice. *J Physiol* 532: 449-457, 2001

38. Persu A, Devuyst O, Lannoy N, Materne R, Brosnahan G, Gabow PA, Pirson Y, Verellen-Dumoulin C: CF gene and cystic fibrosis transmembrane conductance regulator expression in autosomal dominant polycystic kidney disease. *J Am Soc Nephrol* 11: 2285-2296, 2000

39. D'Amico G, Bazzi C: Pathophysiology of proteinuria. *Kidney Int* 63: 809-825, 2003

CHAPTER VI.

TYPE III CARBONIC ANHYDRASE: A NOVEL RENAL ISOFORM THAT PLAYS A ROLE IN DENT'S DISEASE AND PROXIMAL TUBULE DYSFUNCTION

Philippe Gailly[(1)], François Jouret[(2)], Dominique Martin[(1)], Huguette Debaix[(2)], Jean-Pierre Cosyns[(3)], Toshiho Nishita[(4)], Thomas Willnow[(5)], Pierre J. Courtoy[(6)], Steve J. Scheinman[(7)], Erik I. Christensen[(8)], Olivier Devuyst[(2)]

(1) Division of Cell Physiology, (2) Nephrology, (3) Pathology, and (6) Christian de Duve Institute of Cellular Pathology, Cell Unit, Université catholique de Louvain, Brussels, Belgium; (4) Laboratory of Veterinary Physiology, Azabu University, Sagamihara-Shi, Japan; (5) Max Delbrück Center for Molecular Medicine, Berlin, Germany; (7) Department of Medicine, State University of New-York, Syracuse, USA; (8) University of Aarhus, Aarhus, Denmark.

Manuscript in preparation

Summary

The loss of the Cl^- transporter ClC-5 in Dent's disease patients and *Clcn5*$^{Y/-}$ mice causes a severe PT dysfunction. However the metabolic consequences and adaptation mechanisms to such disorder remain unknown. First, real-time RT-PCR, immuno-blotting and -staining demonstrated higher cell proliferation and oxidative stress in *Clcn5*$^{Y/-}$ PT cells. Transcriptome comparison between *Clcn5*$^{Y/-}$ and *Clcn5*$^{Y/+}$ kidneys was next performed to isolate genes involved in adaptation mechanisms. Real-time RT-PCR and immunoblotting confirmed a 4-fold induction of type III carbonic anhydrase (CAIII) in *Clcn5*$^{Y/-}$ samples. In normal kidney, CAIII expression was ~5-fold lower than CAII, with a segmental distribution restricted to scattered PT cells. The number of CAIII-positive PT cells in *Clcn5*$^{Y/-}$ kidney dramatically increased, without enhanced apoptosis. These findings were confirmed in human *CLCN5* mutated kidney samples, as well as in the megalin knockout mice. Moreover CAIII expression in HK-2 PT cells was significantly induced following exposure to H_2O_2 (1 mM). In conclusion, we report on a novel renal CA isozyme located in scattered PT cells. The induction of CAIII expression in distinct models of renal Fanconi syndrome and H_2O_2-exposed PT cells suggests that this isozyme might protect the PT from oxidative damage.

6.1. Introduction

The epithelial cells lining the PT are highly specialized to reabsorb ions, glucose, amino acids, vitamins, proteins, and other nutrients from the primitive urine filtrated by the glomeruli. In particular, several grams of albumin and hundreds of milligrams of LMW proteins are daily filtered, and avidly recaptured by PT cells through receptor-mediated endocytosis (Birn, 2006). This endocytic pathway involves two multiligand-binding receptors, megalin and cubilin, that are abundantly expressed at the brush border of PT cells (Christensen, 2002). Ligand binding and interactions between both receptors induce their internalization into coated vesicles at the apical membrane of PT cells and their subsequent delivery to endosomes and lysosomes for ligand processing and receptor recycling. This endocytotic trafficking is dependent on a progressive acidification from early to late endosomes and finally to lysosomes (Marshansky, 2002). In PT cells, the endosomal acidification is driven by the electrogenic V-ATPase, in parallel with a Cl^- conductance necessary for the electro-neutrality (Wagner, 2004). Although the nature of the endosomal Cl^- conductance is still debated, recent findings about the Cl^- transporter ClC-5 have provided new insights into PT endocytic pathway (Jentsch, 2005).

Acquired or inherited dysfunctions of the PT, collectively named “renal Fanconi syndrome”, are associated with LMW proteinuria due to defective receptor-mediated endocytosis of PT cells. Chronic exposure to cadmium inhibits the V-ATPase and impairs endosomal acidification, thereby causing severe PT damage characterized by constant LMW proteinuria (Bernard, 2004). Likewise the functional loss of cubilin in Imerslund-Gräsbeck disease (Aminoff, 1999), as well as the genetic inactivation of megalin in mice (Leheste, 2003), leads to tubular reabsorption deficiency, with increased urinary excretion of LMW proteins. Mutations in *CLCN5* gene, which encodes the endosomal voltage-gated Cl^- transporter ClC-5, are associated with Dent’s disease, an X-linked renal tubular disorder characterized by LMW proteinuria and hypercalciuria, associated with

glucosuria, amino-aciduria, phosphaturia, nephrocalcinosis, and nephrolithiasis (Fisher, 1994; Lloyd, 1996). Genetic inactivation of *Clcn5* gene in mice causes renal tubular defects that mimic human Dent's disease, including severe PT dysfunction with impaired endocytosis and trafficking defects (Piwon, 2000; Wang, 2000; Christensen, 2003). Despite the severity of the renal Fanconi syndrome, the metabolic outcomes at the cellular level remain poorly understood. Recently, Wilmer et al. have reported an increased oxidative stress and altered redox status in primary PT cells derived form urine of patients with cystinosis, the most frequent cause of inborn Fanconi syndrome (Wilmer, 2005). These observations suggest that PT dysfunction might be associated with increased solicitation of cell oxidative defences.

In this study, we have used *Clcn5* knockout mice, as a well-defined model of renal Fanconi syndrome (Wang, 2000), in order to investigate the metabolic consequences and adaptative mechanisms to PT dysfunction. Particularly, a differential display procedure based on amplified fragment length polymorphism (AFLP) was performed on *Clcn5*$^{Y/-}$ *versus* *Clcn5*$^{Y/+}$ kidneys (Vos, 1995), and identified *Car3* gene as a candidate gene of such cellular response. Type III carbonic anhydrase (CAIII) belongs to the family of zinc metalloenzymes that reversibly hydrate carbon dioxide. In the kidney, type II and IV CA represent the most abundant CA isozymes, where they participate in correct urine acidification and Na^+ homeostasis. Here we report on (i) the segmental and subcellular distribution of CAIII in mouse kidney; (ii) its increased expression in *Clcn5*$^{Y/-}$ kidneys, which are characterized by higher cell turn-over and oxidative stress; (iii) and its induction in samples from the two kidneys of a patient with Dent's disease. These findings were validated in the *megalin* KO mouse model of PT dysfunction, and further investigated in HK-2 PT cells exposed to oxidant conditions. As a whole, these results support that CAIII may protect PT cells against oxidative damage in case of renal Fanconi syndrome.

6.2. Materials and Methods

Mouse models. Experiments were conducted on 12 pairs of 12-week-old (n=6) and 1-year-old (n=6) *Clcn5* wild-type (Y/+) and KO (Y/-) mice. Renal function of young *Clcn5*$^{Y/-}$ mice was within normal range, whereas plasma creatinine level was tripled in old *Clcn5*$^{Y/-}$ mice in comparison to age-matched controls. The *Clcn5*$^{Y/-}$ mice, generated by targeted deletion of the exon VI of *Clcn5*, have been extensively characterized and shown to mimic the phenotype of human Dent's disease (Wang, 2000). Real-time RT-PCR studies were performed on kidneys from two additional mouse models of human renal Fanconi syndrome, i.e. 3 pairs of *megalin* KO mice (Willnow, 1996), and 3 pairs of *Ctns* KO mice (Cherqui, 2002). The *megalin* KO mice exhibit a specific defect in PT endocytic apparatus resulting in impaired uptake of filtered LMW proteins, without significant alteration of glucose, electrolyte and amino acid transports (Leheste, 1999). The *Ctns* KO mice present no signs of proximal tubulopathy despite the severe PT defects observed in children with infantile cystinosis, which suggests alternative rescue pathways in mice (Cherqui, 2002). All samples were obtained in accordance with NIH guidelines for the care and use of laboratory animals, and with the approval of the Committee for Animal Rights of the Université catholique de Louvain.

RNA extraction and double strand cDNA synthesis. Total RNA was extracted from frozen mouse kidneys using Trizol reagent (Invitrogen, Merelbeke, Belgium). The concentration of each RNA sample was obtained from optical densitometry (260 nm) measurements and RNA quality was confirmed using agarose gel electrophoresis. Poly(A)+ RNA were prepared from 75 μg of total RNA using Dynabeads Oligo$(dT)_{25}$ (Invitrogen). First strand cDNA was synthesized from 500 ng of Poly(A)+ RNA using Superscript II RNase H^- Reverse Transcriptase (Invitrogen) in a total volume of 20 μl at 37°C for 50 min. Double strand cDNA was synthesised in the same vial using T4 DNA Polymerase and purified using QIAquick Extraction Kit (Qiagen, Venlo, The Netherlands).

AFLP reactions. The AFLP protocol was essentially performed as previously described (Vos, 1995). cDNA samples were digested with *Eco*RI and *Mse*I (Fermentas, Vilnius, Lithuania) for 2 h at 37°C. Restriction fragments were next ligated to *Eco*RI and *Mse*I double strand adapters for 2 h at 20°C. The *Eco*RI and *Mse*I adapters were prepared by mixing equimolar amounts of the oligonucleotide (Table 6.1): Ad1-*Eco*, Ad2-*Eco* (for *Eco*RI adapter) and Ad1-*Mse*, Ad2-*Mse* (for *Mse*I adapter). The restriction fragments with ligated adapters were diluted (10X) with TE buffer (100 mM Tris-HCl, 10 mM EDTA, pH 8.0), and further used as a template for the pre-amplification reaction. This step was performed in 20 cycles (94°C, 30 sec; 56°C, 1 min; 72°C, 1 min) with *Eco*-P0 and *Mse*-P0 primers corresponding to *Eco*RI and *Mse*I adapters without extension. Following the pre-amplification step, the product was diluted (10X) with TE buffer and 5 μl were used for selective amplification, as following: 33 cycles including 9 touchdown cycles comprising a decrease of the annealing

temperature from 65°C to 56°C, which was maintained for 24 cycles. Twelve primer combinations were used for selective amplification: *Eco*-PAA and *Mse*-PAA or *Mse*-PAC or *Mse*-PAT, *Eco*-PAC and *Mse*-PAA or *Mse*-PAC or *Mse*-PAT, *Eco*-PAG and *Mse*-PAA or *Mse*-PAC or *Mse*-PAT, *Eco*-PAT and *Mse*-PAA or *Mse*-PAC or *Mse*-PAT. All amplification reactions were performed in the iCycler thermal cycler (Bio-Rad, Nazareth, Belgium). Selective amplification products were denatured at 95°C for 3 min in an equal volume of formamide dye and separated on sequencing gels (6% polyacrylamide, 6 M urea) at 60 W. Gels were dried onto Whatman paper and exposed to Kodak BioMax film (Amersham Biosciences, Buckinghamshire, UK) overnight at -80°C. The bands of interest were selected, removed from the gel and soaked in water. AFLP fragments were recovered by PCR under the same conditions as used for the selective amplification. Reamplified cDNAs were visualised on a 1.5% (w/v) agarose gel, subcloned into pGEM-T easy vector (Promega, Leiden, The Netherlands) and sequenced (Genome Express, Meylan, France). Each reamplified AFLP fragment was compared against all sequences in the non-redundant databases using BLAST sequence alignment program: http://www.ncbi.nlm.nih.gov/BLAST/ (Altschul, 1990).

Table 6.1. Adapters and primers used for AFLP

Name	Nucleotide sequence
Ad1-*Eco*	5' CTCGTAGACTGCGTACC 3'
Ad2-*Eco*	5' AATTGGTACGCAGTCTAC 3'
Ad1-*Mse*	5' GACGATGAGTCCTGAG 3'
Ad2-*Mse*	5' TACTCAGGACTCAT 3'
Eco-P0	5' GACTGCGTACCAATTC 3'
Mse-P0	5' GATGAGTCCTGAGTAA 3'
Eco-PAA	5' GACTGCGTACCAATTCAA 3'
Eco-PAC	5' GACTGCGTACCAATTCAC 3'
Eco-PAG	5' GACTGCGTACCAATTCAG 3'
Eco-PAT	5' GACTGCGTACCAATTCAT 3'
Mse-PAA	5' GATGAGTCCTGAGTAAAA 3'
Mse-PAC	5' GATGAGTCCTGAGTAAAC 3'
Mse-PAT	5' GATGAGTCCTGAGTAAAT 3'

Real-time RT-PCR. Total RNA (2.7 µg) was treated with DNase I (Invitrogen) and reverse-transcribed into cDNA using SuperScript III RNase H^- Reverse Transcriptase (Invitrogen). Changes in mRNA expression levels were determined by real-time RT-PCR (iCycler IQ System, Bio-Rad) using SYBR Green I detection of single PCR product accumulation. Specific primers for *Car2, Car3,*

PCNA, Ki67, cyclin E, osteopontin, catalase, Type I SOD, thioredoxin, HPRT1 and *GAPDH* were designed using Beacon Primer Designer 2.0 (Premier Biosoft International, Palo Alto, CA) and are summarized in Table 6.2. The PCR products were size-fractionated on 1.5% agarose gel, stained with ethidium bromide, purified by QIAquick Gel Extraction Kit (Qiagen) and subsequently sequenced by Genome Express. Real-time RT-PCR analyses were performed in duplicate with 200 nM of both forward and reverse primers in a final volume of 25 µl using 1 Unit of Platinum Taq DNA Polymerase, 6 mM $MgSO_4$, 400 µM dNTP and SYBR Green I (Invitrogen) diluted 1/100,000. The PCR mix contained 10 nM fluorescein for initial well-to-well fluorescence normalization. PCR conditions were as follows: 94°C for 3 min, 40 cycles of 30 sec at 95°C, 15 sec at 61°C and 1 min at 72°C. The melting temperature of the PCR product was checked at the end of each PCR by recording SYBR Green fluorescence increase upon slow renaturing DNA. For each assay, standard curves were prepared by serial 4-fold dilutions of WT mouse kidney cDNA. The efficiencies of the amplifications with each primer set were calculated from the slope of the standard curve [efficiency = $(10^{-1/slope}) - 1$] and were close to 1 (Table 6.2). The relative changes in Target mRNA / GAPDH (or HPRT1) mRNA ratio between *Clcn5*$^{Y/+}$ and *Clcn5*$^{Y/-}$ samples were determined by using the formula: Efficiency $^{\Delta\Delta Ct}$.

Table 6.2. Primers used for real-time RT-PCR

	Forward	Reverse	Length	Efficiency
Mouse				
car2	5' CTTGAAGCACTGCATTCCAT 3'	5' CACGATCCAGGTCACA CATT 3'	153	1.03 ± 0.09
car3	5' CTTGATGC CCTGGACAAAAT 3'	5' GAGCCGTGGTAGGTCCAATA 3'	110	1.04 ± 0.11
PCNA	5' TTGGAATCCCAGAACAGGAG 3'	5' ATTGCCAAGCTCTCCACTTG 3'	155	1.02 ± 0.20
Ki67	5' TGCAAAGGTAGAGGCTCCAT 3'	5' CAGGTAGGCCAGAGCAAGT 3'	152	1.03 ± 0.17
osteopontin	5' TCCAATCGTCCCTACAGTCG 3'	5' CGCTCTTCATGTGAGAGGTG 3'	146	0.98 ± 0.08
catalase	5' CATGGTCTGGGACTTCTGGA 3'	5' GACTGCCTCTCCATCTGCAT 3'	151	0.97 ± 0.27
Type I SOD	5' GGGTTCCACGTCCATCAGTA 3'	5' CAGTCACATTGCCCAGGTCT 3'	136	1.10 ± 0.09
thioredoxin	5' TGATCAAGCCCTTCTTCCAT 3'	5' CCCACCTTTTGACCCTTTTT 3'	151	1.00 ± 0.20
gapdh	5' TGCACCACCAACTGCTTAGC 3'	5' GGATGCAGGGATGATGTTCT 3'	176	1.04 ± 0.03
hprt1	5' ACATTGTGGCCCTCTGTGTG 3'	5' TTATGTCCCCCGTTGACTGA 3'	162	0.99 ± 0.01
Man				
CA2	5' CCCTGGATGGCACTTACAG 3'	5' CAGCTTTCCCAAAATCCCCA 3'	149	1.01 ± 0.10
CA3	5' GCCGGGACTACTGGACCTA 3'	5' CGTTCTCAGCACTGGAGAG 3'	144	0.97 ± 0.11
PCNA	5' ACGTCTCTTTGGTGCAGCTC 3'	5' GCGTTATCTTCGGCCCTTAG 3'	157	0.98 ± 0.30
OSTEOPONTIN	5' ATGGCCGAGGTGATAGTGTG 3'	5' GATGGCCTTGTATGCACCAT 3'	146	1.10 ± 0.30
CATALASE	5' TGGCTCATTTTGACCGAGAG 3'	5' GCGATGGGAGTCTTCTTTCC 3'	148	0.95 ± 0.26
THIOREDOXIN	5' TCAGCCACGTGGTGTGGG 3'	5' TGGAATGTTGGCATGCATTT 3'	152	1.20 ± 0.30
GAPDH	5' GGGGCTCTCCAGAACATCAT 3'	5' TCTAGACGGCAGGTCAGGT 3'	149	0.97 ± 0.12

Antibodies. Immuno-blotting and -staining analyses were performed with mouse monoclonal antibodies against CAIII (Spectral, Toronto, Canada) (Azzazy, 1998); against V-ATPase E1 subunit (a gift of Dr. S. Gluck, University of California, San Francisco, CA, USA) (Brown, 1988); against PCNA (clone PC-10, Dako, Heverlee, Belgium); and against β-actin (Sigma, St-Louis, MO); rat monoclonal against Ki67 antigen (clone TEC-3, Dako); rabbit polyclonal antibodies against CAIII (Nishita, 2002); and against the water channel aquaporin-1 (Chemicon, Temecula, CA); and sheep polyclonal antibodies anti-CAII (Serotec, Oxford, UK).

Immunoblotting. Cytosolic proteins were isolated from kidney, and prepared as previously described (Wang, 2000). Briefly, tissues were homogenized in ice-cold buffer (0.25 M sucrose, 20 mM imidazole, pH 7.4, 1 mM EDTA) containing Complete^{TM} protease inhibitors (Roche, Vilvoorde, Belgium). A low-speed "nuclear" fraction was pelleted from the homogenate by centrifugation at 1000 *g* for 10 min and extracted twice by resuspension sedimentation. The resulting supernatant was centrifuged at 100,000 *g* for 60 min at 4°C in a 50Ti fixed-angle rotor (Beckman, Palo Alto, CA). The supernatant was considered as the cytosolic fraction, and the high-speed pellet as the membrane compartment. Protein concentration was determined using bicinchoninic acid protein assay (Pierce, Aalst, Belgium). Proteins (20 μg) were separated through SDS-PAGE and transferred onto nitrocellulose membrane (BioRad). After blocking, membranes were incubated overnight at 4°C with primary antibodies, rinsed and incubated for 1 h at room temperature with the appropriate secondary peroxidase-labelled antibody (Dako). The immunoreactive bands were detected using enhanced chemiluminescence (Amersham Biosciences). Normalization for β-actin was obtained after stripping the blots and reprobing with the anti-β-actin antibody. Specificity of the immunoblot was determined by incubation with non-immune rabbit or mouse IgG (Vector Laboratories, Brussels, Belgium). Densitometry analysis was performed with a Canon CanoScan8000F using the NIH Image V1.60 software. All immunoblots were at least performed in triplicate.

Immunostaining. Kidneys were fixed for 6 h at 4°C in 4% formaldehyde (Boehringer Ingelheim, Heidelberg, Germany) in 0.1 M phosphate buffer, pH 7.4, prior to embedding in paraffin. Six-μm thick sections were rehydrated and incubated for 30 min with 0.3% hydrogen peroxide to block endogenous peroxidase. After incubation with PBS 10% normal goat serum for 20 min, sections were incubated for 45 min with primary antibodies in PBS 2% BSA. After washes, sections were incubated with appropriate biotinylated secondary antibodies (Vector Laboratories), washed and incubated for 45 min with the avidin-biotin peroxydase complex (Vectastain Elite, Vector Laboratories) and aminoethylcarbazole. All immunostaining were preformed at room temperature in a humidified chamber. Control experiments included incubation (i) in the absence of primary antibody, (ii) with non-immune rabbit or mouse IgG (Vector Laboratories).

Apoptosis assay. Apoptotic cells were detected by the terminal deoxynucleotidyl transferase-mediated deoxyuridine triphosphate nick end labeling (TUNEL) method (Cell Death detection kit, Roche). Sections were pre-treated with 20 μg/ml proteinase K for 20 minutes. Positive control sections were first treated with 100 μg/ml DNAse I for 10 minutes at room temperature, whereas omission of transferase was regarded as negative control.

Detection of superoxide anion (O_2^-) generation. The *in situ* production of superoxide in kidney samples was assessed using the hydroethidine (HE, dihydroethidium bromide) fluorescence method (Piech, 2003). HE is freely permeable to cells, and is oxidized by O_2^- to red fluorescent ethidium bromide. After excitation at 480 nm, ethidium bromide emits light at a wavelength of 610 nm. After embedding in Tissue Tek OCT compound (Sakura Finetek, Zoeterwoude, The Netherlands), kidneys were snap-frozen in pre-cooled isopentane, cut into 5-mm-thick cryosections, and stored at –80°C. The HE 5 mM stabilized solution in DMSO (Invitrogen) was diluted to 2 x 10^{-6} M in water before use. Fifty μl of HE solution was applied on tissue sections and cover-slipped. The slides were incubated at 37°C for 30 min in a light-protected and humidified chamber. Red fluorescence from HE-treated *Clcn5*$^{Y/+}$ and *Clcn5*$^{Y/-}$ samples was measured during 5 ms using the software KS400 (Zeiss, Zaventem, Belgium) through a Zeiss Axiovert S100 microscope equipped with an Axiocam camera.

Immunogold labelling. Kidneys were fixed by retrograde perfusion through the aorta with 2% formaldehyde in 0.1 M sodium cacodylate buffer, pH 7.2. Tissues were trimmed into small blocks, further fixed by immersion for 1 hour in 1% formaldehyde, infiltrated with 2.3 M sucrose for 30 min and frozen in liquid nitrogen. Cryosections (70-90 nm) were obtained at -100^{o}C with an FCS Reichert Ultracut S cryoultramicrotome as previously described (Christensen, 1995), and were incubated with rabbit anti-CAIII at 4^{o}C overnight followed by incubation for 1 hour with 10 nm goat anti-rabbit gold particles (BioCell, Cardiff, UK). The cryosections were embedded in methylcellulose containing 0.3% uranyl acetate and studied in a Philips CM100 electron microscope. Control sections were incubated with secondary antibody alone or with non-specific rabbit serum.

Human samples. Studies were conducted on frozen and formalin-fixed kidney samples from the two kidneys obtained after bilateral nephrectomy of an end-stage patient with Dent's disease. Clinical features of this patient bearing a "G to A" missense mutation (Gly506Glu) in *CLCN5* gene were reported previously (Frymoyer, 1991; Lloyd, 1996). Comparative real-time RT-PCR and immunoblotting studies used 4 end-stage kidneys (chronic interstitial nephritis) removed during renal transplantation as controls. These samples were snap-frozen in liquid nitrogen and stored at –80°C, or routinely fixed in 4% formaldehyde. The use of these samples has been approved by the Ethical Review Board of the Université catholique de Louvain.

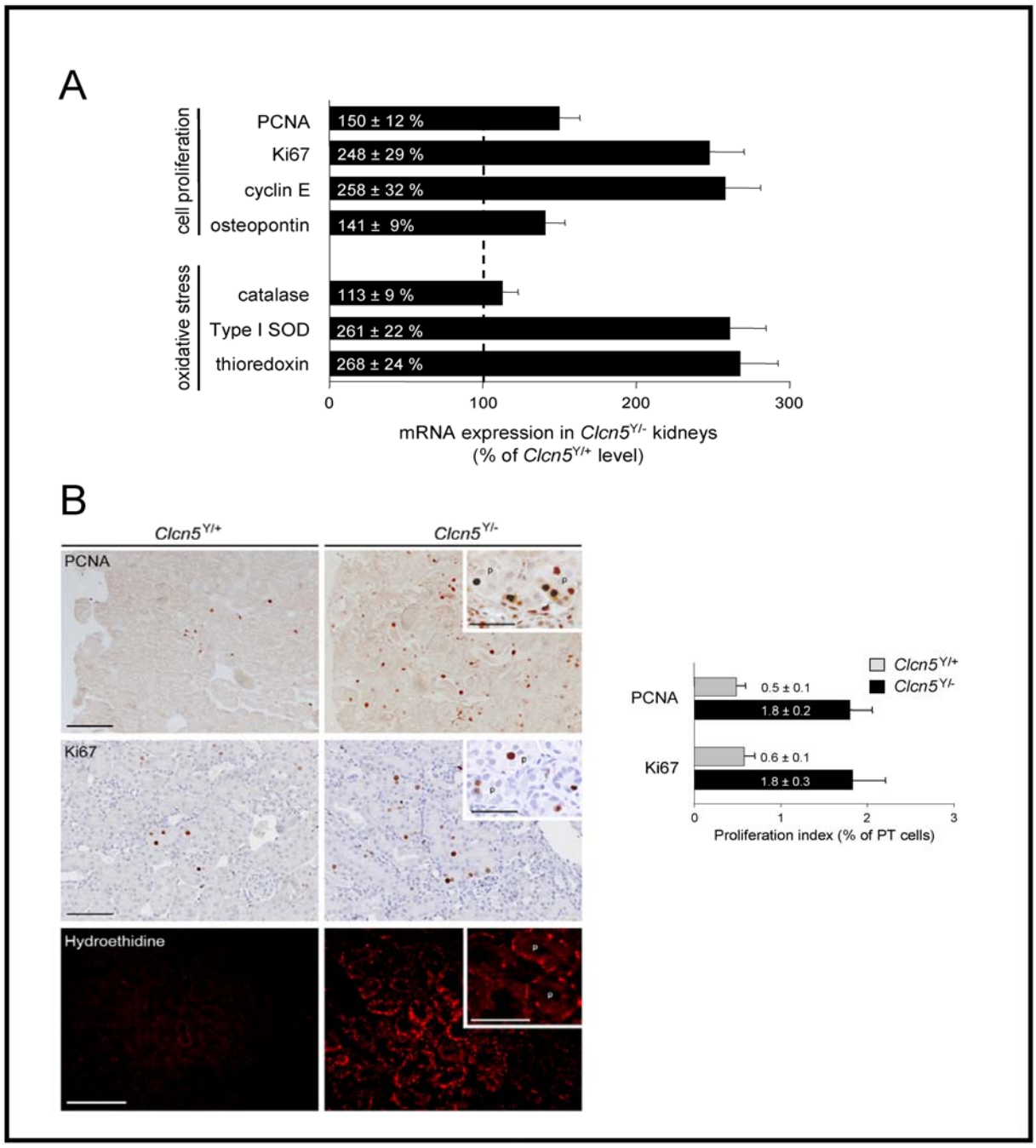

Figure 6.1. Cell proliferation and oxidative stress in ClC-5-deficient kidney

Panel A. Real-time RT-PCR quantification of mRNA expression of proliferative cell nuclear antigen (PCNA), Ki67, cyclin E, osteopontin, catalase, Type I superoxide dismutase (SOD) and thioredoxin in kidneys from *Clcn5*$^{Y/-}$ *vs. Clcn5*$^{Y/+}$ 12-week-old mice (*n=6 pairs*). The mRNA levels were adjusted to GAPDH before quantification, and calculated upon the formula: Efficiency$^{\Delta\Delta Ct}$. The *Clcn5*$^{Y/-}$ kidneys show an increased expression of both cell turnover and oxidative stress markers. Values are presented as mean ratio ± SD, with *Clcn5*$^{Y/+}$ level set at 100%.

Panel B Immunostaining for proliferation markers, proliferative cell nuclear antigen (PCNA) and Ki67, and measurement of superoxide generation in *Clcn5*$^{Y/+}$ and *Clcn5*$^{Y/-}$ kidneys. Counting of PCNA- and Ki67-positive cells along PT (p in insets) indicates a ~3-fold increase of proliferating PT cells in *Clcn5*$^{Y/-}$ *vs. Clcn5*$^{Y/+}$ kidneys (*n=4 pairs*). Values are presented as means ± SD. The detection of red fluorescent ethidium bromide for 5 ms shows a positive signal in *Clcn5*$^{Y/-}$ PT (p in insets), in strong contrast to *Clcn5*$^{Y/+}$ samples (*n=3 pairs*). Bars: 100 μm (insets, 50 μm).

HK-2 (human kidney 2) cells culture. The HK-2 cell line was obtained from ATCC (Teddington, UK). Cells were grown on keratinocyte-serum free medium (GIBCO-BRL 17005-042, Invitrogen) with 5 ng/ml recombinant epidermal growth factor, 50 μg/ml bovine pituitary extract, 50 U/ml penicillin, and 50 μg/ml streptomycin, at 37°C in 95% air/5% CO_2 incubator. When the cultures reached confluence, subculture was prepared using a 0.02% EDTA-0.05% trypsin solution (Invitrogen). After 24h-deprivation of serum, HK-2 cells (passage 12) were treated with H_2O_2 (1 mM). At various times *post* H_2O_2-treatment, cells were trypsinized, washed twice in cold PBS, and centrifuged at 300 *g* for 5 min. The pellet was frozen and stored at -80°C for further use.

Statistics. Results are expressed as means ± SD. Comparisons between samples from *Clcn5*$^{Y/+}$ and *Clcn5*$^{Y/-}$ mice were made by Student unpaired *t*-tests. The significance level was set at $p<0.05$.

6.3. Results

6.3.1. Metabolic outcomes of ClC-5 inactivation in mouse kidney

Real-time RT-PCR for cell turnover and differentiation markers, such as proliferative cell nuclear antigen (PCNA), Ki67, cyclin E and osteopontin, showed a higher expression in 12-week-old *Clcn5*$^{Y/-}$ *vs.* *Clcn5*$^{Y/+}$ mouse kidneys (Figure 6.1, panel A). In addition, real-time RT-PCR analyses for distinct reactive oxygen species (ROS) scavengers, such as type I superoxide dismutase (SOD) and thioredoxin, but not catalase, indicated an increased solicitation of cell oxidative defences in *Clcn5*$^{Y/-}$ samples in comparison to control kidneys (Figure 6.1, panel A). Similar results were obtained in 1-year-old *Clcn5*$^{Y/-}$ mice (data not shown).

Immunohistochemistry detected a significantly higher number of PCNA- and Ki67-positive cells in ClC-5 deficient samples (~2% of PT cells) than in controls (~0.5% of PT cells) (Figure 6.1, panel B). Moreover, comparative measurement of ethidium bromide fluorescence from *Clcn5*$^{Y/+}$ and *Clcn5*$^{Y/-}$ kidneys demonstrated an increased production of superoxide O_2^- anion in *Clcn5*$^{Y/-}$ PT cells (Figure 6.1, panel B). These data demonstrate that the inactivation of ClC-5 causes severe cellular outcomes in PT cells, with higher cell turnover and major oxidative stress.

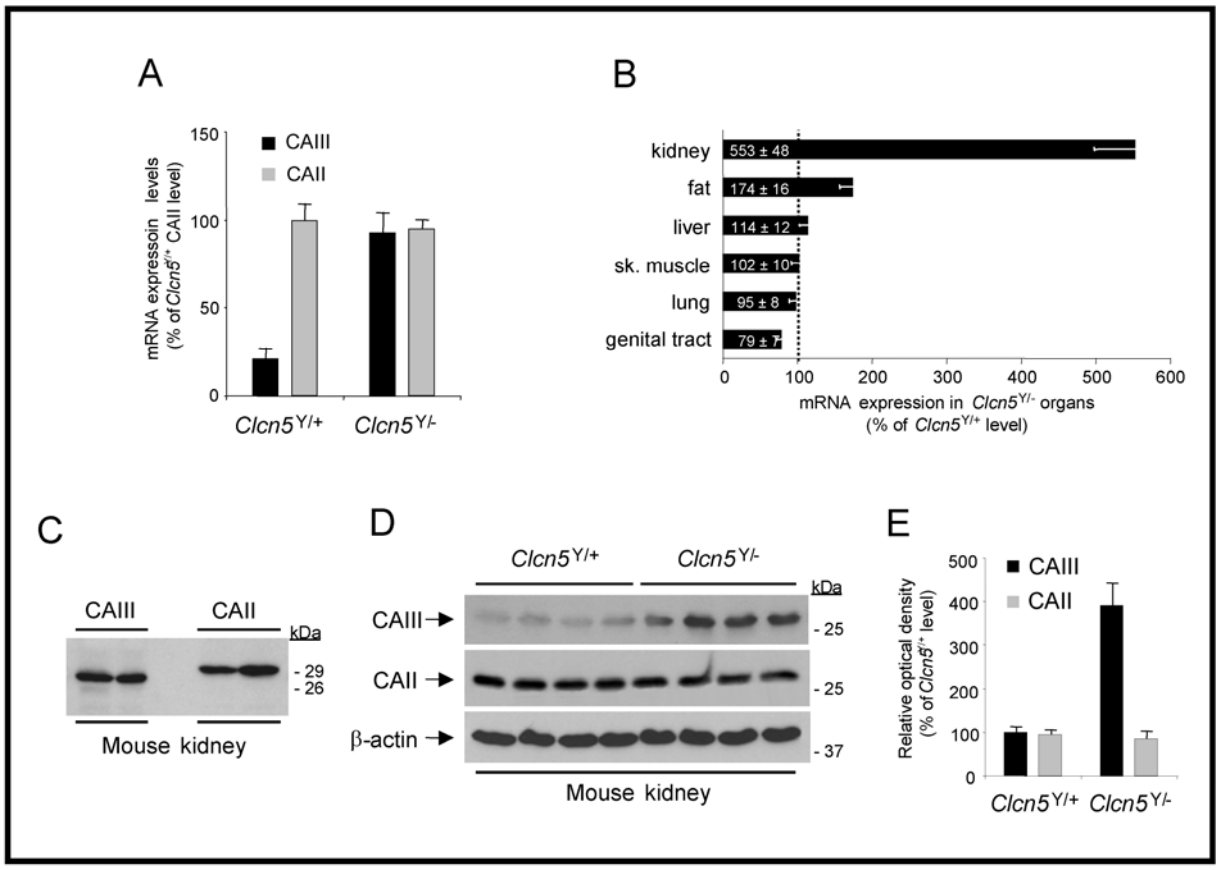

Figure 6.2. Increased expression of CAIII in *Clcn5*$^{Y/-}$ *vs*. *Clcn5*$^{Y/+}$ kidneys

Panel A. Real-time RT-PCR quantification of mRNA expression of type III and II CA isozymes in *Clcn5*$^{Y/-}$ *vs. Clcn5*$^{Y/+}$ kidneys (*n=6 pairs*). The mRNA levels were adjusted to reporter genes, GAPDH or HPRT1, and then compared between *Clcn5*$^{Y/-}$ *vs. Clcn5*$^{Y/+}$ samples, using the formula: Ratio = Efficiency$^{\Delta\Delta Ct}$. In normal mouse kidneys, CAIII mRNA expression represents only ~20% of CAII. By contrast, in *Clcn5*$^{Y/-}$ samples, CAIII expression is increased ~5 times, with no change in CAII level.

Panel B. Real-time RT-PCR quantification of CAIII mRNA expression in *Clcn5*$^{Y/-}$ *vs. Clcn5*$^{Y/+}$ kidneys, epididymal fat, liver, skeletal muscle (*vastus lateralis*), lung and male genital tract (*n=6 pairs*). After adjustment of mRNA levels to the reporter gene GAPDH, CAIII mRNA quantification was compared between *Clcn5*$^{Y/-}$ *vs. Clcn5*$^{Y/+}$ samples, using the formula: Ratio = Efficiency$^{\Delta\Delta Ct}$. The induction of CAIII expression caused by ClC-5 deficiency involves mostly kidneys and epididymal fat, with no significant changes in other *Clcn5*$^{Y/-}$ organs.

Panel C. Characterization of the antibodies directed against type III and II CA isozymes. Twenty μg of cytosolic proteins from total mouse kidneys were separated by SDS-PAGE and blotted onto nitrocellulose membrane. Rabbit polyclonal antibodies anti-CAIII (1/1000) detect a unique band around ~28 kDa, whereas CAII is identified by sheep polyclonal antibodies (1/2000) at a slightly higher molecular weight, without cross-reactivity.

Panels D-E. Representative immunoblots for CAIII and CAII in *Clcn5*$^{Y/+}$ and *Clcn5*$^{Y/-}$ kidneys. Twenty μg of cytosolic proteins were loaded in each lane. Blots were probed as in (C), and after stripping, for β-actin (1/10,000). Densitometry analyses show that CAIII expression is ~4-fold higher in *Clcn5*$^{Y/-}$ kidneys than in controls, whereas CAII abundance is unchanged.

6.3.2. Comparison of *Clcn5*$^{Y/+}$ and C*lcn5*$^{Y/-}$ renal transcriptomes

In order to identify differentially expressed genes possibly involved in adaptation mechanisms, the AFLP procedure was comparatively performed on 12-week-old *Clcn5*$^{Y/-}$ and *Clcn5*$^{Y/+}$ kidneys (n = 4 pairs). Using ~ one third of the possible AFLP primer combinations (see section 4), a total of 10 cDNA bands were reproducibly identified as differentially expressed in *Clcn5*$^{Y/-}$ *vs. Clcn5*$^{Y/+}$ kidneys. One of these bands, significantly upregulated in *Clcn5*$^{Y/-}$ samples, was identified in the GenBank database using the BLAST program (http://www.ncbi.nlm.nih.gov/BLAST/), as a transcript of *Car3* (GenBank accession number: M27796), encoding Type III carbonic anhydrase (CAIII). The other cDNA bands, which were differentially expressed in *Clcn5*$^{Y/-}$ vs. control kidneys, corresponded to unidentified mouse contigs.

Quantitative real-time RT-PCR analyses were next used to compare the mRNA expression of CAIII in 12-week-old *Clcn5*$^{Y/-}$ *vs. Clcn5*$^{Y/+}$ kidneys (Figure 6.2, panel A). In parallel, the mRNA expression of CAII, which represents the most abundant CA isozyme in kidney, was quantified in the very samples. In normal kidney, CAIII mRNA expression was ~5-fold lower than CAII. In contrast, CAIII transcript was significantly upregulated in ClC-5 deficient kidneys (Ratio: 553% ± 48 of *Clcn5*$^{Y/+}$ level, n=6), whereas CAII mRNA expression remained unchanged (94% ± 8 of *Clcn5*$^{Y/+}$ level). Of note, CAIII mRNA expression remained increased ~5-fold in uremic kidneys from 1-year-old *Clcn5*$^{Y/-}$ mice in comparison to age-matched controls (data not shown).

The increased expression of CAIII mRNA associated with the loss of ClC-5 was specific to the kidney, as CAIII mRNA expression levels in liver, skeletal muscle (*vastus lateralis*) and lung from *Clcn5*$^{Y/-}$ mice were unchanged (Figure 6.2, panel B). Of note, CAIII mRNA expression was less than doubled in *Clcn5*$^{Y/-}$ epididymal fat. These data demonstrate the usefulness of the AFLP procedure coupled with real-time RT-PCR to compare the transcriptome of distinct groups of mice. Here, this technique evidenced a significant and kidney-specific induction of *Car3* mRNA expression in *Clcn5*$^{Y/-}$ *versus Clcn5*$^{Y/+}$ mice.

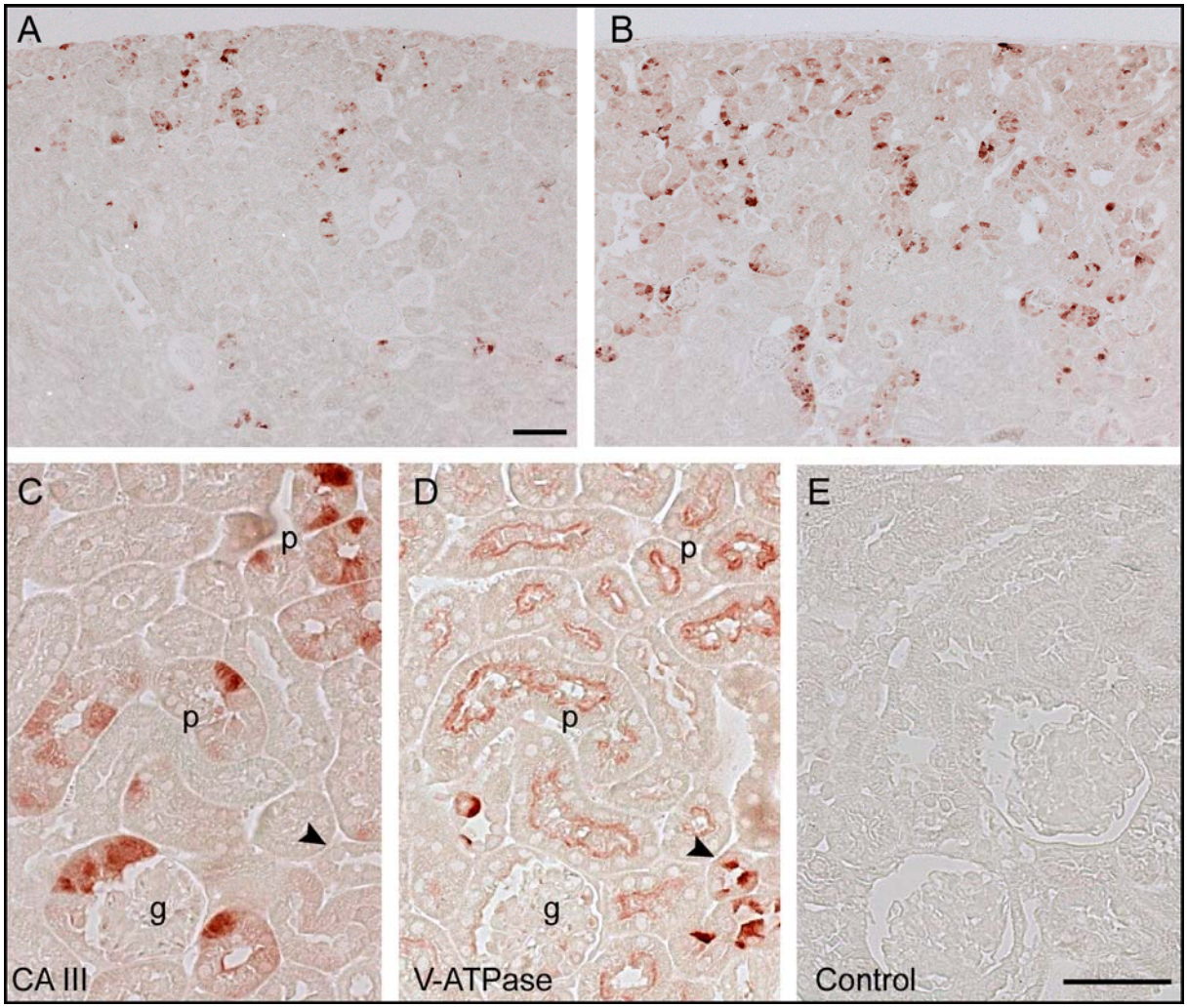

Figure 6.3. Scattered distribution of CAIII in mouse proximal tubule

Immunostaining for CAIII (panels A-C) and V-ATPase E1 subunit (panel D) in *Clcn5*$^{Y/+}$ (panels A, C-E) and *Clcn5*$^{Y/-}$ (panel B); C-D are serial sections (p, proximal tubule; g, glomerulus). In mouse control kidney, CAIII is present in some tubules in the outer cortex (A). In *Clcn5*$^{Y/-}$ kidney, CAIII distribution includes both outer and inner cortices, with a ~4-fold increased number of CAIII-positive cells (B). At higher magnification, CAIII is located in a subset of PT cells (C), identified by co-staining for the V-ATPase (D). The α-type intercalated cells of the collecting duct, also positive for the V-ATPase, are strictly negative for CAIII (C-D, arrowheads). No signal is detected after incubation with non-immune rabbit IgG (E).Bars: 100 μm (A-B); 50 μm (C-E).

6.3.3. Expression of CAIII in *Clcn5*$^{Y/-}$ and *Clcn5*$^{Y/+}$ kidney

The specificity of the sheep polyclonal anti-CAII and rabbit polyclonal anti-CAIII antibodies was first demonstrated by the lack of cross-reactivity between these isozymes, which are characterized by a slightly distinct molecular weight (http://us.expasy.org/) (Figure 6.2, panel C). Next, immunoblotting analyses confirmed the consistent up-regulation of CAIII in 12-week-old ClC-5 deficient kidneys (Figure 6.2, panels D-E). Densitometry analyses showed that CAIII was ~4 times more abundant in *Clcn5*$^{Y/-}$ than in control samples (385% ± 43 of *Clcn5*$^{Y/+}$, n=4), while CAII expression was not modified. These data were confirmed by using a commercial mouse monoclonal antibody directed against CAIII (data not shown). These results support the data obtained by real-time RT-PCR, and further demonstrate that CAIII expression is significantly and specifically increased at both mRNA and protein levels in ClC-5 deficient kidneys.

6.3.4. Cellular and subcellular distribution of CAIII in mouse kidney

In normal kidney, a weak immunoreactive signal for CAIII was observed in some tubules located in the outer cortex (Figure 6.3, panel A). At higher magnification, the staining pattern was restricted to a subset of cells lining the PT, identified by their apical reactivity for the E1 subunit of the V-ATPase (Figure 6.3, panels C-D). In ClC-5 deficient kidney, the total number of CAIII-positive PT cells in the outer cortex was increased ~4-fold (17.1% *vs*. 4.2% of *Clcn5*$^{Y/+}$ PT cells) (Figure 6.3, panel B). In addition, immunoreactive signal for CAIII was detected in PT of the inner cortex. No signal was detected with non-immune rabbit IgG (Figure 6.3, panel E). The number of PT cells undergoing apoptosis, based on the classical TUNEL reaction, was similar in *Clcn5*$^{Y/+}$ and *Clcn5*$^{Y/-}$ kidneys (data not shown).

Subcellular fractionation of mouse kidneys demonstrated that CAIII was predominantly located in the cytosol, with residual distribution in membrane and nuclear fractions, as reported previously in adipocytes and hepatocytes (Tweedie, 1989). Immunogold analyses showed that in normal kidney cortex, CAIII distribution was mainly cytosolic, also including the apical brush border microvilli (Figure 6.4, panels A and D). Nuclei were labelled (Figure 6.4, panels C and F), and a possible endosomal labelling could not be excluded (Figure 6.4, panel B). No significant signal

was noticed in mitochondria (Figure 6.4, panel E). In *Clcn5*$^{Y/-}$ samples, CAIII labelling appeared stronger than in *Clcn5*$^{Y/+}$ kidneys, with a similar distribution (Figure 6.4, panels F *vs.* C). Altogether these data demonstrate that the CAIII isozyme is present in mouse kidney, with a subcellular distribution including the cytosol, the nucleus and the brush border of a subset of cells lining the PT in the outer cortex. The loss of the Cl^- transporter ClC-5 causes a significant increase of CAIII expression in PT cells of both outer and inner cortices, with a similar subcellular localization.

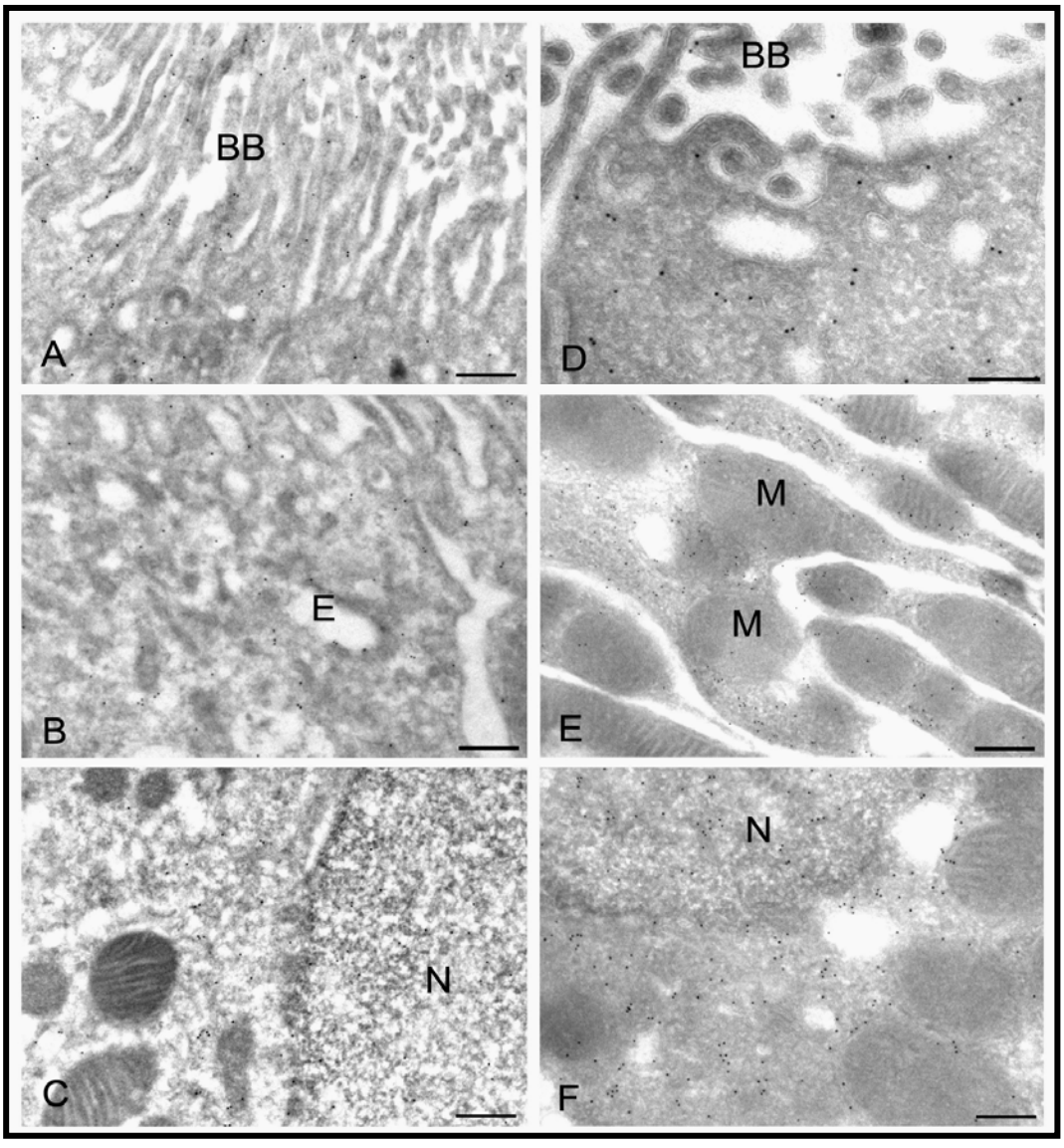

Figure 6.4. Subcellular distribution of CAIII in *Clcn5*$^{Y/+}$ and *Clcn5*$^{Y/-}$ kidneys
EM immunocytochemistry for CAIII on ultrathin cryosections from renal cortex of *Clcn5*$^{Y/+}$ (A-C) and *Clcn5*$^{Y/-}$ mice (D-F). Labeling appears stronger in the *Clcn5*$^{Y/-}$ samples than in controls. The labeling is mainly cytosolic, extending to the apical brush border (BB) microvilli (A, D). Nuclei (N) are also labelled (C, F) and a possible endosomal labelling (E) in (B) can not be excluded. The very low signal in mitochondria (M in E) was considered to be background. Bars. A-C and F: 0.5 μm; D: 0.3 μm; and E: 0.8 μm.

6.3.5. Upregulation of CAIII in human Dent's disease kidney

The data obtained in the *Clcn5*$^{Y/-}$ mouse model were assessed in kidney samples from one patient with Dent's disease due to a loss-of-function mutation of *CLCN5* (Gly506Glu) (Frymoyer, 1991; Lloyd, 1996). In comparison to 4 distinct end-stage kidney samples with chronic interstitial nephritis, Dent's kidney was characterized by a ~5-fold up-regulation of CAIII at both mRNA and protein levels (Figure 6.5, panels A-B). In addition, real-time RT-PCR studies showed that the functional loss of ClC-5 was associated with an induction of PCNA and thioredoxin expression, which reflects a higher cell turnover and oxidative stress, respectively (Figure 6.5, panel C). Despite tissue damage due to the end-stage renal disease, the expression of CAIII could be located in PT cells, identified by co-staining with the water channel aquaporin-1 (Figure 6.5, panel D).

These results demonstrate at the human level that the functional loss of ClC-5 is associated with metabolic responses of PT cells, including cell proliferation, protection against oxidative damage and induction of CAIII.

6.3.6. Expression of CAIII mRNA in distinct mouse models of PT dysfunction

As demonstrated above, the severe PT dysfunction caused by the functional loss of ClC-5 is associated with increased expression of CAIII in both mouse and man PT cells (Figures 6.2-5). In order to clarify whether CAIII induction was specifically caused by ClC-5 inactivation or participated in a common cell response to PT dysfunction, CAIII mRNA expression was investigated in two additional mouse models of human renal Fanconi syndrome, namely the megalin- and cystinosin-deficient mice. These models can be distinguished from each other by the severity of PT defects, as summarized in section 6.2. The expression of CAIII mRNA was significantly increased in *megalin* KO (262 ± 22% of WT level, *n=3 pairs*), whereas no changes were observed in *Ctns* KO samples.

These results indicate that the induction of CAIII expression directly correlates with the severity of PT dysfunction, suggesting that this isozyme participates in the general cellular response to PT dysfunction.

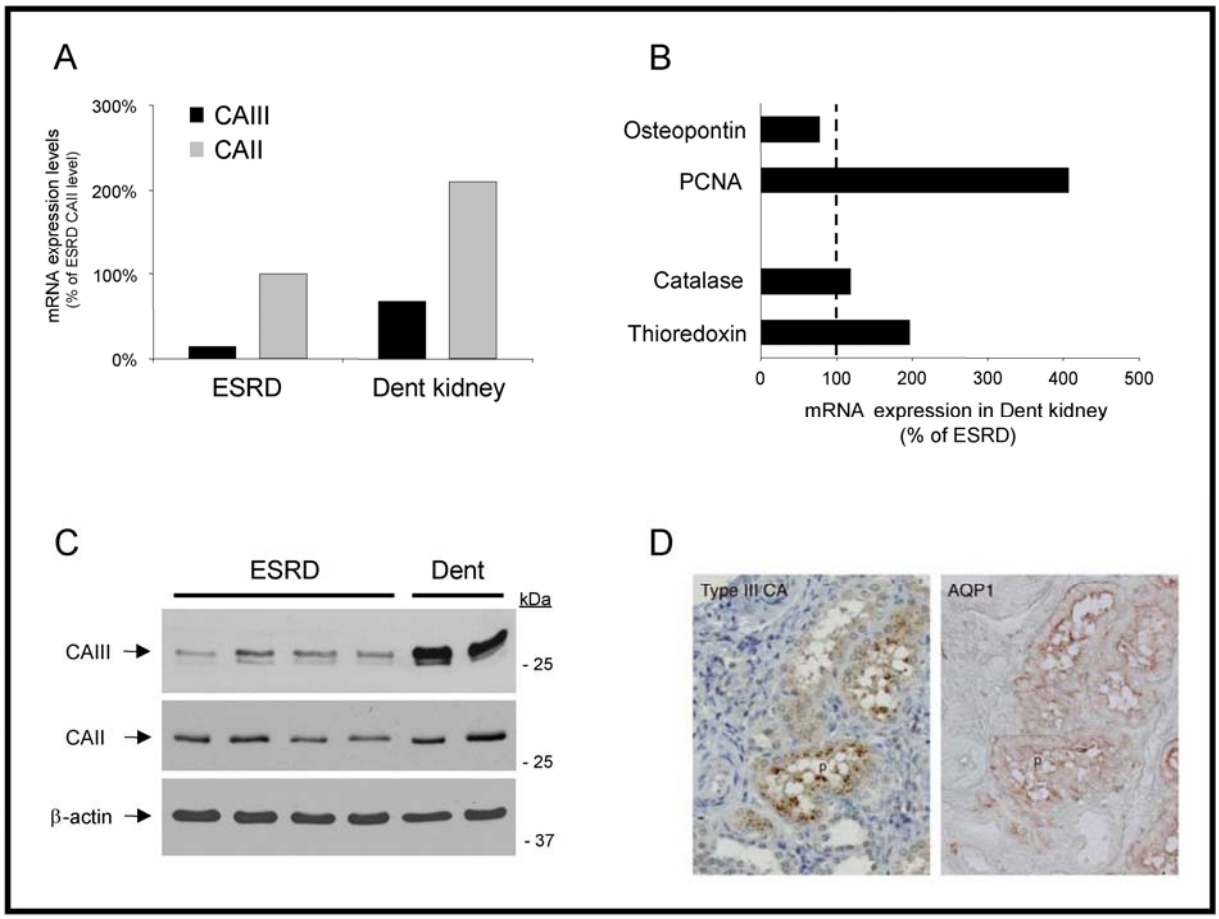

Figure 6.5. Expression and distribution of CAIII in human Dent's disease kidney

Panels A and B. Real-time RT-PCR quantification of mRNA expression of type III and II CA isozymes (A), osteopontin, PCNA, catalase and thioredoxin (B) in end-stage renal disease (ESRD) kidneys with Dent's disease (*n=1 patient*) vs. with an unrelated pathology (*n=4 patients*). The mRNA levels were adjusted to the reporter gene GAPDH, and quantified using the formula: Ratio = Efficiency$^{\Delta\Delta Ct}$. In Dent's disease samples, CAIII mRNA expression is ~4-fold higher than in controls, with a variable increase of CAII level. In addition, PCNA and thioredoxin mRNA are increased in Dent's samples *vs.* controls.

Panel C. Representative immunoblotting for CAIII and CAII isozymes in human ESRD kidneys with Dent's disease and with an unrelated pathology. Blots were probed with antibodies against CAIII (1/1000) or CAII (1/2000), and after stripping, β-actin (1/10,000). CAIII expression is ~5-fold higher in Dent's disease kidneys than in controls, with no change in CAII expression level.

Panel D. Immunostaining for CAIII (A) and aquaporin-1 (B) in human Dent's disease kidney. CAIII is located diffusely in some PT cells (p), identified by staining for the water channel, AQP1.

6.3.7. Induction of CAIII expression in PT cells exposed to H_2O_2

The HK-2 cell line derives from normal man PT cells immortalized by transduction with human HPV-16 E6/E7 genes. At baseline, a weak expression of CAII and CAIII can be detected in HK-2 cells at both mRNA and protein levels. Exposure of HK-2 cells to 1 mM H_2O_2 induced a significant increase in CAIII mRNA expression as early as 3 hours postincubation, with a maximal level observed at 6 hours posttreatment (Figure 6.6). Immunoblotting analyses showed an early and stable induction of CAIII from 6 hours postincubation with H_2O_2. Similar results were obtained with *Opossum kidney* (OK) cells, which represent another established model of PT cells. Exposure of OK cells to 0.3 mM H_2O_2 was associated with an increased expression of CAIII from 6 hours postincubation (data not shown). These data demonstrate that, under oxidative conditions such as exposure to H_2O_2, PT cells rapidly increase their expression of CAIII.

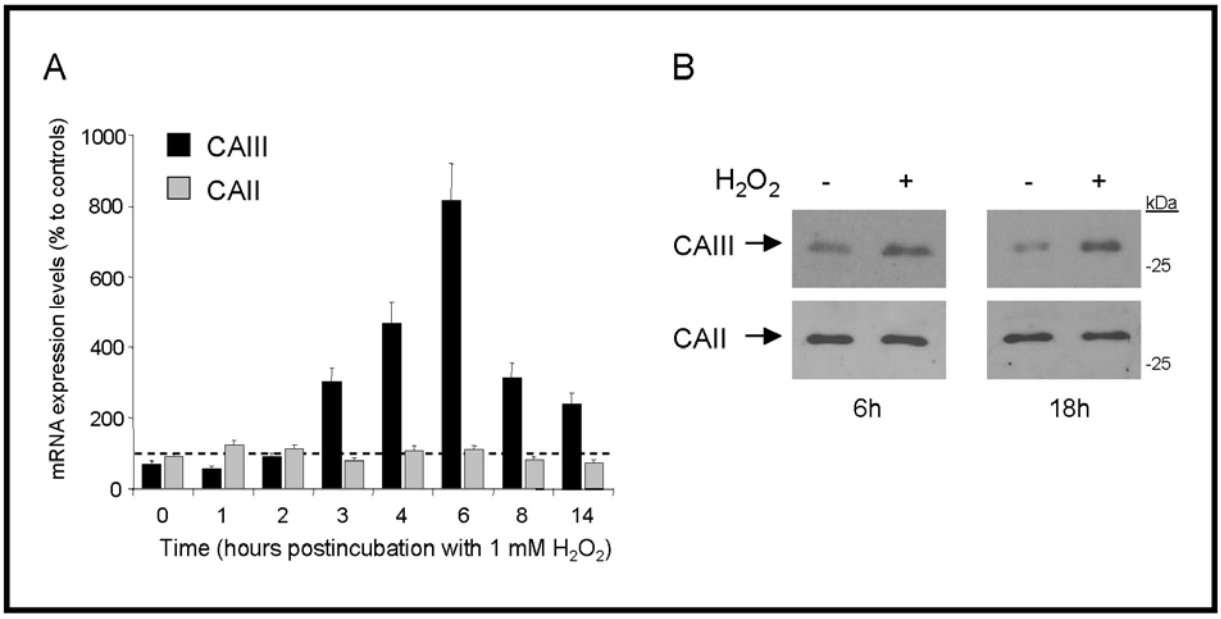

Figure 6.6. Time-course of CAIII expression in HK-2 cells after H_2O_2 exposure

Panel A. Real-time RT-PCR analyses of CAIII and CAII mRNA abundance in HK-2 cells after the indicated times of exposure to H_2O_2 (1 mM). Quantifications were done after adjustment to GAPDH mRNA levels and in comparison to time-matched controls. The expression of CAIII mRNA significantly increases from 3 hours *post* H_2O_2 treatment, whereas no changes are observed in CAII mRNA level. Values are presented as means ± SD.

Panel B. Representative immunoblotting for CAIII and CAII expression in HK-2 cells at various time-points following exposure to H_2O_2 (1 mM). Thirty μg proteins were loaded, blotted onto nitrocellulose membrane, and incubated with antibodies anti-CAIII (1/1000) or anti-CAII (12000). In comparison to non-treated cells, H_2O_2-treated HK-2 cells show an increased expression of CAIII from 6 hours posttreatment, with no change in CAII abundance.

6.4. Discussion

In this study, we report that CAIII is a novel kidney CA isozyme expressed in scattered PT cells. In ClC-5-deficient kidney, the severe PT dysfunction is associated with induction of cell oxidative defences and higher cell proliferation, as well as increased expression of CAIII at both mRNA and protein levels. This induction is specific to the kidney, since no significant changes in CAIII expression are observed in other *Clcn5*$^{Y/-}$ organs investigated. Moreover, CAIII induction is also observed in megalin-deficient kidney, as well as in PT cells exposed to oxidant conditions.

Type III CA belongs to the family of zinc metallo-enzymes that reversibly hydrate CO_2, thus generating hydrogen and bicarbonate ions essential for acid-base homeostasis, respiration, ureagenesis, lipidogenesis, urinary acidification and bone resorption (Sly, 1995; Lindskog, 1997). At least 15 different isoforms, with 11 catalytically active isozymes, have been described in the mammals, with distinct kinetic properties and tissue distribution. Subcellularly, four of the active CA isozymes are cytosolic (CAI, CAII, CAIII, and CAVII), four are membrane-bound (CAIV, CAIX, CAXII and CAXIV), two are mitochondrial (CA VA and VB), and one is a secretory isoform (CA VI) (Mori, 1999). In the kidney, type II and IV CA represent the two main isozymes, and are located in PT cells where they concurrently participate in H^+ secretion and HCO_3^- reabsorption, as well as to salt homeostasis. In addition CAII is present in the cytosol of the IC of the CD, where it ensures net urinary acidification (Giebisch, 2003b). The functional loss of CAII causes Guibaud-Vainsel disease, an inherited syndrome characterized by renal tubular acidosis, osteopetrosis, and cerebral calcifications (Sly, 1985). Other CA isozymes have been located in mouse kidney, i.e. CA XIII and CAXIV, but their specific role, as well as their interactions with CAII and CAIV in this organ, remains unknown (Mori, 1999; Lehtonen, 2004).

Type III CA is distinguishable from the other CA isozymes by several features, particularly its resistance to sulfonamide inhibitors and its low CO_2 hydration ability which represents ~2% of CAII activity (Jewell, 1991). Its lower catalytic turnover is in part explained by the replacement of a histidine at residue 64 by a lysine, which is not

efficient for H^+ transfer during catalysis (Jewell, 1991). In addition, at residue 198, the phenyl side chain of CAIII (Phe instead of Leu in CAII) causes a further steric constriction in CAIII active site, which may be responsible for lower catalytic activity and resistance to acetazolamide (LoGrasso, 1991; Duda, 2005). Although CAIII is abundantly expressed in the cytosol of skeletal muscle cells, adipocytes and hepatocytes, its function, as well as its regulation, remains unclear (Kim, 2004). The concentration of CAIII in rat male liver was found to be 30 times greater than that in females, with a marked reduction after castration (Carter, 2001). However, comparative real-time RT-PCR studies in mouse kidney did not find any significant difference in CAIII mRNA expression between 15-week-old male and female samples (*n=5*, data not shown). Two reactive sulfhydryl groups of CAIII are rapidly reduced and S-thiolated by glutathione after *in vivo* and *in vitro* exposure to oxidative conditions (Chai, 1991). CAIII may be S-thiolated by two different non-enzymatic mechanisms and dethiolated by enzymatic reactions (glutaredoxin and thioredoxin-like) in intact liver cells. These observations, as well as its protective role against hydrogen-peroxide induced apoptosis (Raisanen, 1999), suggest that CAIII isozyme may function as an oxyradical scavenger and thus protect cells from oxidative stresses, such as renal ischemia-reperfusion injury and aging (Eaton, 2003; Cabiscol, 1995). Recently, Kim et al have postulated that CAIII may have evolved into a percarbonic acid anhydrase, which would mediate $H_2O_2 + CO_2 \leftrightarrow H_2CO_4$ (Kim, 2004; Richardson, 2003).

The metabolic outcomes of acquired or hereditary PT dysfunction remain unclear. Cadmium-induced nephropathy is clearly associated with increased ROS production, which depletes endogenous radical scavengers and cause cell oxidative damage (Thevenod, 1999). In addition, recent studies have demonstrated elevated oxidized glutathione in PT epithelial cells derived from patients with cystinosis (Wilmer, 2005). Here, we show that the PT dysfunction caused by the functional loss of ClC-5 is associated with higher cell turnover and increased cellular response to oxidant damage, as well as induction of CAIII expression. The upregulation of CAIII in *Clcn5*$^{Y/-}$ mice was restricted to the kidney, with no changes observed in the other

CAIII-expressing organs. These findings were also observed in kidney samples of a patient with Dent's disease, with a previously reported "G to A" missense mutation in *CLCN5* (Frymoyer, 1991; Lloyd, 1996). Interestingly, the investigation of another mouse model of PT dysfunction caused by the inactivation of megalin (Willnow, 1996), showed similar features in terms of cell proliferation and response to oxidative stress, as well as a significant increase of renal CAIII expression in megalin-deficient kidneys. Moreover the exposure of PT cells to oxidant conditions caused a rapid and consistent response of CAIII.

In conclusion, we report on CAIII, a novel kidney CA isozyme with a distribution restricted to scattered PT cells. The induction of CAIII expression in Dent's disease, in megalin-deficient kidneys and in PT cells exposed to oxidative stress suggests that this isozyme may participate to the common cellular response against oxidative damage in case of PT dysfunction.

Acknowledgements

The authors are grateful to C. Antignac, M-C. Gubler, and E. Van Schaftingen for helpful discussion, and thank V. Beaujean, Y. Cnops, B. Marien, H. Sidelmann, M. Van Schoor and L. Wenderickx for excellent technical assistance. The *Clcn5* mice were kindly provided by W.B. Guggino (Dept. of Physiology, Johns Hopkins University Medical School, Baltimore, MD).

CHAPTER VII.

IN VIVO INVESTIGATION OF PROXIMAL TUBULE DYSFUNCTION IN CONSCIOUS MICE BY SINGLE PHOTON EMISSION COMPUTED TOMOGRAPHY

François Jouret[(1)], Stéphan Walrand[(2)], Pierre J. Courtoy[(3)], Stanislas Pauwels[(2)], Olivier Devuyst[(1)] and François Jamar[(2)]

(1) Division of Nephrology, (2) Laboratory of Molecular Imaging and Experimental Radiotherapy, and (3) Christian de Duve Institute of Cellular Pathology, CELL Unit, Université catholique de Louvain, Brussels, Belgium

Manuscript in preparation

Summary

Investigations of mouse kidney function are usually performed *ex vivo*, with definite ethical and technical obstacles. Therefore, the development of *in vivo* imaging techniques represents an attractive alternative for such functional studies. Here, SPECT studies (Linoview) were conducted on control and *Clcn5* knockout conscious mice as a model of Dent's disease to *in vivo* assess PT functions. SPECT quantification of ^{123}I-β_2-microglobulin and ^{99m}Tc-DMSA renal uptake demonstrated a major defect in both PT apical endocytosis and basolateral transport in *Clcn5*$^{Y/-}$ mice. Conversely dynamic ^{99m}Tc-MAG3 secretion studies detected no differences between *Clcn5*$^{Y/+}$ and *Clcn5*$^{Y/-}$ mice. In conclusion, SPECT allowed the *in vivo* investigation of mouse PT functions with (i) avoidance of animal anaesthesia and sacrifice, (ii) comparison of distinct radiotracer biodistribution in the same animals, (iii) and dynamic imaging to achieve pharmacokinetic evaluations. The data further suggest a severe defect in both apical and basolateral PT functions in *Clcn5*$^{Y/-}$ mice, without alteration of the secretory pathway.

7.1. Introduction

Transgenic mouse strains have become a widely used research tool to investigate the anatomy and physiology of developing and mature organs (Rao, 2000). However, most studies are usually performed *ex vivo*, with definite ethical and technical obstacles. Therefore many efforts have been made to develop *in vivo* functional imaging techniques in mice, such as PET (Positron Emission Tomography) or SPECT (Single Photon Emission Computed Tomography) (Lewis, 2002; Beekman, 2005; Walrand, 2005). Indeed high-resolution imaging would allow the fine visualization of organs *in vivo*. The feasibility of repetitive biodistribution studies in the same animal would help compare the handling of distinct radiolabeled compounds, without interindividual variance. Moreover quantitative biodistribution analyses starting at the time of drug injection would help establish the pharmacokinetic parameters of new drugs in rodents, as a prerequisite for further human applications. Intervention studies would enable to non-invasively evaluate tissue responses to different acute or prolonged experimental conditions, such as variable regimens of drug administration. Finally, *in vivo* imaging would circumvent the complexity of *ex vivo* approaches, such as radioactivity counting or (chemi-) fluorescence imaging, and would avoid animal sacrifice, which represents *per se* a considerable improvement from an ethical point of view (Directive 86/609/EC).

Among its numerous potential applications, SPECT may be especially useful to non-invasively investigate the urinary tract in normal and genetically modified rodents: quantification of renal function, dynamic imaging, and parenchymal scanning (de Jong, 2005). Similarly to routine investigations in man, two main classes of radioactive compounds, i.e. glomerular and tubular tracers, can be used for renal studies in mice (Trejtnar, 2002; Maisey, 2003). On one hand, glomerular tracers, such as ^{99m}Tc-labeled diethylenetriamine pentaacetic acid and ^{51}Cr-labeled ethylenediamine tetraacetic acid, are passively cleared from the plasma by glomerular filtration, without significant tubular reabsorption or secretion (Trejtnar, 2002). On the other hand, tubular tracers are classified into two sub-classes of molecules, which are either retained in renal parenchyma (captation) or excreted into the urine after tubular uptake

from the plasma (secretion). ^{99m}Tc-labeled dimercaptosuccinic acid (^{99m}Tc-DMSA) accumulates in the renal cortex and minimally excreted into the urine, thereby providing cortex imaging with fine resolution (Moretti, 1984). The renal uptake of ^{99m}Tc-DMSA from peri-tubular capillaries has been shown to be mediated by the co-transporter NaC3 (SLC13A3) located in the basolateral membrane of S3 PT cells (Burckhardt, 2002). Thus, ^{99m}Tc-DMSA uptake can also be used as a marker of PT dysfunction in inherited and in drug-induced renal disorders (Van Luijk, 1984; Anninga, 1994). ^{99m}Tc-labeled mercaptoacetyltriglycine (^{99m}Tc-MAG3), a radiolabeled analogue of p-aminohippurate, is cleared from plasma by tubular secretion, and is regarded as the almost perfect tubular agent for dynamic renography since there is hardly any glomerular filtration (Müller-Suur, 1989; Maisey, 2003). Recent *in vitro* studies based on transport experiments in *Xenopus* oocytes have proposed a model for ^{99m}Tc-MAG3 secretion by PT cells (Shikano, 2004). First ^{99m}Tc-MAG3 is actively extracted from peri-tubular plasma through the organic anion transporter OAT1 in exchange for intracellular dicarboxylates (Burckhardt, 2003). The segmental distribution of OAT1 in the nephron includes all segments of the PT (Motohashi, 2002). This exchanger allows the intracellular accumulation of ^{99m}Tc-MAG3 at high levels in PT cells, and its subsequent exit at the brush border following its electrochemical gradient. The molecular counterpart of ^{99m}Tc-MAG3 apical transport remains debated (Shikano, 2004), although p-aminohippurate apical transport seems mediated by the human Type 1 Na^+-dependent phosphate transporter NPT1 and/or the multidrug resistance protein MRP2 (Burckhardt, 2001). In addition to these classical radiotracers, other compounds can be specifically radiolabeled with gamma emitters to investigate particular kidney functions by SPECT. For example, PT apical receptor-mediated endocytosis of filtered LMW proteins may be investigated by quantification of ^{123}I-β_2-microglobulin uptake (Christensen, 2003).

We report on the use of a small-animal SPECT prototype (Linoview Systems, Amsterdam, the Netherlands) to investigate PT functions, i.e. apical and basolateral uptakes and secretion, in control and *Clcn5* KO mice, an established model of Dent's disease. Dent's disease is an X-linked renal tubulopathy characterized by LMW

proteinuria and renal Fanconi syndrome, associated with hypercalciuria, nephrocalcinosis, and nephrolithiasis (Lloyd, 1996; Scheinman, 1998). Dent's disease is caused by mutations in the *CLCN5* gene, which encodes the endosomal H^+/Cl^- exchanger ClC-5 predominantly expressed in the kidney (Fisher, 1994; Jentsch, 2005). Similarly genetic inactivation of *Clcn5* gene in mice leads to severe PT dysfunction (Piwon, 2000; Wang, 2000), with impaired receptor-mediated endocytosis and intracellular trafficking (Christensen, 2003). In this well-defined model of PT dysfunction, we conducted a series of experiments to demonstrate the feasibility and benefits of *in vivo* SPECT imaging to explore PT functions in conscious mice.

7.2. Materials and methods

Animals. Experiments were conducted on 4 C57/bl6 20-week-old mice and 6 pairs of 20-week-old *Clcn5* wild-type (*Clcn5*$^{Y/+}$) and KO (*Clcn5*$^{Y/-}$) male mice. No significant differences of weight (30.4 g ± 0.8) and plasma creatinine levels (0.31 mg/dL ± 0.04) were noted between the 2 groups. The *Clcn5*$^{Y/-}$ mice, generated by targeted deletion of the exon VI of *Clcn5*, have been extensively characterized (Wang, 2000). Restricted kidney infarction was induced by clamping the superior pole of the organ for 30 min under anaesthesia. All procedures were performed in accordance with NIH guidelines for the care and use of laboratory animals, and with the approval of the Committee for Animal Rights of the Université catholique de Louvain.

Radiochemicals. Human β_2-microglobulin (Sigma, St-Louis, MO) was iodinated with ^{123}I-sodium (GE Healthcare, Brussels, Belgium) and Iodobeads™ (Pierce, Aalst, Belgium) as previously described (Christensen, 2003). Radiopharmaceutical purity was in excess of 92%, and remained stable over time. Commercial kits of dimercaptosuccinic acid (TechneScan® DMSA) or mercaptoacetyltriglycine (TechneScan® MAG3) were obtained from Tyco HealthCare (Mechelen, Belgium). Both tracers were radiolabeled with ^{99m}Tc Na-pertechnetate (Tyco HealthCare) following the standard procedure. Radiopharmaceutical purity was in excess of 99%, as confirmed by instant thin-layer chromatography.

Autoradiography. Seven minutes after iv injection of 620 ng/g of body weight of ^{125}I-β_2-microglobulin, kidneys were exsanguinated *in situ*, removed, and fixed for 6h at 4°C in 4% formaldehyde. Ten-µm slices were prepared, treated with emulsion reagent (Ilford Scientific Product, Wilrijk, Belgium), and revealed four weeks later.

SPECT system. The animal SPECT device (Linoview Systems, Amsterdam, The Netherlands) is made of four 2- by 5-in. γ-ray detectors based on pixelated CsI(Na) scintillators (5-mm thickness, 21 x 52 pixels of 2.44 x 2.44 mm) (Figure 7.1). The intrinsic spatial resolution is 2.5 mm, the intrinsic energy resolution at 140 keV is 35%, and the intrinsic sensitivity in an energy window of 35% width centered on the photopeak is 42%. The detectors are fitted with a rake collimator equipped with an adjustable slit aperture (0-5 mm), made of 2 iridium square rods (2 x 2 x 60 mm) (Walrand, 2005).

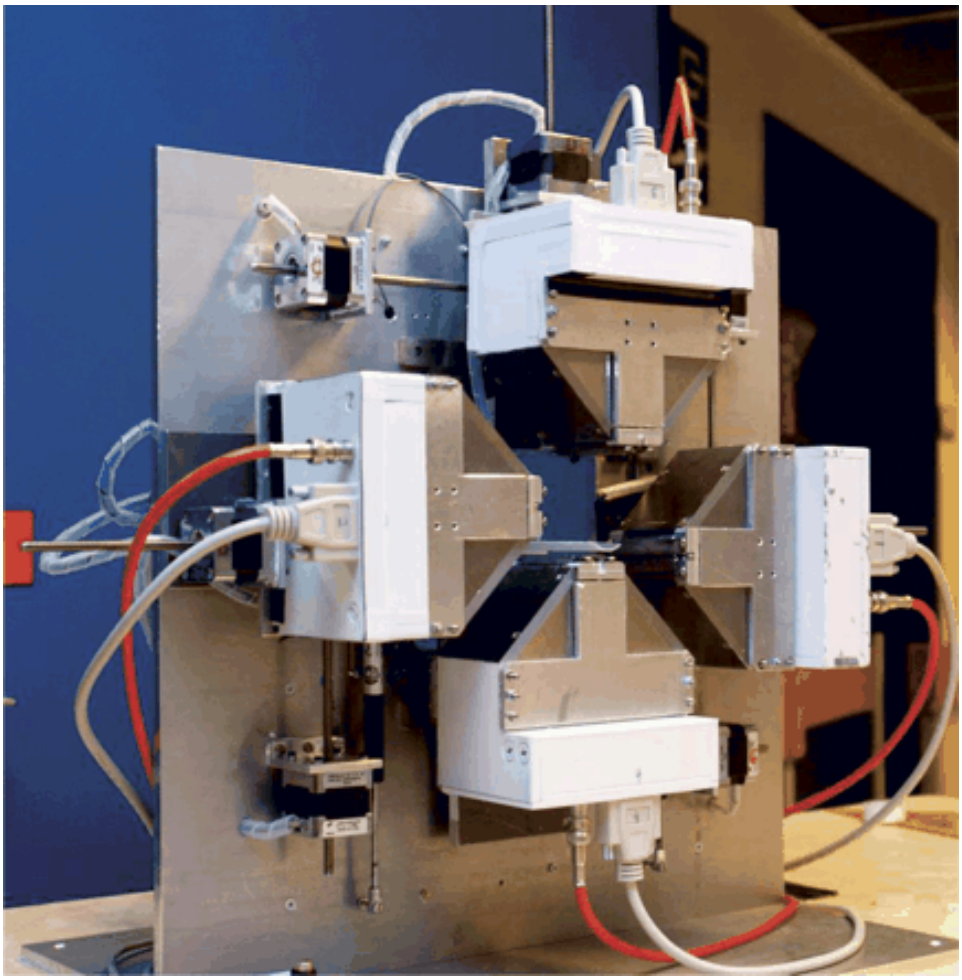

Figure 7.1. Linoview SPECT device (Linoview Systems)
Courtesy of S. Walrand

Acquisition procedure. All kinetic studies were performed on conscious mice placed in a special plastic holder to prevent animal motion during imaging. Static SPECT was obtained every hour (acquisitions of 5 min each) during 6 hours after iv injection of 700 μCi of ^{99m}Tc-DMSA (n=4 pairs). At 6 hours postinjection, a 30 min-acquisition was performed under anaesthesia in order to obtain high-resolution images. Continuous dynamic SPECT (acquisitions of 15 sec each) was performed over 30 minutes after iv injection of 600 μCi of ^{99m}Tc-MAG3 (n=3 pairs) or 200 μCi ^{123}I-β_2-microglobulin (n=3 pairs), respectively. In addition, dynamic ^{99m}Tc-MAG3 SPECT was performed before and following anaesthesia (ketamine [Merial, Brussels, Belgium], 100 μg/g; xylazine [Bayer, Antwerp, Belgium], 10 μg/g) in two control mice. The linear motion of the detectors were set in such a way that the 4 slit apertures would draw the narrowest rectangle possible around the animal. Typically the distance between the actual contours and the collimator aperture was ~3 mm. Acquisitions were performed in continuous motion. The linear acquisition generates linograms forming a complete set of tomographic data allowing the reconstruction of the activity map (Walrand, 2002).

Data processing. Reconstructions were performed using the maximum-likelihood expectation maximization algorithm with attenuation correction but no scatter correction nor spatial resolution recovery (Shepp, 1982; Lange, 1984). Time-activity curves were generated. ^{99m}Tc-MAG3 dynamic parameters were calculated by fitting the curves to a 2-exponential model. The glomerular filtration rate (GFR) of ^{123}I-β_2-microglobulin was assessed by fitting the "blood" curve (region of interest centred on the heart) by the exponential function:

$$A\,e^{-kt} \qquad (1)$$

The GFR can be calculated as:

$$GFR = k\,V_p \qquad (2)$$

where Vp is the plasma volume. Only the period between 30 and 180 sec postinjection was considered in order to avoid the influence of the bolus injection and the effect of ^{123}I-β_2-microglobulin tubular reabsorption and metabolization. The plasma volume of the mice was approximated using a standard blood volume (8% body weight) and 0.45 as haematocrit value (Qi, 2004). All kinetic parameters of renal uptake were calculated using SigmaPlot 2000 (Systat Software GmbH, Erkrath, Germany).

Statistics. Results are expressed as means ± standard deviation (SD). Comparisons between *Clcn5*$^{Y/+}$ and *Clcn5*$^{Y/-}$ mice were made by Student non-paired *t*-tests. The significance level was set at $p<0.05$. Inter-assay variability was calculated by the ratio [(SDx100)/mean].

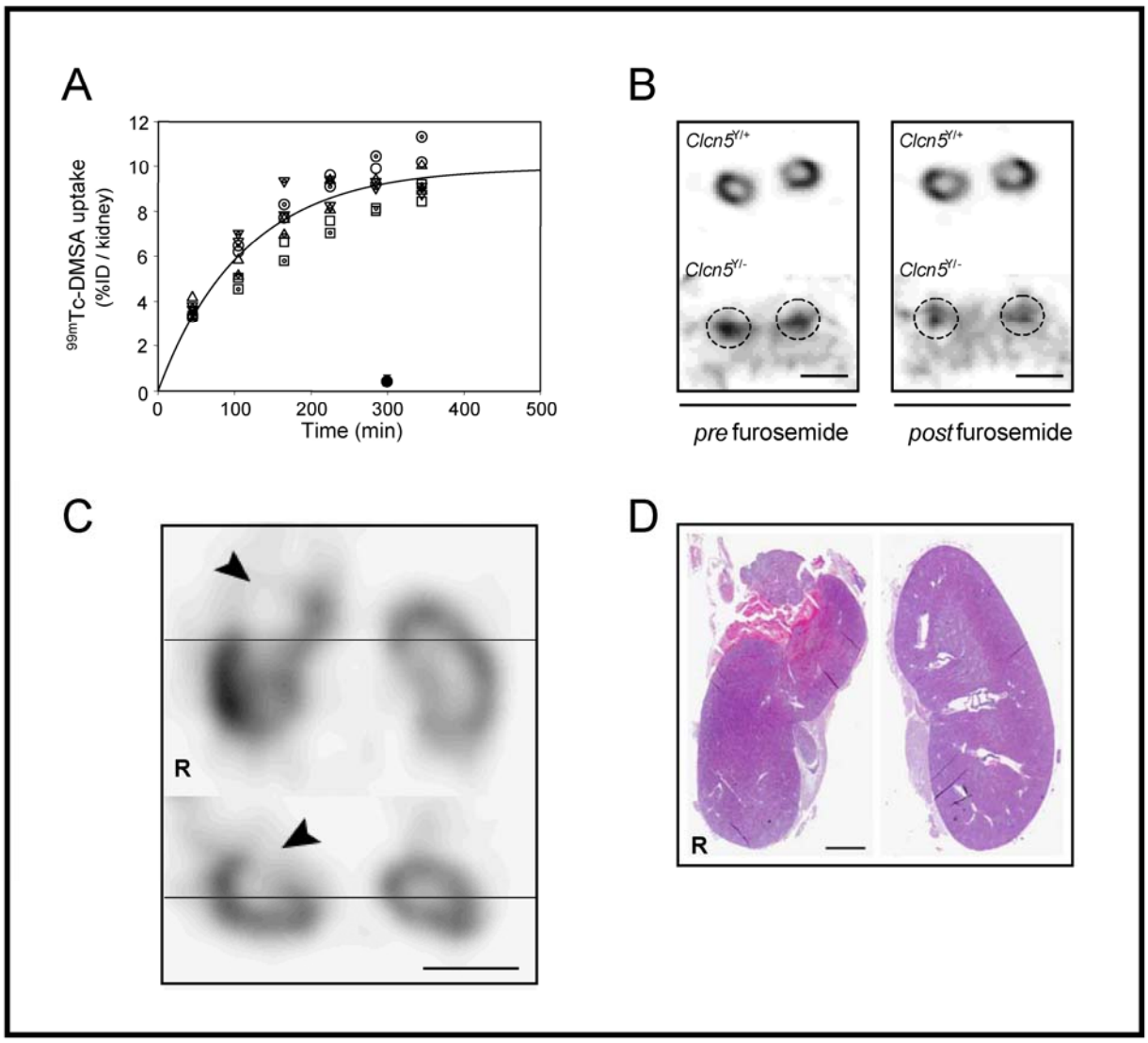

Figure 7.2. Uptake of ^{99m}Tc-DMSA in *Clcn5*$^{Y/-}$ *versus Clcn5*$^{Y/+}$ mice

Panel A. Repetitive static SPECT analysis of ^{99m}Tc-DMSA uptake in control mice (*n=8 kidneys from 4 mice*). The same symbol is used for one given animal, with empty and dotted symbols representing the left and right kidneys, respectively. The asymptotic curve was fitted on the mean uptake data, and shows a plateau phase from 6 hours postinjection. Renal uptake of ^{99m}Tc-DMSA is abolished in *Clcn5*$^{Y/-}$ mice (*n=8 kidneys from 4 mice*).

Panel B. Representative ^{99m}Tc-DMSA SPECT imaging of *Clcn5*$^{Y/+}$ and *Clcn5*$^{Y/-}$ kidneys (transverse slices at 6 hours postinjection) before and after furosemide administration (10 mg/kg BW). In *Clcn5*$^{Y/+}$ kidney, the tracer remains concentrated over the cortex area, even after furosemide injection. In contrast, ^{99m}Tc-DMSA signal is minimal in *Clcn5*$^{Y/-}$ mice, located in the pelvis, and rapidly cleared after furosemide injection. Dotted circles represent the cortical contours in *Clcn5*$^{Y/-}$ kidneys. Bar: 5 mm.

Panel C. ^{99m}Tc-DMSA SPECT image after experimental infarction of the upper right kidney (R). Coronal (upper panel) and transverse (lower panel) slices show no activity tracer in the infarcted area (arrowheads). Bar: 5 mm.

Panel D. Hematoxylin-eosine staining of kidneys corresponding to Panel C. The superior pole of the right kidney (R) is necrotic, whereas normal histology is observed elsewhere in the cortex. Bar: 2 mm.

7.3. Results

7.3.1. Renal uptake of ^{99m}Tc-DMSA in *Clcn5*$^{Y/+}$ *versus Clcn5*$^{Y/-}$ mice

The kinetics of ^{99m}Tc-DMSA renal uptake in control mice showed a progressive increase ($T_{1/2}$ ~75min) to a plateau level (Figure 7.2, panel A). At 6 hours postinjection, the activity uptake was close to the steady state, reaching 9.8 ± 0.4% of injected dose / kidney. Of note, SPECT quantification of uptake was previously shown to fit with measurements obtained by standard *ex vivo* counting (Walrand, 2005). Statistical calculations of the inter-assay coefficient of variation (CV, 5.6%) demonstrated a high reproducibility of this procedure. At steady state, the spatial resolution of ^{99m}Tc-DMSA SPECT imaging enabled a clear delineation of the radioactivity distributed over the functional renal cortex, whereas the medulla and the pelvis area (~1 mm) showed no detectable signal (Figure 7.2, panel C). When a focal kidney infarction was generated, SPECT imaging showed a lack of cortical accumulation of the tracer in the infarcted zone, in strict correlation with pathological examination (Figure 7.2, panel D).

The uptake of ^{99m}Tc-DMSA in *Clcn5*$^{Y/-}$ mice, investigated in identical conditions, was completely abolished (Table 7.1), with a small residual activity detected in the pelvis (Figure 7.2, panel B). Following furosemide injection, no significant changes were observed in controls, whereas most of the ^{99m}Tc-DMSA signal was cleared from *Clcn5*$^{Y/-}$ animals (Figure 7.2, panel B).

These results demonstrate that the spatial resolution obtained by SPECT imaging clearly delineates the radioactivity distributed over the functional renal cortex. In control mice, the kinetics of ^{99m}Tc-DMSA uptake in mouse kidney is similar to the asymptotic curve observed in man. Furthermore, the lack of cortical retention of ^{99m}Tc-DMSA clearly demonstrate a profound dysfunction of the basolateral uptake in *Clcn5*$^{Y/-}$ PT cells.

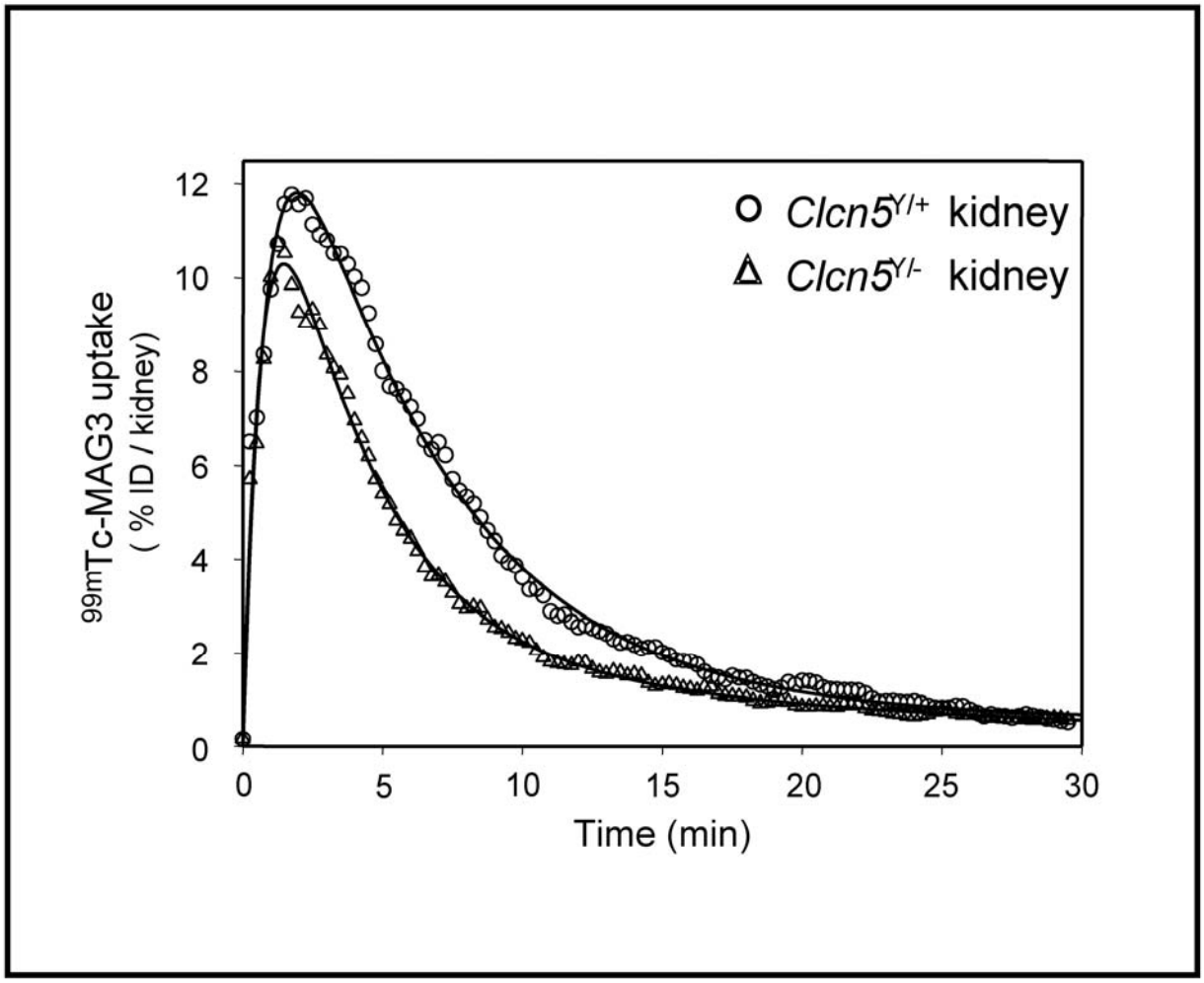

Figure 7.3. Secretion of ^{99m}Tc-MAG3 in *Clcn5*$^{Y/-}$ *versus Clcn5*$^{Y/+}$ mice

In both *Clcn5*$^{Y/-}$ *versus Clcn5*$^{Y/+}$ mice, dynamic SPECT shows a rapid ^{99m}Tc-MAG3 kidney uptake, followed by its secretion into the urine (*n=6 kidneys from 3 mice of each genotype*). The elimination of the tracer from the kidney is slightly faster in Clcn5$^{Y/-}$ mice than in controls. (% ID: % of injected dose)

7.3.2. Renal secretion of ^{99m}Tc-MAG3 in *Clcn5*$^{Y/+}$ *versus Clcn5*$^{Y/-}$ mice

The handling of ^{99m}Tc-MAG3 in control mice was characterized by a rapid extraction from blood ($T_{1/2IN}$, 0.4 ± 0.1 min), maximal renal accumulation between 90 and 120 seconds after iv injection (11.7 ± 1.6% of injected dose / kidney), and subsequent tubular secretion ($T_{1/2OUT}$, 4.7 ± 0.4 min) (Figure 7.3). Inter-assay variability in ^{99m}Tc-MAG3 secretion parameters was low (CV_{IN}, 12.2%; CV_{OUT}, 9.1%) in conscious mice. Conversely, dynamic studies performed on the same animals after ketamine-xylazine anaesthesia showed variable curves, with delayed clearance of ^{99m}Tc-MAG3 in anaesthetised mice. As a whole, the kinetic parameters of ^{99m}Tc-MAG3 handling were not significantly different between *Clcn5*$^{Y/-}$ and *Clcn5*$^{Y/+}$ mice (Table 7.1), except for a faster elimination in *Clcn5*$^{Y/-}$ mice (Figure 7.3). This most probably reflects the polyuria-polydypsia syndrome observed in such animals (Wang, 2000). These data demonstrate the feasibility of dynamic SPECT kidney imaging in conscious mice with a timeframe of 30 minutes. Importantly, comparative dynamic studies before and after anaesthesia showed a marked but variable effect of anaesthesia on ^{99m}Tc-MAG3 secretion and excretion. However the functional loss of ClC-5 was not associated with significant changes of ^{99m}Tc-MAG3 uptake and secretion.

7.3.3. Renal uptake of ^{123}I-β_2-microglobulin in *Clcn5*$^{Y/+}$ *versus Clcn5*$^{Y/-}$ mice

Dynamic SPECT quantification of apical ^{123}I-β_2-microglobulin uptake in control mice showed a rapid glomerular filtration followed by a progressive accumulation of ^{123}I-β_2-microglobulin in the kidney cortex, with maximal activity (6.4 ± 0.8% of injected dose / kidney) measured at 7 min postinjection (Figure 7.4). Efficient breakdown of ^{123}I-β_2-microglobulin in PT cells induced ^{123}I reflux to circulating blood and a subsequent decrease of renal activity. Indeed, biochemical analyses demonstrated that the ^{123}I present in *Clcn5*$^{Y/+}$ urine at 60 min postinjection was mostly free iodine (92.1 ± 2.5% of total urine activity). In strong contrast, *Clcn5*$^{Y/-}$ mice showed a severe defect in ^{123}I-β_2-microglobulin reabsorption (see Table 7.1), with

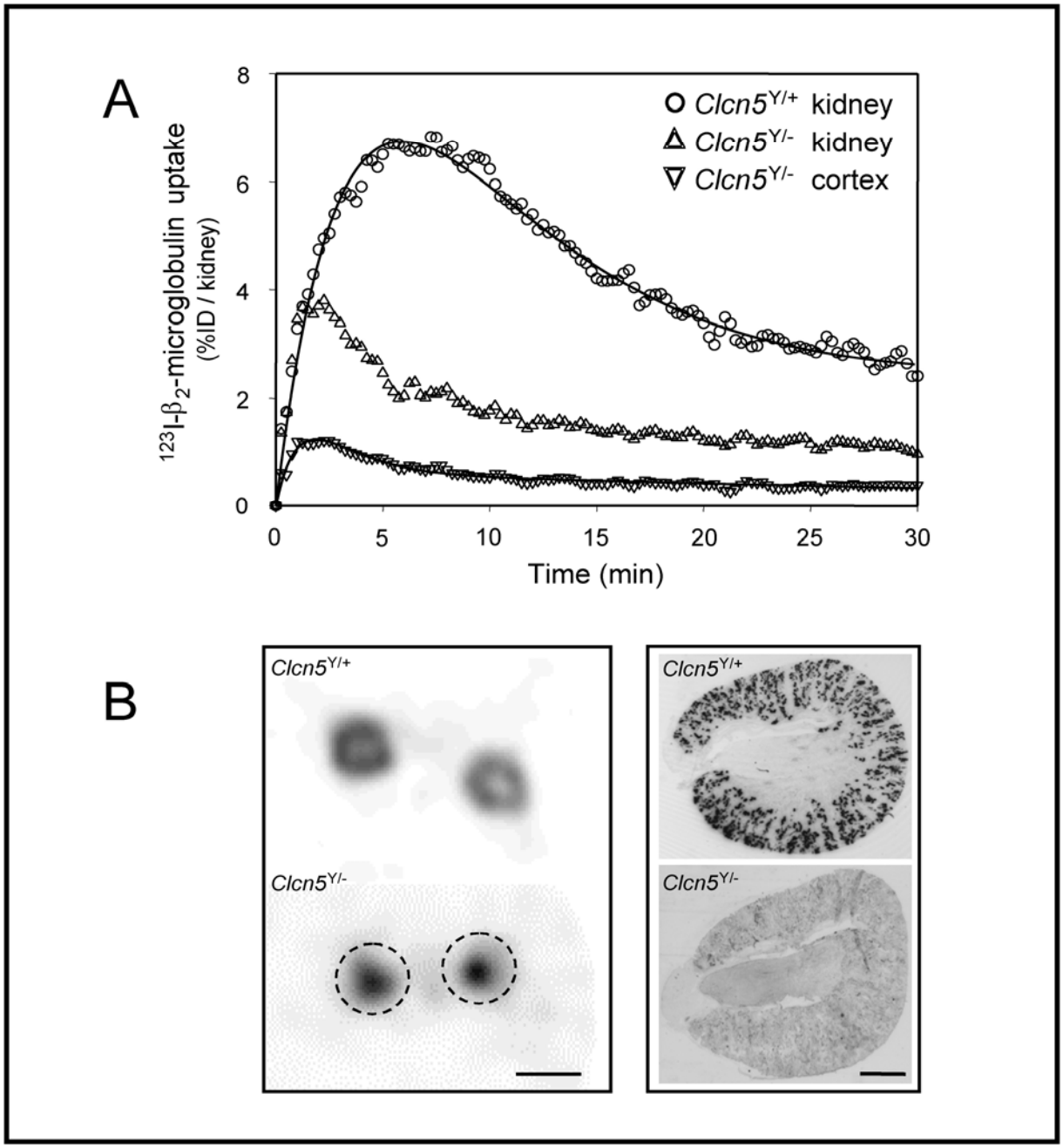

Figure 7.4. Uptake of ^{123}I-β$_2$-microglobulin in *Clcn5*$^{Y/-}$ *versus Clcn5*$^{Y/+}$ mice

Panel A. Dynamic SPECT analysis of ^{123}I-β$_2$-microglobulin uptake in *Clcn5*$^{Y/+}$ (O) and *Clcn5*$^{Y/-}$ (△) kidneys, and *Clcn5*$^{Y/-}$ cortex (▽). The curves show the average of 6 distinct kidneys in each group. In *Clcn5*$^{Y/+}$ mice, ^{123}I-β$_2$-microglobulin progressively accumulates in the cortex, with subsequent breakdown and release of free ^{123}I to the circulation. In *Clcn5*$^{Y/-}$ mice, the minimal ^{123}I-β$_2$-microglobulin uptake in the cortex can be distinguished from the strong signal detected in the pelvis region, which reflects the glomerular filtration and the urinary loss of the tracer.

Panel B. Representative distribution of β$_2$-microglobulin at 7 min postinjection in *Clcn5*$^{Y/+}$ and *Clcn5*$^{Y/-}$ kidney: *in vivo* SPECT imaging vs. autoradiography (transverse sections). In *Clcn5*$^{Y/+}$ kidney, ^{123}I-β$_2$-microglobulin is strictly located in the cortex area, with a segmental distribution including the PT. In strong contrast, most ^{123}I-β$_2$-microglobulin is located in the pelvis of the *Clcn5*$^{Y/-}$ mouse, and no significant signal can be detected in the cortex. Dotted circles in left panel represent the cortical contours in *Clcn5*$^{Y/-}$ kidney. Bars: 5 mm (left panel); 1 mm (right panel).

predominant urinary loss of intact ^{123}I-β_2-microglobulin (62.2 ± 4.2% of total urine activity) (Figure 7.4). Likewise, autoradiography analyses performed at 7 minutes postinjection of ^{125}I-β_2-microglobulin showed a strong signal in PT of control kidney, whereas no significant uptake of ^{125}I-β_2-microglobulin could be detected in *Clcn5*$^{Y/-}$ kidney (Figure 7.4, panel B). Both *in vivo* and *ex vivo* investigations of β_2-microglobulin uptake were performed on the same animals. Of note, the calculated glomerular filtration rate (~0.22 ± 0.02 ml/min) was similar in both *Clcn5*$^{Y/-}$ and control mice.

Based on 30-min dynamic SPECT acquisitions, these data, as a whole, established the first *in vivo* kinetic measurement of kidney receptor-mediated endocytosis in conscious mice. This further confirmed the major PT apical dysfunction caused by the functional loss of ClC-5 (Wang, 2000; Christensen, 2003).

Table 7.1. Summary of SPECT quantifications in *Clcn5*$^{Y/+}$ *versus Clcn5*$^{Y/-}$ mice

	***Clcn5*$^{Y/+}$**	***Clcn5*$^{Y/-}$**	***p* value**
^{99m}Tc-DMSA			
Uptake (% ID / kidney)	9.3 ± 0.5	0.4 ± 0.1	< 0.01
^{123}I-β_2-microglobulin			
T_{max} (min)	[6.75 ; 7.25]	[1.75 ; 3]	< 0.01
$U_{at\ 7min}$ (% ID / kidney)	6.4 ± 0.8	0.5 ± 0.2	< 0.01
^{99m}Tc-MAG3			
$T_{1/2\ IN}$ (min)	0.4 ± 0.1	0.4 ± 0.1	NS
$T_{1/2\ OUT}$ (min)	4.7 ± 0.5	4.2 ± 1.2	NS

Data are expressed as means ± SD. Non-paired Student t-test was used to compare *Clcn5*$^{Y/-}$ to *Clcn5*$^{Y/+}$ mice (% ID: % of injected dose).

7.3. Discussion

The data reported in this study demonstrate the feasibility and the benefits of both static and dynamic SPECT studies to investigate PT functions in conscious mice. The renal uptake of ^{99m}Tc-DMSA allows a fine resolution of the functional cortex. Dynamic ^{99m}Tc-MAG3 SPECT studies further investigate PT basolateral captation and apical secretion, whereas the handling of ^{123}I-β_2-microglobulin especially assesses apical receptor-mediated endocytosis in PT cells. Particularly, our SPECT studies suggest that the functional loss of ClC-5 causes a severe defect in both apical and basolateral PT functions, without alteration of the secretory pathway.

The renal uptake of ^{99m}Tc-DMSA in mice shows a progressive accumulation in kidney cortex, matching standard curves reported in man (Moretti, 1984). At the plateau phase (~6 hours postinjection), SPECT nephrography gives a millimetric resolution of the cortex apart from the medulla and the pelvis. Moreover, functional imaging by ^{99m}Tc-DMSA SPECT clearly identifies restricted kidney damage such as infarction. Such characterization of ^{99m}Tc-DMSA handling in conscious mice shows a low inter-assay variability, and supports the usefulness of SPECT for repetitive and long-term biodistribution studies, as well as intervention studies in the same animals. Likewise, dynamic ^{99m}Tc-MAG3 SPECT demonstrates the feasibility of continuous monitoring of drug handling in conscious mice from the time of intravenous injection. Clearance studies in mice are thus far performed by different approaches at various experimental levels, such as repetitive blood and urine sampling, kidney perfusion technique, or isolated functionally intact tubules (Trejtnar, 2002). Although providing useful information about renal physiology, these techniques are complex and time-consuming, and may be biased by the procedure itself, such as the need for anaesthesia (Rao, 2000). Our findings emphasize the versatile adverse impact of ketamine/xylazine anaesthesia on baseline renal function, urging caution in interpreting data from anaesthetized mice (Yang, 1999). SPECT imaging in conscious mice offers thus an attractive alternative for such *in vivo* functional investigations. As an example, the

dynamic SPECT quantification of β_2-microglobulin renal uptake establishes the first *in vivo* time-course of PT receptor-mediated endocytosis in conscious mice. Moreover, mathematical analyses of ^{123}I-β_2-microglobulin biodistribution enable to precisely determine *in vivo* the glomerular filtration rate in mouse (Qi, 2004). The radiolabeled LMW protein is largely filtered by the glomeruli, avidly captured in the renal cortex, and rapidly degraded with subsequent release of the radiotracer and residual peptide/amino acids to peri-tubular capillaries (Birn, 2006). Free iodine is then filtered by the glomeruli and lost in urine, as demonstrated here in control mice.

To further assess the usefulness of SPECT imaging in the evaluation of PT function, SPECT analyses were performed comparatively on control and *Clcn5* KO mice, which represent a well-defined model of severe PT dysfunction, with constant LMW proteinuria (Wang, 2000). Recently, the functional loss of ClC-5 was associated with a major and selective loss of the multiligand receptors, megalin and cubilin, at the brush border, reflecting a generalized trafficking defect in PT cells (Christensen, 2003). For the first time, our study aims to non-invasively investigate PT activities in this mouse model of inherited PT dysfunction in order to establish correlates between *ex vivo* findings and *in vivo* behaviour. This may have important implications for the evaluation of drugs or regimens aimed to prevent PT deficiency in conditions where tubular injury is anticipated (e.g. chemotherapy). First, the dramatic defect in PT apical receptor-mediated endocytosis previously reported in *Clcn5*$^{Y/-}$ mice by *ex vivo* counting (Christensen, 2003), is confirmed by *in vivo* SPECT quantification of ^{123}I-β_2-microglobulin uptake. Dynamic studies demonstrate that the glomerular filtration rate of ^{123}I-β_2-microglobulin is similar in both *Clcn5*$^{Y/+}$ and *Clcn5*$^{Y/-}$ mice, whereas its tubular reabsorption occurring mostly in S1-S2 PT segments is significantly impaired in *Clcn5*$^{Y/-}$ mice, with subsequent loss into the urine as the native labeled protein. Similarly to β_2-microglobulin clearance, the renal handling of ^{99m}Tc-DMSA has been regarded as an indicator of PT function in man and animal models (Van luijk, 1984; Anninga, 1994). For example, treatment of rats with Na-maleate induces a typical

renal Fanconi syndrome, with LMW proteinuria, glucosuria, phosphaturia, and marked reduction of ^{99m}Tc-DMSA uptake (Provoost, 1985). In our study, SPECT quantification of ^{99m}Tc-DMSA renal capture shows that the genetic inactivation of *Clcn5* is associated with the lack of accumulation of the tracer in the renal cortex, suggesting a severe defect in PT basolateral function. It is likely that the residual signal detected in the pelvis area of *Clcn5*$^{Y/-}$ mice – and cleared following furosemide injection – represents a small glomerular filtration of ^{99m}Tc-DMSA, an accessory pathway of renal handling described with this tracer (Müller-Suur, 1995). Transport of ^{99m}Tc-DMSA in PT cells is mediated by the co-transporter NaC3 (SLC13A3), which couples the downhill movement of Na^+ to the concentrative uptake of succinate (Markovich, 2004). Recent *in vitro* studies have shown that the co-expression of non-conducting fragments of ClC-5 with NaC transporter alters its translation and/or trafficking in *Xenopus* oocytes, resulting in decreased expression at the surface membrane (Mo, 2004). The severe deficit in both apical and basolateral uptake reported here in *Clcn5*$^{Y/-}$ mice further supports a generalized intracellular trafficking in PT cells caused by the functional loss of ClC-5 (Piwon, 2000; Christensen, 2003).

Renal scintigraphy with the analogue of p-aminohippurate, ^{99m}Tc-MAG3, can provide excellent image quality, even in patients with severely decreased renal function (Itoh, 2001). Our results demonstrate that the PT dysfunction caused by the functional loss of ClC-5 is not associated with a defect in ^{99m}Tc-MAG3 renal handling. The strong contrast between the complete loss of ^{99m}Tc-DMSA uptake and the preserved ^{99m}Tc-MAG3 secretion in *Clcn5* KO kidney suggests that these two pathways are not functionally dependent on each other (Shikano, 2004). These data further support distribution studies showing the absence of co-localization of NaC3 and OAT1 in S1-S2 PT segments (Burckhardt, 2003). Additional SPECT studies using mouse models invalidated for distinct organic anion transporters may help establish the metabolic pathways responsible for the handling of these particular radiotracers, as well as those for other drugs and metabolites.

In conclusion, SPECT analysis represents a novel approach to characterize *in vivo* the renal function in conscious mice. Acute and/or repetitive biodistribution studies allow to define the pharmacokinetic parameters of distinct radiolabeled compounds, as a prerequisite for further human applications. It should be kept in mind that such methodology will not substitute the sophisticated armamentarium that is currently available for function analyses. In particular, spatial resolution of SPECT remains limited to the millimeter range and cannot compete with classical microscopic techniques, including all their possible refinements, nor with the more recently evolving live-microscopy methods. Although most pharmacokinetic studies can be performed with a temporal resolution of 5-10 seconds, this may not be sufficient to explore almost instantaneous functions such as organ activation or cell trafficking. Nevertheless, the development of creative approaches like *in vivo* SPECT analysis using devices dedicated to small animal imaging will permit further functional investigations of transgenic mouse strains, and finally help better understand renal physiology or functions in general.

Acknowledgements

The authors thank M-F. van den Hove for helpful discussion, and V. Beaujean, Y. Cnops, G. Dom, M. Helbo, T. Lac, A. Saliez and P. Van Der Smissen for excellent technical assistance. The *Clcn5*$^{Y/-}$ mice were kindly provided by W.B. Guggino and S.E. Guggino (Dept. of Physiology, Johns Hopkins University Medical School, Baltimore, MD).

CHAPTER VIII. DISCUSSION AND PERSPECTIVES

The first part of our project investigates the expression, segmental distribution, and maturation of the Cl^- transporter ClC-5 and the multisubunit complex V-ATPase in the developing kidney. These studies indicate that the segmental co-distribution of ClC-5 and the V-ATPase in PT cells is essentially acquired at E15.5 in mice and during the second trimester of gestation in man (**Chapter II**). These results complete previous observations that the establishment of the brush border and endocytic compartments in PT cells coincides with the onset of glomerular filtration (Biemesderfer, 1992). The ability of PT cells to reabsorb filtered LMW proteins *in utero* is further suggested by the progressive decrease of the [LMW proteins] in the AF during late gestation (Cagdas, 2000). Accordingly, the disruption of PT endocytic pathway observed in congenital PT disorders like cystinosis, Dent's disease, OCRL syndrome, and Imerslund–Gräsbeck disease, may result in LMW proteinuria detected during early infancy.

The developmental pattern of ClC-5 is characterized by a complex maturation of ClC-5 isoforms, which may result from alternative splicing variants and/or post-translational modifications like N-glycosylation and phosphorylation. Recent studies have identified at least 4 different in-frame start sites for the transcription of *CLCN5* gene, with tissue-specific expression of the variants (Ludwig, 2003). By analogy, two transcripts for *CLCN3* have been identified in man developing lung, with a differential expression in fœtal *versus* mature tissues (Lamb, 2001). The ontogeny and segmental distribution of ClC-5 variants is also likely to differ in the developing kidney. The

hypothesis is that the earliest and transient appearance of ClC-5 in the branching UB may correspond to fœtal isoforms possibly involved in fluid secretion and lumen formation, as previously suggested by the detection of the aquaporin-2 and the Cl^- channel CFTR at this location (Devuyst, 1996a-b). Conversely, the progressive increase in mature ClC-5 isoforms that parallels the induction of the V-ATPase during late nephrogenesis may reflect PT maturation. Northern blotting and *in situ* hybridization analyses are needed to clarify the respective roles of ClC-5 variants during kidney organogenesis. In addition, post-translational modifications such as N-glycosylation may account for the variability in the apparent molecular mass of ClC-5 observed in foetal vs. adult samples, as well as in different tissues. As an example, deglycosylation studies with N-glycosidase F have recently demonstrated that ClC-5 bears more glycan chains in the thyroid gland than in the kidney (van den Hove, 2006). Several functional roles for N-glycans have been reported including cell adhesion, signal transduction, and protein sorting (Gut, 1998). Further investigations on the complex maturation of ClC-5 during development and in the different tissues may help precise its precise role in the different cellular compartments, namely the endosomes and the plasma membrane. In any case, the absence of overt developmental abnormalities in *Clcn5* KO mice suggests that ClC-5 is not required for kidney development. However, investigations of ClC-5-deficient fœtuses may help characterize PT receptor-mediated endocytic pathway *in utero*, and further identify early compensatory mechanisms in PT dysfunction.

In addition to PT cells, ClC-5 and the V-ATPase are co-detected in the apical area of α-type IC from E15.5 in mouse nephrogenesis and at the end of the second trimester in human gestation (**Chapter II**). The structure of the V-ATPase located in the plasma membrane of mature IC differs from the ubiquitous complex by the presence of IC-specific subunit isoforms. Our studies demonstrate a strong contrast between the developmental patterns of ubiquitous *versus* IC-specific V-ATPase subunits during kidney organogenesis (**Chapter III**). The early expression of ubiquitous subunits of the V-ATPase in the developing kidney, with a preferential distribution in endosomes, confirms its essential role for mouse development, as well as its participation in PT maturation. Conversely, the expression of IC-specific V-ATPase isoforms appears induced by the forkhead trasncription factor Foxi1 in late

nephrogenesis, in parallel with other IC markers. These results corroborate the model proposed by Blomqvist et al. for IC differentiation from a common epithelial precursor along the CD (Blomqvist, 2004), and further support that maturation of acid-base secretory functions in this nephron segment occurs around birth (Bonnici, 2004). Nevertheless, the developmental pathway by which Foxi1 determines the identity of the IC may be more complex. For instance, Foxi1 may interact positively or negatively with other transcription factors (e.g. the paired-box PAX family) implicated in cell specification, as reported for other forkhead members (Clifton-Bligh, 1998). Furthermore, its absence could also be responsible for principal cell differentiation. Thus, the identification of the role of Foxi1 in cell specification along the CD and the possible association of *FOXI1* mutations with hereditary distal RTA represent an exciting new chapter in the field of nephrogenesis and congenital tubular disorders.

The typical developmental pattern of IC-specific subunit isoforms of the V-ATPase represents a useful tool to further characterize any newly discovered subunit. Our investigations of the novel V0 d2 subunit reveal a progressive induction during late nephrogenesis in parallel with the IC-specific a4 and B1, which differs from the ontogeny of the ubiquitously expressed d1 and E1 subunits (**Chapter IV**). The distribution of d2 appears restricted to the V-ATPase located in the plasma membrane of IC and osteoclasts. Of note, these cells are of different embryological origin, and the role of the transcription factor Foxi1 in bone development and/or remodeling remains unknown. The murine d2 isoform can be co-immunoprecipitated from renal tissue with the B1 but not the ubiquitously expressed B2 subunit, which further supports that d2 is only present in the specialized IC-specific V-ATPase complex (Sun-Wada, 2003). The specificity of d2 distribution further proposes *ATP6V0D2* gene as a candidate gene for inherited distal RTA and osteopetrosis, as observed in Guibaud-Vainsel syndrome (marble brain disease, OMIM +259730) caused by mutations in *CA2*. In conclusion, our comparative ontogeny of the Cl^- transporter ClC-5 and the multisubunit complex V-ATPase provides new insight into the complex maturation of PT cells and IC, and helps decipher the pathophysiology of early phenotypic variants of Dent's disease and inherited distal RTA.

* * *

The spectrum of CF-related disorders has broadened considerably over the last decade, and includes many milder cases, which are associated with a longer survival and a potential for developing complications in multiple organs. Our investigations support that the functional loss of CFTR is associated with impaired receptor-mediated endocytosis in renal PT cells, leading to LMW proteinuria in both mouse and man (**Chapter V**). The segmental and subcellular distribution of CFTR along the nephron includes predominantly (but not exclusively) S3 PT cells, in which it co-localizes with ClC-5 and the V-ATPase in apical endosomes. Previous studies support a role for CFTR in the acidification of intracellular organelles along the endosomal and biosynthetic pathways, with a possible involvement in intracellular trafficking (Bradbury, 1999). Particularly, the defect in acidification of the *trans*-Golgi network caused by the functional loss of CFTR may impair post-translational maturation (e.g. sialylation, glycosylation) and targeting of secreted proteins. Our results show a decrease of cubilin expression in the S3 PT segment of *Cftr*$^{-/-}$ mice without significant changes observed at the mRNA level, suggesting an enhanced degradation and/or a trafficking defect of cubilin-AMN complexes in PT cells. The apical sorting of this complex is indeed dependent on the correct glycosylation of cubilin extracellular domains (Coudroy, 2005), and further deglycosylation studies on CF vs. control kidneys may help precise the role of CFTR in cubam maturation. These data give explanation for the reduced vitamin B12 absorption, as well as the enhanced renal clearance of aminoglycosides observed in CF patients. However, the renal phenotype observed in *Cftr*$^{-/-}$ mice and CF patients remains minor in comparison to *Clcn5*$^{Y/-}$ mice and patients with Dent's disease. The magnitude in the endocytic defect caused by CFTR vs. ClC-5 loss likely reflects the differences in segmental distribution and functional regulation between these Cl^- transporters. In addition, tissue-specific protective mechanisms, such as the occurrence of functional CFTR splice variants and/or alternative pathways for Cl^- conductance, may account for the discrete nature of renal manifestations in CF.

Our immunoblotting studies show that the electrophoretic mobility of N-glycosylated CFTR is different in kidney vs. lung, although CFTR core protein is

located at ~150kDa in both tissue samples. Since the stability and function of CFTR in the plasma membrane is dependent on its glycosylation maturation, the distinctive CFTR processing in kidney may reflect differential trafficking/targeting within tubular cells. Particularly, the mutant ΔF508-CFTR shows defective processing and maturation to the fully glycosylated form, resulting in its retention in the ER by molecular chaperones and degradation via the ubiquitin-proteasome pathway. However, ΔF508-CFTR can function as cAMP-regulated Cl^- channel, both in the ER and at the plasma membrane under permissive conditions. The severity in ΔF508-CFTR processing defect has been shown to be tissue-specific, suggesting that the variable CF phenotype in different organs reflects the heterogeneity of residual CFTR expression. Previous studies have demonstrated the presence of cAMP-dependent Cl^- permeability in intestine and gallbladder of the $Cftr^{\Delta F/\Delta F}$ mice used in our studies. Our investigations further support a large individual variability in the residual expression of ΔF508-CFTR protein in $Cftr^{\Delta F/\Delta F}$ kidney. These observations may account for the variable phenotype noted on $Cftr^{\Delta F/\Delta F}$ mice that are characterized by either unchanged or increased urinary excretion of LMW proteins. Conversely, all CF patients examined in our series harbour at least one ΔF508 mutation (as expected from the prevalence of this mutation in our Caucasian population), and show a significant LMW proteinuria vs. age- and gender-matched controls. Further investigations may help unravel the differences in CFTR processing in rodent vs. human kidney, as well as the functional consequences of the ΔF508 mutation. In addition, the characterization of the renal phenotype in a series of CF patients harbouring mutations of different type and severity (e.g. Type I mutations particularly present in the Ashkenazi Jewish population), as well as in "control patients" with similar disease like chronic bronchitis, may substantiate our findings, and eventually establish novel genotype-phenotype correlations.

As a whole, the preferential distribution of CFTR in the straight part of the PT supports a segmental differentiation of mouse PT. By analogy to other species, this segment may be particularly involved in the secretion of metabolites and drugs (Wright, 2004). In the near future, we plan to perform comparative clearance studies in

Cftr$^{-/-}$, *Cftr*$^{\Delta F/\Delta F}$ and control mice by SPECT (see **Chapter VII**) to address the putative role of CFTR along the secretory activity of PT cells. The direct or indirect interactions between CFTR and organic anion transporters located in PT brush border may result in enhanced tubular clearance of certain drugs, as indeed observed in patients with CF (Woodland, 1998). In any case, the functional loss of CFTR is associated with a moderate but significant defect in LMW protein handling in mouse and man, supporting a role of CFTR within intracellular organelles along the endocytic pathway in renal PT cells. This renal phenotype, which can trigger interstitial renal disease, must be integrated in the multi-systemic complications increasingly observed in CF patients.

* * *

The metabolic outcomes of the renal Fanconi syndrome at the cellular level remain unknown, although recent studies have suggested increased sollicitation of cell oxidative defences in acquired and inherited PT dysfunction. Our investigations in both man and mouse show that the functional loss of ClC-5 in Dent's disease is associated with higher cell turnover and increased cellular response to oxidant damage, as well as the induction of CAIII expression (**Chapter VI**). The upregulation of CAIII in *Clcn5*$^{Y/-}$ mice is restricted to the kidney, with no changes observed in the other CAIII-expressing organs. Moreover, a significant increase of renal CAIII expression is also observed in megalin-deficient mice, as well as in PT cells exposed to H_2O_2.

Type III CA belongs to the family of zinc metallo-enzymes that reversibly hydrate CO_2, of which at least 15 different isoforms have been identified in mammals. Type III CA is abundantly expressed in the cytosol of skeletal muscle cells, adipocytes and hepatocytes. In contrast to most CA isozymes, two unique amino acids in its catalytic site confer resistance to sulfonamide inhibitors and result in low CO_2 hydration ability. In addition, CAIII exhibits two reactive sulfhydryl groups that are rapidly S-glutathiolated following exposure to oxidative conditions. Recent *in vitro* studies proposed that CAIII acts as oxyradical scavenger and protects cells from H_2O_2-

induced apoptosis. Moreover, structural analyses suggest that CAIII has evolved into a percarbonic acid anhydrase, which would mediate $H_2O_2 + CO_2 \leftrightarrow H_2CO_4$. Our observations support that CAIII isozyme participates in the common cellular response against oxidative damage in case of PT dysfunction. These findings will be soon investigated in distinct *in vitro* models of PT cells invalidated for ClC-5 (siRNA) in order to decipher the role of CAIII induction observed in Dent's disease. Moreover, we are currently characterizing a CAIII-deficient mouse model recently engineered by Kim et al. (Kim, 2004). This *in vivo* model will help us define the role of CAIII in baseline kidney function and in acquired renal Fanconi syndrome (e.g. cadmium-induced nephropathy). Finally, recent observations indicate that the abundance of CAIII urinary excretion may reflect the severity of PT dysfunction in man and mouse, suggesting CAIII as a potential novel biomarker of renal Fanconi syndrome. This will be further evaluated by quantification of urine [CAIII] in patients suffering from various acquired or toxic kidney diseases.

During embryogenesis, CAIII is regarded as an early mesodermal marker, with a distribution including the myotomes, the notochord, and the developing adipocytes. Since nephrogenesis involves reciprocal induction between mesodermal structures, namely the mesonephric UB and the metanephric mesenchyme, one could speculate that CAIII also participates in kidney development. Our preliminary results (immunoblotting and real-time RT-PCR analyses) show an early and strong induction (from E13.5 to E15.5) of CAIII, followed by a rapid decrease of its expression throughout nephrogenesis. Immunostaining detects CAIII in stromal cells surrounding differentiating UB, as early as E13.5. From E15.5, CAIII-positive cells are located around pelvis and developing ureter, and can be identified as smooth muscle cells. Although no specific signal is observed in any stage of nephron differentiation, CAIII is detected after birth in some scattered cells of the PT, like in adult kidney. These observations prompted us to investigate CAIII expression in dysplastic kidney samples. Renal dysplasia refers to altered metanephric differentiation likely due to intra-uterine urinary obstruction or insufficient fœtal urine production. The histopathology of renal dysplasia includes islands of hyaline cartilage and poorly

branched primitive ducts surrounded by stromal/mesenchymal-type cells. Preliminary data indicate that CAIII is present in some cells of these fibromuscular collars. These observations provide new insights into the differentiation and fate of renal stromal cells, as well as into the ureterogenesis. Further investigations of kidney development in CAIII-deficient mice, as well as the characterization of CAIII distribution in human dysplastic kidneys and in animal models of *in utero* urinary obstruction, may help decipher the contribution of the metanephric stroma in the pathophysiology of renal dysplasia.

Thus the identification of CAIII in the developing and mature kidney has opened a new field of investigations in the pathophysiology of distinct human diseases like renal dysplasia and renal Fanconi syndrome, which may lead to direct clinical applications.

* * *

The development of creative approaches to investigate both anatomy and function of small laboratory animals has been stimulated by the increasing availability of transgenic mouse models of gene deletion and human disease. Although the literature is abundant on *in vitro* studies performed on mouse samples, there is a relative paucity of *in vivo* functional studies in mice, in part due to the technical difficulties associated with their small size and the lack of detailed information about anaesthesia influence and normal physiological parameters (Rao, 2000). Therefore, the development of *in vivo* imaging techniques, like small-animal PET or SPECT, represents an attractive alternative for structural and functional studies in mice. Moreover these techniques may circumvent the complexity of *ex vivo* approaches and avoid animal sacrifice, which represents *per se* a considerable improvement from an ethical point of view.

In the last part of our project, we use the well-defined *Clcn5* KO mouse model of PT dysfunction to demonstrate the feasibility and benefits of SPECT imaging to explore PT functions in conscious mice (**Chapter VII**). Our *in vivo* SPECT studies

first confirm the severe deficit in PT apical receptor-mediated endocytosis previously reported in *Clcn5*$^{Y/-}$ mice by standard *ex vivo* procedures (Christensen, 2003). In addition, we show that the functional loss of ClC-5 is associated with defective PT basolateral transport, without alteration of the secretory pathway. Importantly, our data also demonstrate the unpredictable adverse impact of ketamine/xylazine anaesthesia on baseline renal function, urging caution in interpreting data from anaesthetized mice.

Numerous applications can be extrapolated from these experiments. For example, the feasibility of repetitive biodistribution studies in the same animal will allow comparisons of distinct compound handling, without the pitfalls of inter-individual variance. Likewise, quantitative biodistribution analyses starting at the time of drug injection will determine the pharmacokinetic parameters of new drugs in rodents before any human applications. Intervention studies will enable to non-invasively evaluate tissue responses to different acute or prolonged experimental conditions, such as drug administration at different dosages. Although SPECT spatial resolution will never compete with classical microscopic techniques, the development of such devices dedicated to small animal imaging will permit further functional investigations of transgenic mouse strains, and finally help better understand *in vivo* renal physiology or functions in general.

* * *

PERSONAL CONTRIBUTIONS

Original articles

- **Jouret F**, Igarashi T, Gofflot F, Wilson PD, Karet FE, Thakker RV, Devuyst O: Comparative ontogeny, processing, and segmental distribution of the renal chloride channel, ClC-5. *Kidney Int* 2004, 65: 198-208

- **Jouret F,** Debaix H, Devuyst O: A catalog of gene expression in the developing kidney. *Kidney Int* 2004, 66: 867-8

- Smith AN, **Jouret F**, Bord S, Borthwick KJ, Al-Lamki RS, Wagner CA, Ireland DC, Cormier-Daire V, Frattini A, Villa A, Kornak U, Devuyst O, Karet FE: Vacuolar H^+-ATPase d2 subunit: molecular characterization, developmental regulation, and localization to specialized proton pumps in kidney and bone. *J Am Soc Nephrol* 2005, 16: 1245-56

- **Jouret F**, Auzanneau C, Debaix H, Wada GH, Pretto C, Marbaix E, Karet FE, Courtoy PJ, Devuyst O: Ubiquitous and kidney-specific subunits of vacuolar H^+-ATPase are differentially expressed during nephrogenesis. *J Am Soc Nephrol* 2005, 16: 3235-46

- van den Hove MF, Croizet-Berger K, **Jouret F**, Guggino SE, Guggino WB, Devuyst O, Courtoy PJ: The loss of the chloride channel, ClC-5, delays apical iodide efflux and induces an euthyroid goiter in the mouse thyroid gland. *Endocrinology* 2006, 147: 1287-96

- Sacré A, **Jouret F**, Manicourt D, Devuyst O: Topiramate induces Type 3 renal tubular acidosis by inhibiting renal carbonic anhydrase. *Nephrol Dial Transplant* 2006, in press

Review articles

- Devuyst O, **Jouret F**, Auzanneau C, Courtoy PJ: Chloride channels and endocytosis: new insights from Dent's disease and ClC-5 knockout mice. *Nephron Physiol*. 2005, 99: 69-73

- **Jouret F**, Courtoy PJ, Devuyst O: Lithiase rénale et tubulopathie complexe : le paradigme de la maladie de Dent. In: *Actualités Néphrologiques de l'Hôpital Necker 2006*, Flammarion Médecine-Sciences, Paris, 2006, pp105-17

Abstracts and presentations at international meetings

- **Jouret F**, Igarashi T, Wilson PD, Jentsch TJ, Thakker RV, Courtoy PJ, Devuyst O: Ontogeny, processing, and segmental distribution of the renal chloride channel ClC-5. *J Am Soc Nephrol* 12: 33A, 2001 (*Poster*, The American Society of Nephrology, San Francisco, CA, 2001)

- **Jouret F**, Wilson PD, Thakker RJ, Devuyst O: Ontogeny, processing, and segmental distribution of the renal chloride channel ClC-5. *Nephrol Dial Transplant*, A3 (W21): 555, 2003 (*Oral Communication*, World Congress of Nephrology, Berlin, 2003)

- **Jouret F**, Debaix H, Karet FE, Devuyst O: Comparative ontogeny of the chloride channel ClC-5 and the vacuolar H^+-ATPase during nephrogenesis. *J Am Soc Nephrol* 14: 312A, 2003 (*Poster*, The American Society of Nephrology, San Diego, CA, 2003)

- Devuyst O, **Jouret F**, Dom G, Guggino WB, Cassiman J-J, De Jonge HR and Courtoy PJ: Low-molecular-weight protein handling is largely preserved in cystic fibrosis kidney. *J Am Soc Nephrol* 14: 319A, 2003 (*Poster*, The American Society of Nephrology, San Diego, 2003)

- **Jouret F**, Auzanneau C, Smith AN, Courtoy PJ, Karet FE, Devuyst O: Ubiquitous and kidney-specific subunits of the vacuolar H^+-ATPase are differentially expressed during nephrogenesis. *J Am Soc Nephrol* 15: 71A, 2004 (*Poster*, The American Society of Nephrology, St Louis, MO, 2004)

- **Jouret F**, Gailly Ph, Christensen EI, Devuyst O: Type III carbonic anhydrase, a mesodermal marker, plays a differential role during nephrogenesis and in mature Kidney. *J Am Soc Nephrol* 15: 414A, 2004 (*Poster*, The American Society of Nephrology, St Louis, MO, 2004)

- **Jouret F**, Gailly Ph, Cosyns J-P, Scheinman SJ, Christensen EI, Gubler M-C, Devuyst O: La maladie de dent révèle la présence de l'anhydrase carbonique de type III dans le rein : implications dans la dysfonction tubulaire proximale et durant la néphrogenèse. (*Oral Communication*, Confrontations anatomo-cliniques de Tenon, Paris, 2005)

- **Jouret F**, Dom G, Guggino WB, Cassiman J-J, De Jonge HR, Courtoy PJ, Devuyst O: Cystic fibrosis is associated with a defect in low-molecular-weight protein handling in the kidney. *Nephrol Dial Transplant*, 20 (S5): v197, 2005 (*Oral Communication*, The European Renal Association – European Dialysis Transplantation Association, Istanbul, 2005)

- **Jouret F**, Auzanneau C, Smith AN, Courtoy PJ, Karet FE, Devuyst O: Ubiquitous and kidney-specific subunits of the vacuolar H^+-ATPase are differentially expressed during nephrogenesis. *Nephrol Dial Transplant*, 20 (S5): v22, 2005 (*Poster*, The ERA-EDTA congress, Istanbul, 2005)

- **Jouret F**, Gailly Ph, Willnow TE, Scheinman SJ, Guggino WB, Christensen EI, Devuyst O: Role of Type III carbonic anhydrase in proximal tubule function: lessons from Dent's disease and C*lcn5* knockout mouse. *J Am Soc Nephrol* 16: 62A, 2005 (*Oral Communication*, The American Society of Nephrology, Philadelphia, PA, 2005)

REFERENCES

Accardi A, Miller C: Secondary active transport mediated by a prokaryotic homologue of ClC Cl^- channels. *Nature* 2004, 427: 803-7

Adams DS, Robinson KR, Fukumoto T, Yuan S, Albertson RC, Yelick P, Kuo L, McSweeney M, Levin M: Early, H+-V-ATPase-dependent proton flux is necessary for consistent left-right patterning of non-mammalian vertebrates. *Development* 2006, 133: 1657-71

Aijaz S, Balda MS, Matter K: Tight junctions: molecular architecture and function. *Int Rev Cytol* 2006, 248: 261-98

Al-Awqati Q: Plasticity in epithelial polarity of renal intercalated cells: targeting of the H^+-ATPase and band 3. *Am J Physiol* 1996, 270: C1571-80

Alper SL, Natale J, Gluck S, Lodish HF, Brown D: Subtypes of intercalated cells in rat kidney collecting duct defined by antibodies against erythroid band 3 and renal vacuolar H+-ATPase. *Proc Natl Acad Sci U S A* 1989, 86: 5429-33

Altschul SF, Gish W, Miller W, Myers EW, Lipman DJ: Basic local alignment search tool. *J Mol Biol* 1990, 215: 403-10

Aminoff M, Carter JE, Chadwick RB, Johnson C, Grasbeck R, Abdelaal MA, Broch H, Jenner LB, Verroust PJ, Moestrup SK, de la Chapelle A, Krahe R: Mutations in CUBN, encoding the intrinsic factor-vitamin B12 receptor, cubilin, cause hereditary megaloblastic anaemia 1. *Nat Genet* 1999, 21: 309-13

Anninga JK, Valdes Olmos RA, de Kraker J, van Tinteren H, Hoefnagel CA, van Royen EA: Technetium-99m dimercaptosuccinic acid and ifosfamide tubular dysfunction in children with cancer. *Eur J Nucl Med* 1994, 21: 658-62

Azzazy HM, Cummings PJ, Ambrozak DR, Christenson RH: Production and characterization of monoclonal antibodies to human carbonic anhydrase III. Hybridoma. 1998, 17: 553-8

Barasch J, Kiss B, Prince A, Saiman L, Gruenert D, al-Awqati Q: Defective acidification of intracellular organelles in cystic fibrosis. *Nature* 1991, 352: 70-3

Bard J: The metanephros. In: *The Kidney, from normal development to congenital disease*, edited by Vize PD, Woolf AS and Bard JBL. Academic Press (Elsevier), Orlando, 2003, pp139-43

Barriere H, Tauc M, Poujeol P: Use of knock-out mouse models for the study of renal ion channels. *J Membr Biol* 2004, 198: 113-24

Bastani B: Immunocytochemical localization of the vacuolar H^+-ATPase pump in the kidney. *Histol Histopathol* 1997, 12: 769-79

Bateman A: The structure of a domain common to archaebacteria and the homocystinuria disease protein. *Trends Biochem Sci* 1997, 22: 12-3

Baum M, Biemesderfer D, Gentry D, Aronson PS: Ontogeny of rabbit renal cortical NHE3 and NHE1: effect of glucocorticoids. *Am J Physiol* 1995, 268: F815-20

Baum M, Quigley R, Satlin L: Maturational changes in renal tubular transport. *Curr Opin Nephrol Hypertens* 2003, 12: 521-6

Beekman FJ, van der Have F, Vastenhouw B, van der Linden AJ, van Rijk PP, Burbach JP, Smidt MP: U-SPECT-I: a novel system for submillimeter-resolution tomography with radiolabeled molecules in mice. *J Nucl Med* 2005, 46: 1194-200

Bergeron M, Gougoux A, Vinay P: The renal Fanconi syndrome. In: *The Metabolic and Molecular Bases of Inherited Diseases*, edited by Scriver CH, Beaudet AL, Sly WS, Valle D. McGraw-Hill, New York, 1995, pp 3691-704

Bernard A: Renal dysfunction induced by cadmium: biomarkers of critical effects. *Biometals* 2004, 17: 519-23

Biemesderfer D, Dekan G, Aronson PS, Farquhar MG: Assembly of distinctive coated pit and microvillar microdomains in the renal brush border. *Am J Physiol* 1992, 262: F55-67

Birn H, Verroust PJ, Nexo E, Hager H, Jacobsen C, Christensen EI, Moestrup SK: Characterization of an epithelial approximately 460-kDa protein that facilitates endocytosis of intrinsic factor-vitamin B12 and binds receptor-associated protein. *J Biol Chem* 1997, 272: 26497-504

Birn H, Vorum H, Verroust PJ, Moestrup SK, Christensen EI: Receptor-associated protein is important for normal processing of megalin in kidney proximal tubules. *J Am Soc Nephrol* 2000, 11: 191-202

Birn H, Christensen EI: Renal albumin absorption in physiology and pathology. *Kidney Int* 2006, 69: 440-9

Blomqvist SR, Vidarsson H, Fitzgerald S, Johansson BR, Ollerstam A, Brown R, Persson AE, Bergstrom G G, Enerback S: Distal renal tubular acidosis in mice that lack the forkhead transcription factor, Foxi1. *J Clin Invest* 2004, 113: 1560-70

Bonnici B, Wagner CA: Postnatal expression of transport proteins involved in acid-base transport in mouse kidney. *Pflugers Arch* 2004, 448: 16-28

Bork P, Beckmann G: The CUB domain. A widespread module in developmentally regulated proteins. *J Mol Biol* 1993, 231: 539-45

Borthwick KJ, Karet FE: Inherited disorders of the H^+-ATPase. *Curr Opin Nephrol Hypertens* 2002, 11: 563-68

Bradbury NA: Intracellular CFTR: localization and function. *Physiol Rev* 1999, 79: S175-91

Brent RL, Averich E, Drapiewski VA: Production of congenital malformations using tissue antibodies. I. Kidney antisera. *Proc Soc Exp Biol Med* 1961, 106: 523-6

Breton S, Wiederhold T, Marshansky V, Nsumu NN, Ramesh V, Brown D: The B1 subunit of the H^+ATPase is a PDZ domain-binding protein. Colocalization with NHE-RF in renal B-intercalated cells. *J Biol Chem* 2000, 275: 18219-24

Broackes-Carter FC, Mouchel N, Gill D, Hyde S, Bassett J, Harris A: Temporal regulation of CFTR expression during ovine lung development: implications for CF gene therapy. *Hum Mol Genet* 2002, 11: 125-31

Brown D, Hirsch S, Gluck S: Localization of a proton-pumping ATPase in rat kidney. *J Clin Invest* 1988, 2: 2114-26

Brown D, Breton S: H^+-V-ATPase-dependent luminal acidification in the kidney collecting duct and the epididymis/vas deferens: vesicle recycling and transcytotic pathways. *J Exp Biol* 2000, 203: 137-45

Brown D: Targeting of membrane transporters in renal epithelia: when cell biology meets physiology. *Am J Physiol Renal Physiol* 2000, 278: F192-201

Bruce LJ, Cope DL, Jones GK, Schofield AE, Burley M, Povey S, Unwin RJ, Wrong O, Tanner MJ: Familial distal renal tubular acidosis is associated with mutations in the red cell anion exchanger (Band 3, AE1) gene. *J Clin Invest* 1997, 100: 1693-707

Bu G, Rennke S: Receptor-associated protein is a folding chaperone for low density lipoprotein receptor-related protein. *J Biol Chem* 1996, 271: 22218-24

Burckhardt G, Bahn A, Wolff NA: Molecular physiology of renal p-aminohippurate secretion. *News Physiol Sci* 2001, 16: 114-8

Burckhardt BC, Drinkuth B, Menzel C, Konig A, Steffgen J, Wright SH, Burckhardt G: The renal Na^+-dependent dicarboxylate transporter, NaDC-3, translocates dimethyl- and disulfhydryl-compounds and contributes to renal heavy metal detoxification. *J Am Soc Nephrol* 2002, 13: 2628-38

Burckhardt BC, Burckhardt G: Transport of organic anions across the basolateral membrane of proximal tubule cells. *Rev Physiol Biochem Pharmacol* 2003, 146: 95-158

Burdett P, Lizana J, Eneroth P, Bremme K: Proteins of human amniotic fluid. II. Mapping by two-dimensional electrophoresis. *Clin Chem* 1982, 28: 935-40

Burghard R, Pallacks R, Gordjani N, Leititis JU, Hackeloer BJ, Brandis M: Microproteins in amniotic fluid as an index of changes in fetal renal function during development. *Pediatr Nephrol* 1987, 1: 574-80

Burrow CR, Devuyst O, Li X, Gatti L, Wilson PD: Expression of the β_2-subunit and apical localization of Na^+-K^+-ATPase in metanephric kidney. *Am J Physiol* 1999, 277: F391-403

Cabiscol E, Levine RL: Carbonic anhydrase III. Oxidative modification in vivo and loss of phosphatase activity during aging. *J Biol Chem* 1995, 270: 14742-7

Cagdas A, Aydinli K, Irez T, Temizyurek K, Apak MY: Evaluation of the fetal kidney maturation by assessment of amniotic fluid alpha-1 microglobulin levels. *Eur J Obstet Gynecol Reprod Biol* 2000, 90: 55-61

Canessa CM, Schild L, Buell G, Thorens B, Gautschi I, Horisberger JD, Rossier BC: Amiloride-sensitive epithelial Na^+ channel is made of three homologous subunits. *Nature* 1994, 367: 463-7

Carter N, Lonnerholm G, Meyerson B, Wistrand P: Androgen-linked control of carbonic anhydrase III expression occurs in rat perivenous hepatocytes; an immunocytochemical study. *Ups J Med Sci* 2001, 106: 67-76

Cebotaru V, Kaul S, Devuyst O, Cai H, Racusen L, Guggino WB, Guggino SE: High citrate diet delays progression of renal insufficiency in the ClC-5 knockout mouse model of Dent's disease. *Kidney Int* 2005, 68: 642-52

Chai YC, Jung CH, Lii CK, Ashraf SS, Hendrich S, Wolf B, Sies H, Thomas JA: Identification of an abundant S-thiolated rat liver protein as carbonic anhydrase III; characterization of S-thiolation and dethiolation reactions. *Arch Biochem Biophys* 1991, 284: 270-88

Chan JC: The influence of dietary intake on endogenous acid production. Theoretical and experimental background. *Nutr Metab* 1974, 16: 1-9

Chatelet F, Brianti E, Ronco P, Roland J, Verroust P: Ultrastructural localization by monoclonal antibodies of brush border antigens expressed by glomeruli (I. Renal distribution). *Am J Pathol* 1986, 122: 500-11

Cheng SH, Gregory RJ, Marshall J, Paul S, Souza DW, White GA, O'Riordan CR, Smith AE: Defective intracellular transport and processing of CFTR is the molecular basis of most cystic fibrosis. *Cell* 1990, 63: 827-34

Chernova MN, Jiang L, Friedman DJ, Darman RB, Lohi H, Kere J, Vandorpe DH, Alper SL: Functional comparison of mouse slc26a6 anion exchanger with human SLC26A6 polypeptide variants: differences in anion selectivity, regulation, and electrogenicity. *J Biol Chem* 2005, 280: 8564-80

Cherqui S, Sevin C, Hamard G, Kalatzis V, Sich M, Pequignot MO, Gogat K, Abitbol M, Broyer M, Gubler MC, Antignac C: Intralysosomal cystine accumulation in mice lacking cystinosin, the protein defective in cystinosis. *Mol Cell Biol* 2002, 22: 7622-32

Cho EA and Dressler GR: The formation and development of nephrons. In: *The Kidney, from normal development to congenital disease*, edited by Vize PD, Woolf AS and Bard JBL. Academic Press (Elsevier), Orlando, 2003, pp197

Christensen EI, Gliemann J, Moestrup SK: Renal tubule gp330 is a calcium binding receptor for endocytic uptake of protein. *J Histochem Cytochem* 1992, 40: 1481-90

Christensen EI, Nielsen S, Moestrup SK, Borre C, Maunsbach AB, de Heer E, Ronco P, Hammond TG, Verroust P: Segmental distribution of the endocytosis receptor gp330 in renal proximal tubules. *Eur J Cell Biol* 1995, 66: 349-64

Christensen EI, Birn H, Verroust P, Moestrup SK: Membrane receptors for endocytosis in the renal proximal tubule. *Int Rev Cytol* 1998, 180: 237-84

Christensen EI, Birn H: Megalin and cubilin: multifunctional endocytic receptors. *Nat Rev Mol Cell Biol* 2002, 3: 256-66

Christensen EI, Verroust PJ: Megalin and cubilin, role in proximal tubule function and during development. *Pediatr Nephrol* 2002, 17: 993-9

Christensen EI, Devuyst O, Dom G, Nielsen R, Van der Smissen P, Verroust P, Leruth M, Guggino WB, Courtoy PJ: Loss of chloride channel ClC-5 impairs endocytosis by defective trafficking of megalin and cubilin in kidney proximal tubules. *Proc Natl Acad Sci U S A* 2003, 100: 8472-7

Clarke LL, Grubb BR, Yankaskas JR, Cotton CU, McKenzie A, Boucher RC: Relationship of a non-cystic fibrosis transmembrane conductance regulator-mediated chloride conductance to organ-level disease in *Cftr*(-/-) mice. *Proc Natl Acad Sci U S A* 1994, 91: 479-83

Claustres M: Molecular pathology of the CFTR locus in male infertility. *Reprod Biomed Online* 2005, 10: 14-41

Clifton-Bligh RJ, Wentworth JM, Heinz P, Crisp MS, John R, Lazarus JH, Ludgate M, Chatterjee VK: Mutation of the gene encoding human TTF-2 associated with thyroid agenesis, cleft palate and choanal atresia. *Nat Genet* 1998, 19: 399-401

Coakley RJ, Taggart C, McElvaney NG, O'Neill SJ: Cytosolic pH and the inflammatory microenvironment modulate cell death in human neutrophils after phagocytosis. *Blood* 2002, 100: 3383-91

Colledge WH, Abella BS, Southern KW, Ratcliff R, Jiang C, Cheng SH, MacVinish LJ, Anderson JR, Cuthbert AW, Evans MJ.: Generation and characterization of a ΔF508 cystic fibrosis mouse model. *Nat Genet* 1995, 10: 445-52

Conner SD, Schmid SL: Regulated portals of entry into the cell. *Nature* 2003, 422: 37-44

Coudroy G, Gburek J, Kozyraki R, Madsen M, Trugnan G, Moestrup SK, Verroust PJ, Maurice M: Contribution of cubilin and amnionless to processing and membrane targeting of cubilin-amnionless complex. *J Am Soc Nephrol* 2005, 16: 2330-7

Crawford I, Maloney PC, Zeitlin PL, Guggino WB, Hyde SC, Turley H, Gatter KC, Harris A, Higgins CF: Immunocytochemical localization of the cystic fibrosis gene product CFTR. *Proc Natl Acad Sci U S A* 1991, 88: 9262-6

Davies SA, Goodwin SF, Kelly DC, Wang Z, Sozen MA, Kaiser K, Dow JA: Analysis and inactivation of vha55, the gene encoding the vacuolar ATPase B-subunit in Drosophila melanogaster reveals a larval lethal phenotype. *J Biol Chem* 1996, 271: 30677-84

de Jong M, Barone R, Krenning E, Bernard B, Melis M, Visser T, Gekle M, Willnow TE, Walrand S, Jamar F, Pauwels S: Megalin is essential for renal proximal tubule reabsorption of (111)In-DTPA-octreotide. *J Nucl Med* 2005, 46: 1696-700

Delaney SJ, Alton EW, Smith SN, Lunn DP, Farley R, Lovelock PK, Thomson SA, Hume DA, Lamb D, Porteous DJ, Dorin JR, Wainwright BJ.: Cystic fibrosis mice carrying the missense mutation G551D replicate human genotype-phenotype correlations. *EMBO J* 1996, 15: 955-63

Dent CE, Friedman M: Hypercalcuric rickets associated with renal tubular damage. *Arch Dis Child* 1964, 39: 240-9

Denning GM, Anderson MP, Amara JF, Marshall J, Smith AE, Welsh MJ: Processing of mutant cystic fibrosis transmembrane conductance regulator is temperature-sensitive. *Nature* 1992, 358: 761-4

Devidas S, Guggino WB: The cystic fibrosis transmembrane conductance regulator and ATP. *Curr Opin Cell Biol* 1997, 9: 547-52

Devuyst O, Burrow CR, Schwiebert EM, Guggino WB, Wilson PD: Developmental regulation of CFTR expression during human nephrogenesis. *Am J Physiol* 1996, 271: F723-35

Devuyst O, Burrow CR, Smith BL, Agre P, Knepper MA, Wilson PD: Expression of aquaporins-1 and -2 during nephrogenesis and in autosomal dominant polycystic kidney disease. *Am J Physiol* 1996, 271: F169-83

Devuyst O, Beauwens R: Ion transport and cystogenesis: the paradigm of autosomal dominant polycystic kidney disease. *Adv Nephrol Necker Hosp* 1998, 28: 439-78

Devuyst O, Christie PT, Courtoy PJ, Beauwens R, Thakker RV: Intra-renal and subcellular distribution of the human chloride channel, CLC-5, reveals a pathophysiological basis for Dent's disease. *Hum Mol Genet* 1999, 8: 247-57

Devuyst O, Guggino WB: Chloride channels in the kidney: lessons learned from knockout animals. *Am J Physiol Renal Physiol* 2002, 283: F1176-91

Dorin JR, Dickinson P, Alton EW, Smith SN, Geddes DM, Stevenson BJ, Kimber WL, Fleming S, Clarke AR, Hooper ML, et al: Cystic fibrosis in the mouse by targeted insertional mutagenesis. *Nature* 1992, 359: 211-5

Doyle DA, Morais Cabral J, Pfuetzner RA, Kuo A, Gulbis JM, Cohen SL, Chait BT, MacKinnon R: The structure of the potassium channel: molecular basis of K^+ conduction and selectivity. *Science* 1998, 280: 69-77

Duda DM, Tu C, Fisher SZ, An H, Yoshioka C, Govindasamy L, Laipis PJ, Agbandje-McKenna M, Silverman DN, McKenna R: Human carbonic anhydrase III: structural and kinetic study of catalysis and proton transfer. *Biochemistry* 2005, 44: 10046-53

Dutzler R, Campbell EB, Cadene M, Chait BT, MacKinnon R: X-ray structure of a ClC chloride channel at 3.0 A reveals the molecular basis of anion selectivity. *Nature* 2002, 415: 287-94

Eaton P, Jones ME, McGregor E, Dunn MJ, Leeds N, Byers HL, Leung KY, Ward MA, Pratt JR, Shattock MJ: Reversible cysteine-targeted oxidation of proteins during renal oxidative stress. *J Am Soc Nephrol* 2003, 14: S290-6

Eckman EA, Cotton CU, Kube DM, Davis PB: Dietary changes improve survival of CFTR S489X homozygous mutant mouse. *Am J Physiol* 1995, 269: L625-30

Edelmann CM, Soriano JR, Boichis H, Gruskin AB, Acosta MI: Renal bicarbonate reabsorption and hydrogen ion excretion in normal infants. *J Clin Invest* 1967, 46:1309-17

Edmonds RD, Silva IV, Guggino WB, Butler RB, Zeitlin PL, Blaisdell CJ: ClC-5: ontogeny of an alternative chloride channel in respiratory epithelia. *Am J Physiol Lung Cell Mol Physiol* 2002, 282: L501-7

Egan ME, Glockner-Pagel J, Ambrose C, Cahill PA, Pappoe L, Balamuth N, Cho E, Canny S, Wagner CA, Geibel J, Caplan MJ: Calcium-pump inhibitors induce functional surface expression of ΔF508-CFTR protein in cystic fibrosis epithelial cells. *Nat Med* 2002, 8: 485-92

Eggermont E, De Boeck K: Small-intestinal abnormalities in cystic fibrosis patients. *Eur J Pediatr* 1991, 150: 824-8

Ekblom P, Ekblom M, Fecker L, Klein G, Zhang HY, Kadoya Y, Chu ML, Mayer U, Timpl R: Role of mesenchymal nidogen for epithelial morphogenesis in vitro. *Development* 1994, 120: 2003-14

Ellsworth RE, Jamison DC, Touchman JW, Chissoe SL, Braden Maduro VV, Bouffard GG, Dietrich NL, Beckstrom-Sternberg SM, Iyer LM, Weintraub LA, Cotton M, Courtney L, Edwards J, Maupin R, Ozersky P, Rohlfing T, Wohldmann P, Miner T, Kemp K, Kramer J, Korf I, Pepin K, Antonacci-Fulton L, Fulton RS, Minx P, Hillier LW, Wilson RK, Waterston RH, Miller W, Green ED: Comparative genomic sequence analysis of the human and mouse cystic fibrosis transmembrane conductance regulator genes. *Proc Natl Acad Sci U S A* 2000, 97: 1172-7

Estévez R, Boettger T, Stein V, Birkenhager R, Otto E, Hildebrandt F, Jentsch TJ: Barttin is a Cl^- channel β-subunit crucial for renal Cl^- reabsorption and inner ear K^+ secretion. *Nature* 2001, 414: 558-61

Faundez V, Hartzell HC: Intracellular chloride channels: determinants of function in the endosomal pathway. *Sci STKE* 2004, 233: re8

Feraille E, Doucet A: Sodium-potassium-adenosinetriphosphatase-dependent sodium transport in the kidney: hormonal control. *Physiol Rev* 2001, 81: 345-418

Finberg KE, Wagner CA, Bailey MA, Paunescu TG, Breton S, Brown D, Giebisch G, Geibel JP, Lifton RP: The B1-subunit of the H^+-ATPase is required for maximal urinary acidification. *Proc Natl Acad Sci U S A* 2005, 102: 13616-21

Fisher SE, Black GC, Lloyd SE, Hatchwell E, Wrong O, Thakker RV, Craig IW: Isolation and partial characterization of a chloride channel gene which is expressed in kidney and is a candidate for Dent's disease (an X-linked hereditary nephrolithiasis). *Hum Mol Genet* 1994, 3: 2053-9

Fisher SE, van Bakel I, Lloyd SE, Pearce SH, Thakker RV, Craig IW: Cloning and characterization of CLCN5, the human kidney chloride channel gene implicated in Dent disease (an X-linked hereditary nephrolithiasis). *Genomics* 1995, 29: 598-606

French PJ, van Doorninck JH, Peters RH, Verbeek E, Ameen NA, Marino CR, de Jonge HR, Bijman J, Scholte BJ: A ΔF508 mutation in mouse cystic fibrosis transmembrane conductance regulator results in a temperature-sensitive processing defect in vivo. *J Clin Invest* 1996, 98: 1304-12

Frymoyer PA, Scheinman SJ, Dunham PB, Jones DB, Hueber P, Schroeder ET: X-linked recessive nephrolithiasis with renal failure. *N Engl J Med* 1991, 325: 681-6

Fuller CM, Benos DJ: CFTR! *Am J Physiol* 1992, 263: C267-86

Fyfe JC, Ramanujam KS, Ramaswamy K, Patterson DF, Seetharam B: Defective brush-border expression of intrinsic factor-cobalamin receptor in canine inherited intestinal cobalamin malabsorption. *J Biol Chem* 1991, 266: 4489-94

Gabriel SE, Clarke LL, Boucher RC, Stutts MJ: CFTR and outward rectifying chloride channels are distinct proteins with a regulatory relationship. *Nature* 1993, 363: 263-8

Gadsby DC, Vergani P, Csanady L: The ABC protein turned chloride channel whose failure causes cystic fibrosis. *Nature* 2006, 440: 477-83

Gekle M, Mildenberger S, Freudinger R, Schwerdt G, Silbernagl S: Albumin endocytosis in OK cells: dependence on actin and microtubules and regulation by protein kinases. *Am J Physiol* 1997, 272: F668-77

Gekle M: Renal tubule albumin transport. *Annu Rev Physiol* 2005, 67:573-94

Gibney EM, Goldfarb DS: The association of nephrolithiasis with cystic fibrosis. *Am J Kidney Dis* 2003, 42: 1-11

Giebisch G and Windhager E: Organization of the urinary system. In: *Medical Physiology*, edited by Boron WF and Boulpaep EL. Saunders (Elsevier Science), Philadelphia, PA, 2003, pp737-56

Giebisch G and Windhager E: Transport of acids and bases. In: *Medical Physiology*, edited by Boron WF and Boulpaep EL. Saunders (Elsevier Science), Philadelphia, PA, 2003, pp845-60

Gomez RA, Norwood VF, Tufro-McReddie A: Development of the kidney vasculature. *Microsc Res Tech* 1997, 39: 254-60

Groman JD, Meyer ME, Wilmott RW, Zeitlin PL, Cutting GR: Variant cystic fibrosis phenotypes in the absence of CFTR mutations. *N Engl J Med* 2002, 347: 401-7

Grubb BR, Vick RN, Boucher RC: Hyperabsorption of Na^+ and raised Ca^{2+}-mediated Cl^- secretion in nasal epithelia of CF mice. *Am J Physiol* 1994, 266: C1478-83

Grubb BR, Boucher RC: Pathophysiology of gene-targeted mouse models for cystic fibrosis. *Physiol Rev* 1999, 79: S193-214

Gruber G, Wieczorek H, Harvey WR, Muller V: Structure-function relationships of A-, F- and V-ATPases. *J Exp Biol* 2001, 204: 2597-605

Gu F, Gruenberg J: ARF1 regulates pH-dependent COP functions in the early endocytic pathway. *J Biol Chem* 2000, 275: 8154-60

Guggino WB: The cystic fibrosis transmembrane regulator forms macromolecular complexes with PDZ domain scaffold proteins. *Proc Am Thorac Soc* 2004, 1: 28-32

Günther W, Luchow A, Cluzeaud F, Vandewalle A, Jentsch TJ: ClC-5, the chloride channel mutated in Dent's disease, colocalizes with the proton pump in endocytotically active kidney cells. *Proc Natl Acad Sci U S A* 1998, 95: 8075-80

Gupta N, Tarif SR, Seikaly M, Baum M: Role of glucocorticoids in the maturation of the rat renal Na^+/H^+ antiporter (NHE3). *Kidney Int* 2001, 60: 173-81

Gut A, Kappeler F, Hyka N, Balda MS, Hauri HP, Matter K: Carbohydrate-mediated Golgi to cell surface transport and apical targeting of membrane proteins. *EMBO J* 1998, 17: 1919-29

Hanaoka K, Devuyst O, Schwiebert EM, Wilson PD, Guggino WB: A role for CFTR in human autosomal dominant polycystic kidney disease. *Am J Physiol* 1996, 270: C389-99

Hasty P, O'Neal WK, Liu KQ, Morris AP, Bebok Z, Shumyatsky GB, Jilling T, Sorscher EJ, Bradley A, Beaudet AL.: Severe phenotype in mice with termination mutation in exon 2 of cystic fibrosis gene. *Somat Cell Mol Genet* 1995, 21: 177-87

He Q, Fyfe JC, Schaffer AA, Kilkenney A, Werner P, Kirkness EF, Henthorn PS: Canine Imerslund-Grasbeck syndrome maps to a region orthologous to HSA14q. *Mamm Genome* 2003, 14: 758-64

He Q, Madsen M, Kilkenney A, Gregory B, Christensen EI, Vorum H, Hojrup P, Schaffer AA, Kirkness EF, Tanner SM, de la Chapelle A, Giger U, Moestrup SK, Fyfe JC: Amnionless function is required for cubilin brush-border expression and intrinsic factor-cobalamin (vitamin B12) absorption in vivo. *Blood* 2005, 106: 1447-53

Henneman CE, Anderson GV, Tejavej A, Gross HA, Heiman ML: Fetal maturation and amniotic fluid. *Am J Obstet Gynecol* 1970, 108: 302-7

Herak-Kramberger CM, Brown D, Sabolic I: Cadmium inhibits vacuolar H^+-ATPase and endocytosis in rat kidney cortex. *Kidney Int* 1998, 53: 1713-26

Higgins CF: ABC transporters: from microorganisms to man. *Annu Rev Cell Biol* 1992, 8: 67-113

Hjalm G, Murray E, Crumley G, Harazim W, Lundgren S, Onyango I, Ek B, Larsson M, Juhlin C, Hellman P, Davis H, Akerstrom G, Rask L, Morse B: Cloning and sequencing of human gp330, a Ca^{2+}-binding receptor with potential intracellular signaling properties. *Eur J Biochem* 1996, 239: 132-7

Hoopes RR Jr, Raja KM, Koich A, Hueber P, Reid R, Knohl SJ, Scheinman SJ: Evidence for genetic heterogeneity in Dent's disease. *Kidney Int* 2004, 65: 1615-20

Hoopes RR Jr, Shrimpton AE, Knohl SJ, Hueber P, Hoppe B, Matyus J, Simckes A, Tasic V, Toenshoff B, Suchy SF, Nussbaum RL, Scheinman SJ: Dent Disease with mutations in OCRL1. *Am J Hum Genet* 2005, 76: 260-7

Horster M: Embryonic epithelial membrane transporters. *Am J Physiol Renal Physiol* 2000, 279: F982-96

Hryciw DH, Wang Y, Devuyst O, Pollock CA, Poronnik P, Guggino WB: Cofilin interacts with ClC-5 and regulates albumin uptake in proximal tubule cell lines. *J Biol Chem* 2003, 278: 40169-76

Hryciw DH, Ekberg J, Pollock CA, Poronnik P: ClC-5: A chloride channel with multiple roles in renal tubular albumin uptake. *Int J Biochem Cell Biol* 2006, 38: 1036-42

Huber S, Braun G, Burger-Kentischer A, Reinhart B, Luckow B, Horster M: CFTR mRNA and its truncated splice variant (TRN-CFTR) are differentially expressed during collecting duct ontogeny. *FEBS Lett* 1998, 423: 362-6

Hulander M, Kiernan AE, Blomqvist SR, Carlsson P, Samuelsson EJ, Johansson BR, Steel KP, Enerback S: Lack of pendrin expression leads to deafness and expansion of the endolymphatic compartment in inner ears of Foxi1 null mutant mice. *Development* 2003, 130: 2013-25

Hunton DB, Long WK, Tsumagari HY: Meconium ileus equivalent: an adult complication of fibrocystic disease. *Gastroenterology* 1966, 50: 99-106

Hurtado-Lorenzo A, Skinner M, El Annan J, Futai M, Sun-Wada GH, Bourgoin S, Casanova J, Wildeman A, Bechoua S, Ausiello DA, Brown D, Marshansky V: V-ATPase interacts with ARNO and Arf6 in early endosomes and regulates the protein degradative pathway. *Nat Cell Biol* 2006, 8: 124-36

Hyde K, Reid CJ, Tebbutt SJ, Weide L, Hollingsworth MA, Harris A: The cystic fibrosis transmembrane conductance regulator as a marker of human pancreatic duct development. *Gastroenterology* 1997, 113: 914-9

Igarashi T, Günther W, Sekine T, Inatomi J, Shiraga H, Takahashi S, Suzuki J, Tsuru N, Yanagihara T, Shimazu M, Jentsch TJ, and Thakker RV: Functional characterization of renal chloride channel, *CLCN5*, mutations associated with Dent's Japan disease. *Kidney Int* 1998, 54: 1850-6

Igarashi T, Sekine T, Inatomi J, Seki G: Unraveling the molecular pathogenesis of isolated proximal renal tubular acidosis. *J Am Soc Nephrol* 2002, 13: 2171-7

Imrie JR, Fagan DG, Sturgess JM: Quantitative evaluation of the development of the exocrine pancreas in cystic fibrosis and control infants. *Am J Pathol* 1979, 95: 697-707

Inoue H, Noumi T, Nagata M, Murakami H, Kanazawa H: Targeted disruption of the gene encoding the proteolipid subunit of mouse vacuolar H^+-ATPase leads to early embryonic lethality. *Biochim Biophys Acta* 1999, 1413: 130-8

Itoh K: ^{99m}Tc-MAG3: review of pharmacokinetics, clinical application to renal diseases and quantification of renal function. *Ann Nucl Med* 2001, 15: 179-90

Iwata M, Imamura H, Stambouli E, Ikeda C, Tamakoshi M, Nagata K, Makyio H, Hankamer B, Barber J, Yoshida M, Yokoyama K, Iwata S: Crystal structure of a central stalk subunit C and reversible association/dissociation of vacuole-type ATPase. *Proc Natl Acad Sci U S A* 2004, 101: 59-64

Izzedine H, Launay-Vacher V, Isnard-Bagnis C, Deray G: Drug-induced Fanconi's syndrome. *Am J Kidney Dis* 2003, 41: 292-309

Jentsch TJ, Steinmeyer K, Schwarz G: Primary structure of Torpedo marmorata chloride channel isolated by expression cloning in Xenopus oocytes. *Nature* 1990, 348: 510-4

Jentsch TJ, Stein V, Weinreich F, Zdebik AA: Molecular structure and physiological function of chloride channels. *Physiol Rev* 2002, 82: 503-68

Jentsch TJ, Maritzen T, Zdebik AA: Chloride channel diseases resulting from impaired transepithelial transport or vesicular function. *J Clin Invest* 2005, 115: 2039-46

Jewell DA, Tu CK, Paranawithana SR, Tanhauser SM, LoGrasso PV, Laipis PJ, Silverman DN: Enhancement of the catalytic properties of human carbonic anhydrase III by site-directed mutagenesis. *Biochemistry* 1991, 30: 1484-90

Kalantry S, Manning S, Haub O, Tomihara-Newberger C, Lee HG, Fangman J, Disteche CM, Manova K, Lacy E: The amnionless gene, essential for mouse gastrulation, encodes a visceral-endoderm-specific protein with an extracellular cysteine-rich domain. *Nat Genet* 2001, 27: 412-6

Kalatzis V, Antignac C: New aspects of the pathogenesis of cystinosis. *Pediatr Nephrol* 2003, 18: 207-15

Kalin N, Claass A, Sommer M, Puchelle E, Tummler B: ΔF508 CFTR protein expression in tissues from patients with cystic fibrosis. *J Clin Invest* 1999, 103: 1379-89

Karet FE: Inherited distal renal tubular acidosis. *J Am Soc Nephrol* 2002, 13: 2178-84

Karashima S, Hattori S, Ushijima T, Furuse A, Nakazato H, Matsuda I: Developmental changes in carbonic anhydrase II in the rat kidney. *Pediatr Nephrol* 1998, 12: 263-8

Katz SM, Krueger LJ, Falkner B: Microscopic nephrocalcinosis in cystic fibrosis. *N Engl J Med* 1988, 319: 263-6

Karet FE, Gainza FJ, Gyory AZ, Unwin RJ, Wrong O, Tanner MJ, Nayir A, Alpay H, Santos F, Hulton SA, Bakkaloglu A, Ozen S, Cunningham MJ, di Pietro A, Walker WG, Lifton RP: Mutations in the chloride-bicarbonate exchanger gene AE1 cause autosomal dominant but not autosomal recessive distal renal tubular acidosis. *Proc Natl Acad Sci U S A* 1998, 95: 6337-42

Karet FE, Finberg KE, Nelson RD, Nayir A, Mocan H, Sanjad SA, Rodriguez-Soriano J, Santos F, Cremers CW, Di Pietro A, Hoffbrand BI, Winiarski J, Bakkaloglu A, Ozen S, Dusunsel R, Goodyer P, Hulton SA,

Wu DK, Skvorak AB, Morton CC, Cunningham MJ, Jha V, Lifton RP: Mutations in the gene encoding B1 subunit of H^+-ATPase cause renal tubular acidosis with sensorineural deafness. *Nat Genet* 1999, 21: 84-90

Karp SL and Molitoris BA: Establishment of polarity in epithelial cells of the developing nephron. In: *The Kidney, from normal development to congenital disease*, edited by Vize PD, Woolf AS and Bard JBL. Academic Press (Elsevier), Orlando, 2003, pp211-20

Kawasaki-Nishi S, Bowers K, Nishi T, Forgac M, Stevens TH: The amino-terminal domain of the vacuolar proton-translocating ATPase a subunit controls targeting and in vivo dissociation, and the carboxyl-terminal domain affects coupling of proton transport and ATP hydrolysis. *J Biol Chem* 2001, 276: 47411-20

Kemp BE: Bateman domains and adenosine derivatives form a binding contract. *J Clin Invest* 2004, 113: 182-4

Kerjaschki D, Farquhar MG: The pathogenic antigen of Heymann nephritis is a membrane glycoprotein of the renal proximal tubule brush border. *Proc Natl Acad Sci U S A* 1982, 79: 5557-61

Kerjaschki D, Farquhar MG: Immunocytochemical localization of the Heymann nephritis antigen (GP330) in glomerular epithelial cells of normal Lewis rats. *J Exp Med* 1983, 157: 667-86

Kibble JD, Neal AM, Colledge WH, Green R, Taylor CJ: Evidence for cystic fibrosis transmembrane conductance regulator-dependent sodium reabsorption in kidney, using *Cftr*^{tm2cam} mice. *J Physiol* 2000, 526: 27-34

Kibble JD, Balloch KJ, Neal AM, Hill C, White S, Robson L, Green R, Taylor CJ: Renal proximal tubule function is preserved in *Cftr*^{tm2cam} ΔF508 cystic fibrosis mice. *J Physiol* 2001, 532: 449-57

Kim J, Tisher CC, Madsen KM: Differentiation of intercalated cells in developing rat kidney: an immunohistochemical study. *Am J Physiol* 1994, 266: F977-90

Kim J, Cha JH, Tisher CC, Madsen KM: Role of apoptotic and nonapoptotic cell death in removal of intercalated cells from developing rat kidney. *Am J Physiol* 1996, 270: F575-92

Kim G, Lee TH, Wetzel P, Geers C, Robinson MA, Myers TG, Owens JW, Wehr NB, Eckhaus MW, Gros G, Wynshaw-Boris A, Levine RL: Carbonic anhydrase III is not required in the mouse for normal growth, development, and life span. *Mol Cell Biol* 2004, 24: 9942-7

Kristiansen M, Kozyraki R, Jacobsen C, Nexo E, Verroust PJ, Moestrup SK: Molecular dissection of the intrinsic factor-vitamin B12 receptor, cubilin, discloses regions important for membrane association and ligand binding. *J Biol Chem* 1999, 274: 20540-4

Kriz W, Bankir L: A standard nomenclature for structures of the kidney. The Renal Commission of the International Union of Physiological Sciences (IUPS). *Kidney Int* 1988, 33: 1-7

Kurth I, Hentschke M, Hentschke S, Borgmeyer U, Gal A, Hubner CA: The forkhead transcription factor Foxi1 directly activates the AE4 promoter. *Biochem J* 2006, 393: 277-83

Laing CM, Toye AM, Capasso G, Unwin RJ: Renal tubular acidosis: developments in our understanding of the molecular basis. *Int J Biochem Cell Biol* 2005, 37: 1151-61

Laitinen L, Virtanen I, Saxen L: Changes in the glycosylation pattern during embryonic development of mouse kidney as revealed with lectin conjugates. *J Histochem Cytochem* 1987, 35: 55-65

Lamb FS, Graeff RW, Clayton GH, Smith RL, Schutte BC, McCray PB Jr: Ontogeny of *CLCN3* chloride channel gene expression in human pulmonary epithelium. *Am J Respir Cell Mol Biol* 2001, 24: 376-81

Lange K, Carson R: EM reconstruction algorithms for emission and transmission tomography. *J Comput Assist Tomogr* 1984, 8: 306-16

Lange PF, Wartosch L, Jentsch TJ, Fuhrmann JC: ClC-7 requires Ostm1 as a β-subunit to support bone resorption and lysosomal function. *Nature* 2006, 440: 220-3

Larson JE, Morrow SL, Happel L, Sharp JF, Cohen JC: Reversal of cystic fibrosis phenotype in mice by gene therapy in utero. *Lancet* 1997, 349: 619-20

Larson JE, Cohen JC: Developmental paradigm for early features of cystic fibrosis. *Pediatr Pulmonol* 2005, 40: 371-7

Larsson L, Lonnerholm G: Carbonic anhydrase in the metanephrogenic zone of the human fetal kidney. *Biol Neonate* 1985, 48: 168-71

Leheste JR, Rolinski B, Vorum H, Hilpert J, Nykjaer A, Jacobsen C, Aucouturier P, Moskaug JO, Otto A, Christensen EI, Willnow TE: Megalin knockout mice as an animal model of low molecular weight proteinuria. *Am J Pathol* 1999, 155: 1361-70

Leheste JR, Melsen F, Wellner M, Jansen P, Schlichting U, Renner-Muller I, Andreassen TT, Wolf E, Bachmann S, Nykjaer A, Willnow TE: Hypocalcemia and osteopathy in mice with kidney-specific megalin gene defect. *FASEB J* 2003, 17: 247-9

Lehtonen S, Lehtonen E, Olkkonen VM: Vesicular transport and kidney development. *Int J Dev Biol* 1999, 43: 425-33

Lehtonen J, Shen B, Vihinen M, Casini A, Scozzafava A, Supuran CT, Parkkila AK, Saarnio J, Kivela AJ, Waheed A, Sly WS, Parkkila S: Characterization of CA XIII, a novel member of the carbonic anhydrase isozyme family. *J Biol Chem* 2004, 279: 2719-27

Letz B, Korbmacher C: cAMP stimulates CFTR-like Cl^- channels and inhibits amiloride-sensitive Na^+ channels in mouse CCD cells. *Am J Physiol* 1997, 272: C657-66

Lewis JS, Achilefu S, Garbow JR, Laforest R, Welch MJ: Small animal imaging. Current technology and perspectives for oncological imaging. *Eur J Cancer* 2002, 38: 2173-88

Li C, Naren AP: Macromolecular complexes of cystic fibrosis transmembrane conductance regulator and its interacting partners. *Pharmacol Ther* 2005, 108: 208-23

Lindskog S: Structure and mechanism of carbonic anhydrase. *Pharmacol Ther* 1997, 74: 1-20

Lloyd SE, Pearce SH, Fisher SE, Steinmeyer K, Schwappach B, Scheinman SJ, Harding B, Bolino A, Devoto M, Goodyer P, Rigden SP, Wrong O, Jentsch TJ, Craig IW, Thakker RV: A common molecular basis for three inherited kidney stone diseases. *Nature* 1996, 379: 445-9

LoGrasso PV, Tu CK, Jewell DA, Wynns GC, Laipis PJ, Silverman DN: Catalytic enhancement of human carbonic anhydrase III by replacement of phenylalanine198 with leucine. *Biochemistry* 1991, 30: 8463-70

Lowe M: Structure and function of the Lowe syndrome protein OCRL1. *Traffic* 2005, 6: 711-9

Ludwig M, Waldegger S, Nuutinen M, Bokenkamp A, Reissinger A, Steckelbroeck S, Utsch B: Four additional *CLCN5* exons encode a widely expressed novel long CLC-5 isoform but fail to explain Dent's phenotype in patients without mutations in the short variant. *Kidney Blood Press Res* 2003, 26: 176-84

Ludwig M, Doroszewicz J, Seyberth HW, Bokenkamp A, Balluch B, Nuutinen M, Utsch B, Waldegger S: Functional evaluation of Dent's disease-causing mutations: implications for ClC-5 channel trafficking and internalization. *Hum Genet* 2005, 117: 228-37

Lyon A, Bilton D: Fertility issues in cystic fibrosis. *Paediatr Respir Rev* 2002, 3: 236-40

Maisey M: Radionuclide renography: a review. *Curr Opin Nephrol Hypertens* 2003, 12: 649-52

Maranda B, Brown D, Bourgoin S, Casanova JE, Vinay P, Ausiello DA, Marshansky V: Intra-endosomal pH-sensitive recruitment of the Arf-nucleotide exchange factor ARNO and Arf6 from cytoplasm to proximal tubule endosomes. *J Biol Chem* 2001, 276: 18540-50

Markovich D, Murer H: The SLC13 gene family of sodium sulphate/carboxylate cotransporters. *Pflugers Arch* 2004, 447: 594-602

Marshansky V, Ausiello DA, Brown D: Physiological importance of endosomal acidification: potential role in proximal tubulopathies. *Curr Opin Nephrol Hypertens* 2002, 11: 527-37

Marvao P, De Jesus Ferreira MC, Bailly C, Paulais M, Bens M, Guinamard R, Moreau R, Vandewalle A, Teulon J: Cl^- absorption across the thick ascending limb is not altered in cystic fibrosis mice. A role for a pseudo-CFTR Cl^- channel. *J Clin Invest* 1998, 102: 1986-93

McGrath SA, Basu A, Zeitlin PL: Cystic fibrosis gene and protein expression during fetal lung development. *Am J Respir Cell Mol Biol* 1993, 8: 201-8

Miller C: Open-state substructure of single chloride channels from Torpedo electroplax. *Philos Trans R Soc Lond B Biol Sci* 1982, 299: 401-11

Miller C: ClC chloride channels viewed through a transporter lens. *Nature* 2006, 440: 484-9

Miller RC, Wolf EJ, Gould M, Macri CJ, Charnas LR: Fetal oculocerebrorenal syndrome of Lowe associated with elevated maternal serum and amniotic fluid alpha-fetoprotein levels. *Obstet Gynecol* 1994, 84: 77-80

Mo L, Wills NK: ClC-5 chloride channel alters expression of the epithelial sodium channel (ENaC). *J Membr Biol* 2004, 202: 21-37

Moestrup SK, Cui S, Vorum H, Bregengard C, Bjorn SE, Norris K, Gliemann J, Christensen EI: Evidence that epithelial glycoprotein 330/megalin mediates uptake of polybasic drugs. *J Clin Invest* 1995, 96: 1404-13

Moestrup SK, Kozyraki R, Kristiansen M, Kaysen JH, Rasmussen HH, Brault D, Pontillon F, Goda FO, Christensen EI, Hammond TG, Verroust PJ: The intrinsic factor-vitamin B12 receptor and target of teratogenic antibodies is a megalin-binding peripheral membrane protein with homology to developmental proteins. *J Biol Chem* 1998, 273: 5235-42

Morales MM, Carroll TP, Morita T, Schwiebert EM, Devuyst O, Wilson PD, Lopes AG, Stanton BA, Dietz HC, Cutting GR, Guggino WB: Both the wild type and a functional isoform of CFTR are expressed in kidney. *Am J Physiol* 1996, 270: F1038-48

Morales MM, Falkenstein D, Lopes AG: The cystic fibrosis transmembrane regulator (CFTR) in the kidney. *An Acad Bras Cienc* 2000, 72: 399-406

Moretti JL, Rapin JR, Saccavini JC, Lageron A, Le Poncin M, Bardy A: 2,3-Dimercaptosuccinic-acid chelates. 2. Renal localization. *Int J Nucl Med Biol* 1984, 11: 275-9

Mori K, Ogawa Y, Ebihara K, Tamura N, Tashiro K, Kuwahara T, Mukoyama M, Sugawara A, Ozaki S, Tanaka I, Nakao K: Isolation and characterization of CA XIV, a novel membrane-bound carbonic anhydrase from mouse kidney. *J Biol Chem* 1999, 274: 15701-5

Moriyama Y, Nelson N: The purified ATPase from chromaffin granule membranes is an anion-dependent proton pump. *J Biol Chem* 1987, 262: 9175-80

Motohashi H, Sakurai Y, Saito H, Masuda S, Urakami Y, Goto M, Fukatsu A, Ogawa O, Inui K: Gene expression levels and immunolocalization of organic ion transporters in the human kidney. *J Am Soc Nephrol* 2002, 13: 866-74

Moulin P, Igarashi T, Van der Smissen P, Cosyns JP, Verroust P, Thakker RV, Scheinman SJ, Courtoy PJ, Devuyst O: Altered polarity and expression of H^+-ATPase without ultrastructural changes in kidneys of Dent's disease patients. *Kidney Int* 2003, 63: 1285-95

Mount DB, Romero MF: The SLC26 gene family of multifunctional anion exchangers. *Pflugers Arch* 2004, 447: 710-21

Müller-Suur R, Gutsche HU: Tubular reabsorption of technetium-99m-DMSA. *J Nucl Med* 1995, 36: 1654-8

Murata K, Mitsuoka K, Hirai T, Walz T, Agre P, Heymann JB, Engel A, Fujiyoshi Y: Structural determinants of water permeation through aquaporin-1. *Nature* 2000, 407: 599-605

Nagai M, Meerloo T, Takeda T, Farquhar MG: The adaptor protein ARH escorts megalin to and through endosomes. *Mol Biol Cell* 2003, 14: 4984-96

Nakazato H, Hattori S, Furuse A, Kawano T, Karashima S, Tsuruta M, Yoshimuta J, Endo F, Matsuda I: Mutations in the *CLCN5* gene in Japanese patients with familial idiopathic low-molecular-weight proteinuria. *Kidney Int* 1997, 52: 895-900

Nelson RD, Guo XL, Masood K, Brown D, Kalkbrenner M, Gluck S: Selectively amplified expression of an isoform of the vacuolar H^+-ATPase 56-kilodalton subunit in renal intercalated cells. *Proc Natl Acad Sci U S A* 1992, 89: 3541-5

Nelson N, Harvey WR: Vacuolar and plasma membrane proton-adenosinetriphosphatases. *Physiol Rev* 1999, 79: 361-85

Nishi T, Forgac M: The vacuolar H^+-ATPases-nature's most versatile proton pumps. *Nat Rev Mol Cell Biol* 2002, 3: 94-103

Nishita T, Matsuura K, Ichihara N, Asari M: Isolation and measurement of carbonic anhydrase isoenzyme III in plasma, sera, and tissues of dogs. *Am J Vet Res* 2002, 63: 229-35

Norden AG, Lapsley M, Igarashi T, Kelleher CL, Lee PJ, Matsuyama T, Scheinman SJ, Shiraga H, Sundin DP, Thakker RV, Unwin RJ, Verroust P, Moestrup SK: Urinary megalin deficiency implicates abnormal tubular endocytic function in Fanconi syndrome. *J Am Soc Nephrol* 2002, 13: 125-33

Numata M, Ohkuma S, Iseki S: Expression and localization of mRNA for the 16 KD subunit of V-ATPase in the rat embryo. *J Histochem Cytochem* 1995, 43: 761-9

Oka T, Murata Y, Namba M, Yoshimizu T, Toyomura T, Yamamoto A, Sun-Wada GH, Hamasaki N, Wada Y, Futai M: a4, a unique kidney-specific isoform of mouse vacuolar H^+-ATPase subunit a. *J Biol Chem* 2001, 276: 40050-4

O'Neal WK, Hasty P, McCray PB Jr, Casey B, Rivera-Perez J, Welsh MJ, Beaudet AL, Bradley A: A severe phenotype in mice with a duplication of exon 3 in the cystic fibrosis locus. *Hum Mol Genet* 1993, 2: 1561-9

Ornoy A, Arnon J, Katznelson D, Granat M, Caspi B, Chemke J: Pathological confirmation of cystic fibrosis in the fetus following prenatal diagnosis. *Am J Med Genet* 1987, 28: 935-47

Otani H, Yamamura T, Nakao Y, Hattori R, Fujii H, Ninomiya H, Kido M, Kawaguchi H, Osako M, Imamura H, Ohta T, Ohkuma S: Vacuolar H^+-ATPase plays a crucial role in growth and phenotypic modulation of myofibroblasts in cultured human saphenous vein. *Circulation* 2000, 102: III269-74

Overdier DG, Ye H, Peterson RS, Clevidence DE, Costa RH: The winged helix transcriptional activator, HFH-3, is expressed in the distal tubules of embryonic and adult mouse kidney. *J Biol Chem* 1997, 272: 13725-30

Pajor AM: Sodium-coupled transporters for Krebs cycle intermediates. *Annu Rev Physiol* 1999, 61: 663-82

Pasyk EA and Foskett JK: Mutant (ΔF508) cystic fibrosis transmembrane conductance regulator Cl^- channel is functional when retained in endoplasmic reticulum of mammalian cells. *J Biol Chem* 1995, 270: 12347-50

Pendaries C, Tronchere H, Plantavid M, Payrastre B: Phosphoinositide signaling disorders in human diseases. *FEBS Lett* 2003, 546: 25-31

Penney MD, Oleesky DA: Renal tubular acidosis. *Ann Clin Biochem* 1999, 36: 408-22

Picollo A, Pusch M: Chloride/proton antiporter activity of mammalian CLC proteins ClC-4 and ClC-5. *Nature* 2005, 436: 420-3

Piech A, Dessy C, Havaux X, Feron O, Balligand JL: Differential regulation of nitric oxide synthases and their allosteric regulators in heart and vessels of hypertensive rats. *Cardiovasc Res* 2003, 57: 456-67

Piwon N, Günther W, Schwake M, Bosl MR, Jentsch TJ: ClC-5 Cl^--channel disruption impairs endocytosis in a mouse model for Dent's disease. *Nature* 2000, 408: 369-73

Ponting CP, Phillips C, Davies KE, Blake DJ: PDZ domains: targeting signalling molecules to sub-membranous sites. *Bioessays* 1997, 19: 469-479

Poschet JF, Skidmore J, Boucher JC, Firoved AM, Van Dyke RW, Deretic V: Hyperacidification of cellubrevin endocytic compartments and defective endosomal recycling in cystic fibrosis respiratory epithelial cells. *J Biol Chem* 2002, 277: 13959-65

Provoost AP, Van Aken M: Renal handling of technetium-99m DMSA in rats with proximal tubular dysfunction. *J Nucl Med* 1985, 26: 1063-7

Qi Z, Whitt I, Mehta A, Jin J, Zhao M, Harris RC, Fogo AB, Breyer MD: Serial determination of glomerular filtration rate in conscious mice using FITC-inulin clearance. *Am J Physiol Renal Physiol* 2004, 286: F590-6

Rabinowitz R, Peters MT, Vyas S, Campbell S, Nicolaides KH: Measurement of fetal urine production in normal pregnancy by real-time ultrasonography. *Am J Obstet Gynecol* 1989, 161: 1264-6

Raisanen SR, Lehenkari P, Tasanen M, Rahkila P, Harkonen PL, Vaananen HK: Carbonic anhydrase III protects cells from hydrogen peroxide-induced apoptosis. *FASEB J* 1999, 13: 513-22

Rao S, Verkman AS: Analysis of organ physiology in transgenic mice. *Am J Physiol Cell Physiol* 2000, 279: C1-18

Ratcliff R, Evans MJ, Cuthbert AW, MacVinish LJ, Foster D, Anderson JR, Colledge WH: Production of a severe cystic fibrosis mutation in mice by gene targeting. *Nat Genet* 1993, 4: 35-41

Reinhart SC, Norden AG, Lapsley M, Thakker RV, Pang J, Moses AM, Frymoyer PA, Favus MJ, Hoepner JA, and Scheinman SJ: Characterization of carrier females and affected males with X-linked recessive nephrolithiasis. *J Am Soc Nephrol* 1995, 5: 1451-61

Richardson DE, Regino CA, Yao H, Johnson JV: Methionine oxidation by peroxymonocarbonate, a reactive oxygen species formed from CO_2/bicarbonate and hydrogen peroxide. *Free Radic Biol Med* 2003, 35: 1538-50

Riordan JR, Rommens JM, Kerem B, Alon N, Rozmahel R, Grzelczak Z, Zielenski J, Lok S, Plavsic N, Chou JL, et al: Identification of the cystic fibrosis gene: cloning and characterization of complementary DNA. *Science* 1989, 245: 1066-73

Romero MF: Molecular pathophysiology of SLC4 bicarbonate transporters. *Curr Opin Nephrol Hypertens* 2005, 14: 495-501

Royaux IE, Wall SM, Karniski LP, Everett LA, Suzuki K, Knepper MA, Green ED: Pendrin, encoded by the Pendred syndrome gene, resides in the apical region of renal intercalated cells and mediates bicarbonate secretion. *Proc Natl Acad Sci U S A* 2001, 98: 4221-6

Rowe SM, Miller S, Sorscher EJ: Cystic fibrosis. *N Engl J Med* 2005, 352: 1992-2001

Rowntree RK, Harris A: The phenotypic consequences of CFTR mutations. *Ann Hum Genet* 2003, 67: 471-85

Rozmahel R, Wilschanski M, Matin A, Plyte S, Oliver M, Auerbach W, Moore A, Forstner J, Durie P, Nadeau J, Bear C, Tsui LC: Modulation of disease severity in cystic fibrosis transmembrane conductance regulator deficient mice by a secondary genetic factor. *Nat Genet* 1996, 12: 280-7

Sahali D, Mulliez N, Chatelet F, Dupuis R, Ronco P, Verroust P: Characterization of a 280-kD protein restricted to the coated pits of the renal brush border and the epithelial cells of the yolk sac. Teratogenic effect of the specific monoclonal antibodies. *J Exp Med* 1988, 167: 213-8

Sahali D, Mulliez N, Chatelet F, Laurent-Winter C, Citadelle D, Sabourin JC, Roux C, Ronco P, Verroust P: Comparative immunochemistry and ontogeny of two closely related coated pit proteins. The 280-kd target of teratogenic antibodies and the 330-kd target of nephritogenic antibodies. *Am J Pathol* 1993, 142: 1654-67

Sakamoto H, Sado Y, Naito I, Kwon TH, Inoue S, Endo K, Kawasaki M, Uchida S, Nielsen S, Sasaki S, Marumo F: Cellular and subcellular immunolocalization of ClC-5 channel in mouse kidney: colocalization with H^+-ATPase. *Am J Physiol* 1999, 277: F957-65

Samaniego-Picota MD, Whelton A: Aminoglycoside-induced nephrotoxicity in cystic fibrosis: a case presentation and review of the literature. *Am J Ther* 1996, 3: 248-57

Satlin LM, Woda CB, Schwartz GJ: Development of function in the metanephric kidney. In: *The Kidney, from normal development to congenital disease*, edited by Vize PD, Woolf AS and Bard JBL. Academic Press (Elsevier), Orlando, 2003, pp267-326

Scheel O, Zdebik AA, Lourdel S, Jentsch TJ: Voltage-dependent electrogenic chloride/proton exchange by endosomal CLC proteins. *Nature* 2005, 436: 424-7

Scheinman SJ, Pook MA, Wooding C, Pang JT, Frymoyer PA, Thakker RV: Mapping the gene causing X-linked recessive nephrolithiasis to Xp11.22 by linkage studies. *J Clin Invest* 1993, 91: 2351-7

Scheinman SJ: X-linked hypercalciuric nephrolithiasis: clinical syndromes and chloride channel mutations. *Kidney Int* 1998, 53: 3-17

Scheinman SJ, Cox JP, Lloyd SE, Pearce SH, Salenger PV, Hoopes RR, Bushinsky DA, Wrong O, Asplin JR, Langman CB, Norden AG, Thakker RV: Isolated hypercalciuria with mutation in *CLCN5*: relevance to idiopathic hypercalciuria. *Kidney Int* 2000, 57: 232-9

Schild L, Lu Y, Gautschi I, Schneeberger E, Lifton RP, Rossier BC: Identification of a PY motif in the epithelial Na channel subunits as a target sequence for mutations causing channel activation found in Liddle syndrome. *EMBO J* 1996, 15: 2381-7

Schmitz C, Hilpert J, Jacobsen C, Boensch C, Christensen EI, Luft FC, Willnow TE: Megalin deficiency offers protection from renal aminoglycoside accumulation. *J Biol Chem* 2002, 277: 618-22

Schwab K, Patterson LT, Aronow BJ, Luckas R, Liang HC, Potter SS: A catalogue of gene expression in the developing kidney. *Kidney Int* 2003, 64: 1588-604

Schwake M, Friedrich T, Jentsch TJ: An internalization signal in ClC-5, an endosomal Cl^-channel mutated in dent's disease. *J Biol Chem* 2001, 276: 12049-54

Schwartz GJ, Barasch J, Al-Awqati Q: Plasticity of functional epithelial polarity. *Nature* 1985, 318: 368-71

Schwartz GJ, Tsuruoka S, Vijayakumar S, Petrovic S, Mian A, Al-Awqati Q: Acid incubation reverses the polarity of intercalated cell transporters, an effect mediated by hensin. *J Clin Invest* 2002, 109: 89-99

Schwartz GJ, Al-Awqati Q: Role of hensin in mediating the adaptation of the cortical collecting duct to metabolic acidosis. *Curr Opin Nephrol Hypertens* 2005, 14: 383-8

Schwiebert EM, Cid-Soto LP, Stafford D, Carter M, Blaisdell CJ, Zeitlin PL, Guggino WB, Cutting GR: Analysis of ClC-2 channels as an alternative pathway for chloride conduction in cystic fibrosis airway cells. *Proc Natl Acad Sci U S A* 1998, 95: 3879-84

Seetharam B, Christensen EI, Moestrup SK, Hammond TG, Verroust PJ: Identification of rat yolk sac target protein of teratogenic antibodies, gp280, as intrinsic factor-cobalamin receptor. *J Clin Invest* 1997, 99: 2317-22

Segawa H, Kaneko I, Takahashi A, Kuwahata M, Ito M, Ohkido I, Tatsumi S, Miyamoto K: Growth-related renal type II Na/Pi cotransporter. *J Biol Chem* 2002, 277: 19665-72

Sheppard DN, Welsh MJ: Structure and function of the CFTR chloride channel. *Physiol Rev* 1999, 79: S23-45

Shi LB, Fushimi K, Bae HR, Verkman AS: Heterogeneity in ATP-dependent acidification in endocytic vesicles from kidney proximal tubule. Measurement of pH in individual endocytic vesicles in a cell-free system. *Biophys J* 1991, 59: 1208-17

Shikano N, Kanai Y, Kawai K, Ishikawa N, Endou H: Transport of ^{99m}Tc-MAG3 via rat renal organic anion transporter 1. *J Nucl Med* 2004, 45: 80-5

Silva IV, Cebotaru V, Wang H, Wang XT, Wang SS, Guo G, Devuyst O, Thakker RV, Guggino WB, Guggino SE: The ClC-5 knockout mouse model of Dent's disease has renal hypercalciuria and increased bone turnover. *J Bone Miner Res* 2003, 18: 615-23

Sly WS, Whyte MP, Sundaram V, Tashian RE, Hewett-Emmett D, Guibaud P, Vainsel M, Baluarte HJ, Gruskin A, Al-Mosawi M: Carbonic anhydrase II deficiency in 12 families with the autosomal recessive syndrome of osteopetrosis with renal tubular acidosis and cerebral calcification. *N Engl J Med* 1985, 313: 139-45

Sly WS, Hu PY: Human carbonic anhydrases and carbonic anhydrase deficiencies. *Annu Rev Biochem* 1995, 64: 375-401

Smith AN, Skaug J, Choate KA, Nayir A, Bakkaloglu A, Ozen S, Hulton SA, Sanjad SA, Al-Sabban EA, Lifton RP, Scherer SW, Karet FE: Mutations in ATP6N1B, encoding a new kidney vacuolar proton pump 116-kD subunit, cause recessive distal renal tubular acidosis with preserved hearing. *Nat Genet* 2000, 26: 71-5

Smith AN, Finberg KE, Wagner CA, Lifton RP, Devonald MA, Su Y, Karet FE: Molecular cloning and characterization of Atp6n1b: a novel fourth murine vacuolar H^+-ATPase a-subunit gene. *J Biol Chem* 2001, 276: 42382-8

Smith AN, Borthwick KJ, Karet FE: Molecular cloning and characterization of novel tissue-specific isoforms of the human vacuolar H^+-ATPase C, G and d subunits, and their evaluation in autosomal recessive distal renal tubular acidosis. *Gene* 2002, 297: 169-77

Snouwaert JN, Brigman KK, Latour AM, Malouf NN, Boucher RC, Smithies O, Koller BH: An animal model for cystic fibrosis made by gene targeting. *Science* 1992, 257: 1083-8

Steinmeyer K, Schwappach B, Bens M, Vandewalle A, Jentsch TJ: Cloning and functional expression of rat CLC-5, a chloride channel related to kidney disease. *J Biol Chem* 1995, 270: 31172-7

Strange K, Emma F, Jackson PS: Cellular and molecular physiology of volume-sensitive anion channels. *Am J Physiol* 1996, 270: C711-30

Strope S, Rivi R, Metzger T, Manova K, Lacy E: Mouse amnionless, which is required for primitive streak assembly, mediates cell-surface localization and endocytic function of cubilin on visceral endoderm and kidney proximal tubules. *Development* 2004, 131: 4787-95

Stuart RO, Bush KT, Nigam SK: Changes in global gene expression patterns during development and maturation of the rat kidney. *Proc Natl Acad Sci U S A* 2001, 98: 5649-54

Sun-Wada G, Murata Y, Yamamoto A, Kanazawa H, Wada Y, Futai M: Acidic endomembrane organelles are required for mouse postimplantation development. *Dev Biol* 2000, 228: 315-25

Sun-Wada GH, Murata Y, Namba M, Yamamoto A, Wada Y, Futai M: Mouse proton pump ATPase C subunit isoforms (C2-a and C2-b) specifically expressed in kidney and lung. *J Biol Chem* 2003, 278: 44843-51

Svenningsen NW, Lindquist B: Postnatal development of renal hydrogen ion excretion capacity in relation to age and protein intake. *Acta Paediatr Scand* 1974, 63: 721-31

Takeda T, Yamazaki H, Farquhar MG: Identification of an apical sorting determinant in the cytoplasmic tail of megalin. *Am J Physiol Cell Physiol* 2003, 284: C1105-13

Tanner SM, Aminoff M, Wright FA, Liyanarachchi S, Kuronen M, Saarinen A, Massika O, Mandel H, Broch H, de la Chapelle A: Amnionless, essential for mouse gastrulation, is mutated in recessive hereditary megaloblastic anemia. *Nat Genet* 2003, 33: 426-9

Tata F, Stanier P, Wicking C, Halford S, Kruyer H, Lench NJ, Scambler PJ, Hansen C, Braman JC, Williamson R, et al: Cloning the mouse homolog of the human cystic fibrosis transmembrane conductance regulator gene. *Genomics* 1991, 10: 301-7

Thevenod F, Friedmann JM: Cadmium-mediated oxidative stress in kidney proximal tubule cells induces degradation of Na^+/K^+-ATPase through proteasomal and endo-/lysosomal proteolytic pathways. *FASEB J* 1999, 13: 1751-61

Tizzano EF, Chitayat D, Buchwald M: Cell-specific localization of CFTR mRNA shows developmentally regulated expression in human fetal tissues. *Hum Mol Genet* 1993, 2: 219-24

Trejtnar F, Laznicek M: Analysis of renal handling of radiopharmaceuticals. *Q J Nucl Med* 2002, 46: 181-94

Trezise AE, Chambers JA, Wardle CJ, Gould S, Harris A: Expression of the cystic fibrosis gene in human foetal tissues. *Hum Mol Genet* 1993, 2: 213-8

Tsuganezawa H, Kobayashi K, Iyori M, Araki T, Koizumi A, Watanabe S, Kaneko A, Fukao T, Monkawa T, Yoshida T, Kim DK, Kanai Y, Endou H, Hayashi M, Saruta T: A new member of the HCO3(-) transporter superfamily is an apical anion exchanger of β-intercalated cells in the kidney. *J Biol Chem* 2001, 276: 8180-9

Tweedie S, Edwards Y: Mouse carbonic anhydrase III: nucleotide sequence and expression studies. *Biochem Genet* 1989, 27: 17-30

van den Hove MF, Croizet-Berger K, Jouret F, Guggino SE, Guggino WB, Devuyst O, Courtoy PJ: The loss of the chloride channel, ClC-5, delays apical iodide efflux and induces a euthyroid goiter in the mouse thyroid gland. *Endocrinology* 2006, 147: 1287-96

van Doorninck JH, French PJ, Verbeek E, Peters RH, Morreau H, Bijman J, Scholte BJ: A mouse model for the cystic fibrosis ΔF508 mutation. *EMBO J* 1995, 14: 4403-11

van Kuijck MA, van Aubel RA, Busch AE, Lang F, Russel FG, Bindels RJ, van Os CH, Deen PM: Molecular cloning and expression of a cyclic AMP-activated chloride conductance regulator: a novel ATP-binding cassette transporter. *Proc Natl Acad Sci U S A* 1996, 93: 5401-6

van Luijk WH, Ensing GJ, Meijer S, Donker AJ, Piers DA: Is the relative ^{99m}Tc-DMSA clearance a useful marker of proximal tubular dysfunction? *Eur J Nucl Med* 1984, 9: 439-42

Veeze HJ, Halley DJ, Bijman J, de Jongste JC, de Jonge HR, Sinaasappel M: Determinants of mild clinical symptoms in cystic fibrosis patients. Residual chloride secretion measured in rectal biopsies in relation to the genotype. *J Clin Invest* 1994, 93: 461-6

Vos P, Hogers R, Bleeker M, Reijans M, van de Lee T, Hornes M, Frijters A, Pot J, Peleman J, Kuiper M: AFLP: a new technique for DNA fingerprinting. *Nucleic Acids Res* 1995, 23: 4407-14

Wagner CA, Giebisch G, Lang F, Geibel JP: Angiotensin II stimulates vesicular H^+-ATPase in rat proximal tubular cells. *Proc Natl Acad Sci U S A* 1998, 95: 9665-8

Wagner CA, Finberg KE, Stehberger PA, Lifton RP, Giebisch GH, Aronson PS, Geibel JP: Regulation of the expression of the Cl-/anion exchanger pendrin in mouse kidney by acid-base status. *Kidney Int* 2002, 62: 2109-17

Wagner CA, Finberg KE, Breton S, Marshansky V, Brown D, Geibel JP: Renal vacuolar H^+-ATPase. *Physiol Rev* 2004, 84: 1263-314

Wagner MC, Molitoris BA: Renal epithelial polarity in health and disease. *Pediatr Nephrol* 1999, 13: 163-70

Wahlstedt-Froberg V, Pettersson T, Aminoff M, Dugue B, Grasbeck R: Proteinuria in cubilin-deficient patients with selective vitamin B12 malabsorption. *Pediatr Nephrol* 2003, 18: 417-21

Walrand S, van Dulmen A, van Rossem H, Pauwels S: Acquisition of linograms in SPECT: implementation and benefits. *Eur J Nucl Med Mol Imaging* 2002, 29: 1188-97

Walrand S, Jamar F, de Jong M, Pauwels S: Evaluation of novel whole-body high-resolution rodent SPECT (Linoview) based on direct acquisition of linogram projections. *J Nucl Med* 2005, 46: 1872-80

Wang SS, Devuyst O, Courtoy PJ, Wang XT, Wang H, Wang Y, Thakker RV, Guggino S, Guggino WB: Mice lacking renal chloride channel, CLC-5, are a model for Dent's disease, a nephrolithiasis disorder associated with defective receptor-mediated endocytosis. *Hum Mol Genet* 2000, 9: 2937-45

Wang Y, Cai H, Cebotaru L, Hryciw DH, Weinman EJ, Donowitz M, Guggino SE, Guggino WB: ClC-5: role in endocytosis in the proximal tubule. *Am J Physiol Renal Physiol* 2005, 289: F850-62

Ward CL, Omura S, Kopito RR: Degradation of CFTR by the ubiquitin-proteasome pathway. *Cell* 1995, 83: 121-7

Wilkens S, Takao I, Forgac M: Three-dimensional structure of the vacuolar ATPase - localization of subunit H by difference imaging and chemical cross-linking. *J Biol Chem* 2004, 279: 41942-9

Willnow TE, Hilpert J, Armstrong SA, Rohlmann A, Hammer RE, Burns DK, Herz J: Defective forebrain development in mice lacking gp330/megalin. *Proc Natl Acad Sci U S A* 1996, 93: 8460-4

Wilmer MJ, de Graaf-Hess A, Blom HJ, Dijkman HB, Monnens LA, van den Heuvel LP, Levtchenko EN: Elevated oxidized glutathione in cystinotic proximal tubular epithelial cells. *Biochem Biophys Res Commun* 2005, 337: 610-4

Wingo CS, Madsen KM, Smolka A, Tisher CC: H^+/K^+-ATPase immunoreactivity in cortical and outer medullary collecting duct. *Kidney Int* 1990, 38: 985-90

Winkler CA, Kittelberger AM, Watkins RH, Maniscalco WM, Schwartz GJ: Maturation of carbonic anhydrase IV expression in rabbit kidney. *Am J Physiol Renal Physiol* 2001, 280: F895-903

Wladimiroff JW, Campbell S: Fetal urine-production rates in normal and complicated pregnancy. *Lancet* 1974, 1: 151-4

Woodland C, Blowey D, Ito S, Spino M, Koren G: Hypothetical framework for enhanced renal tubular secretion of drugs in cystic fibrosis. *Med Hypotheses* 1998, 51: 489-91

Wright JT, Kiefer CL, Hall KI, Grubb BR: Abnormal enamel development in a cystic fibrosis transgenic mouse model. *J Dent Res* 1996, 75: 966-73

Wright SH, Dantzler WH: Molecular and cellular physiology of renal organic cation and anion transport. *Physiol Rev* 2004, 84: 987-1049

Wrong OM, Norden AG, Feest TG: Dent's disease; a familial proximal renal tubular syndrome with low-molecular-weight proteinuria, hypercalciuria, nephrocalcinosis, metabolic bone disease, progressive renal failure and a marked male predominance. *QJM* 1994, 87: 473-93

Wu F, Roche P, Christie PT, Loh NY, Reed AA, Esnouf RM, Thakker RV: Modeling study of human renal chloride channel (hCLC-5) mutations suggests a structural-functional relationship. *Kidney Int* 2003, 63: 1426-32

Zeiher BG, Eichwald E, Zabner J, Smith JJ, Puga AP, McCray PB Jr, Capecchi MR, Welsh MJ, Thomas KR.: A mouse model for the ΔF508 allele of cystic fibrosis. *J Clin Invest* 1995, 96: 2051-64

Zeitlin P: Pharmacologic restoration of ΔF508 CFTR-mediated Cl^- current. *Kidney Int* 2000, 57: 832-7

Zeuzem S, Feick P, Zimmermann P, Haase W, Kahn RA, Schulz I: Intravesicular acidification correlates with binding of ADP-ribosylation factor to microsomal membranes. *Proc Natl Acad Sci U S A* 1992, 89: 6619-23

Zhai XY, Thomsen JS, Birn H, Kristoffersen IB, Andreasen A, Christensen EI. Three-dimensional reconstruction of the mouse nephron. *J Am Soc Nephrol* 2006, 17: 77-88

Zhai XY, Birn H, Jensen KB, Thomsen JS, Andreasen A, Christensen EI: Digital three-dimensional reconstruction and ultrastructure of the mouse proximal tubule. *J Am Soc Nephrol* 2003, 14: 611-9

SUMMARY

The chloride transporters ClC-5 and CFTR (cystic fibrosis transmembrane conductance regulator) and the vacuolar H^+-ATPase (V-ATPase) co-distribute in proximal tubule (PT) cells. In PT endosomes, ClC-5 and the V-ATPase participate in the receptor-mediated endocytic uptake of low-molecular-weight (LMW) proteins from the ultrafiltrate. Mutations in the *CLCN5* gene are associated with Dent's disease, an X-linked renal tubulopathy characterized by early LMW proteinuria, hypercalciuria, nephrolithiasis, and nephrocalcinosis. Likewise, the inhibition of the V-ATPase results in a generalized PT dysfunction, with severe LMW proteinuria. In contrast, the role of CFTR in PT function remains poorly understood, and no overwhelming renal phenotype has been documented in cystic fibrosis (CF). In addition to PT cells, ClC-5 and the V-ATPase co-distribute in the intercalated cells (IC) of the collecting duct, which are mainly involved in acid-base homeostasis. At this location, the V-ATPase complex is located at the plasma membrane, and is made of particular subunit isoforms. Mutations in *ATP6V1B1* and *ATP6V0A4* genes encoding such IC-specific subunits of the V-ATPase cause metabolic acidosis in infancy or early childhood. These clinical observations prompted us to firstly investigate the ontogeny of ClC-5 and the V-ATPase in man and mouse kidney development. Our data support that their segmental distribution in PT cells is acquired during early nephrogenesis, in parallel with the onset of glomerular filtration. Conversely, the developmental pattern of the IC-specific V-ATPase isoforms, including the novel V0 d2 subunit, is characterized by a later appearance, following the induction of the transcription factor Foxi1. Next, our studies have demonstrated that the functional loss of CFTR in two distinct mouse models of CF, as well as in a representative cohort of CF patients harbouring the ΔF508 mutation, is associated with a moderate but significant defect in the reabsorption of LMW proteins. Finally, we have investigated the metabolic outcomes of the severe PT dysfunction observed in the *Clcn5* knockout mice, and postulated a role for Type III carbonic anhydrase in oxidative defences of injured PT cells. In parallel, we have demonstrated the usefulness of a small-animal SPECT (single photon emission computed tomography) prototype to *in vivo* explore PT functions in conscious mice. In conclusion, these studies provide new insights into the implication of the Cl^- transporters ClC-5 and CFTR and the V-ATPase in renal tubular maturation and in the pathophysiology of inherited tubular disorders.

RÉSUMÉ

Les transporteurs de chlorure, ClC-5 et CFTR (cystic fibrosis transmembrane conductance regulator), co-localisent avec la pompe à proton vacuolaire (V-ATPase) dans les cellules du tube proximal (TP). Au niveau des endosomes de ce segment du néphron, ClC-5 et la V-ATPase participent à l'endocytose médiée par récepteur des protéines ultrafiltrées. La perte fonctionnelle de ClC-5 par mutation du gène *CLCN5* cause la maladie de Dent, désordre tubulaire héréditaire lié à l'X associant protéinurie de bas poids moléculaire (BPM) précoce, hypercalciurie, lithiase rénale et néphrocalcinose. De même, l'inhibition de la V-ATPase *in vivo* cause une dysfonction généralisée du TP, caractérisée par une protéinurie de BPM sévère. A contrario, le rôle de CFTR dans la fonction du TP, ainsi que l'effet de son inactivation sur la fonction rénale des patients mucoviscidosiques, restent largement méconnus. En plus du TP, ClC-5 et la V-ATPase co-localisent dans les cellules intercalaires (CI) du néphron distal, qui participent à l'homéostasie acido-basique. Le complexe V-ATPase se trouve à la surface membranaire de ces cellules, où il est composé d'isoformes spécifiques de certaines sous-unités. La perte de ces sous-unités par mutation des gènes *ATP6V1B1* et *ATP6V0A4* entraîne l'apparition d'une acidose métabolique précoce durant l'enfance. Ces observations cliniques nous ont incités à investiguer l'ontogénie de ClC-5 et de la V-ATPase durant le développement rénal chez l'homme et la souris. Nos données indiquent que leur distribution segmentaire au niveau du TP est acquise durant la néphrogenèse précoce, au moment où la filtration glomérulaire commence. A l'inverse, les sous-unités spécifiques de la V-ATPase des CI, y compris la nouvelle sous-unité V0 d2, apparaissent plus tardivement, suivant l'induction du facteur de transcription Foxi1. Dans un second temps, nous avons montré que la perte fonctionnelle de CFTR, dans deux modèles murins de la mucoviscidose et dans une série de patients mucoviscidosiques porteurs de la mutation ΔF508, entraîne un déficit modéré, mais significatif, de la réabsorption tubulaire proximale des protéines de BPM. *In fine*, nous avons investigué les conséquences métaboliques du désordre tubulaire sévère observé chez les souris inactivées pour le gène *Clcn5*, et révélé un possible rôle pour l'anhydrase carbonique de type III dans la défense du TP contre le stress oxydatif. Par ailleurs, la mise au point récente d'un prototype SPECT (single photon emission computed tomography) nous a permis d'explorer *in vivo* la fonction rénale de ces souris. En conclusion, notre étude des transporteurs ClC-5 et CFTR et de la V-ATPase au cours de la maturation tubulaire et dans le rein adulte, permet une meilleure compréhension de la physiopathologie des désordres tubulaires congénitaux.